Contents

1. General Information

All reagents employed were at the highest commercially available purity levels and used as received, unless otherwise specified. Deuterated solvents were purchased at the highest purity level. Carbon dioxide (CO_2) was purchased at the 4.5 grade and used as received.

The nuclear magnetic resonance (NMR) experiments (^1H, ^{13}C, ^{19}F) were performed on Bruker Advance Neo 500 (^1H-frequency 500 MHz) spectrometer operating with the frequency, deuterated solvent, and at the temperature indicated in parentheses. All ^{13}C and ^{19}F spectra were proton-decoupled, indicated by $^{13}C\{^1H\}$ respective $^{19}F\{^1H\}$. Proton and carbon chemical shift values (δ) in d_6-DMSO are reported in parts per million (ppm) downfield in relation to tetramethylsilane (TMS) using the residual undeuterated solvent signal as a secondary internal standard (δ_H = 2.50 ppm and δ_C = 39.52 ppm). Experiments in d_7-DMF were performed using a commercial solution in sealed ampules containing 0.05 v/v% TMS (Cambridge Isotope Laboratories, Inc.), which was used as an internal standard for proton and carbon chemical shift values.

Quantitative $^{13}C\{^1H\}$ was recorded using TopSpin 4.0.5 software in-built inverse gated pulse sequence (C13IG). To ensure complete relaxation, d1 was set to 180 sec.[1] Spectra were recorded with 155 scans (8 h) at 25°C. Fluorine chemical shift (δ) are reported in parts per million (ppm) upfield in relation to $CFCl_3$ (0 ppm), and are uncorrected. To obtain quantitative ^{19}F spectra, d1 was set to 20 sec.[1] All ^{15}N NMR experiments were performed at the natural isotopic abundance of ^{15}N. Chemical shift values (δ) are reported in parts per million (ppm) upfield in relation to nitromethane (0 ppm) using a slightly modified literature method.[2] Briefly, a neat mixture of CH_3NO_2/CD_3NO_2 (9:1) under argon was used as an external standard with the lock on. Unless otherwise mentioned, all ^{15}N NMR experiments were proton-coupled and recorded using TopSpin 4.0.5 software standard pulse sequence (15N) with default settings (d1 = 10 sec). In some cases, the long relaxation time of tertiary nitrogen caused saturation, resulting in loss of signal. As a remedy, TopSpin in-built inverse gated pulse sequence (N15IG) was used. To ensure complete relaxation, d1 was set to 60 sec. Variable temperature experiments were adjusted to the desired temperature and left to equilibrate for an hour before measurement of spectra. Temperatures were calibrated using commercial NMR standard (4% methanol in CD_3OD).

All coupling constants (J) are quoted to the nearest 0.1 Hz with the involved nuclei subscripted, and the resonances are noted as follows: δ chemical shift in ppm (number of nuclei, multiplicity, J value(s), assignment). Splitting patterns are denoted as s (singlet), d (doublet), t (triplet), q (quartet), p (quintet), h (heptet), m (multiplet), or br (broad resonance). In case of signal overlap, 2D NMR experiments (HSQC and/or HMBC) were used as additional techniques for NMR signal assignments.

Infrared spectroscopy was performed with a Bruker ALPHA FT-IR spectrometer equipped with Platinum-ATR module, and operated with Opus 7 software.

The thermogravimetric analysis (TGA) and differential thermal analysis (DTA) were conducted with MettlerToledo TGA850 equipment. The samples (8–13 mg) were placed in alumina crucibles, and heated from 25 to 400 °C at 10 °C/min.

2. In situ NMR Experimental Procedure

Liquid anilines, TMG and d_6-DMSO were stored over activated 3 Å molecular sieves in a glovebox. Solid anilines were azeotropically dried with co-evaporation using dry toluene (3 cycles), then placed under vacuum overnight, and finally transferred to the glovebox. To an oven-dried 8 ml glass vial was added corresponding aniline (0.5 mmol), TMG (62.8 µl, 0.5 mmol) and 0.7 ml d_6-DMSO, in a glovebox. The solution was mixed using a syringe, and transferred to an oven-dried J. Young NMR tube. The tube was sealed, taken out from the glovebox and connected to a Schlenk-line. The lower two thirds of the tube were immersed in an ice-water bath for 1 h, freezing the solution. Next, the tube was lifted out and evacuated with the Schlenk-line, and then back-filled with CO_2 for a total of five cycles. The tube was left to warm to room temperature, while being open to the CO_2-line. After 30 min the tube had reached room temperature. The tube was sealed, and turned upside down three times, to ensure mixing of CO_2 with the solution. Afterwards, the tube was opened to the CO_2-line and the mixing process was repeated every 30 min, for three times. **Efficient mixing is critical for repeatable results.**

CAUTION: Do NOT apply CO_2 if the J. Young NMR tube is placed in liquid nitrogen. Doing this might cause an explosion. It is safer to use an ice-water bath to freeze the solution.

For spectral characterization of in-situ formed mixed carbamates, please section 16.

Yields were determined by ^1H NMR. The values were validated by comparing to integrals obtained with quantitative $^{13}C\{^1H\}$ spectra, and quantitative $^{19}F\{^1H\}$ spectra for fluorinated substrates.

3. Quantifying the Effect of Organic Base

We studied the effect of organic base by replacing TMG with an alternative organic base. For convenience, in a glovebox, we prepared a stock-solution of 4-nitroaniline (4.254 g, 30.80 mmol) in d_6-DMSO in a 10 ml volumetric flask. Dissolving 4-nitroaniline was slightly laborious, therefore we recommend making a more diluted stock-solution.

Typically, to an oven-dried 8 ml glass vial was added 4-nitroaniline stock solution (0.5 mmol, 126 µl), the base (0.5 mmol) and d_6-DMSO (0.6 ml), in this order. The solution was mixed using a syringe, transferred to an oven-dried J. Young NMR tube, and then processed as in the standard in-situ NMR experimental procedure (section 2).

The control experiment without base (Table 1, entry 1) had extra d_6-DMSO (0.7 ml in total) to compensate for lower volume (due to lack of base). The small sharp peak at 124.2 ppm in the carbon spectrum corresponds to free CO_2.[3]

Experiments with DIPA and DIPEA (Table 1, entries 2 and 3) were conducted with a different procedure, because the freebases phase-separated from the frozen d_6-DMSO, even when using liquid N_2. Instead, to an oven-dried 25 ml Schlenk tube with a stir bar was added 4-nitroaniline stock solution (0.5 mmol, 126 µl), the base (0.5 mmol) and d_6-DMSO (0.6 ml), in this order. The tube was sealed, taken out from the glovebox and connected to a Schlenk-line under CO_2 (1 atm). The stopper was replaced with a rubber septum, which was pierced with a needle (0.6 x 30 mm), and the tube was flushed with CO_2 for 10 min while vigorously stirring. The needle was removed and the solution stirred for 1h 30 min. Next, a large Schlenk tube, containing a J. Young NMR tube, was evacuated, filled with CO_2., and the stopper replaced with a rubber septum. The d_6-DMSO solution was rapidly transferred by syringe from the small Schlenk tube to the J. Young NMR tube inside the large Schlenk tube. The septum was removed and the J. Young NMR tube was quickly sealed under CO_2 flow. The reaction was then analyzed by NMR.

The experiment with DBU as a base (Table 1, entry 6) produced significant amounts of precipitate, which caused considerable line broadening. Therefore, we decided to repeat the experiment with 1,3-dimethoxybenzene (DMB) as an internal standard, to accurately quantify the amount of mixed carbamate. Surprisingly, no precipitate formed in the presence of DMB, and the solution remained homogeneous. Consequently, the peaks were much sharper; however, the amount of mixed carbamate was identical to the experiment without DMB. It is possible $DBUH^+$ forms a cation-π interaction with the electron-rich DMB, thereby improving solubility. However, cation-π interaction seems unlikely since there is no change in ^{13}C signals of DMB. Therefore, DBM seems to improve solubility by preventing formation of hydrogen-bonded aggregates.

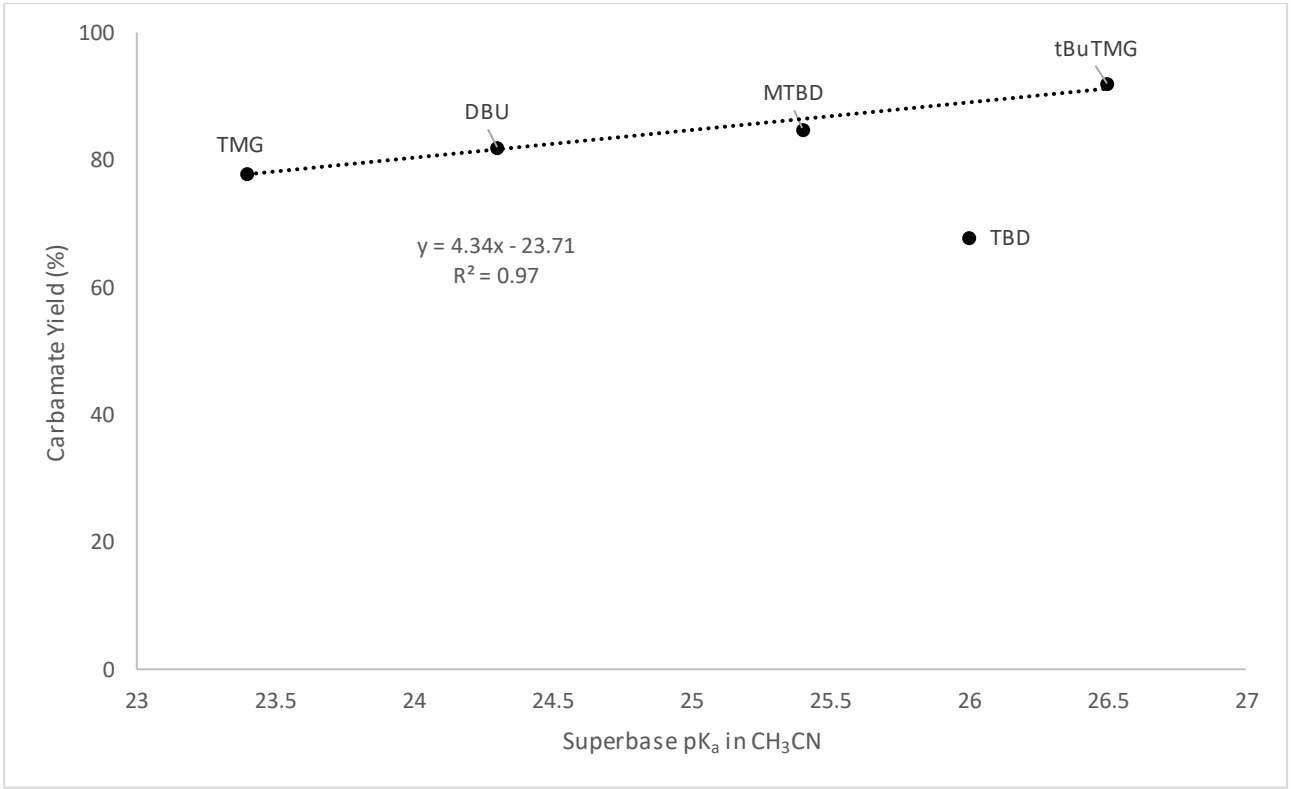

Figure S1. Mixed carbamate yield from 4-nitroaniline as a function of the pK_a of the corresponding superbase in CH_3CN. Yield determined by ^1H NMR on 0.5 mmol scale in d_6-DMSO. TBD was excluded from the plot. When included, there is no correlation (R^2 = 0.04).

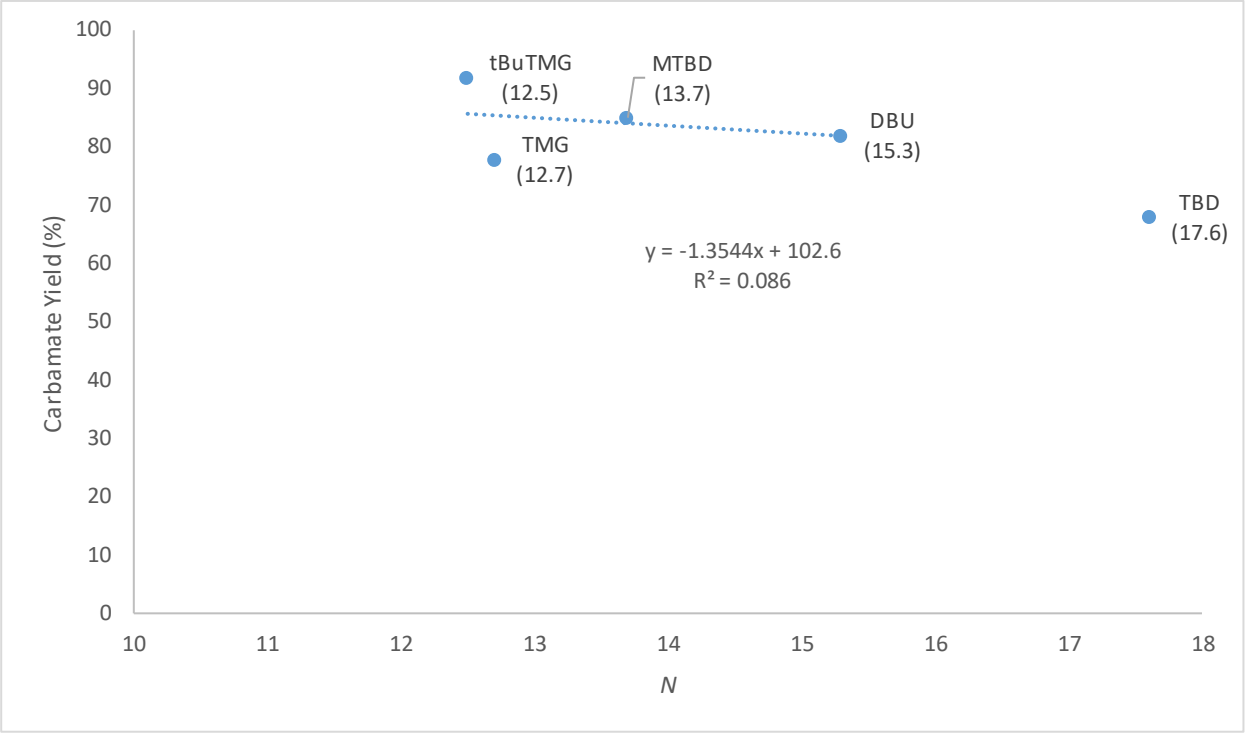

Figure S2. Mixed carbamate yield from 4-nitroaniline as a function of the nucleophilicity parameter *N* (in brackets) of the corresponding superbase in CH_3CN.[4,5] Yield determined by ^1H NMR on 0.5 mmol scale in d_6-DMSO. There is a moderate correlation with TBD included the plot (R^2 = 0.62).

4. Computational Details

All calculations were carried out with the Gaussian09 package, *Rev. D01*.[6] The DFT hybrid functional PBE0[7,8] was employed alongside with the Grimme empirical dispersion correction (D3BJ)[9] and the implicit solvation model (IEFPCM, DMSO).[10–12] Additional calculations were performed with B3LYP-D3 method in order to check the robustness of the results obtained at the PBE0-D3BJ level of theory.

For geometry optimizations, the 6-31+G(d,p) basis set[13] (BS1) was used on all atoms, whereas the 6-311++G(2df,2pd) basis set (BS2) was employed for single point calculations to obtain more accurate electronic energies. A counterpoise correction (CP)[14] was computed at the BS2 level of theory. For steps involving CO_2 insertion, the CP = 0.45 kcal/mol. Standard state conversion (SS)[1516] correction was included in order to convert the computed Gibbs free energy (ΔG°, BS1) at 1 atm into the 1M standard state. It only has an effect for reaction steps where a change in the number of moles occurs. For the reaction A + B = C at 298.15 K, SS = -1.89 kcal/mol.

The final energies ($\Delta G^\circ_{1M,298\ K}$) correspond to:

$$\Delta G^\circ_{1M,298K} = \Delta G_{1atm,\ 298K,BS1} - \Delta E_{1atm,BS1} + \Delta E_{1atm,BS2} + SS_{298K} + CP$$

The computed frequencies at the PBE0/6-31+G(d,p)/IEFPCM level of theory were scaled by 0.955 (see https://cccbdb.nist.gov/vibscalejust.asp).

4.1. Path 1 - Nucleophilic self-carboxylation of 4-nitroaniline in the presence of explicit DMSO solvent

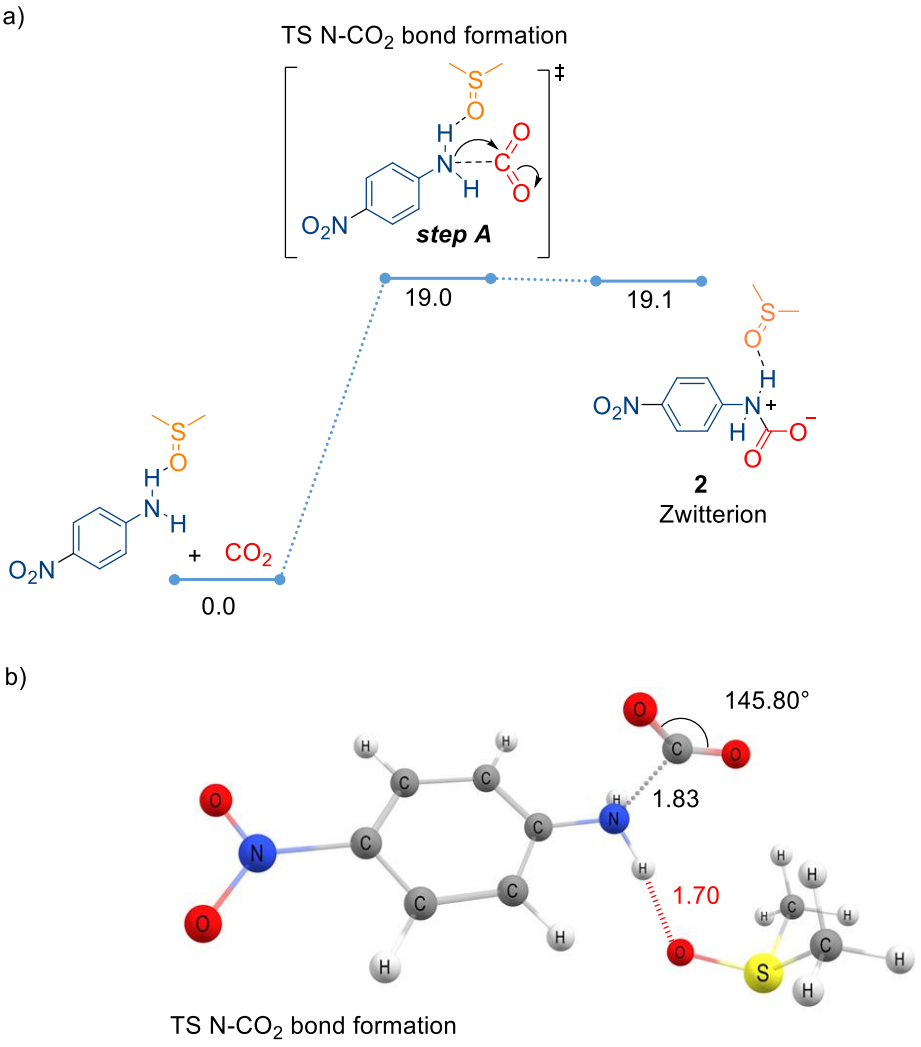

Figure S3. a) Computed Gibbs free energy profile (1 M energies, kcal/mol, 298 K, PBE0-D3BJ/IEFPCM, SS and CP included) for **Path 1** where 4-nitroaniline attacks a free CO_2 in the presence of explicit DMSO solvent. b) TS N-CO_2 could only be located if an explicit DMSO solvent molecule was added to the molecular model to stabilize the emerging positive charge on nitrogen. Distances are in Å.

4.2. Path 2 - Pre-associated 4-NO_2-aniline...TMG complex

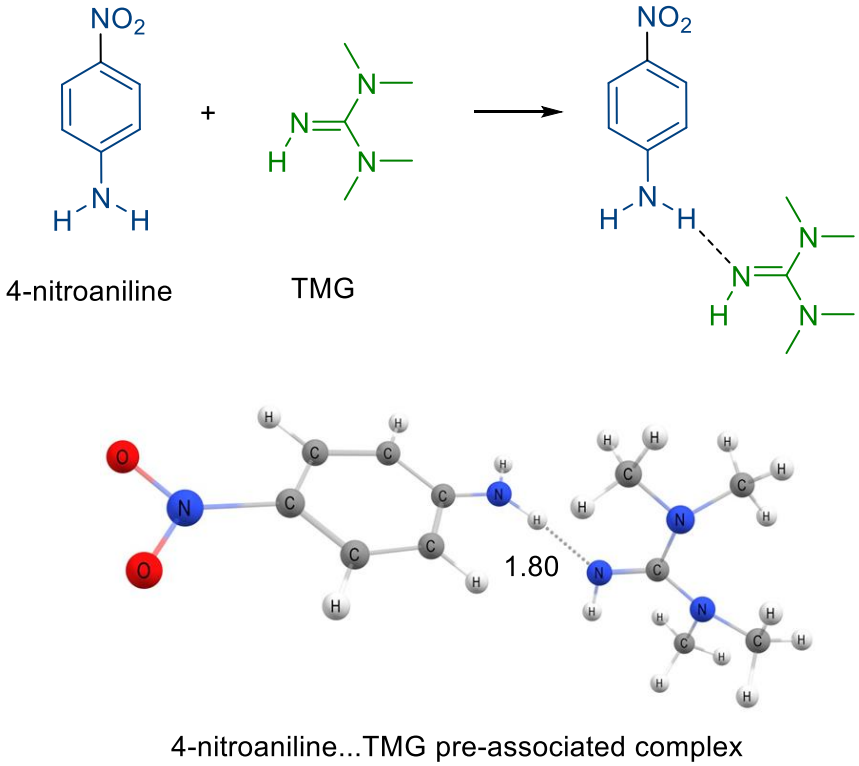

4-nitroaniline...TMG pre-associated complex

Figure S4. a) 4-nitroaniline...TMG pre-associated complex formed before attack on CO_2 occurs. The pre-associated complex is 0.2 kcal/mol more stable than the separated fragments (1 M energies, kcal/mol, 298 K, PBE0-D3BJ/IEFPCM[DMSO], SS and CP included) and is supported by NMR studies (see main text in article). In our computational model, the explicit hydrogen bonding of other bases or anilines or the DMSO solvent cannot be included. Therefore, this model should be considered approximate. Distances are in Å.

4.3 Computed barriers and Gibbs free energies (kcal/mol, 298 K) for formation of mixed carbamates from 4-nitroaniline using different bases in the absence of DMSO, employing PBE0-D3BJ and B3LYP-D3 methods

Table S1. Energies are relative to 4-nitroaniline-superbase and are given as computed (1 atm) and with a standard state correction to 1 M, at PBE0-D3BJ/IEFPCM IEFPCM[DMSO] and B3LYP-D3/IEFPCM[DMSO] level of theories. The energies obtained with B3LYP-D3 are higher, but the same trend is obtained as with PBE0-D3BJ method. The computed barrier for the mixed carbamate formation with TMG (PBE0-D3BJ/IEFPCM) is lower by 1.4 kcal/mol and 3.7 kcal/mol relative to barriers obtained with DIPA and DIPAE, respectively. With B3LYP-D3/IEFPCM method, the barrier for the mixed carbamate formation with TMG is lower by 2.9 kcal/mol and 4.2 kcal/mol relative to barriers obtained with DIPA and DIPAE, respectively.

		PBE0-D3BJ		B3LYP-D3	
Entry	Base	$\Delta G^{\neq}$	ΔG_r	$\Delta G^{\neq}$	ΔG_r
		1 atm [1 M]	1 atm [1 M]	1 atm [1 M]	1 atm [1 M]
1	DIPEA	22.5 [20.6]	1.0 [-0.9]	25.6 [23.7]	4.5 [2.7]
2	DIPA	20.2 [18.3]	0.9 [-1.0]	24.3 [22.4]	3.2 [1.3]
3	TMG	18.8 [16.9]	-0.8 [-2.7]	21.4 [19.5]	2.7 [0.8]
4	tBuTMG	18.4 [16.5]	-5.4 [-7.3]	-	

4.4 Computed barriers and Gibbs free energies (kcal/mol, 298 K) for formation of mixed carbamates from 4-nitroaniline using DIPEA, DIPA and TMG superbases, at B3LYP-D3/IEFPCM level of theory and in the presence of DMSO

Table S2. Energies are relative to 4-nitroaniline-superbase and are given as computed (1 atm) and with a standard state correction to 1 M, at B3LYP-D3/IEFPCM level of theory. The energies obtained with B3LYP-D3 gave the same trend as PBE0-D3BJ. The barrier for the mixed carbamate formation with TMG (B3LYP-D3/IEFPCM) is lower by 3.8 kcal/mol and 3.9 kcal/mol relative to barriers obtained with DIPA and DIPAE, respectively.

		B3LYP-D3	
Entry	Base	$\Delta G^{\neq}$	ΔG_r
		1 atm [1 M]	1 atm [1 M]
1	DIPEA	22.7 [20.8]	6.1 [4.2]
2	DIPA	22.6 [20.7]	6.4 [4.5]
3	TMG	18.8 [16.9]	1.1 [-0.8]

4.5 Formation of Zwitterion 4 and Subsequent Dimerization

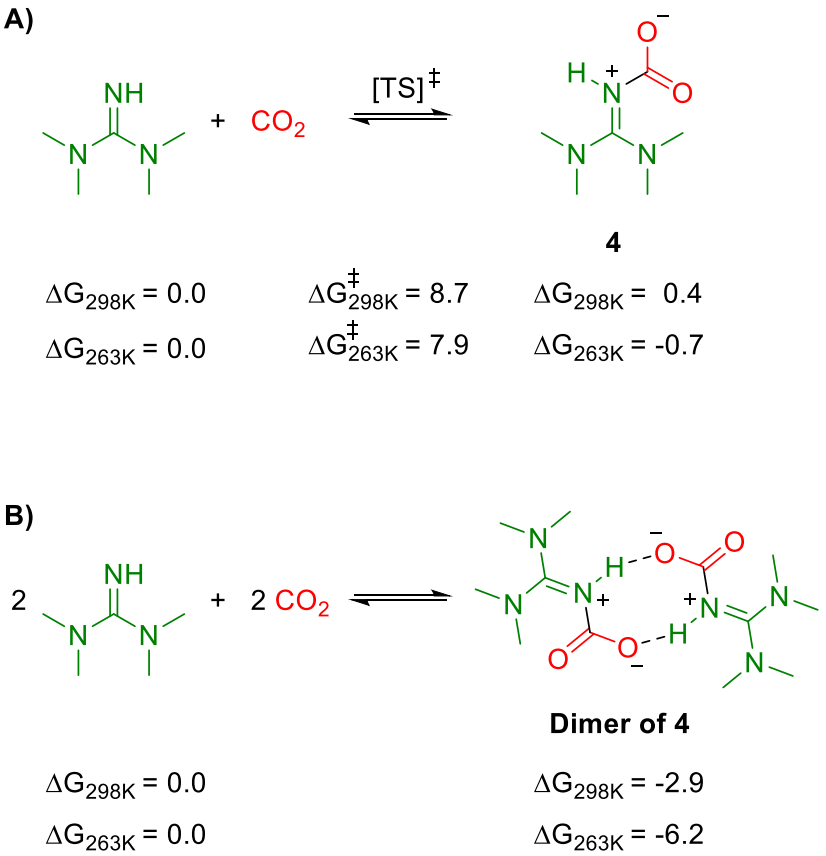

Figure S5. A) Computed barrier and reaction energy for formation of **4** and **B)** reaction energy for formation of the dimer of **4** from TMG and CO_2 (PBE0-D3BJ/IEFPCM[acetonitrile]). Free energies are in kcal/mol, computed at two different temperatures (298K and 263 K), including counterpoise corrections and standard state conversion (1 M) at the respective temperatures.

4.6 Formation of Zwitterions DBU–CO_2 and DBN–CO_2

Table S3. Computed free energies (kcal/mol, PBE0-D3BJ/IEFPCM[DMF], 1 M standard state) for reversible formation of DBU–CO_2 and DBN–CO_2 zwitterions are in kcal/mol, including counterpoise corrections and standard state conversion (1 M).

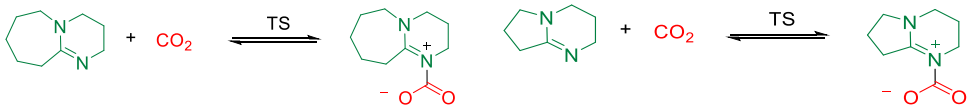

Entry	Temperature	DBU–CO_2		DBN–CO_2	
		$\Delta G^{\neq}$ [1 M]	ΔG_r [1 M]	$\Delta G^{\neq}$ [1 M]	ΔG_r [1 M]
1	298 K	7.1	2.0	5.7	-2.2
2	268 K	6.3	1.0	4.9	-3.2
3	248 K	5.6	0.5	4.5	-3.7
4	233 K	5.5	0.0	4.2	-4.1
4	223 K	5.3	-0.3	3.8	-4.5
5	203 K	4.8	-0.9	3.4	-5.0

4.7 The optimized geometries of DBU–CO_2 and DBN–CO_2

a) Optimized structure of DBU-CO_2 zwitterion

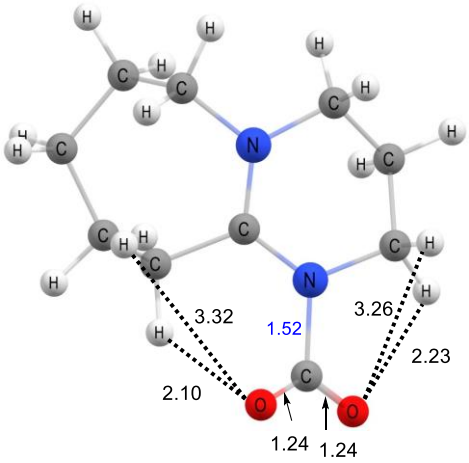

b) Optimized structure of DBN-CO_2 zwitterion

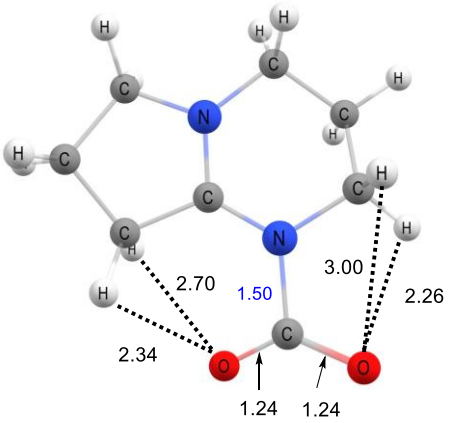

Figure S6. The optimized geometries of a) DBU–CO_2 and b) DBN–CO_2 zwitterions (PBE0-D3BJ/IEFPCM[DMF]). Four C-H···O interactions are observed within each zwitterion. The DBN–CO2 zwitterion has two strong C-H···O interactions (2.26 Å and 2.34 Å), one medium (2.70 Å) and one weak (3.00 Å). On the contrary, DBU–CO_2 zwitterion has two strong C-H···O interactions (2.10 Å and 2.23 Å) and two very weak (3.26 Å and 3.32 Å).

5. Derivation of the Hammett Relationship

In the manuscript, Equation 7 is derived using Equations 5 and 6. Derivation details are described below.

$$K = \frac{[RC_6H_4NHCO_2^-]^2}{[RC_6H_4NH_2]^2[CO_2]} \quad (5)$$

$$F = \frac{[RC_6H_4NHCO_2^-]}{[RC_6H_4NHCO_2^-]+[RC_6H_4NH_2]} \quad (6)$$

First, Equation 6 is rewritten as Equation S1. Further moving of the terms gives Equation S2, which is equal to Equation S3. We then divide both sides in Equation S3 by (1-*F*), giving us Equation S4. At this point, we have expressed the concentration of carbamate [$RC_6H_4HCO_2^-$] as a function of *F* and the concentration of unreacted aniline [$RC_6H_4H_2$].

$$F\,[RC_6H_4NHCO_2^-] + F[RC_6H_4NH_2] = [RC_6H_4NHCO_2^-] \quad (S1)$$

$$F[RC_6H_4NH_2] = [RC_6H_4NHCO_2^-] - F\,[RC_6H_4NHCO_2^-] \quad (S2)$$

$$F[RC_6H_4NH_2] = (1-F)[RC_6H_4NHCO_2^-] \quad (S3)$$

$$[RC_6H_4NHCO_2^-] = \frac{F}{(1-F)}[RC_6H_4NH_2] \quad (S4)$$

We can now substitute [$RC_6H_4HCO_2^-$] in Equation 5, giving us Equation S5. Rearranging the terms gives us Equation S6. At this point, we can eliminate $[RC_6H_4H_2]^2$, giving us Equation 7.

$$K = \frac{(\frac{F}{(1-F)}[RC_6H_4NH_2])^2}{[RC_6H_4NH_2]^2[CO_2]} \quad (S5)$$

$$K = (\frac{F}{1-F})^2 \frac{[RC_6H_4NH_2]^2}{[RC_6H_4NH_2]^2[CO_2]} \quad (S6)$$

$$K = (\frac{F}{1-F})^2 \frac{1}{[CO_2]} \quad (7)$$

In the following step, we insert Equation 7 into Equation 2, giving us Equation S7. Using rules for logarithmic functions, we rewrite Equation S7, giving us Equation S8.

$$\log K = \sigma\rho + \log K_0 \quad (2)$$

$$\log\left(\left(\frac{F}{1-F}\right)^2 \frac{1}{[CO_2]}\right) = \sigma\rho + \log K_0 \quad (S7)$$

$$\log\left(\left(\frac{F}{1-F}\right)^2\right) + \log\left(\frac{1}{[CO_2]}\right) = \sigma\rho + \log K_0 \quad (S8)$$

Further application of logarithm rules allows us to rewrite the terms in Equation S8, resulting in Equation S9. We then move the terms, giving us Equation S10. Finally, we rearrange the terms in Equation S10, resulting in Equation 8. Here, Equation 8 is written in a linear equation format **y = ax + b**. The parenthesis is to emphasize that the terms within make up the intercept **b**.

$$log\left(\left(\frac{F}{1-F}\right)^2\right) - log([CO_2]) = \sigma\rho + log\,K_0 \quad \text{(S9)}$$

$$log\left(\left(\frac{F}{1-F}\right)^2\right) = \sigma\rho + log\,K_0 + log([CO_2]) \quad \text{(S10)}$$

$$log\left(\left(\frac{F}{1-F}\right)^2\right) = \sigma\rho + (log([CO_2]) + log\,K_0) \quad \text{(8)}$$

6. Data Used in the Hammett Study

Table S4. Numerical and experimental data for substituents used in the Hammett study.

Entry	*p*-Substituent	σ [a]	σ$^+$ [a]	*F* [b]	$log\,((\frac{F}{1-F})^2)$
1	SO_2CF_3	0.96	-	0.73	0.863918
2	NO_2	0.78	0.79	0.78	1.099344
3	CN	0.66	0.66	0.80	1.204120
4	CF_3	0.54	0.61	0.85	1.506655
5	OCF_3	0.35	-	0.88	1.730603
6	Cl	0.23	0.11	0.91	2.009598

[a] Data from ref.[17] [b] This work.

As can be seen from **Table S4**, not all substituents have both σ and σ+ values available. Therefore, we replotted data in **Figure 1** (left, see manuscript), restricting us to substituents with σ and σ+ available. **Figure S7** shows correlation with σ (R^2 = 0.99), and **Figure S8** with σ+ (R^2 = 0.94). A better fit is obtained with standard σ values (**Figure S7**).

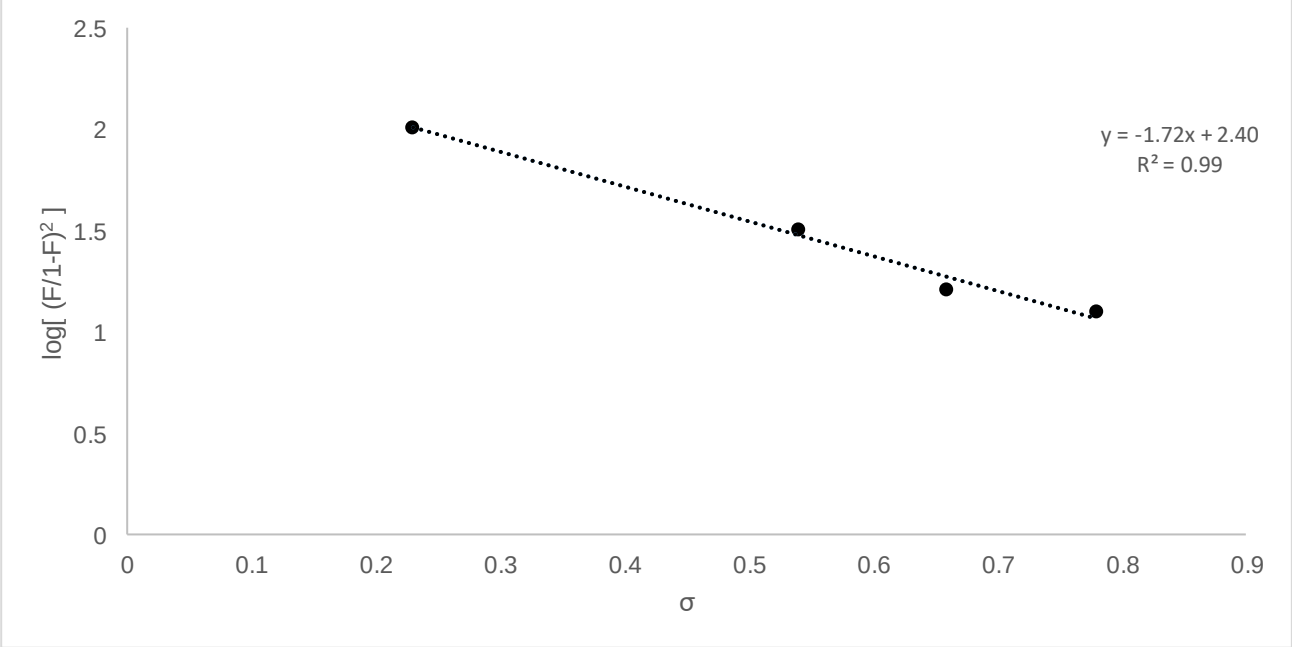

FigureS7. Hammett study of *para*-substituted anilines, showing correlation between log[(F/1-F)2] and standard Hammett values (σ) at 25 °C. Fraction of mixed carbamate (F) in parenthesis. The plot is limited to substituents with reported σ and σ+ values.

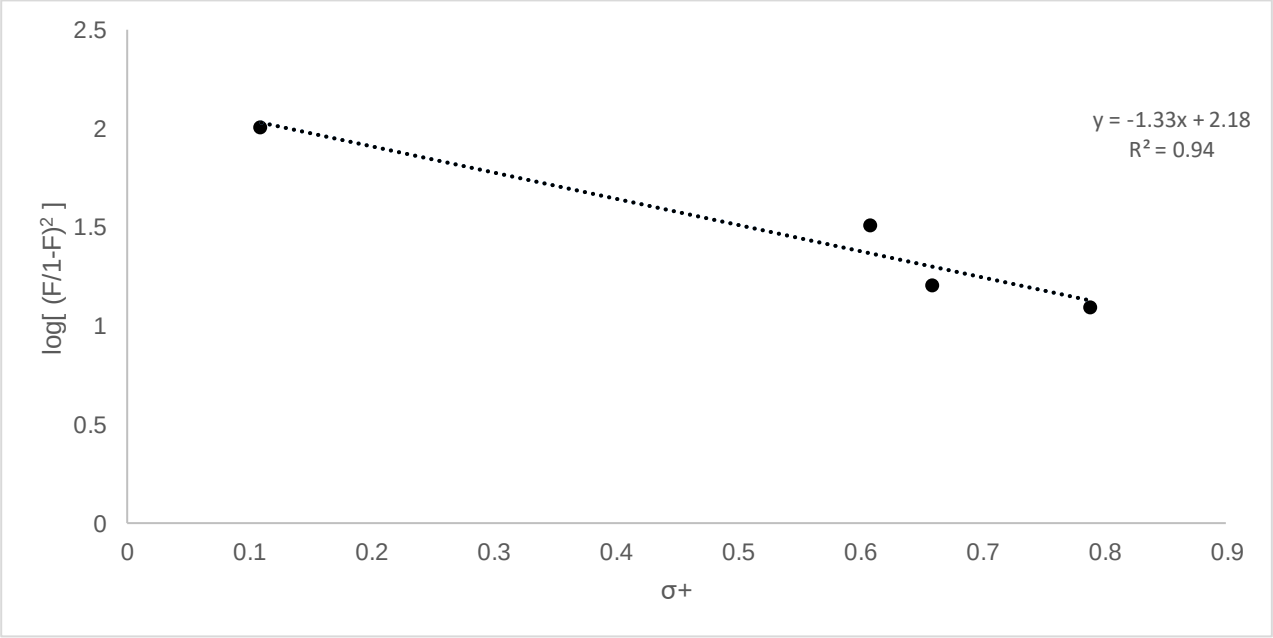

Figure S8. Hammett study of *para*-substituted anilines, showing correlation between log[(F/1-F)2] and positive Hammett values (σ+) at 25 °C. Fraction of mixed carbamate (F) in parenthesis. The plot is limited to substituents with reported σ and σ+ values.

7. Isolation of Zwitterion 4, TMG-CO_2

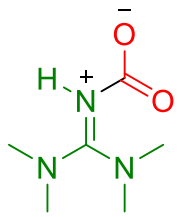

An oven-dried 120 ml Schlenk tube with a stir bar was connected to a Schlenk line, evacuated, and placed under CO_2 (1 atm). Dry TMG (5 ml, 4.58 g, 39.8 mmol) and acetonitrile (40 ml) were added under CO_2 flow while stirring at room temperature. The Schlenk tube was sealed with a rubber septum, which was then pierced with a needle. The solution was stirred rapidly for 30 min, and then the solution was transferred by through a syringe filter to a second oven-dried 120 ml Schlenk tube under CO_2 (1 atm). This removed small amounts of bicarbonate **5**, formed from residual water. The receiving tube had its septum replaced with a glass stopper, the Schlenk adapter was closed, and the tube was placed in a freezer (−25 °C) for two nights.

By this point, large amounts of a white amorphous solid had precipitated in the tube. The tube was removed from the freezer, placed in a cryostatic bath maintained at −25 °C, and connected to a Schlenk line under CO_2. The stopper was replaced with a pre-pierced rubber septum, through which a large spatula was inserted. The white solid was crushed and scraped off the walls of the tube. The cold suspension was transferred by PTFE-tubing to a Schlenk filter funnel with two glass stopcocks (one on side-arm), and filtered. The white solid was dried under a gentle flow of CO_2 until constant weight (ca 3h). Yield 3.93 g (62%).

For NMR analysis, to an oven-dried (and pre-cooled) 25 ml vial with a stir bar was added ca 3 ml dry d_6-DMSO, followed by ca 200 mg of the white solid. The vial was sealed and left to stir for 30 min. During this time, bubbles were observed to rise from the white solid, which sluggishly dissolved partially. When the vial was opened, a clear fizzing sound was heard, similar to when a can of carbonated soft drink is opened. Using a syringe, 0.7 ml was withdrawn from top of the mixture (avoiding the solids), and transferred to an oven-dried (and pre-cooled) Young tube, which was sealed. Many bubbles were visible in the tube. Immediate NMR analysis gave broad signals. When the sample was aged overnight, the bubbles had disappeared, and therefore sharper signals were obtained with identical shifts.

Bicarbonate **5** is stable under vacuum or when stored under argon. In contrast, zwitterion **4**, when placed in a Schlenk-tube, sublimates under vacuum (ca 0.1 mbar) at room temperature. When a separate Schlenk-tube containing zwitterion **4** is briefly opened under argon (ca 30 min) in a glovebox, and resealed, the zwitterion decomposes slowly (ca one month) under the introduced argon atmosphere, forming liquid TMG.

^{1}H NMR (500 MHz, d_6-DMSO, 25 °C): δ 6.58 (1H, br, =N**H**), 2.65 (12H, s, C**H**$_3$)

^{13}C{^{1}H} NMR (125.8 MHz, d_6-DMSO, 25 °C): δ 165.4 (**C**=N), 126.8 (N-**C**O_2^-), 39.1 (N**C**H$_3$)

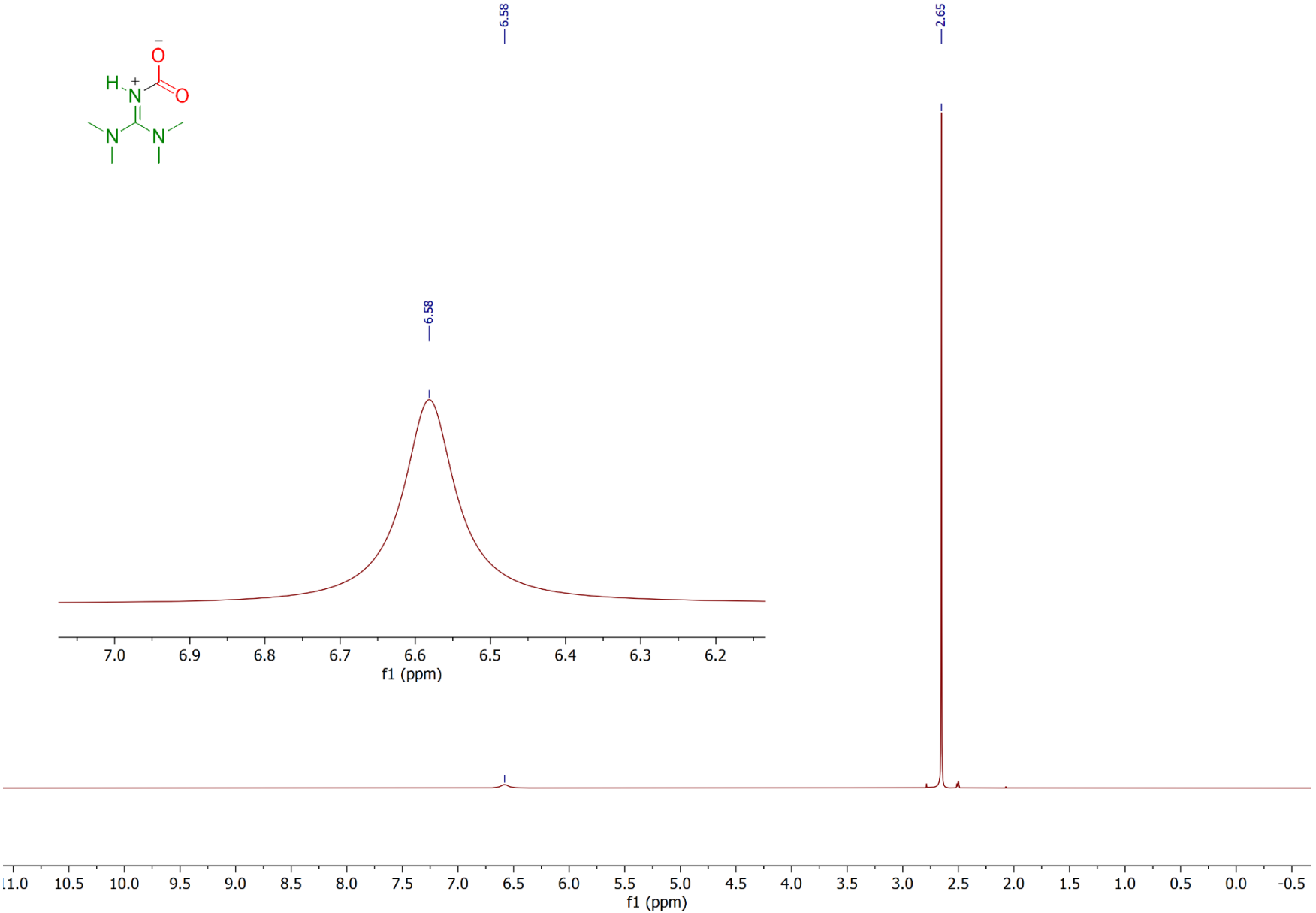

Figure S9. ^{1}H NMR spectra (500 MHz, d_6-DMSO, 25 °C) of isolated zwitterion **4**, TMG-CO_2.

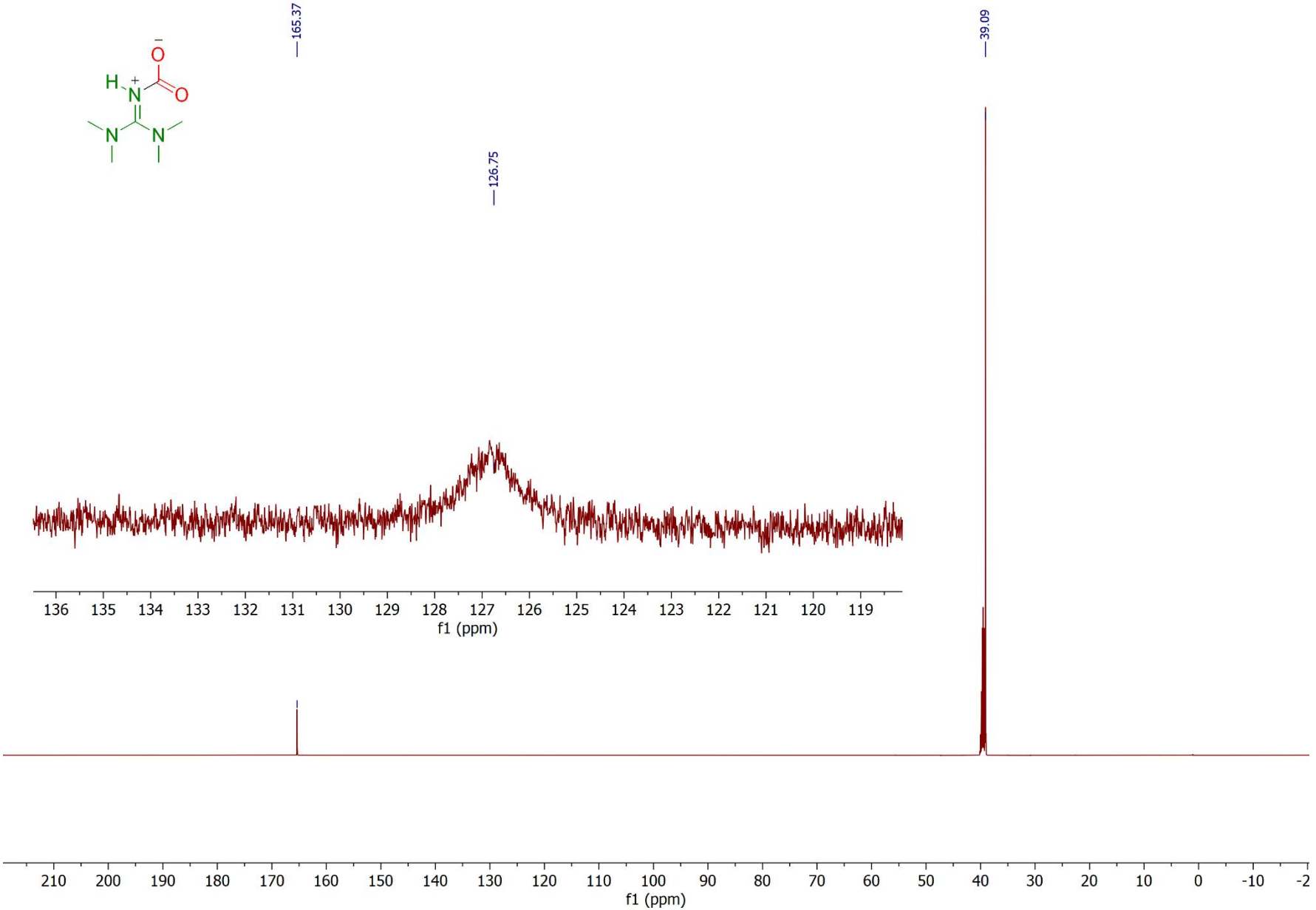

Figure S10. $^{13}C\{^{1}H\}$ NMR spectra (125.8 MHz, d_6-DMSO, 25 °C) of isolated zwitterion **4**, TMG-CO_2.

8. Isolation of Bicarbonate 5, [TMGH$^+$][HCO$_3^-$]

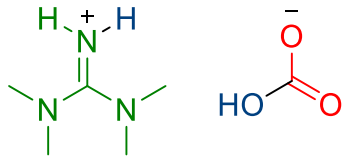

An oven-dried 120 ml Schlenk tube with a stir bar was connected to a Schlenk line, evacuated, and placed under CO_2 (1 atm). While stirring at room temperature under CO_2 flow, dry TMG (5 ml, 4.58 g, 39.8 mmol), acetonitrile (40 ml), and water (0.8 ml, 44 mmol, 1.1 eq) were added, in this order, resulting in immediate exothermic precipitation of a white powder. The solution was stirred rapidly for 30 min. The tube was then connected to an upside-down Schlenk filter funnel with two glass stopcocks (one on side-arm) under CO_2. The whole apparatus was slowly and carefully turned upside down, and the solution filtered using a flow of CO_2. The white solid was collected and transferred under CO_2 to a second oven-dried Schlenk tube, where the solids were dried under vacuum overnight. Yield 5.99 g (85%).

^{1}H NMR (500 MHz, d_6-DMSO, 25 °C): δ 7.60 (1H, br, =N**H**$_2$), 3.75 (1H, br, **H**CO$_3^-$), 2.74 (12H, s, C**H**$_3$)

^{13}C{^{1}H} NMR (125.8 MHz, d_6-DMSO, 25 °C): δ 164.0 (**C**=N), 158.3 (H**C**O$_3^-$), 39.2 (N**C**H$_3$)

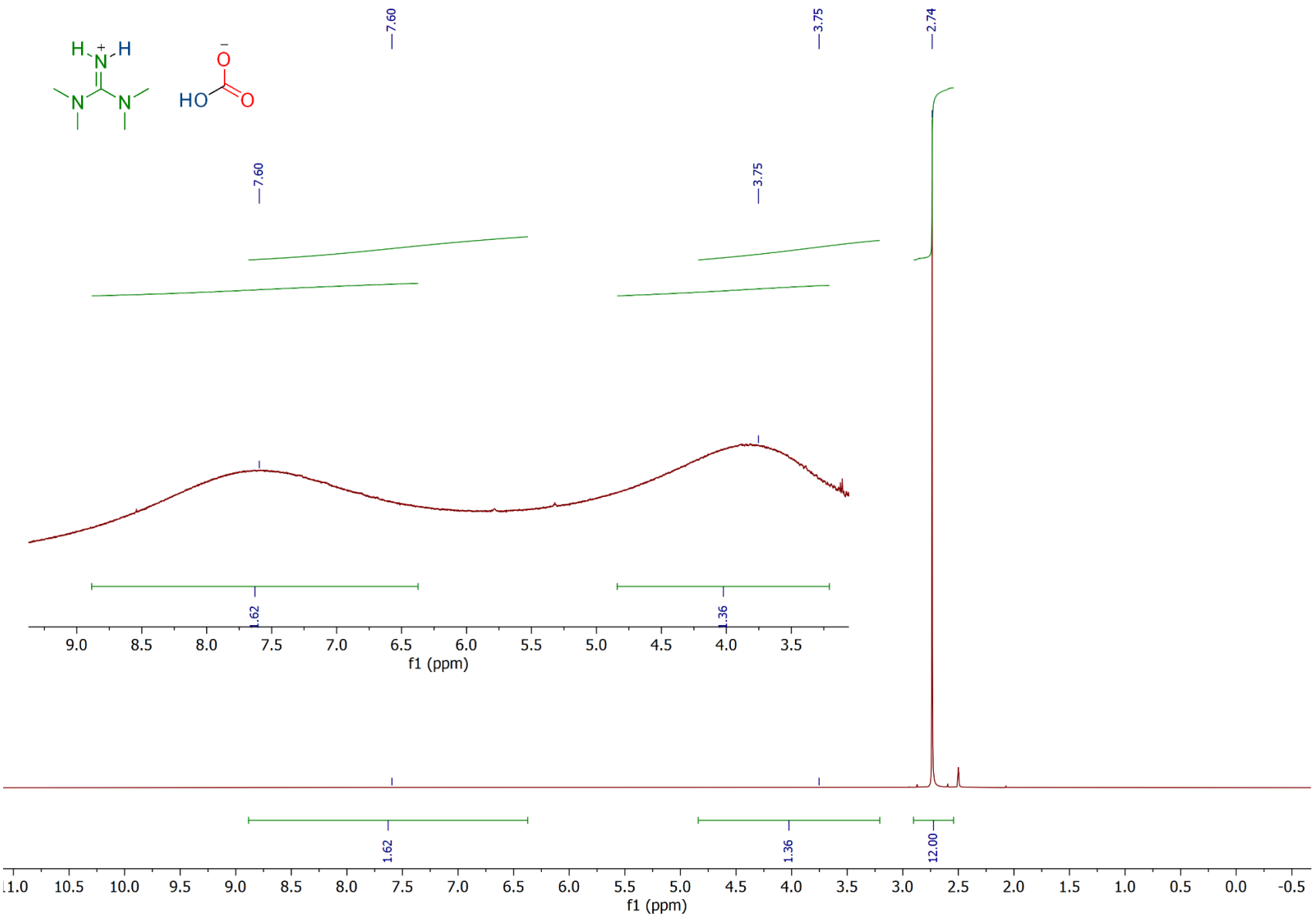

Figure S11. ^{1}H NMR spectra (500 MHz, d_6-DMSO, 25 °C) of bicarbonate **5**, [TMGH^{+}][HCO$_3^{-}$].

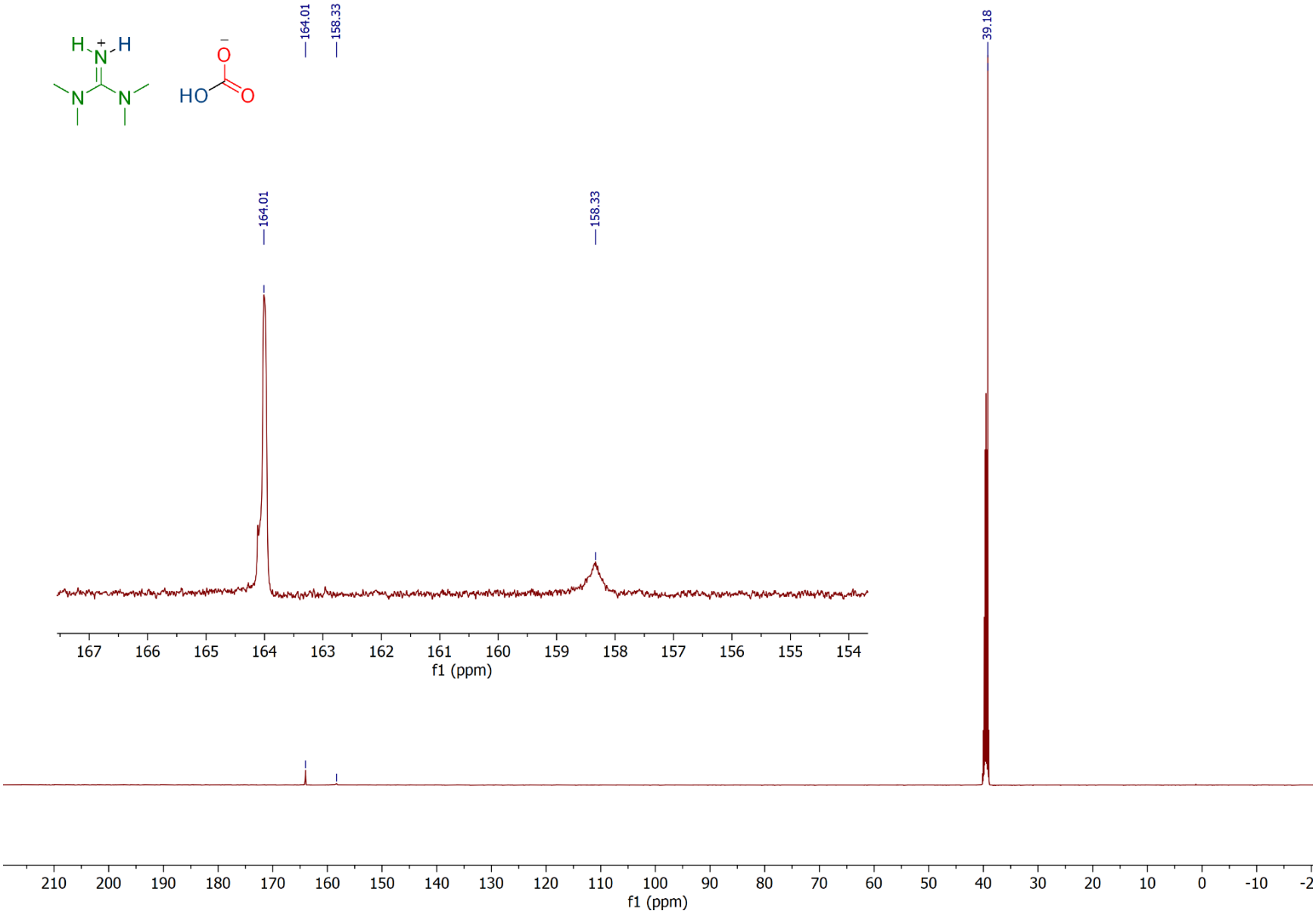

Figure S12. $^{13}C\{^{1}H\}$ NMR spectra (125.8 MHz, d_6-DMSO, 25 °C) of bicarbonate **5**, $[TMGH^+][HCO_3^-]$.

9. In situ NMR Studies of TMG

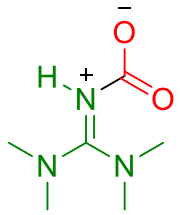

In-situ NMR studies of TMG in d_6-DMSO were performed as described in section 2.

Under argon:

^{1}H NMR (500 MHz, d_6-DMSO, 25 °C): δ 5.34 (1H, s, =N**H**), 2.61 (12H, s, C**H$_3$**)

^{13}C{^{1}H} NMR (125.8 MHz, d_6-DMSO, 25 °C): δ 166.2 (**C**=N), 39.1 (N**C**H$_3$)

Under CO_2:

^{1}H NMR (500 MHz, d_6-DMSO, 25 °C): δ 5.58 (1H, s, =N**H**), 2.62 (12H, s, C**H$_3$**)

^{13}C{^{1}H} NMR (125.8 MHz, d_6-DMSO, 25 °C): δ 165.9 (**C**=N), 126.8 (N-**C**O$_2^-$), 39.1 (N**C**H$_3$)

In-situ NMR studies of TMG in d_7-DMF (**Table S5**) were performed as described in section 2, except an acetone/dry ice bath was used to freeze the solution. Note that free CO_2 in d_7-DMF appears as a sharp signal at 125.5 ppm (**Figure S23**). ^{15}N NMR data of TMG is consistent with a previous report.[18]

Table S5. Chemical shift of TMG in d_7-DMF during variable-temperature NMR experiments.

Atmosphere	T (°C)	δ N**H** (^{1}H)[a]	δ C**H$_3$** (^{1}H)[a]	δ **C**H$_3$ (^{13}C)[a]	δ **C**=N (^{13}C)	δ N-**C**O$_2^-$ (^{13}C)	δ **N**H (^{15}N)	δ **N**Me$_2$ (^{15}N)
Ar	25	5.45	2.65	39.5	167.3	d	-206.4	-328.2
CO_2	25	5.56	2.66	39.5	167.3	125.9 (br)	-207.4	-327.9
CO_2	10	5.69	2.66	39.5	167.2	126.6 (br)	-207.8	-327.2
CO_2	0	5.91	2.68	39.5	166.8	128.7 (br)	-209.5	-326.0
CO_2	-10	6.42 (br)	2.71	39.6	166.2	d	-207.3	d

[a] ^{1}H NMR 500 MHz, **Figure S16**. [b] ^{13}C{^{1}H} NMR 125.8 MHz, **Figure S17-21**. [c] ^{15}N NMR 50.7 MHz, **Figure S22**. [d] Signal not observed.

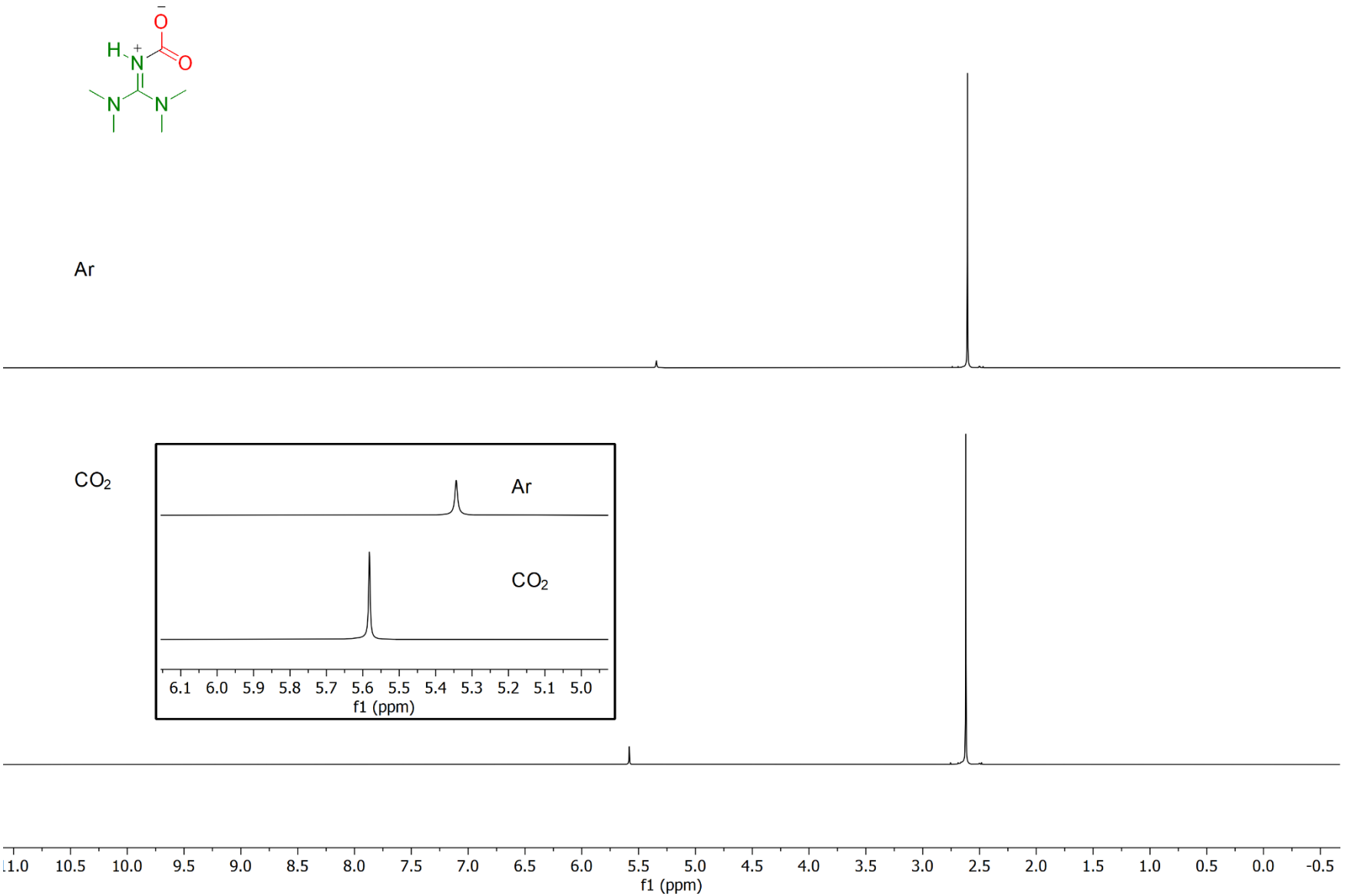

Figure S13. Stacked ^{1}H NMR spectra (500 MHz, d_6-DMSO, 25 °C) of TMG (under Ar) and in-situ generated zwitterion **4**, TMG-CO_2 (under CO_2).

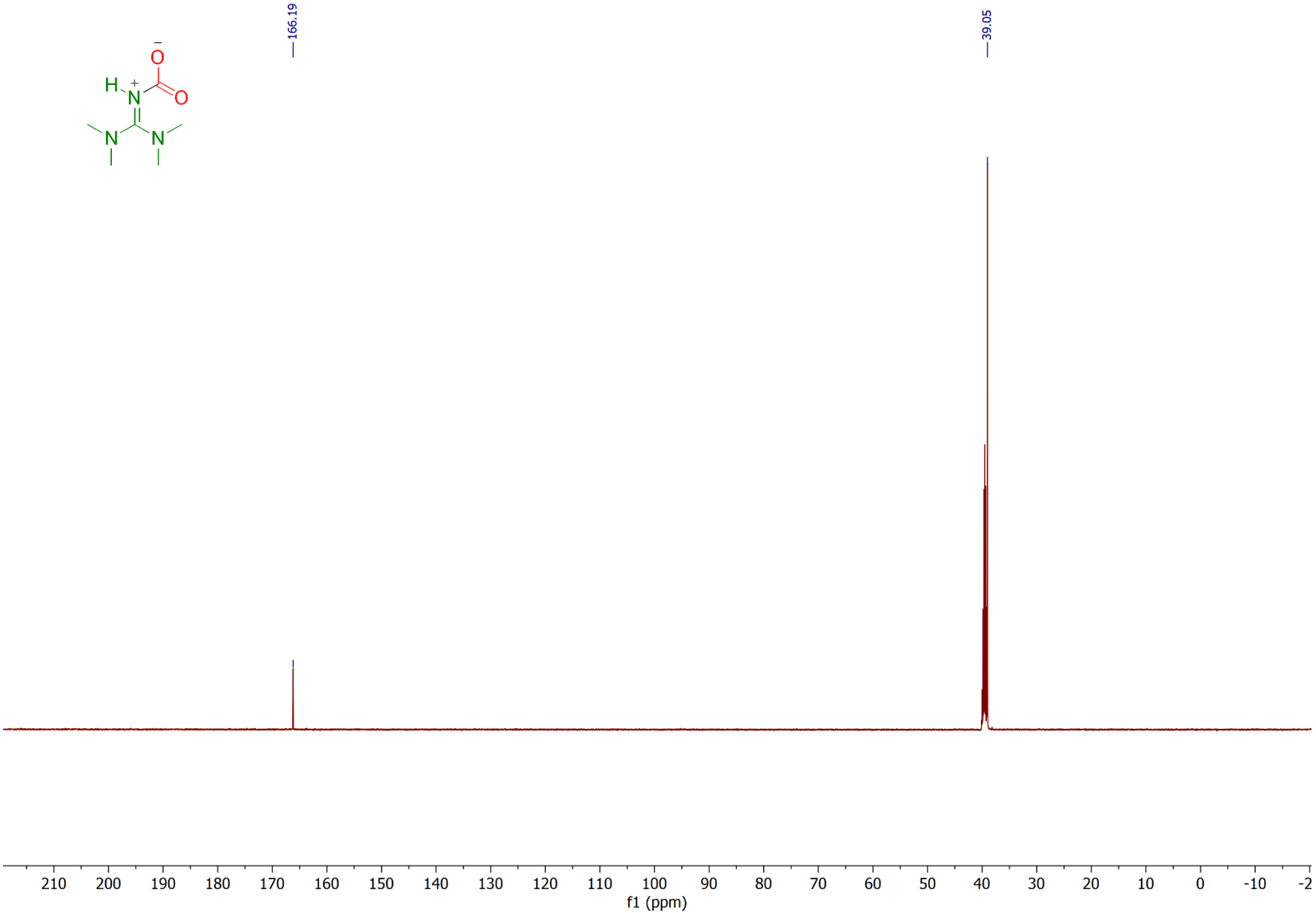

Figure S14. $^{13}C\{^{1}H\}$ NMR spectra (125.8 MHz, d_6-DMSO, 25 °C) of TMG under Ar.

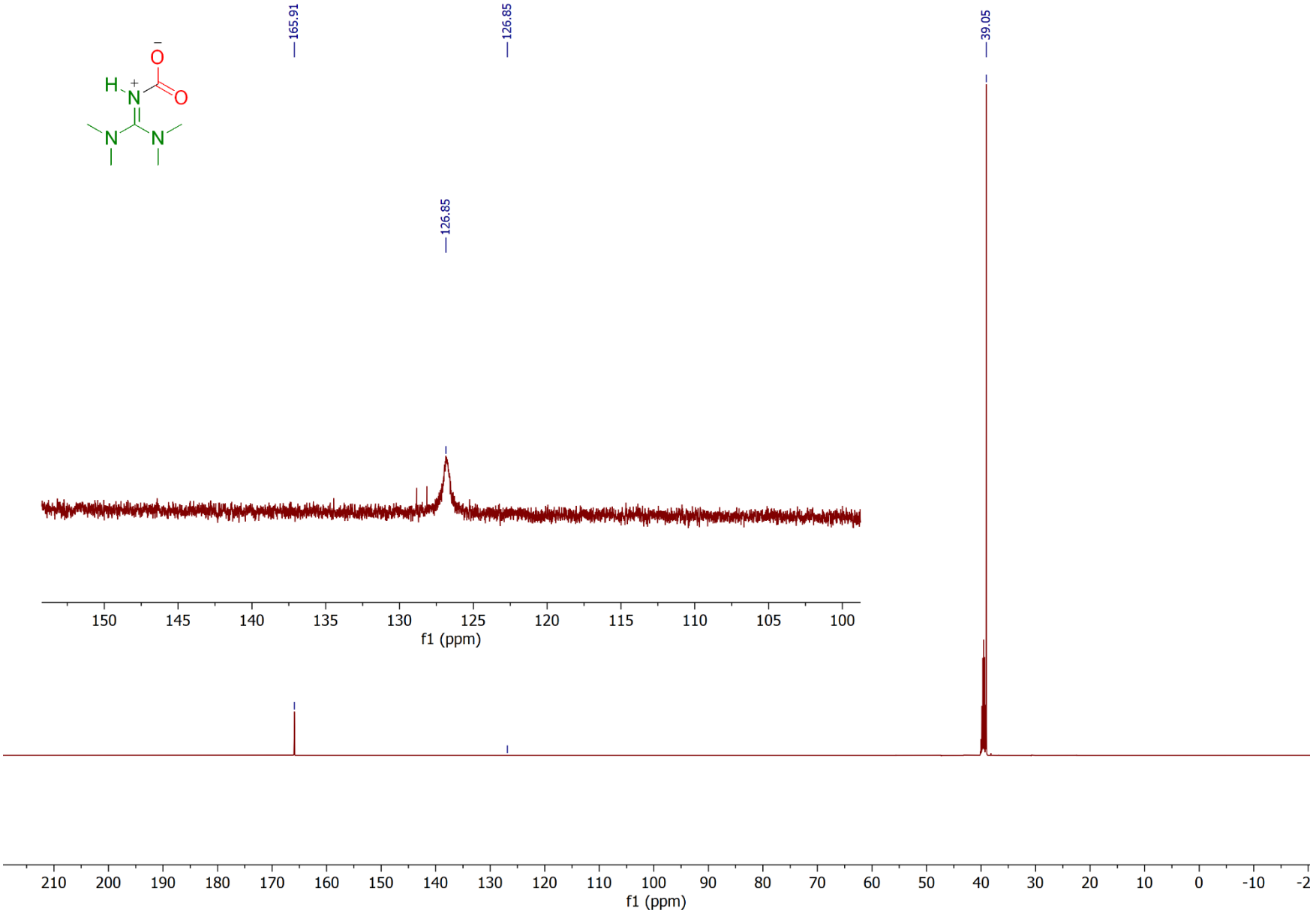

Figure S15. $^{13}C\{^{1}H\}$ NMR spectra (125.8 MHz, d_6-DMSO, 25 °C) of in-situ generated zwitterion **4**, TMG-CO_2 (under CO_2).

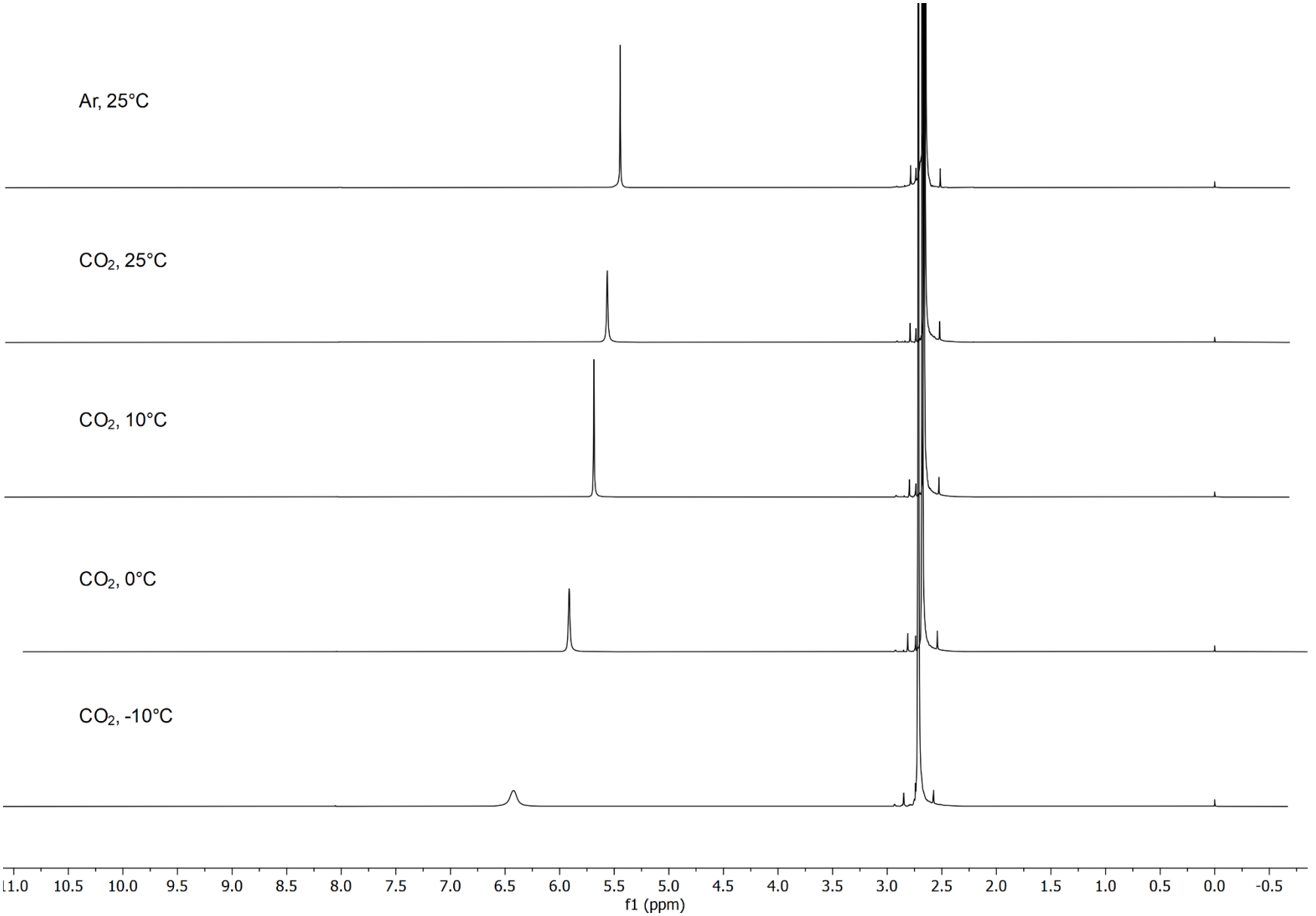

Figure S16. Stacked ^{1}H spectra (500 MHz) of TMG in d_7-DMF.

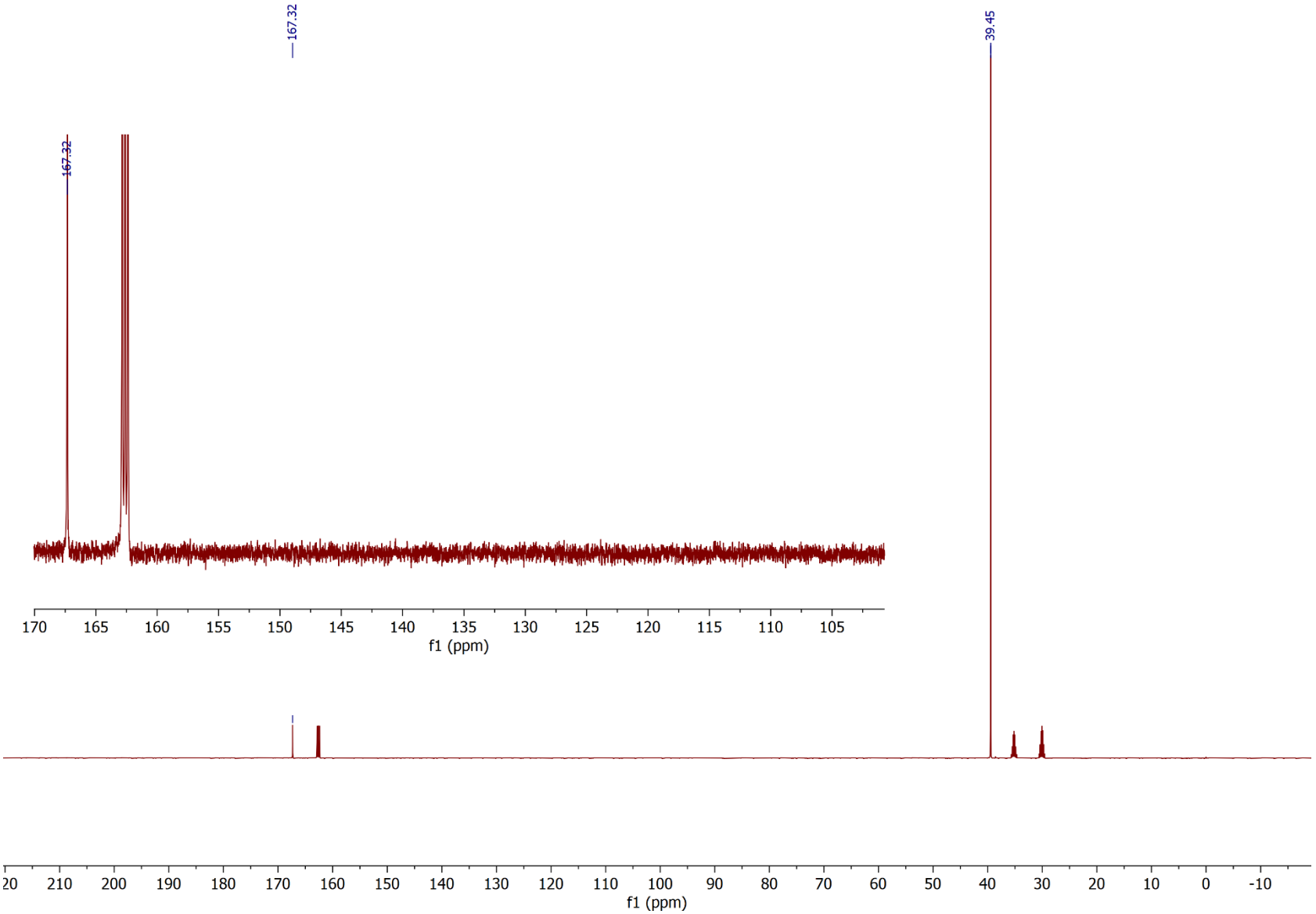

Figure S17. $^{13}C\{^{1}H\}$ spectra (125.8 MHz) of TMG in d_7-DMF under argon at 25°C.

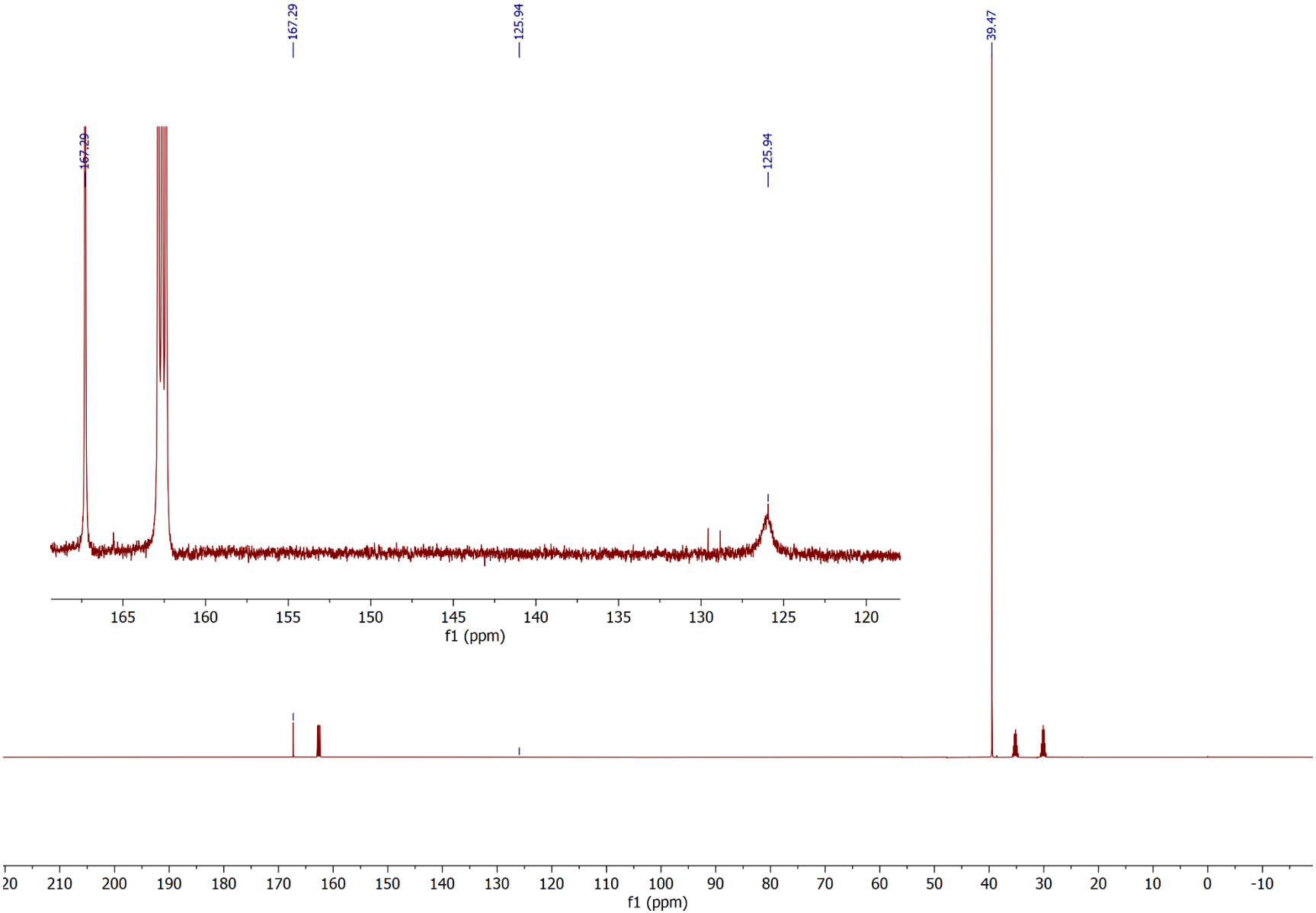

Figure S18. $^{13}C\{^{1}H\}$ spectra (125.8 MHz) of TMG in d_7-DMF under CO_2 at 25°C.

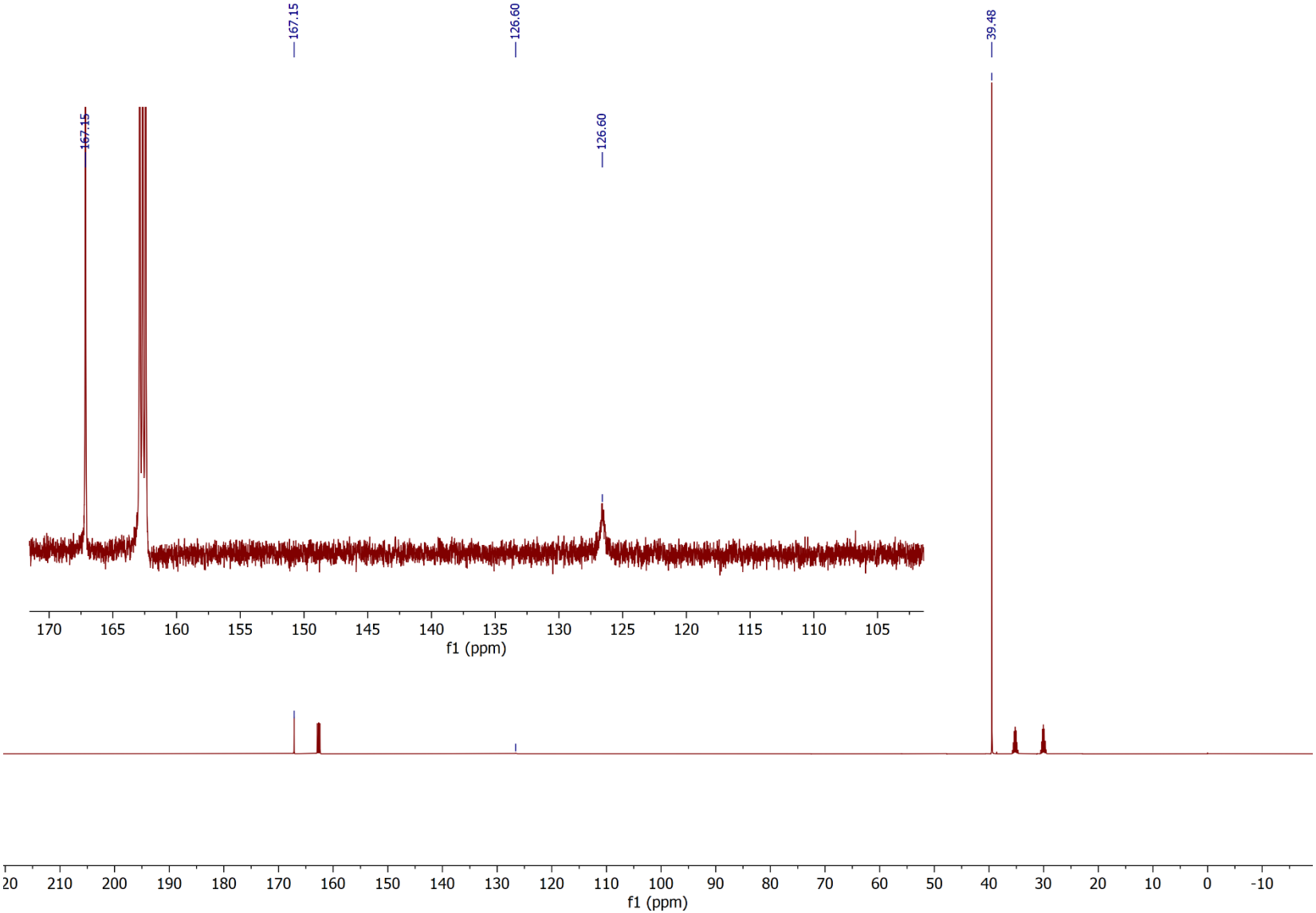

Figure S19. $^{13}C\{^{1}H\}$ spectra (125.8 MHz) of TMG in d_7-DMF under CO_2 at 10°C.

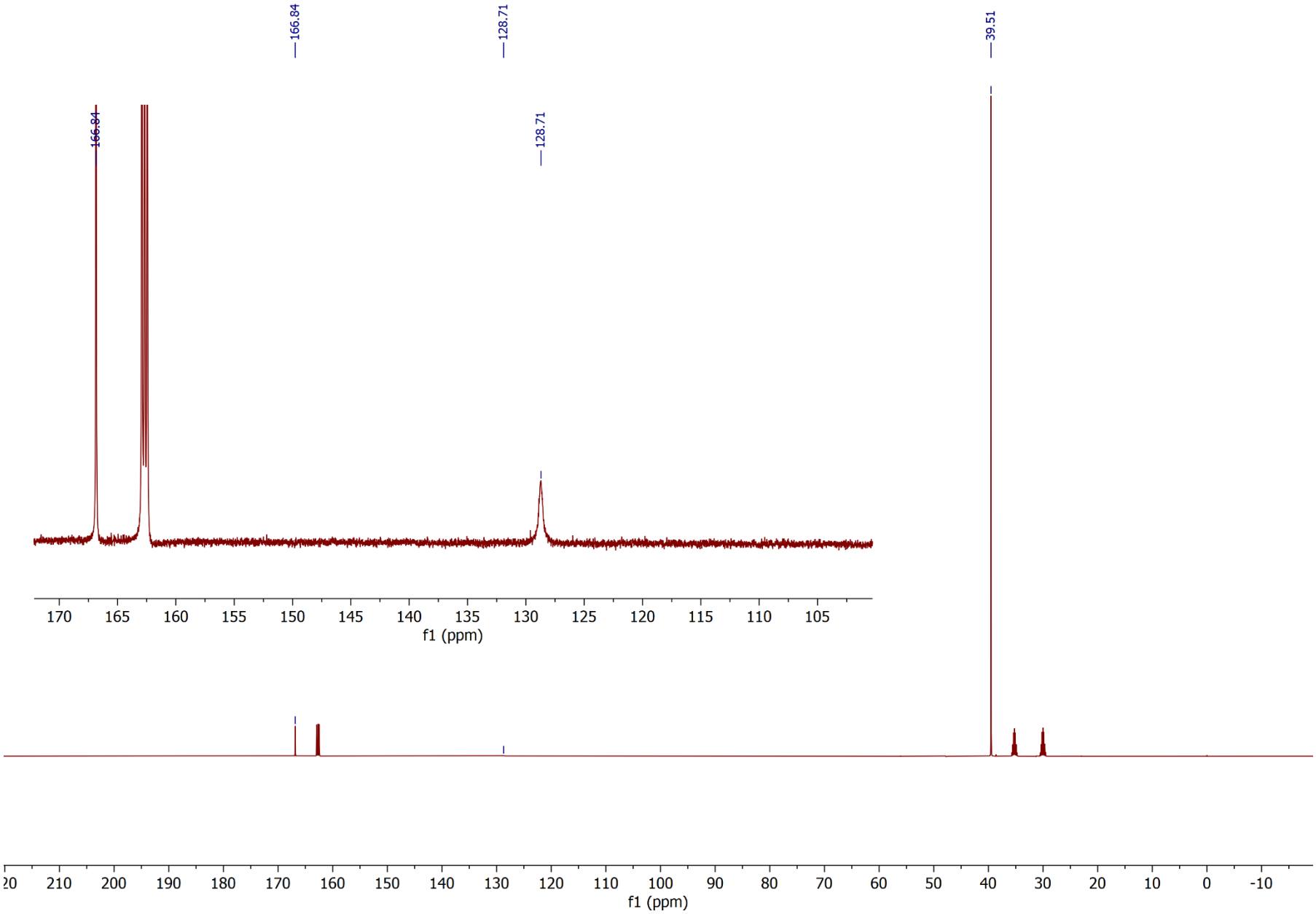

Figure S20. $^{13}C\{^{1}H\}$ spectra (125.8 MHz) of TMG in d_7-DMF under CO_2 at 0°C.

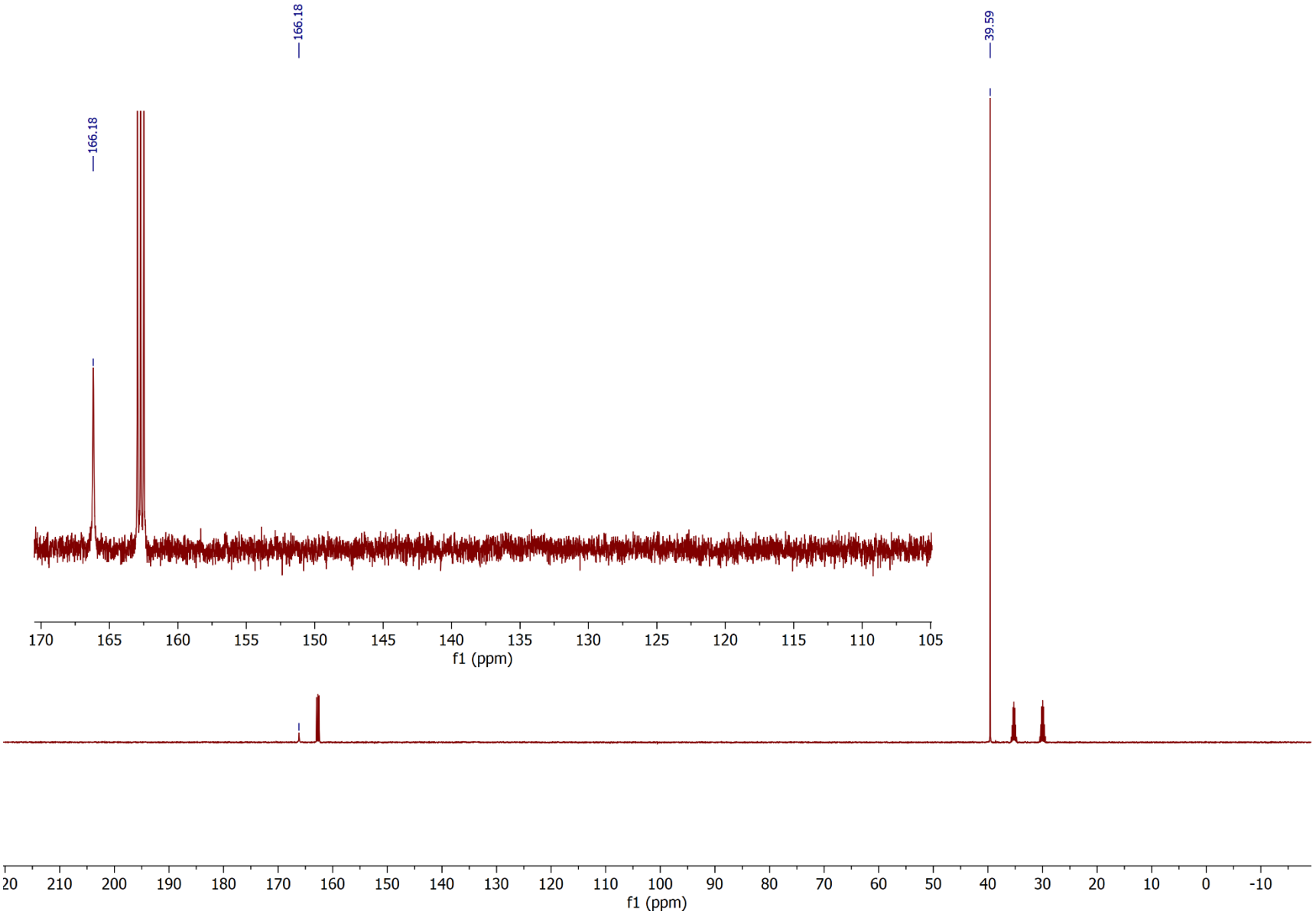

Figure S21. $^{13}C\{^{1}H\}$ spectra (125.8 MHz) of TMG in d_7-DMF under CO_2 at -10°C.

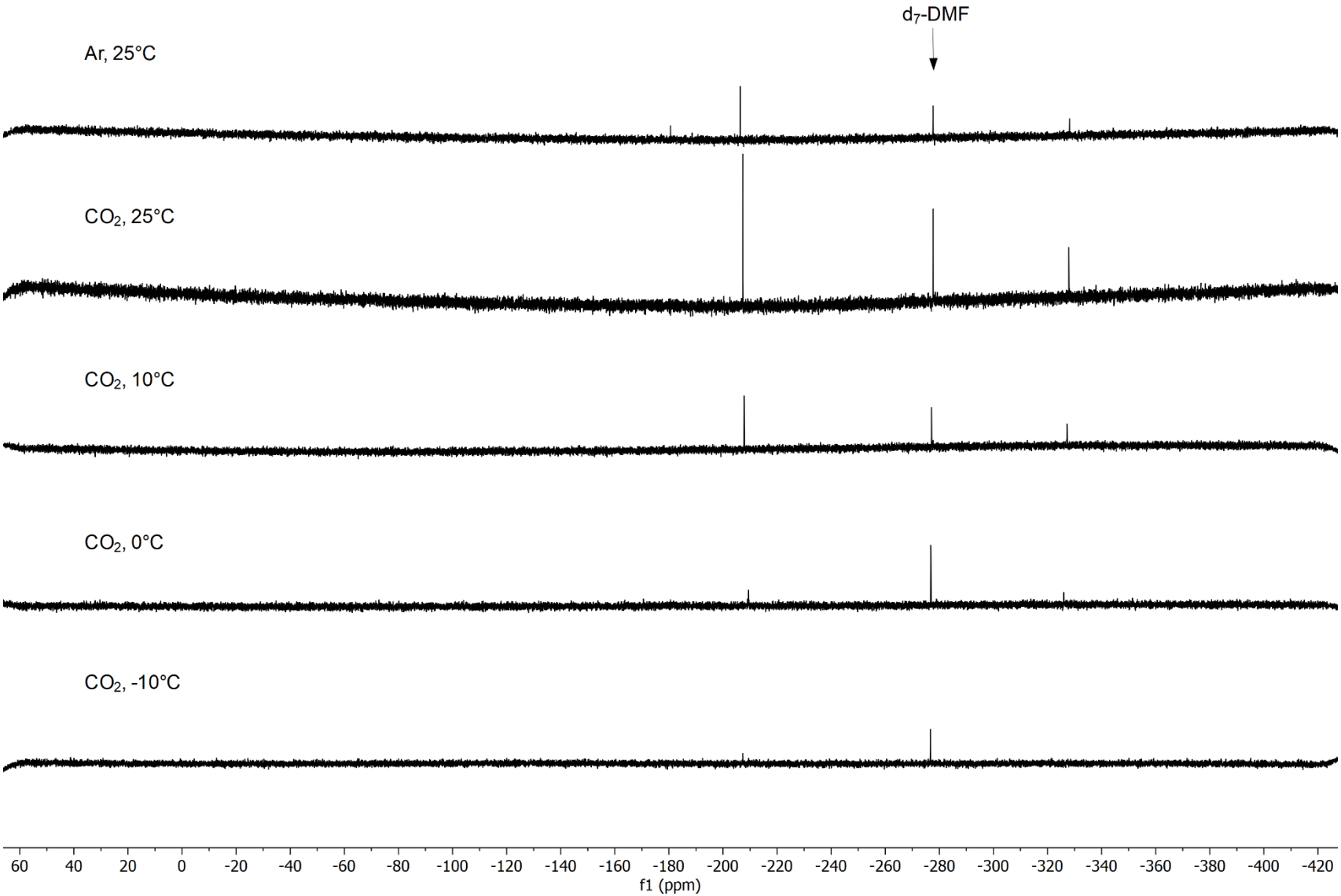

Figure S22. Stacked ^{15}N (^{1}H-coupled) spectra (50.7 MHz) of TMG in d_7-DMF. Signal of d_7-DMF at -277.67 ppm under CO_2 or argon at 25°C.

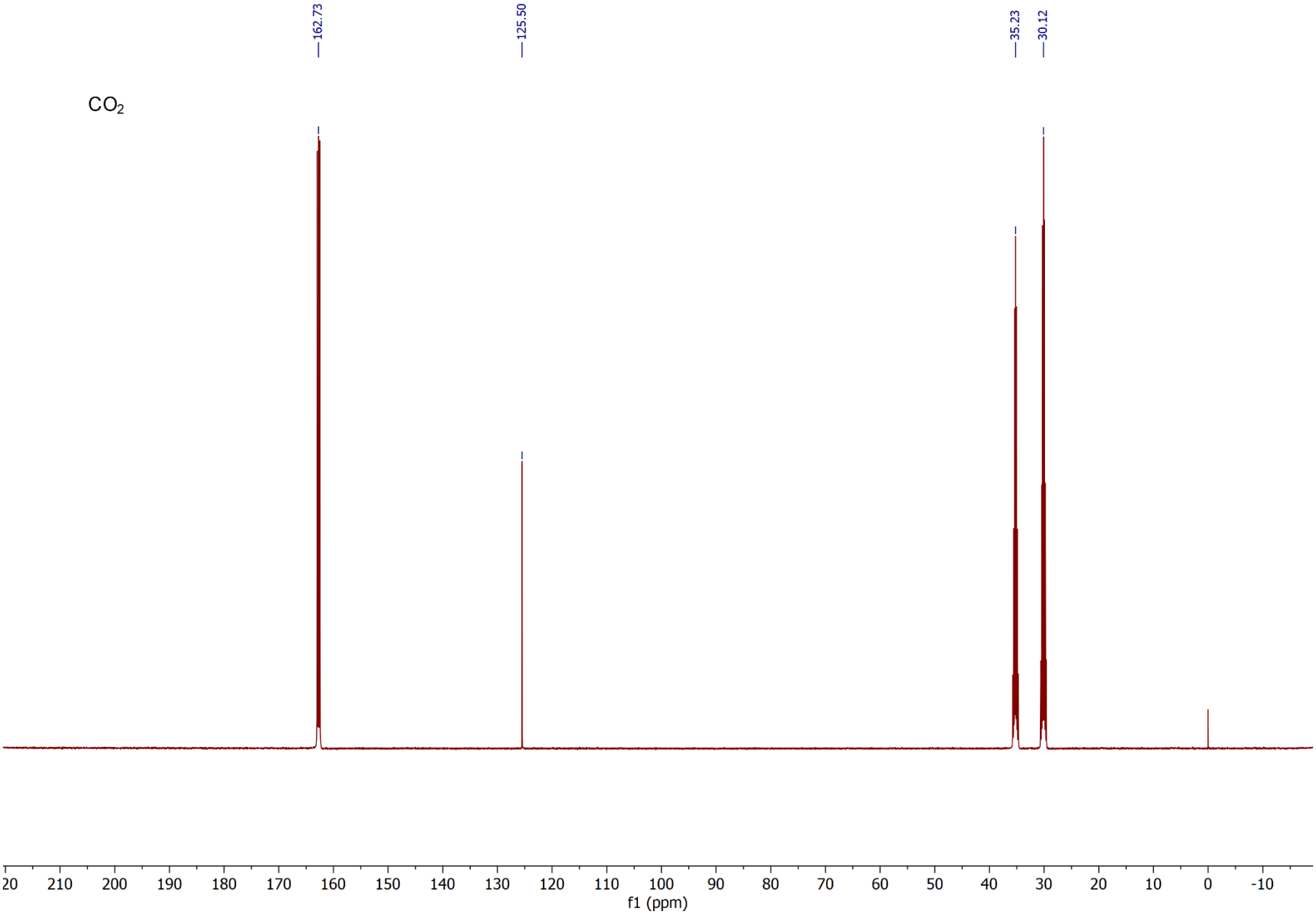

Figure S23. $^{13}C\{^{1}H\}$ NMR (125.8 MHz) of free CO_2 (1 atm) in d_7-DMF at 25°C.

10. In situ NMR Studies of DBN

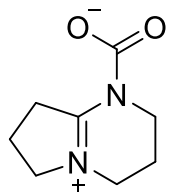

In-situ NMR studies of DBN in d_6-DMSO were performed as described in section 2. Spectroscopic data (including chemical shift of N-**C**O_2^-) is consistent with a previous study performed in CD_3CN.[19] However, DBN seems to be unstable under CO_2, because the clear solution turns brown during the overnight NMR experiment (ca 15 hour $^{13}C\{^1H\}$). The impurities are visible in ^1H and $^{13}C\{^1H\}$ spectra, but no further effort was made to characterize them.

Under argon:

^{1}H NMR (500 MHz, d_6-DMSO, 25 °C): δ 3.17 (2H, t, J = 6.8 Hz), 3.11 (2H, m, overlap), 3.10 (2H, t, J = 6.1 Hz, overlap), 2.22 (2H, t, J = 7.7 Hz), 1.80 (2H, p, J = 7.5 Hz), 1.63 (2H, p, J = 5.8 Hz)

$^{13}C\{^1H\}$ NMR (125.8 MHz, d_6-DMSO, 25 °C): δ 158.9 (**C**=N), 50.6 (**C**H_2CN), 43.4 (**C**H_2CN), 42.5 (**C**H_2CN), 30.4 (**C**H_2), 20.7 (**C**H_2), 19.2 (**C**H_2)

Under CO_2:

^{1}H NMR (500 MHz, d_6-DMSO, 25 °C): δ 3.33 (2H, t, J = 7.1 Hz), 3.28 (2H, t, J = 5.7 Hz), 3.19 (2H, t, J = 6.0 Hz), 2.62 (2H, t, J = 7.9 Hz), 1.86 (2H, p, J = 7.6 Hz), 1.73 (2H, p, J = 5.8 Hz)

$^{13}C\{^1H\}$ NMR (125.8 MHz, d_6-DMSO, 25 °C): δ 161.1 (**C**=N), 136.3 (N-**C**O_2^-), 51.4 (**C**H_2CN), 42.7 (**C**H_2CN), 42.5 (**C**H_2CN), 31.3 (**C**H_2), 20.0 (**C**H_2), 18.9 (**C**H_2)

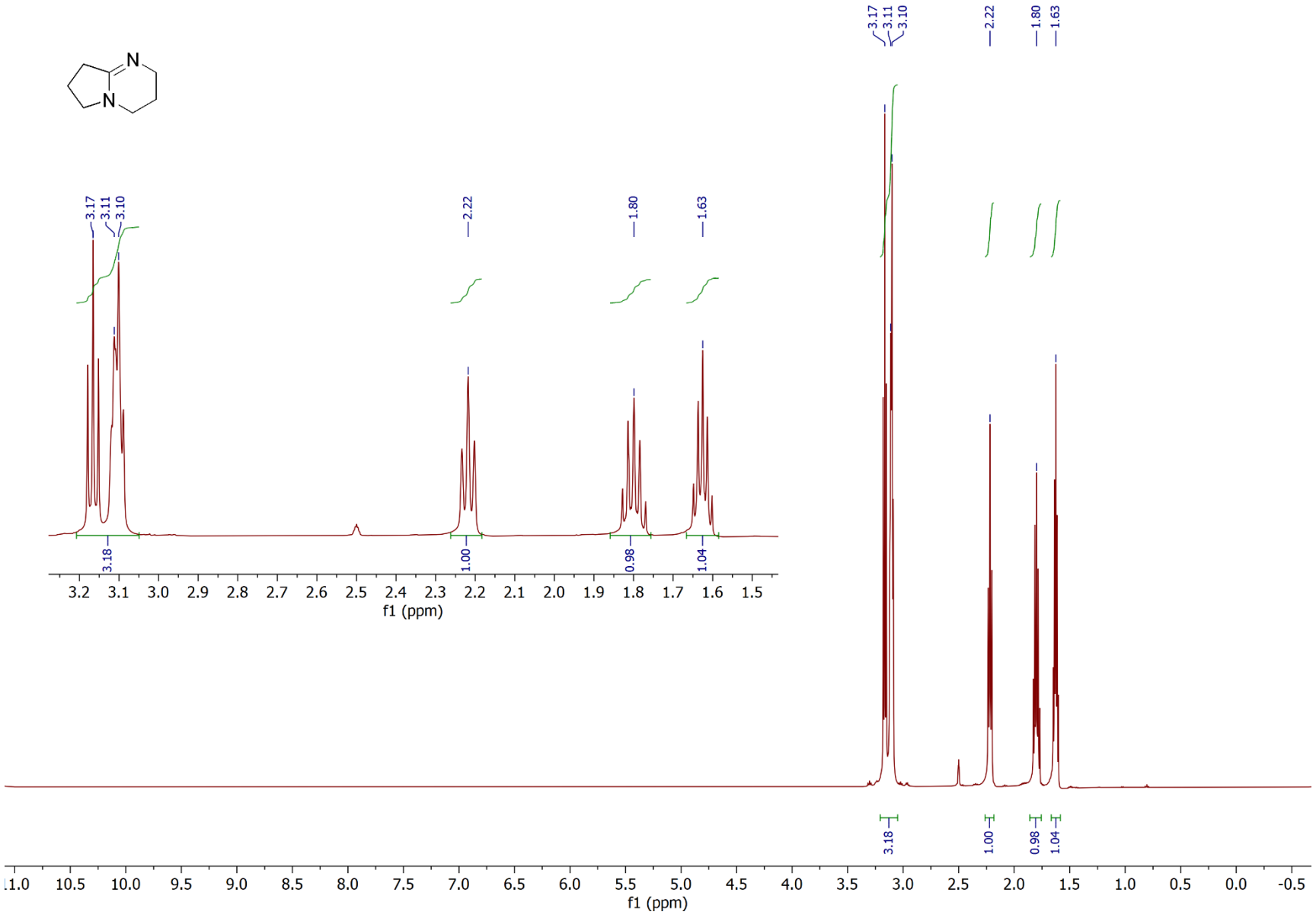

Figure S24. ^{1}H NMR spectra (500 MHz, d_6-DMSO, 25 °C) of DBN under Ar.

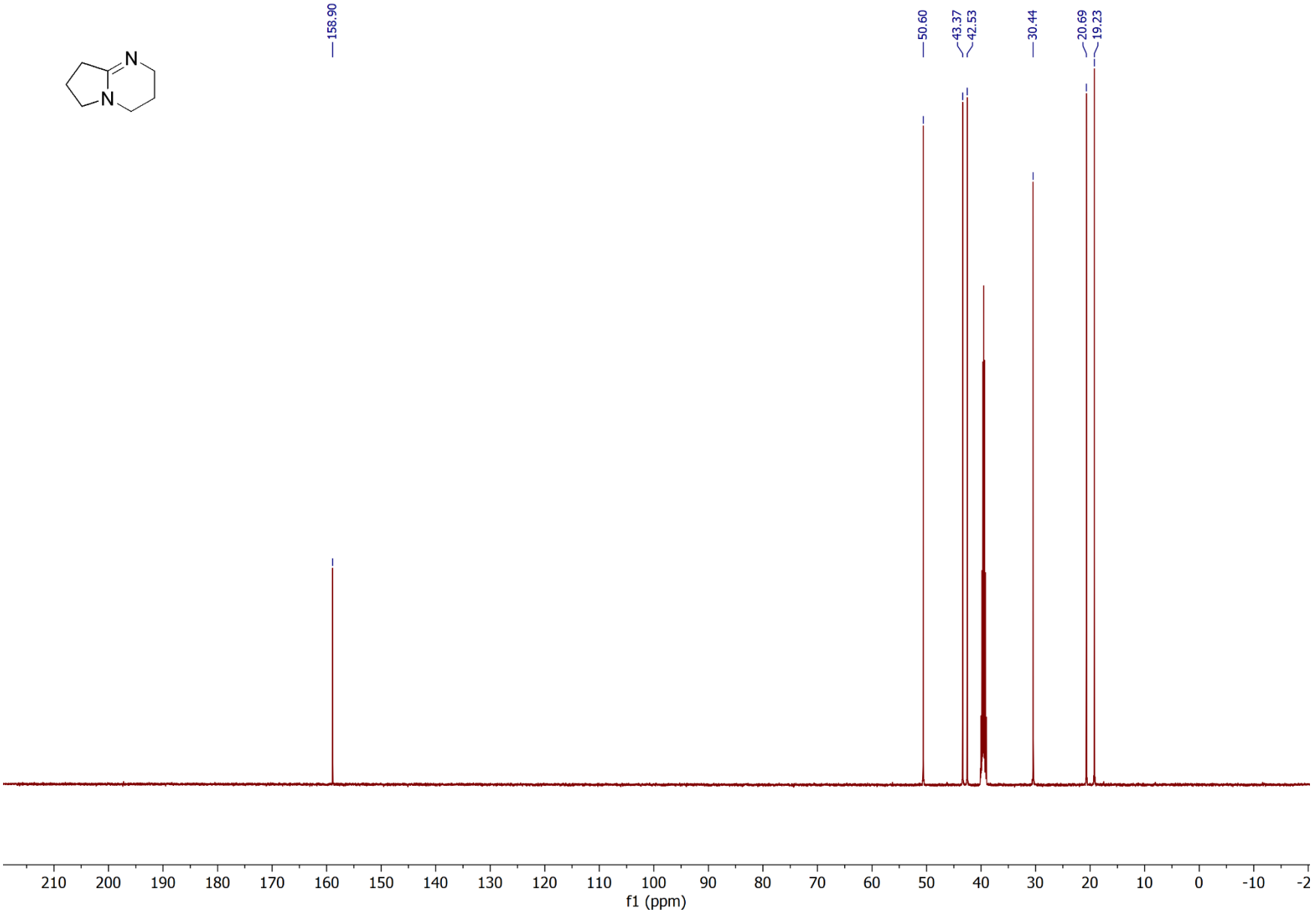

Figure S25. $^{13}C\{^{1}H\}$ NMR spectra (125.8 MHz, d_6-DMSO, 25 °C) of DBN under Ar.

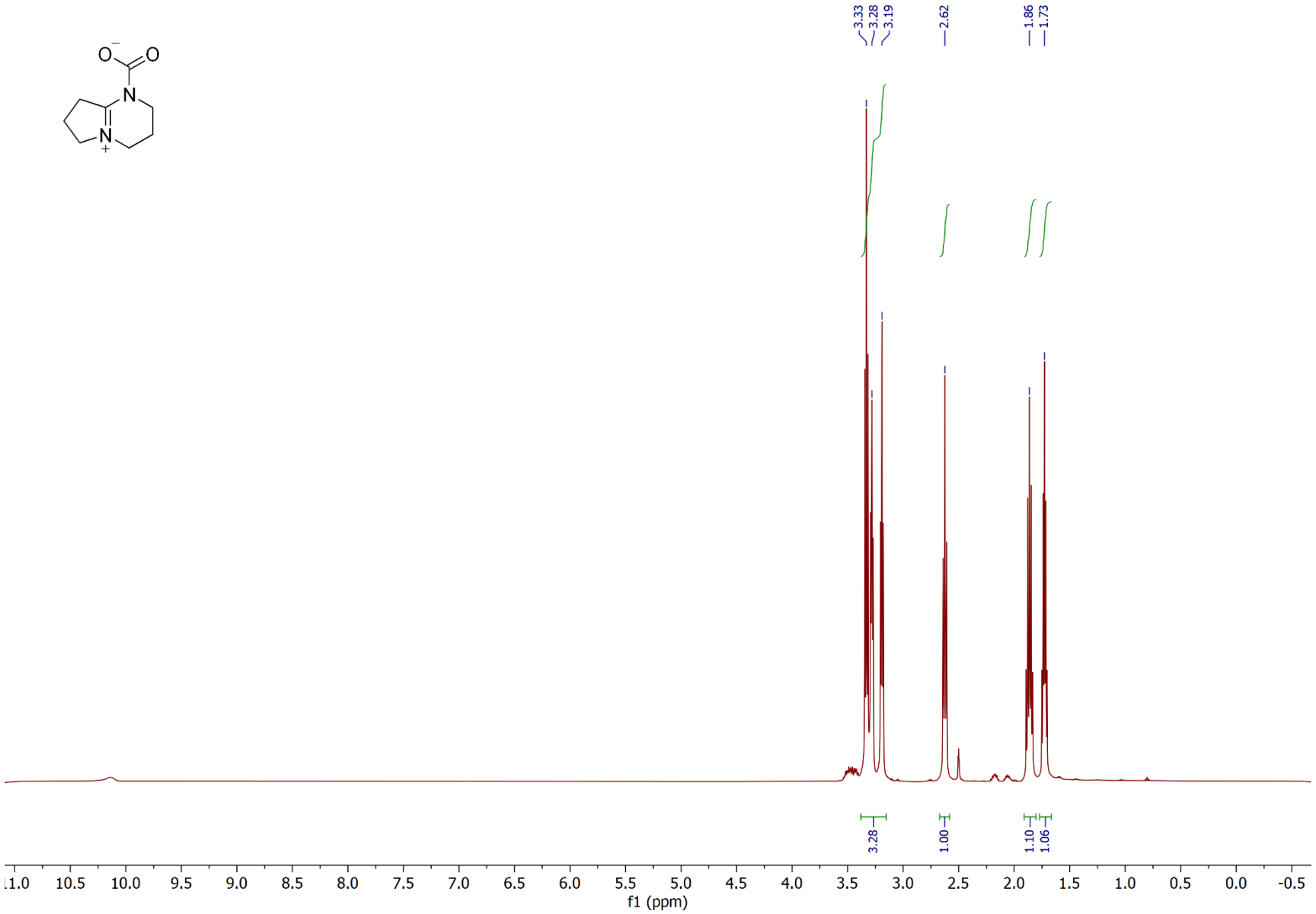

Figure S26. ^{1}H NMR spectra (500 MHz, d_6-DMSO, 25 °C) of DBN under CO_2.

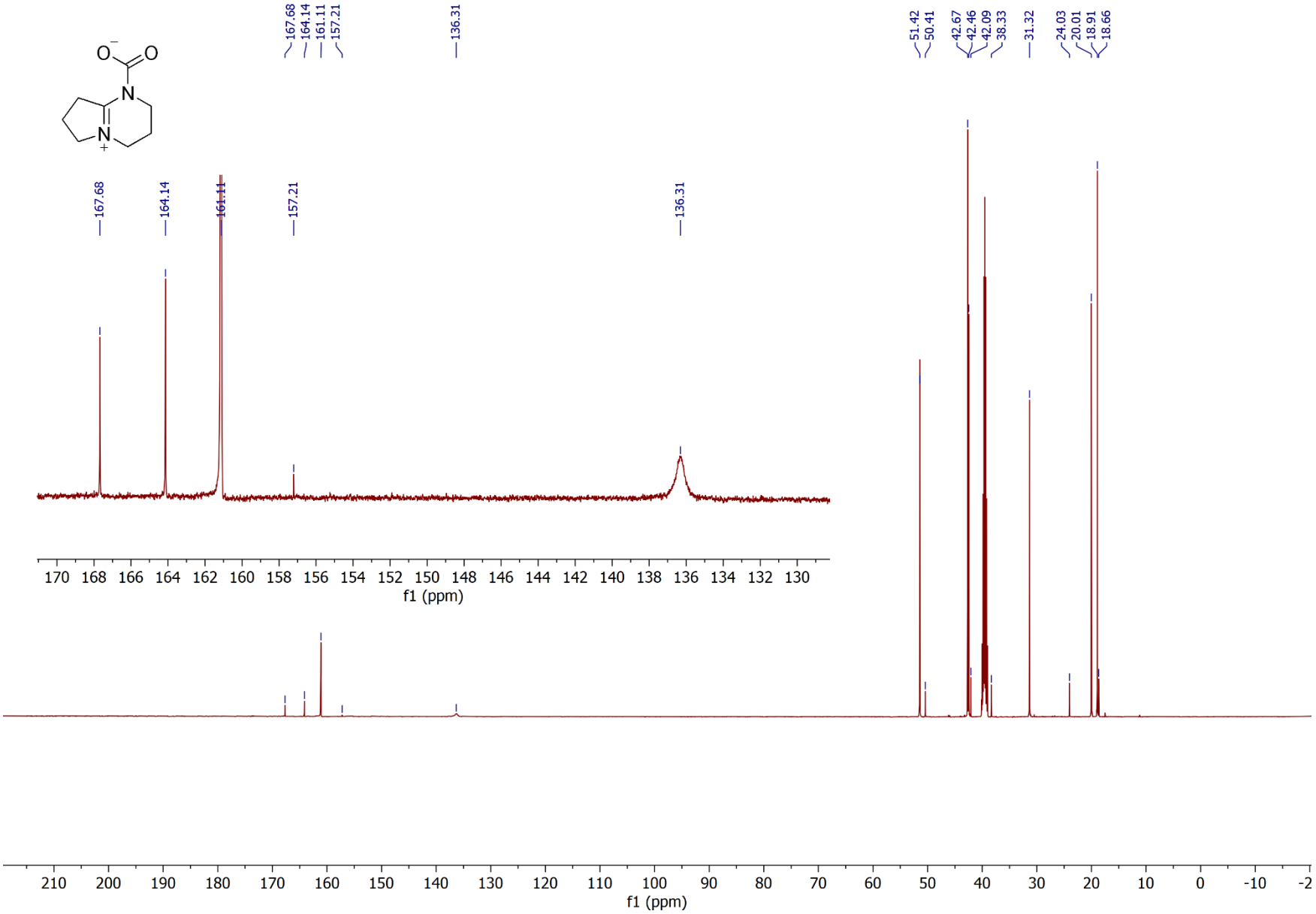

Figure S27. $^{13}C\{^{1}H\}$ NMR spectra (125.8 MHz, d_6-DMSO, 25 °C) of DBN under CO_2.

11. In situ NMR Studies of DBU

In-situ NMR studies of DBU in d_7-DMF were performed as described in section 2, except an acetone/N_2 bath (-95°C) was used to freeze the solution. The mixture of DBU and d_7-DMF freezes at ca -80°C.

For a graphical summary of variable-temperature NMR spectra of DBU, please see **Figure S28**. Previous NMR studies of DBU in $CDCl_3$[20] or CD_3CN[19] have reported no change in ^1H or $^{13}C\{^1H\}$ spectra when CO_2 is applied. Likewise, in our case (d_7-DMF), no obvious change occurs in ^1H or $^{13}C\{^1H\}$ spectra of DBU at 25°C when CO_2 is applied (**Tables S6** and **S7**). However, a ***broad*** signal at 125.6 ppm appears, similar in shape and chemical shift to the carboxylate of TMG–CO_2 (125.9 ppm).

At 25°C, the ***broad*** carboxylate signal of DBU is a characteristic sign of zwitterion formation, because confirmed zwitterions TMG, DBN and various NHI-compounds (for examples, see SI of ref[19]) produce a similar ***broad*** signal. Note that free CO_2 in d_7-DMF appears as a ***sharp*** signal at 125.5 ppm (**Figure S23**). Moreover, 4-nitroaniline (without superbase) exhibits free CO_2 as a ***sharp*** signal. The same ***sharp*** signal is observed when 4-nitroaniline is in the presence of DIPEA (no carboxylation, Table 1, entry 3 in manuscript). From this, we conclude the shape of the appearing signal (under CO_2) is indicative of solution behavior. Systems in rapid equilibrium of carboxylation-decarboxylation produce a ***broad*** $^{13}C\{^1H\}$ signal (carboxylate), whereas unreactive systems produce a ***sharp*** $^{13}C\{^1H\}$ signal (free CO_2). Note that unreactive does not mean inherently inert, as the employed conditions might affect reactivity. For example, 4-nitroaniline is activated for carboxylation by the addition of a superbase.

One reviewer suggested the observed broad signal could originate from an impurity, such as H_2O or D_2O. To exclude the possibility of moisture contamination, we prepared two control samples, one with added H_2O (0.5 equiv to DBU, 0.25 mmol), and a second with trace H_2O (non-dried DBU). After applying CO_2, both control samples contain a white precipitate, which is absent from an anhydrous sample (**Figure S29**). The sample containing trace H_2O was suitable for NMR analysis (we could not shim the other due to large amounts of precipitate). However, even a long $^{13}C\{^1H\}$ NMR experiment (ca 15h) failed to detect any bicarbonate (ca 158 ppm). We conclude DBU bicarbonate salt is very poorly soluble in d_7-DMF, and is highly unlikely to cause the broad signal at 125.6 ppm at 25°C. Note that any TMG–CO_2 samples prepared using the same CO_2-applying method also do not show the presence of bicarbonate (**Figures S19-S21**).

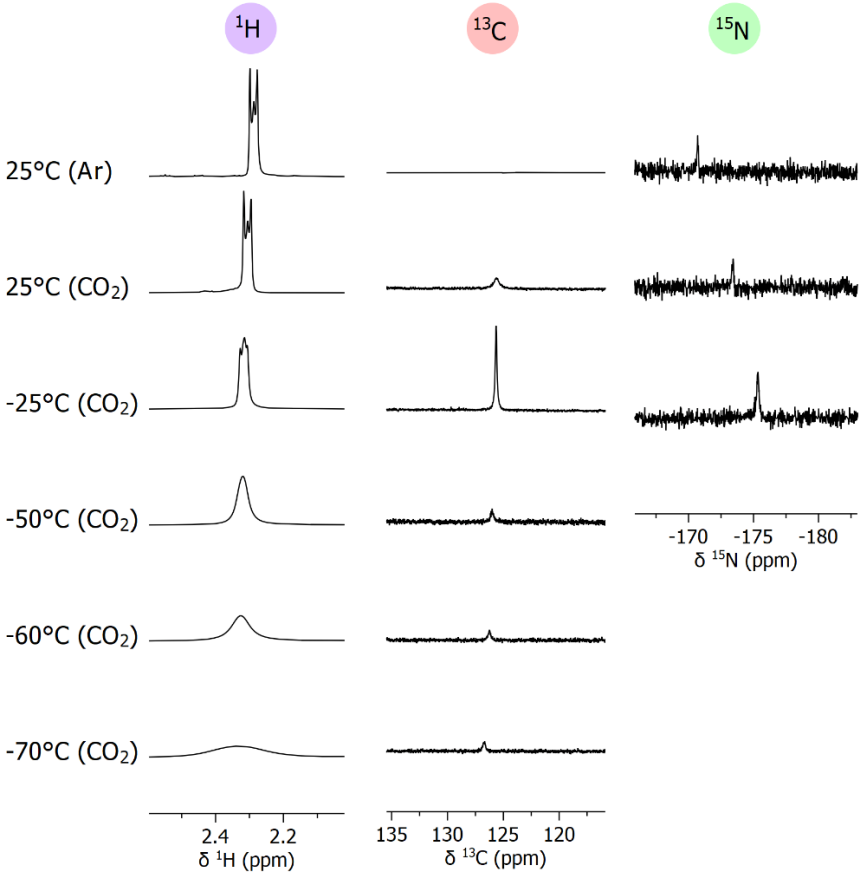

Figure S28. Variable-temperature NMR spectra (selected regions) of in situ generated zwitterion DBU–CO_2 in d_7-DMF.

When temperature is lowered, the broad DBU–carboxylate moves downfield from 125.6 ppm at 25°C, eventually reaching 126.7 ppm at -70°C (**Figure S30**). As control experiments, we measured free CO_2 (no DBU present) at -50°C and -60°C (**Figure S31** and **S32**). Free CO_2 retains the sharp signal shape at these low temperatures, and the chemical shift is largely the same (125.50 ppm at 25°C, 125.53 ppm at -60°C). These experiments demonstrate that the broad carboxylate originates from CO_2 reacting with DBU.

Interestingly, under CO_2, DBU carbons C-6, C-7, and C-9 have a decreased $^{13}C\{^1H\}$ NMR signal intensity of as a function of temperature (**Figure S33** and **S34**). The decrease in intensity is particularly evident at -70°C (**Figure S34**). As a control, we measured DBU under argon in d_7-DMF. There was no noticeable decrease in signal intensity, as all DBU carbons had roughly equal intensities (**Figure S35**). Consequently, the decrease in intensity is not an inherent property of DBU, as the phenomenon occurs only under CO_2. From computed results (section 4.7) we would expect DBU carbons C-6, C-7, and C-9 to be the most affected if there is formation of zwitterionic DBU–CO_2. Bridgehead carbon C-7 should be affected by N-8 coordinating to CO_2, while adjacent methylenes C-6 and C-9 stabilize the forming carboxylate. In this regard, the observed decrease in $^{13}C\{^1H\}$ NMR signal intensity C-6, C-7, and C-9 suggests an increasing concentration of DBU–CO_2 at lower temperatures, which is supported by computational results (section 4.6). **Figures S36-S38** are provided to allow direct comparison of DBU under argon or CO_2 at low temperatures.

DBU under CO_2 displays increasing line broadening of ^1H NMR spectra when temperature is decreased (**Figure S39** and **S40**). Similar line broadening is also observed for a control sample under argon (**Figure S41** and **S42**), indicating most of the line broadening is because of a reduced rate of ring flip at lower temperatures. However, more importantly, differences between the CO_2 sample and argon sample are observed at -70°C (**Figure S43** and **S44**). At this temperature, the sample under CO_2 displays much broader 1H signals of DBU. Particularly striking is that H-6 is a single peak under CO_2, but argon H-6 is split in two. Likewise, H-10 is far better separated from H-3, H-4 and H-5 under argon. Note that small signals are emerging at 3.50 and 2.91, but these are much sharper under argon. An exception to the general behavior appears to be H-9, which is sharper under CO_2. Differences are negligible at -50°C and -60°C (**Figure S45** and **S46**). Overall, the broader signals under CO_2 suggest there is an equilibrium reaction ongoing, which is absent under argon, thereby supporting the formation of DBU–CO_2.

The ^1H and $^{13}C\{^1H\}$ chemical shifts of DBU under CO_2 or argon spare tabulated in **Table S6** and **S7**. Note that under CO_2, the largest $^{13}C\{^1H\}$ changes (compared to Ar, 25°C) are observed for carbons C-6 and C-9, each with a 0.5 ppm upfield shift at -70°C. As temperature is decreased, bridgehead carbon C-7 moves upfield (160.3 ppm, -25°C), and then downfield (160.8 ppm, -70°C). This behavior is absent from the sample under argon. Note that carbons C-6, C-7, and C-9 are known to be more sensitive to protonation of DBU, displaying a larger change in chemical shift compared to other carbons in the structure of DBU.[20,21]

Although the changes for C-6, C-7 and C-9 are modest in our case (0.5 ppm), they are larger than what is observed for the other carbons (0-0.3 ppm). We interpret this fact as evidence for partial quaternization of N-8, although the equilibrium must be unfavorable even at -70°C, since the changes are modest. The lower temperature significantly sharpens the DBU carboxylate signal, as was observed for TMG–CO_2 (**Figure 4** in manuscript). The DBU carboxylate is revealed in a few scans, while at 25°C many hours of scans are required.

Additional support for formation of a DBU–CO_2 zwitterion is obtained from ^{15}N NMR experiments (**Table S8, Figure S47** and **S48**). When CO_2 is applied at 25°C, the imine-like nitrogen N-8 moves upfield by 2.7 ppm, while tertiary N-1 moves downfield by 0.9 ppm. Under similar conditions, TMG imine-like nitrogen moves upfield 1.0 ppm. Since we have confirmed the formation of TMG–CO_2, we interpret the large upfield shift of N-8 as strong evidence of DBU zwitterion formation. At lower temperatures (-25°C), N-8 has moved further upfield (total change 4.7 ppm), and N-1 further downfield (total change 1.7 ppm). These changes, particularly the large upfield shift of N-8, are a strong indicator of partial quaternization. ^{15}N NMR was not recorded at -50°C and below, because the cryogenic conditions could not be maintained long enough for adequate total acquisition time (15h or longer).

To summarize, changes in ^1H and $^{13}C\{^1H\}$ spectra upon applying CO_2 are minor at 25°C, which explains why others have excluded formation of zwitterionic DBU–CO_2.[19,20] The ***broad shape*** of the carboxylate signal at 125.6 ppm is characteristic of a zwitterion, which probably has been previously overlooked. Our low temperature experiments have revealed modest, yet clear changes in ^1H and $^{13}C\{^1H\}$ spectra, consistent with partial quaternization equilibrium. The broad DBU carboxylate is significantly sharpened at lower temperatures, consistent with behavior observed for TMG–CO_2 (**Figure 4** in manuscript). Additionally, the chemical shift of the DBU carboxylate at 25°C differs only by 0.1 ppm from free CO_2, suggesting zwitterionic DBU–CO_2 is highly unstable. At lower temperatures, the broad carboxylate clearly differs in signal shape and chemical shift from free CO_2. Assuming the difference in chemical shift between DBU carboxylate and free CO_2 is equally small in other solvents, it is likely others have mistakenly assigned DBU carboxylate as free CO_2.[19,20] Finally, analysis of ^{15}N NMR spectra provides evidence of N-8 partial quaternization, agreeing with changes in ^1H and $^{13}C\{^1H\}$ spectra, and thereby supporting formation of zwitterionic DBU–CO_2.

Table S6. ^{1}H NMR (500 MHz) data of DBU in d_7-DMF.[a]

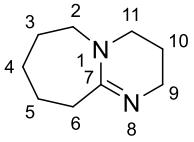

Atmosphere	T (°C)	δ H-6	δ H-10	δ H-2, H-11	δ H-9	δ H-3, H-4, H-5
Ar	25	2.29	1.68	3.18	3.13	1.51-1.60
CO_2	25	2.30	1.69	3.19	3.14	1.52-1.60
CO_2	-25	2.31	1.69	3.21	3.13	1.51-1.60
Ar	-50	2.30	1.68	3.20	3.12	1.51-1.58
CO_2	-50	2.32	1.69	3.21	3.13	1.51-1.59
Ar	-60	2.30	1.67	3.20	3.12	1.54
CO_2	-60	2.33	1.69	3.22	3.13	1.55
Ar	-70	2.22, 2.40	1.72	3.21	3.13	1.33
CO_2	-70	2.33	1.68	3.22	3.13	1.44

[a] IUPAC numeration is given for the molecular structure of DBU.

Table S7. $^{13}C\{^{1}H\}$ NMR (125.8 MHz) data of DBU in d_7-DMF.[a]

Atmosphere	T (°C)	δ C-2	δ C-3	δ C-4	δ C-5	δ C-6	δ C-7	δ C-9	δ C-10	δ C-11	δ N-CO_2^-
Ar	25	52.8	29.1	30.1	26.8	37.5	160.7	44.8	23.4	48.5	b
CO_2	25	52.8	29.1	30.1	26.8	37.3	160.6	44.6	23.3	48.5	125.6
CO_2	-25	52.6	29.0	30.1	26.8	37.2	160.3	44.4	23.2	48.4	125.6
Ar	-50	52.5	29.0	30.1	26.9	37.3	160.5	44.5	23.2	48.2	b
CO_2	-50	52.5	29.0	30.1	26.8	37.1	160.7	44.4	23.1	48.3	126.0
Ar	-60	52.4	29.0	30.1	26.9	37.3	160.5	44.5	23.2	48.2	b
CO_2	-60	52.5	28.9	30.1	26.8	37.1	160.7	44.3	23.1	48.2	126.2
Ar	-70	52.4	29.0	30.1	26.9	37.2	160.5	44.5	23.2	48.2	b
CO_2	-70	52.5	28.9	30.1	26.8	37.0	160.8	44.3	23.1	48.2	126.7

[a] See **Table S6** for IUPAC numeration. [b] Signal not observed.

Table S8. ^{15}N NMR (50.7 MHz) data of DBU in d_7-DMF.[a] Data is consistent with a previous report.[21]

Atmosphere	T (°C)	δ N-8	δ N-1
Ar	25	-170.7	-291.5[b]
CO_2	25	-173.4	-290.6[b]
CO_2	-25	-175.4	-289.8

[a] See **Table S6** for IUPAC numeration. [b] Inverse gated ^{15}N experiment.

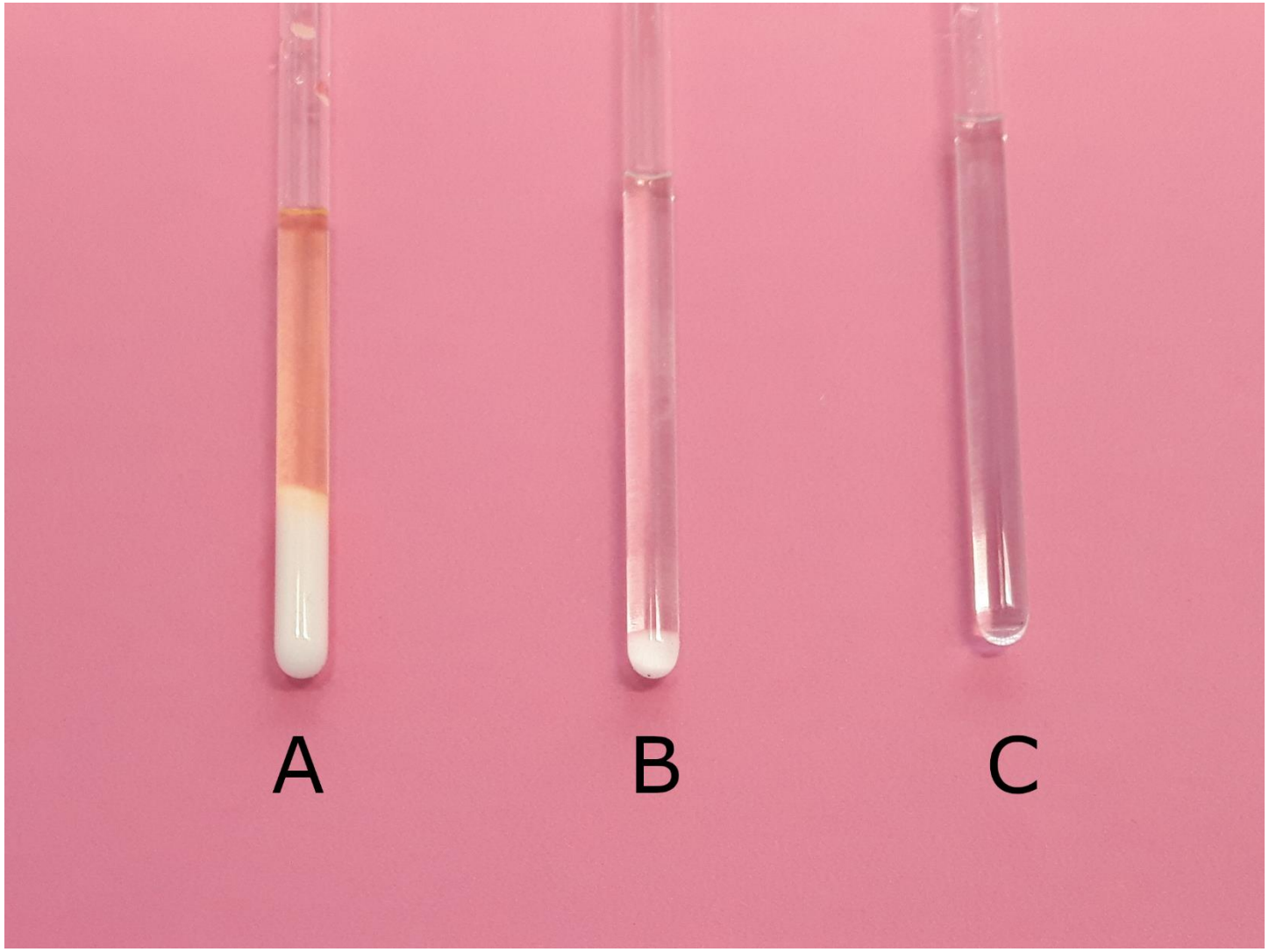

Figure S29. Samples of DBU under CO_2 in d_7-DMF with constant concentration of DBU (0.5 mmol in ca 0.6 ml d_7-DMF).

A) Sample with added H_2O (0.5 equiv to DBU, 0.25 mmol). A large amount of precipitate is formed. Discoloration occurs in a few days.

B) Sample with trace H_2O (non-dried DBU). A small amount of precipitate is visible. A long ^{13}C NMR experiment (ca 15h) failed to detect the presence of any bicarbonate (ca 158 ppm).

C) Sample prepared under anhydrous conditions remains clear.

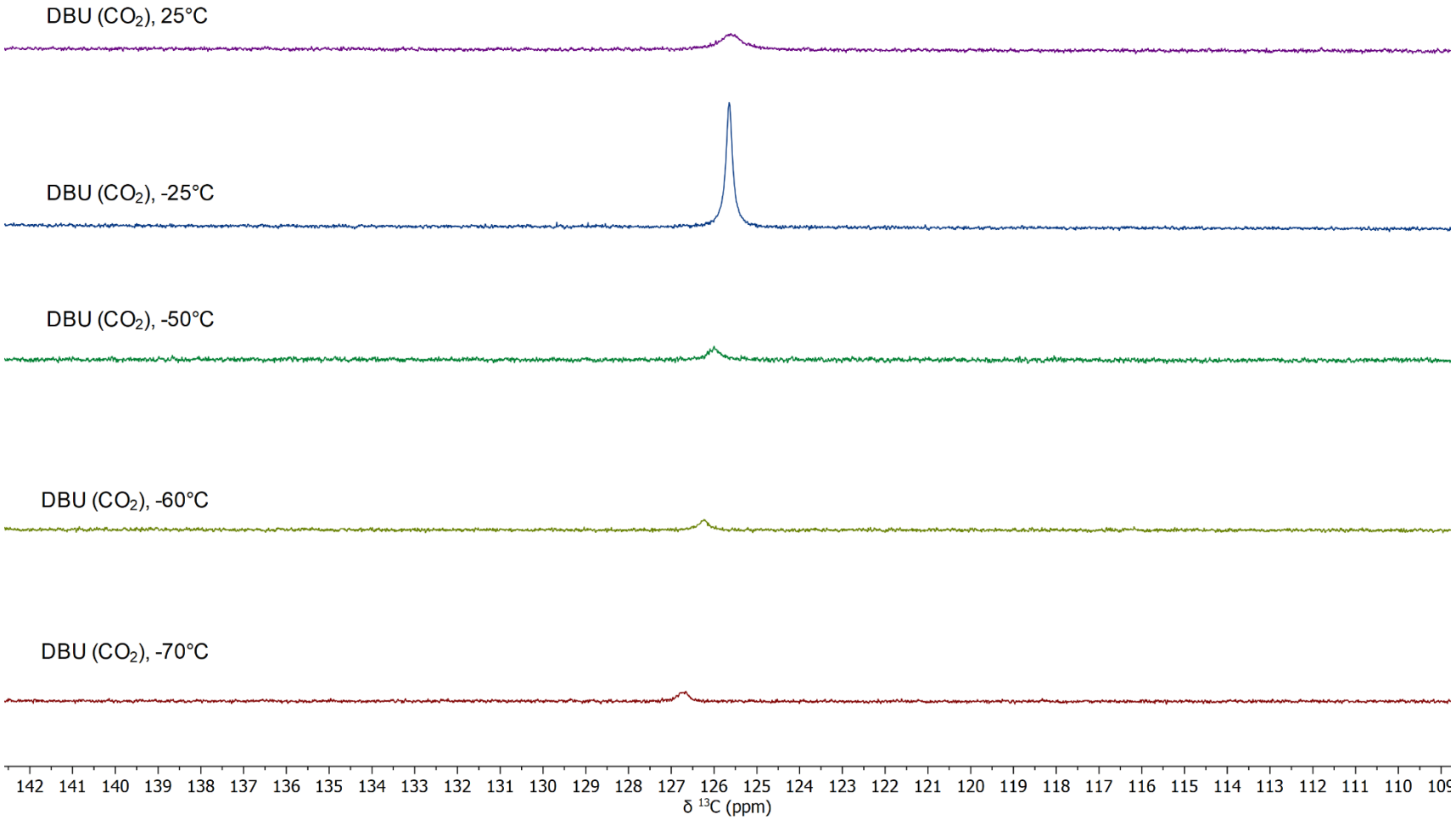

Figure S30. Stacked $^{13}C\{^{1}H\}$ spectra (500 MHz, selected region shown) of DBU under CO_2 (1 atm) in d_7-DMF. Note that experiments at 25°C and -25°C had total acquisition times of ca 24 h, while the others had ca 30 min.

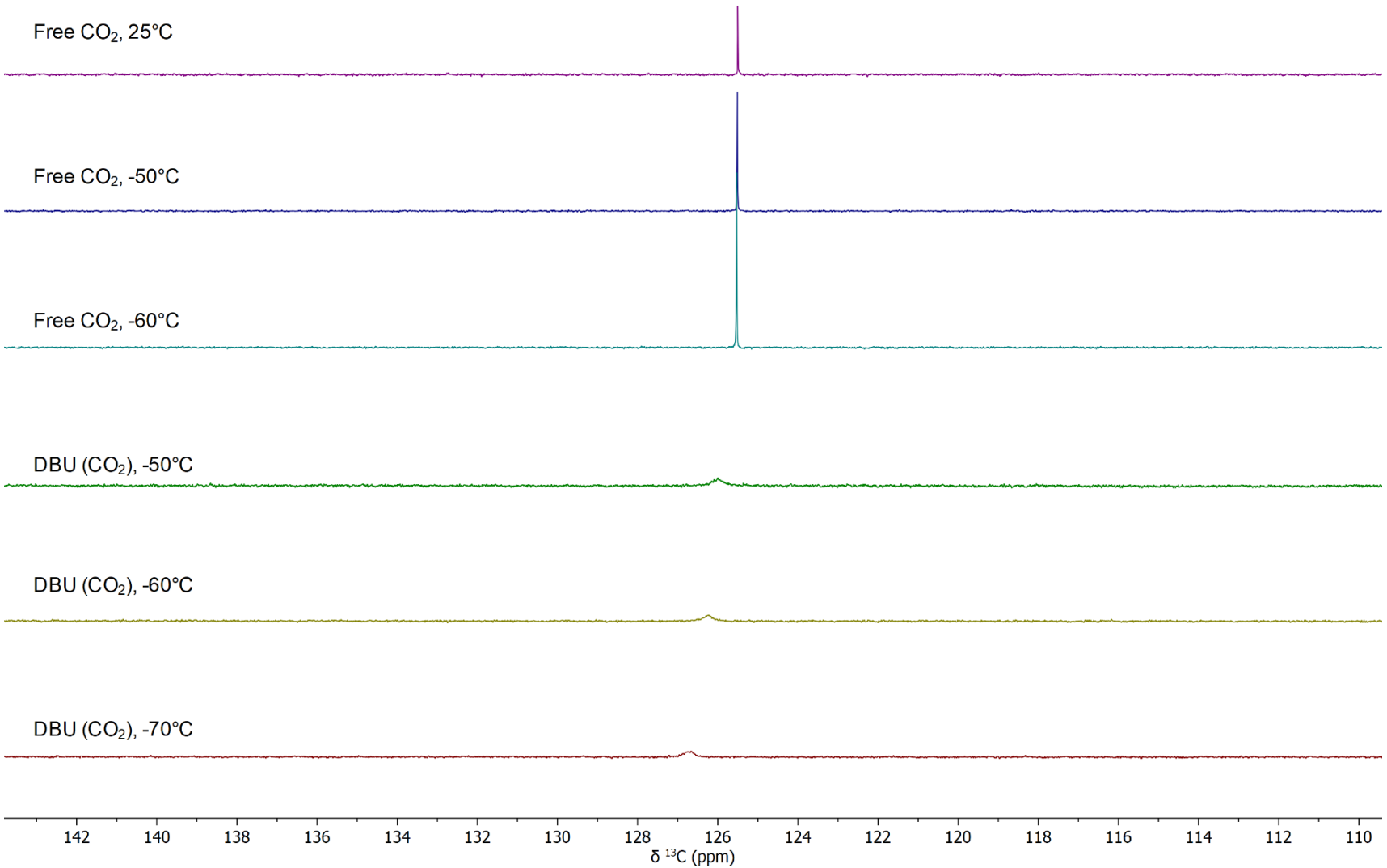

Figure S31. Stacked $^{13}C\{^1H\}$ spectra (500 MHz, selected region shown) of free CO_2 (1 atm) in d_7-DMF, and DBU under CO_2 (1 atm) in d_7-DMF.

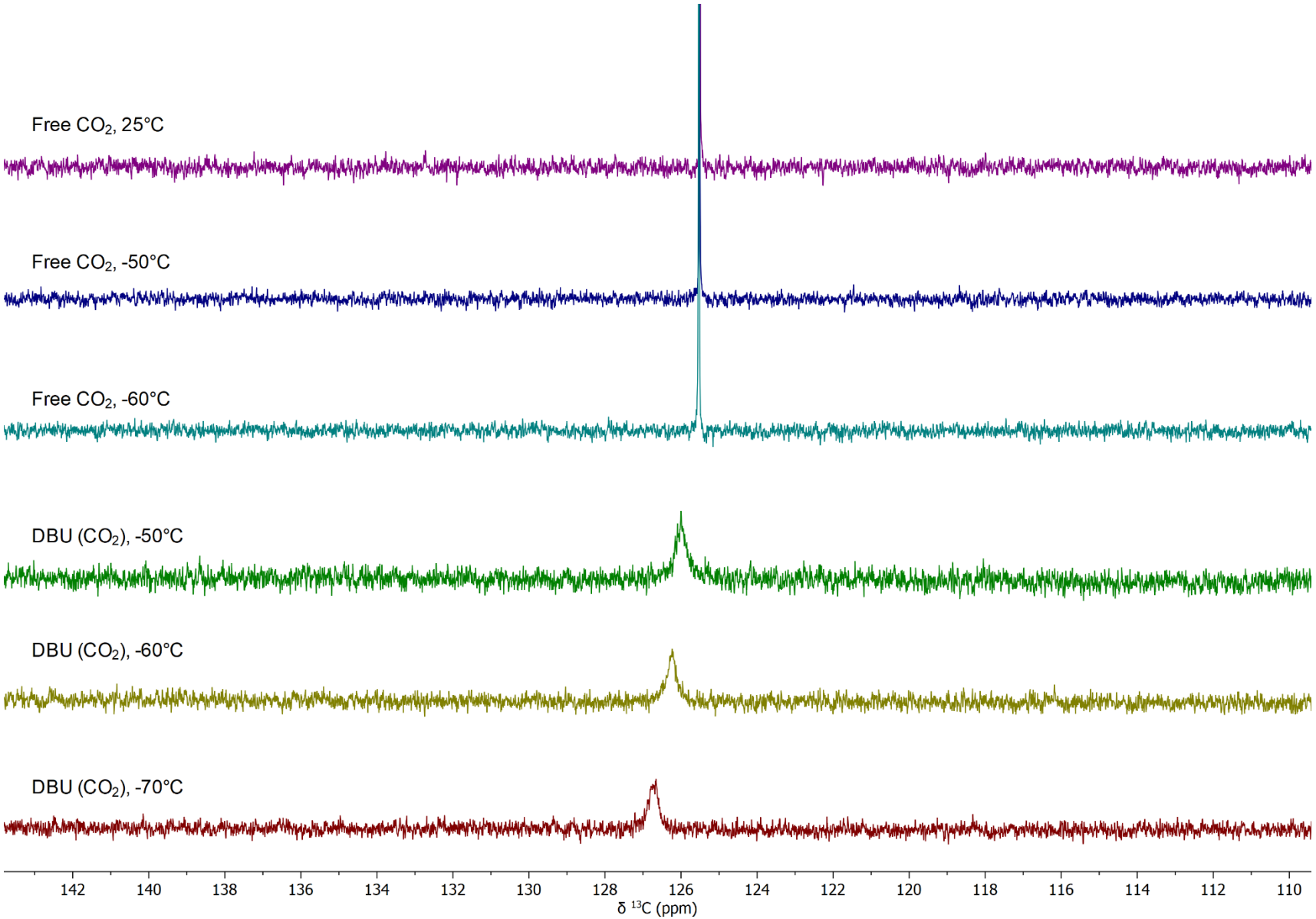

Figure S32. Stacked $^{13}C\{^1H\}$ spectra (500 MHz, selected region shown) of free CO_2 (1 atm) in d_7-DMF, and DBU under CO_2 (1 atm) in d_7-DMF. This is a close up of Figure S31.

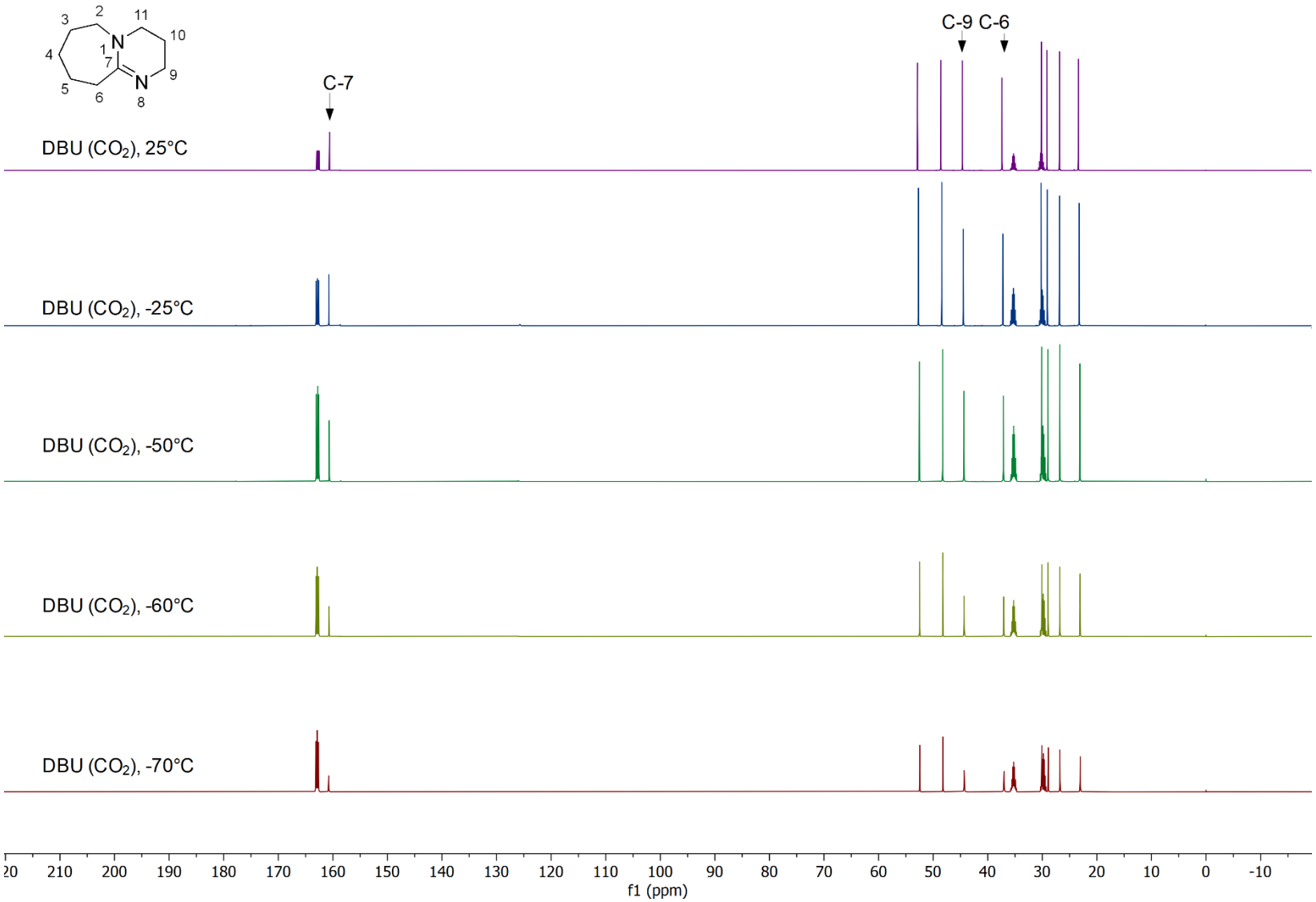

Figure S33. Stacked $^{13}C\{^1H\}$ spectra (500 MHz) of DBU under CO_2 (1 atm) in d_7-DMF. Note the reduction in signal intensity of C-6, C-7 and C-9.

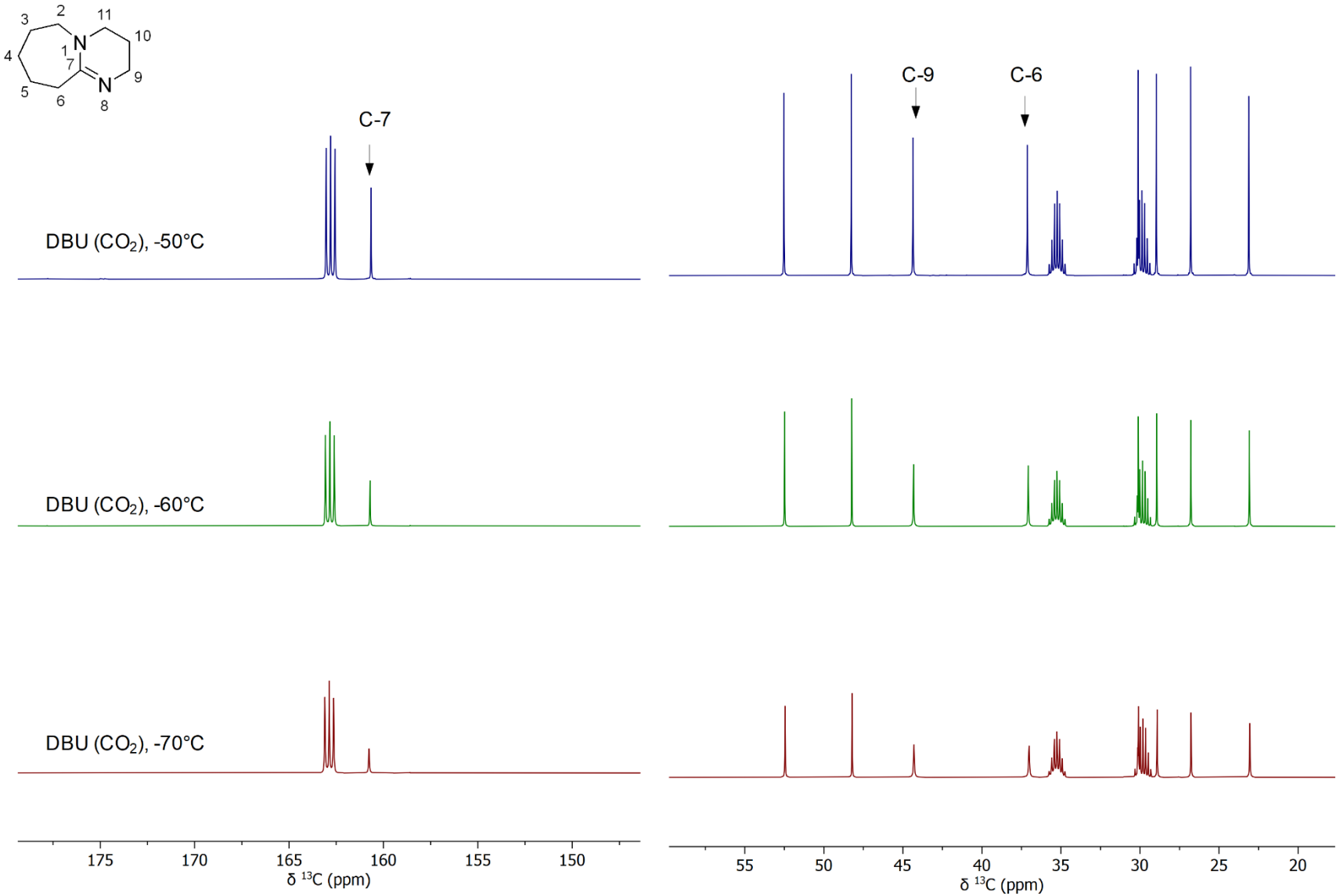

Figure S34. Stacked $^{13}C\{^1H\}$ spectra (500 MHz, selected regions shown) of DBU under CO_2 (1 atm) in d_7-DMF. Note the reduction in signal intensity of C-6, C-7 and C-9.

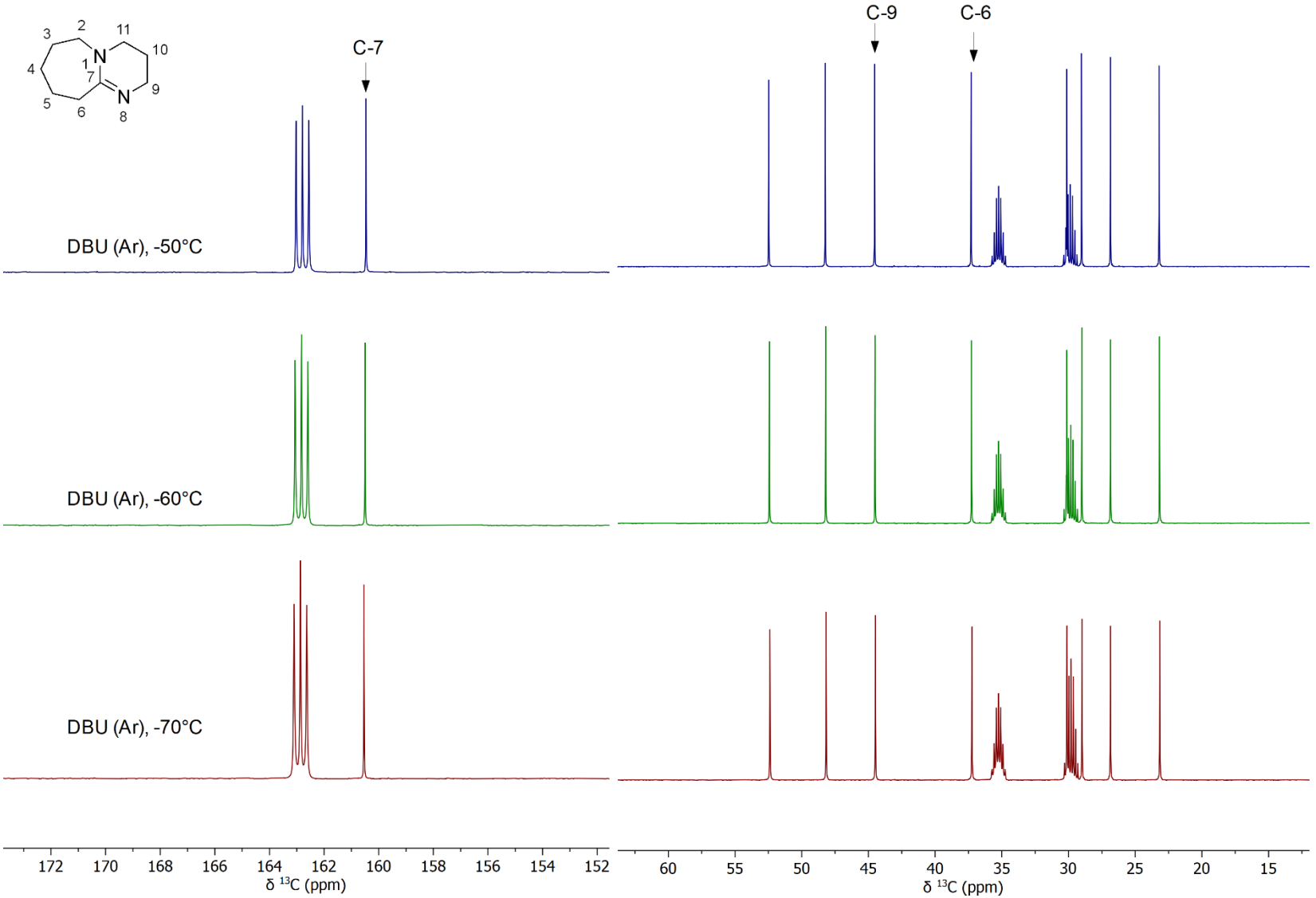

Figure S35. Stacked $^{13}C\{^{1}H\}$ spectra (500 MHz, selected regions shown) of DBU under argon (1 atm) in d_7-DMF. Note there is NO reduction in signal intensity of C-6, C-7 and C-9.

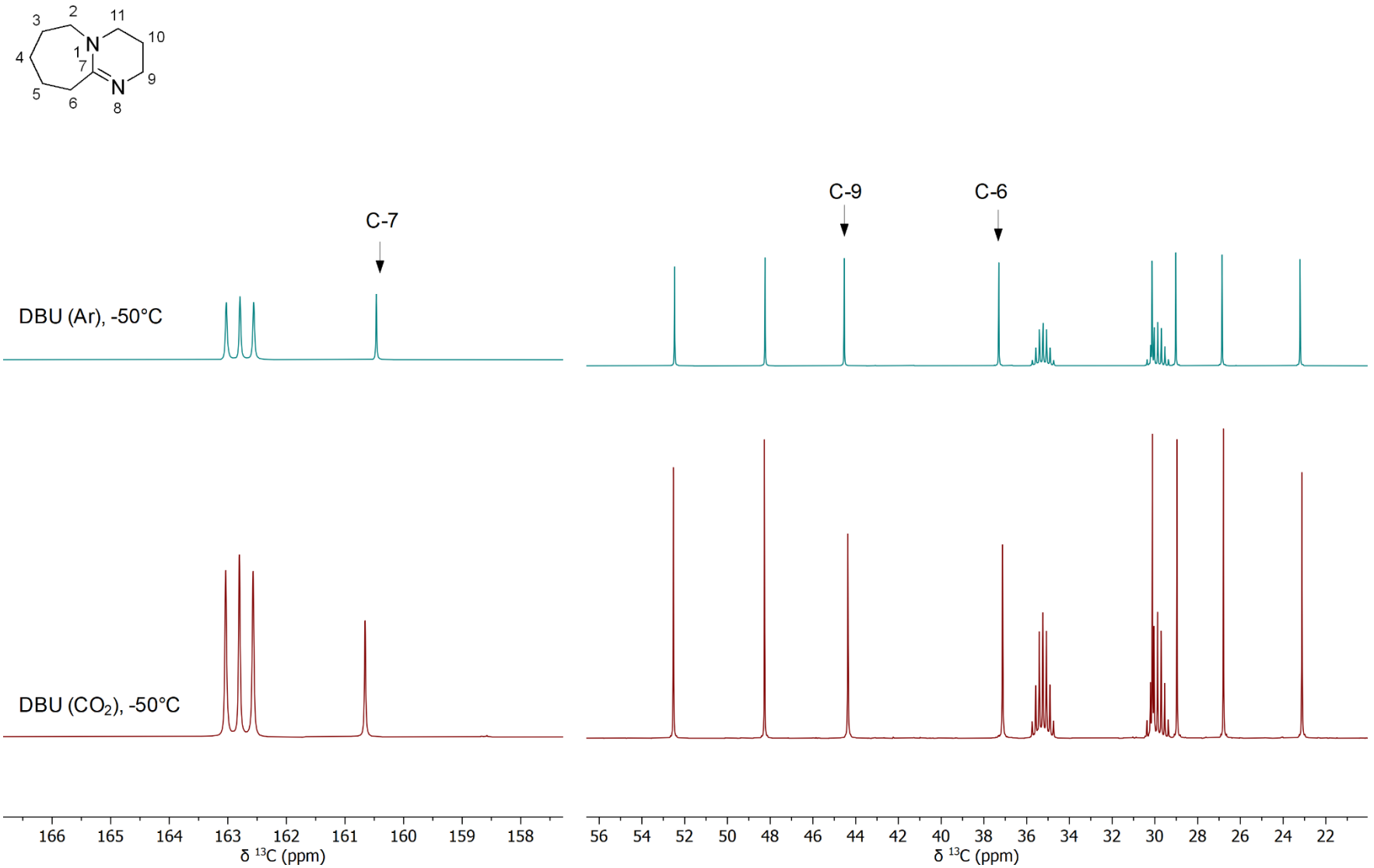

Figure S36. Stacked $^{13}C\{^{1}H\}$ spectra (500 MHz, selected regions shown) of DBU under argon or CO_2 (1 atm) in d_7-DMF.

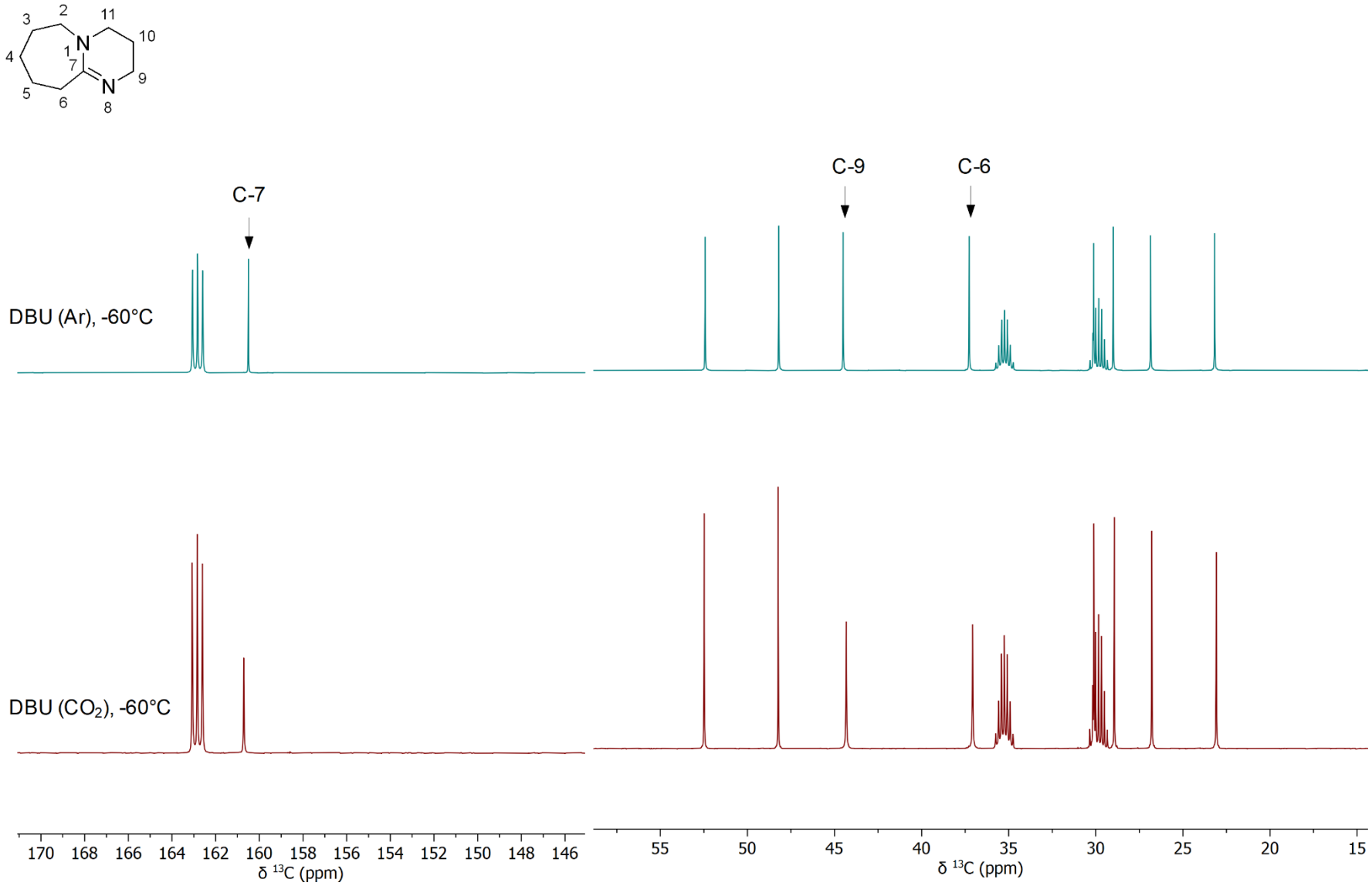

Figure S37. Stacked $^{13}C\{^{1}H\}$ spectra (500 MHz, selected regions shown) of DBU under argon or CO_2 (1 atm) in d_7-DMF.

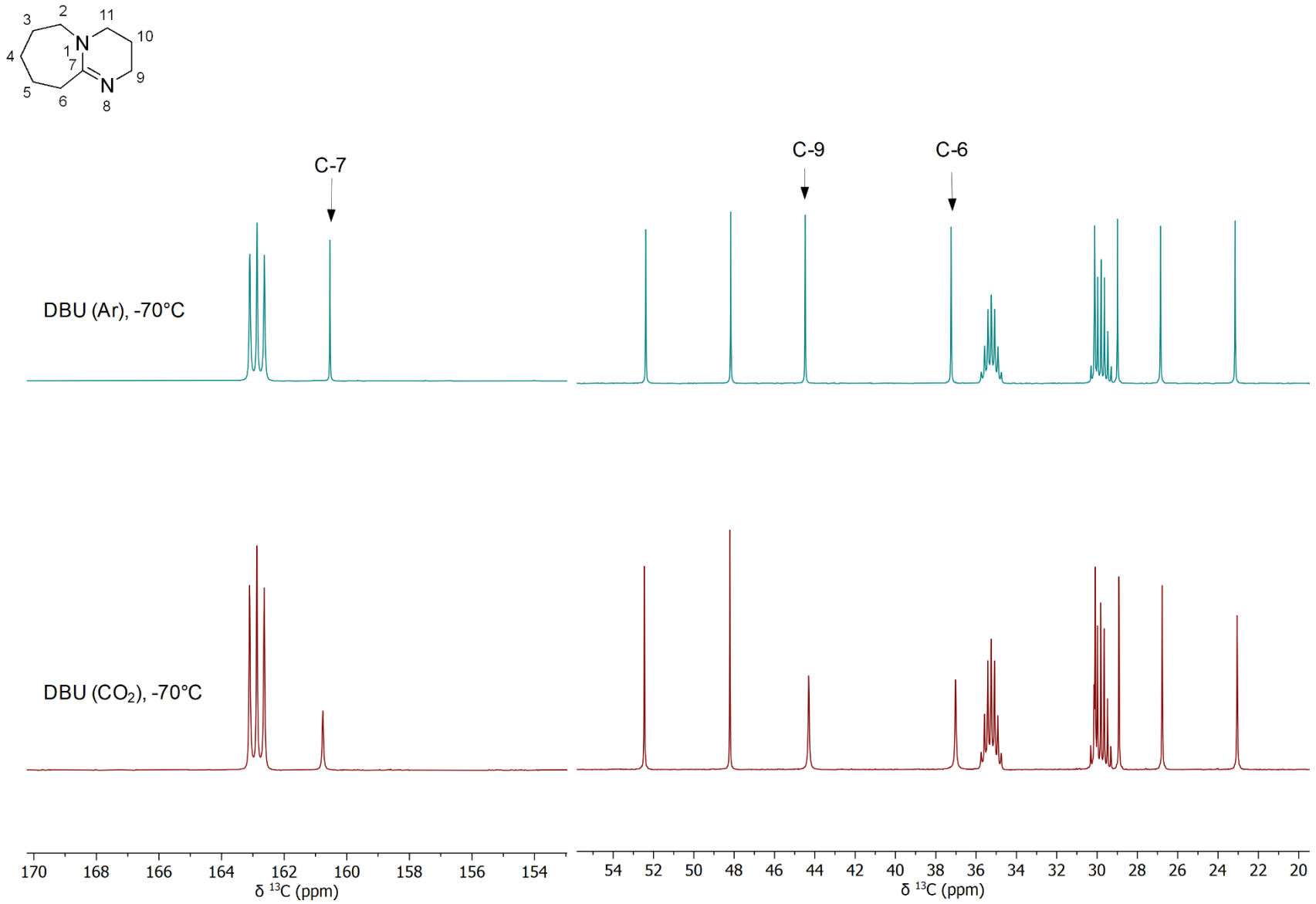

Figure S38. Stacked $^{13}C\{^{1}H\}$ spectra (500 MHz, selected regions shown) of DBU under argon or CO_2 (1 atm) in d_7-DMF.

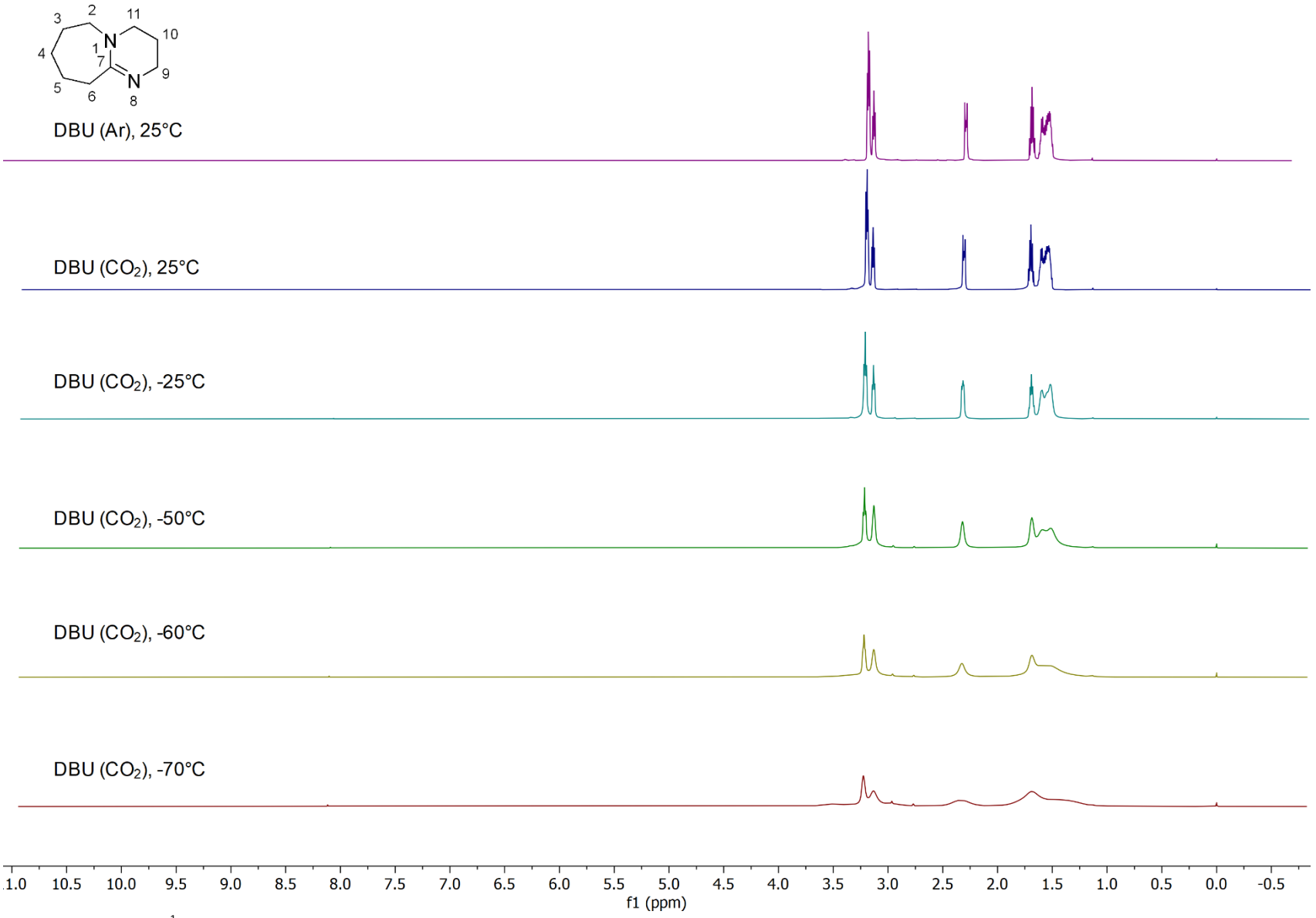

Figure S39. Stacked ^{1}H spectra (500 MHz) of DBU in d_7-DMF.

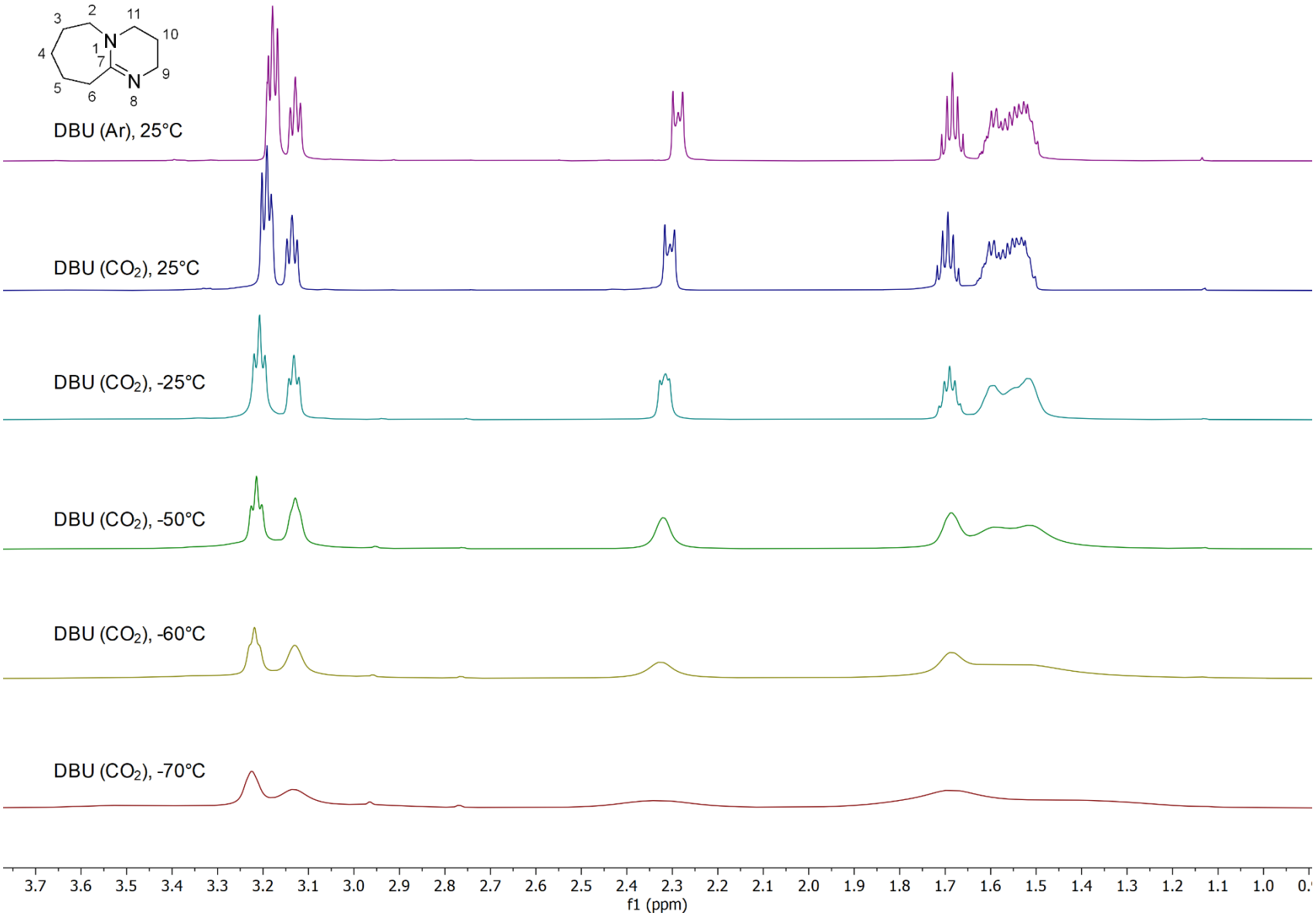

Figure S40. Stacked ^{1}H spectra (500 MHz, aliphatic region shown) of DBU in d_7-DMF.

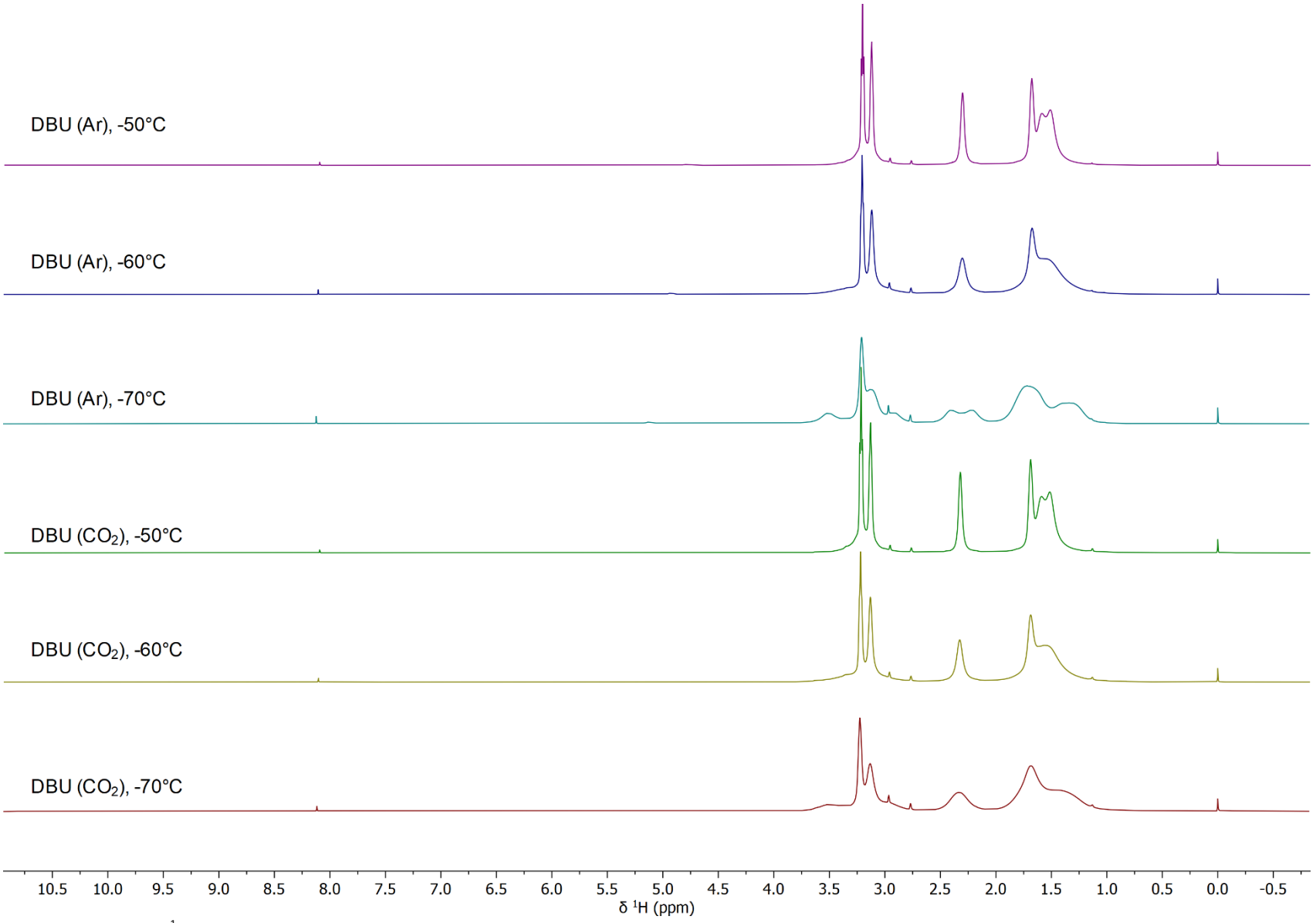

Figure S41. Stacked ^{1}H spectra (500 MHz) of DBU in d_7-DMF.

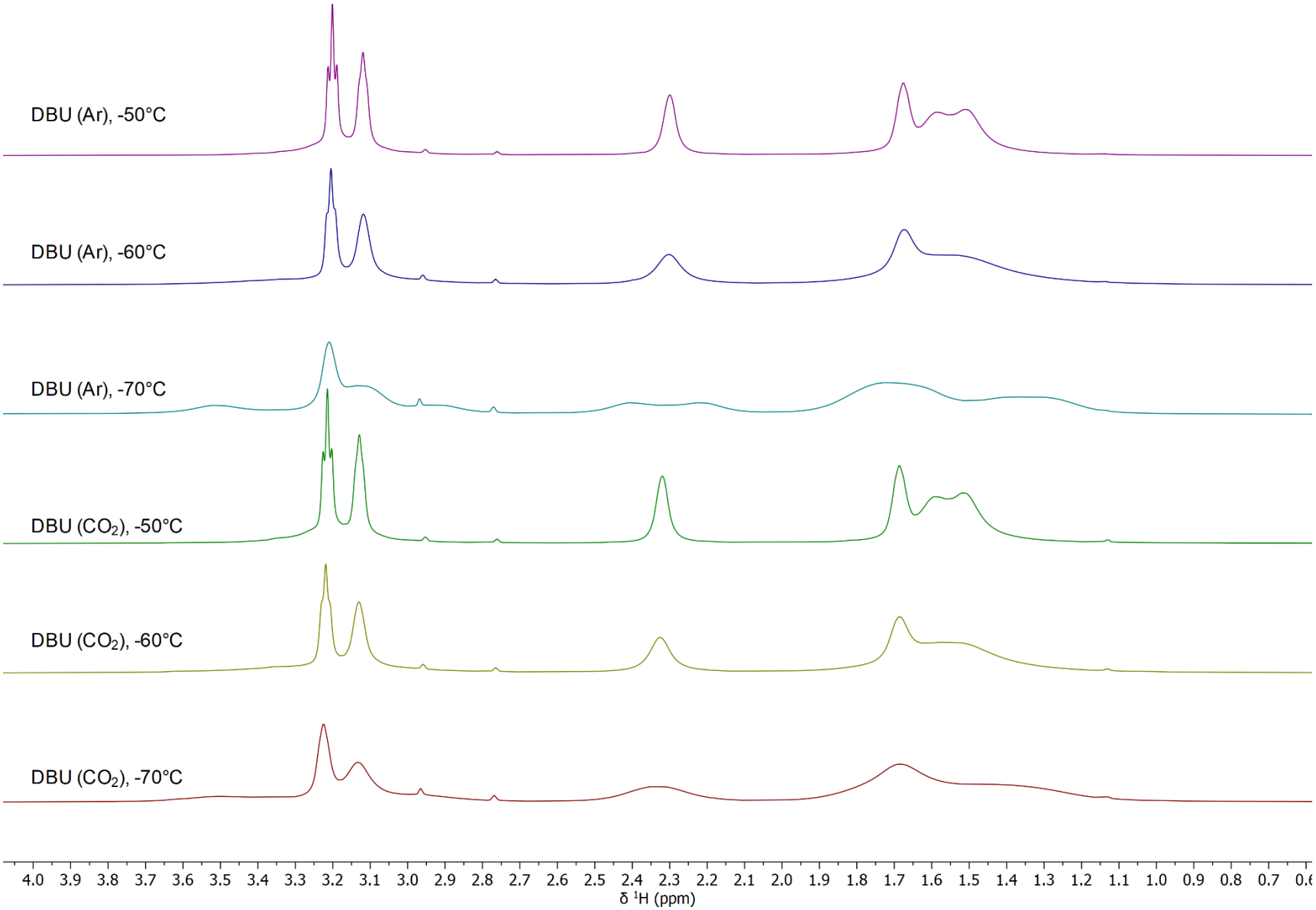

Figure S42. Stacked ^{1}H spectra (500 MHz, aliphatic region shown) of DBU in d_7-DMF.

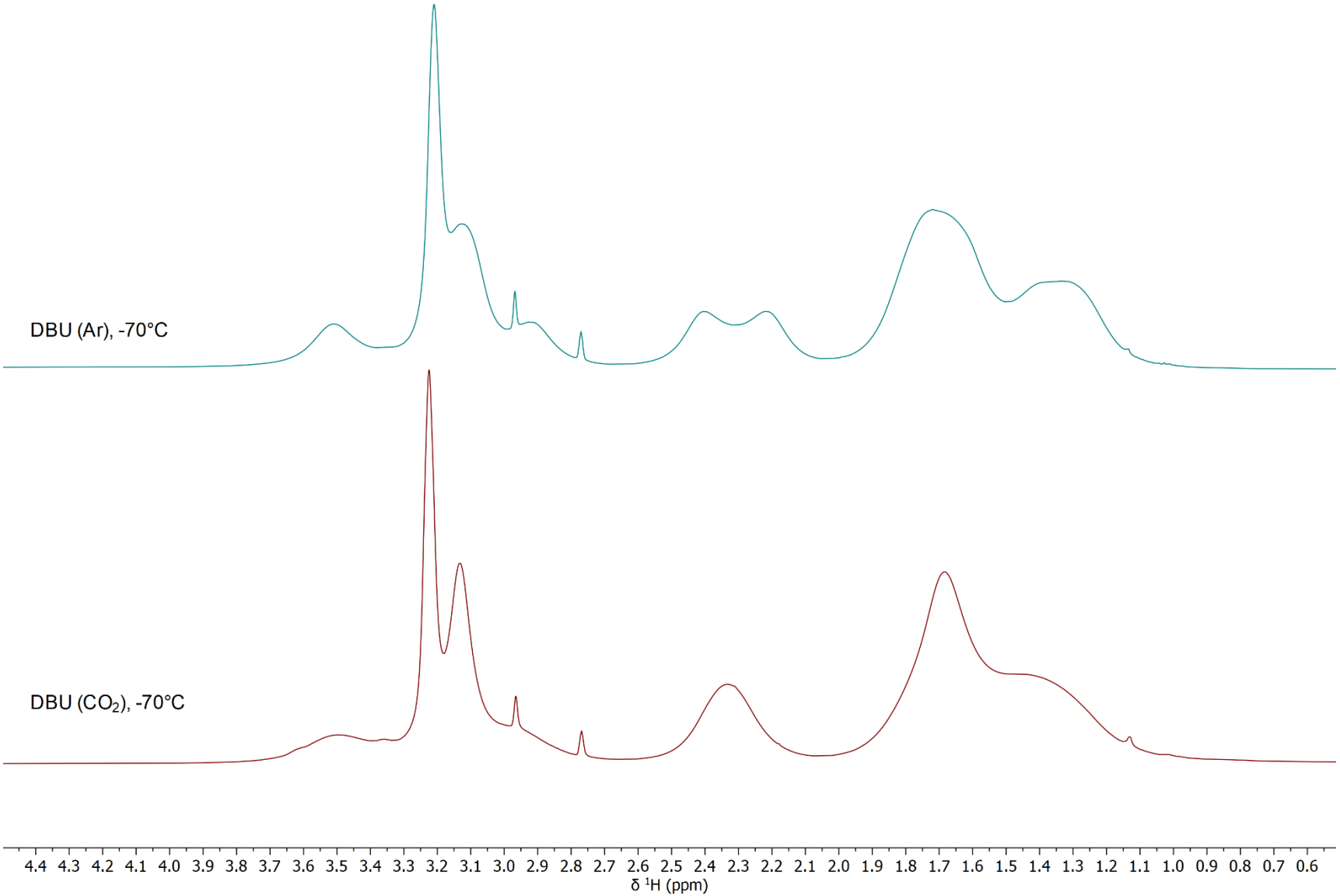

Figure S43. Stacked ^{1}H spectra (500 MHz, aliphatic region shown) of DBU in d_7-DMF at -70°C.

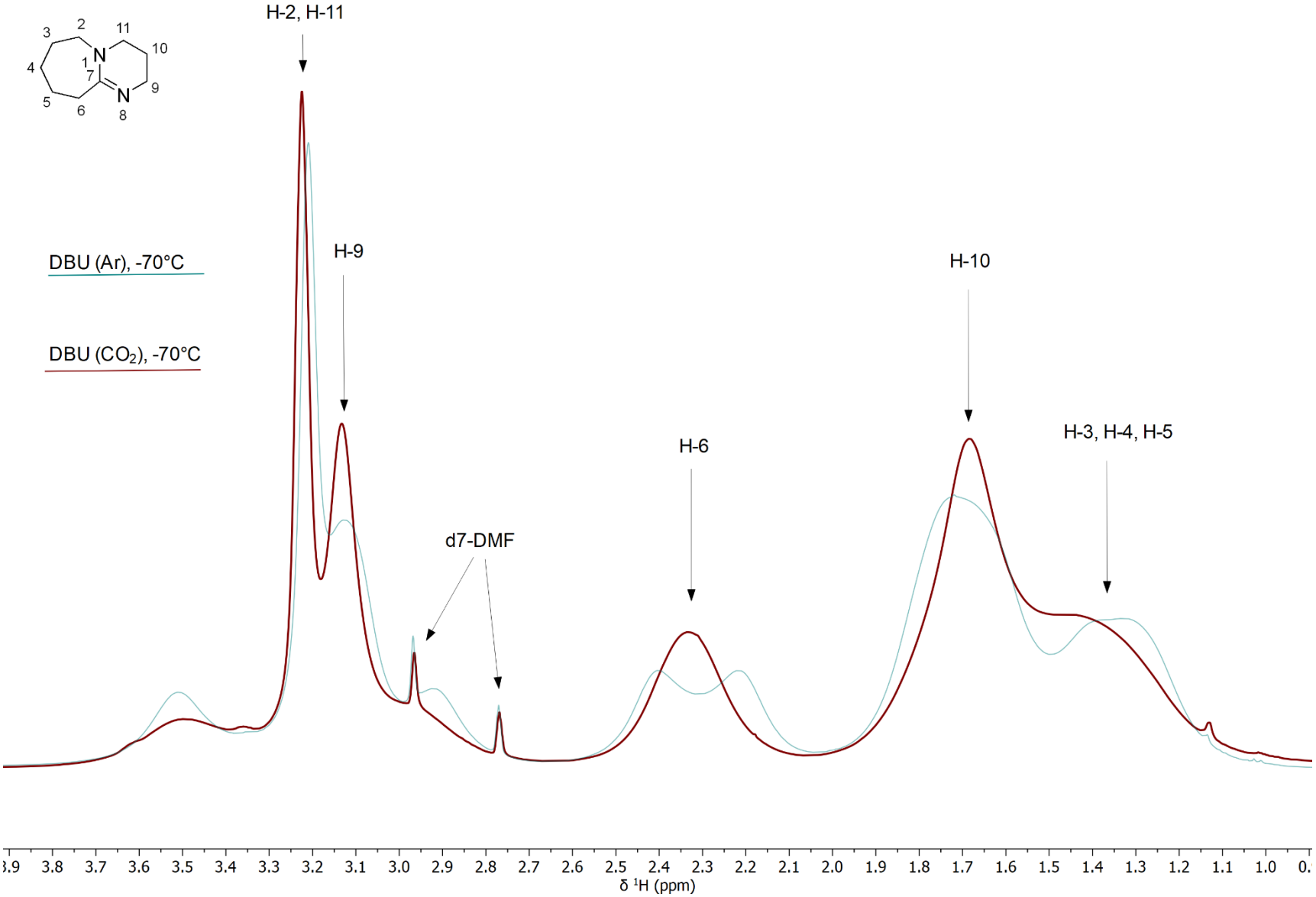

Figure S44. Overlaid ^{1}H spectra (500 MHz, aliphatic region shown) of DBU in d_7-DMF at -70°C.

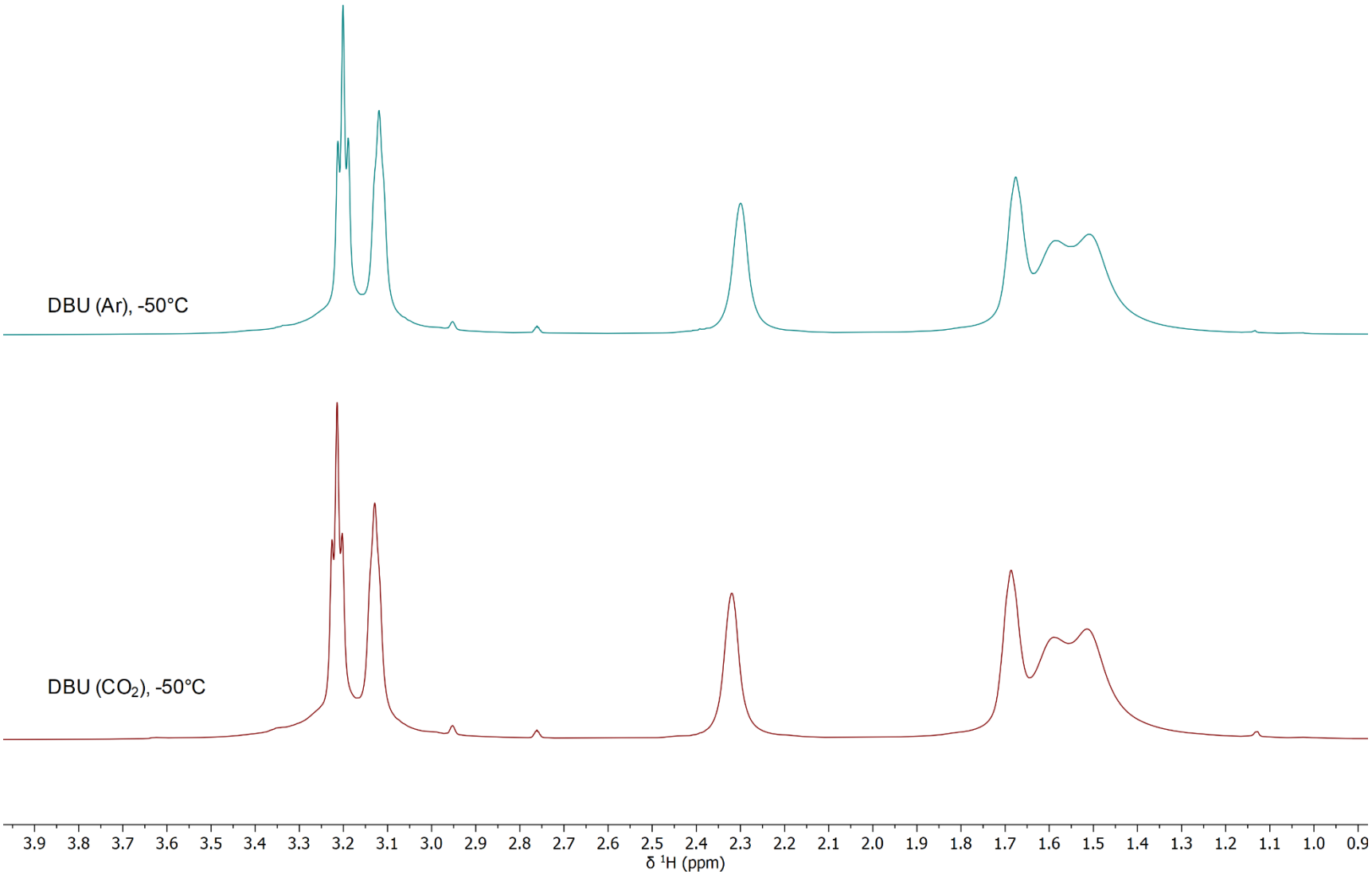

Figure S45. Stacked ^{1}H spectra (500 MHz, aliphatic region shown) of DBU in d_7-DMF at -50°C.

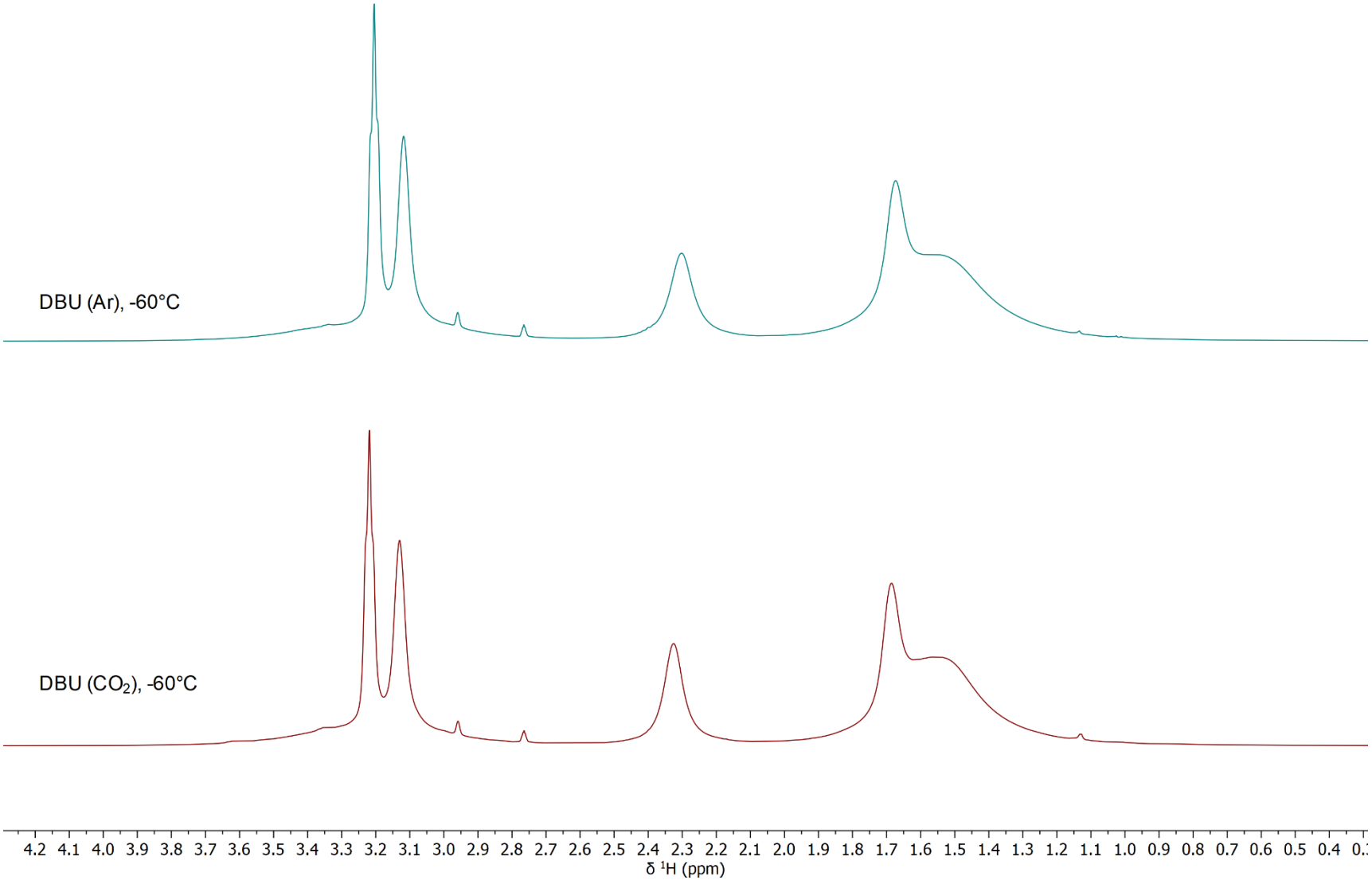

Figure S46. Stacked ^{1}H spectra (500 MHz, aliphatic region shown) of DBU in d_7-DMF at -60°C.

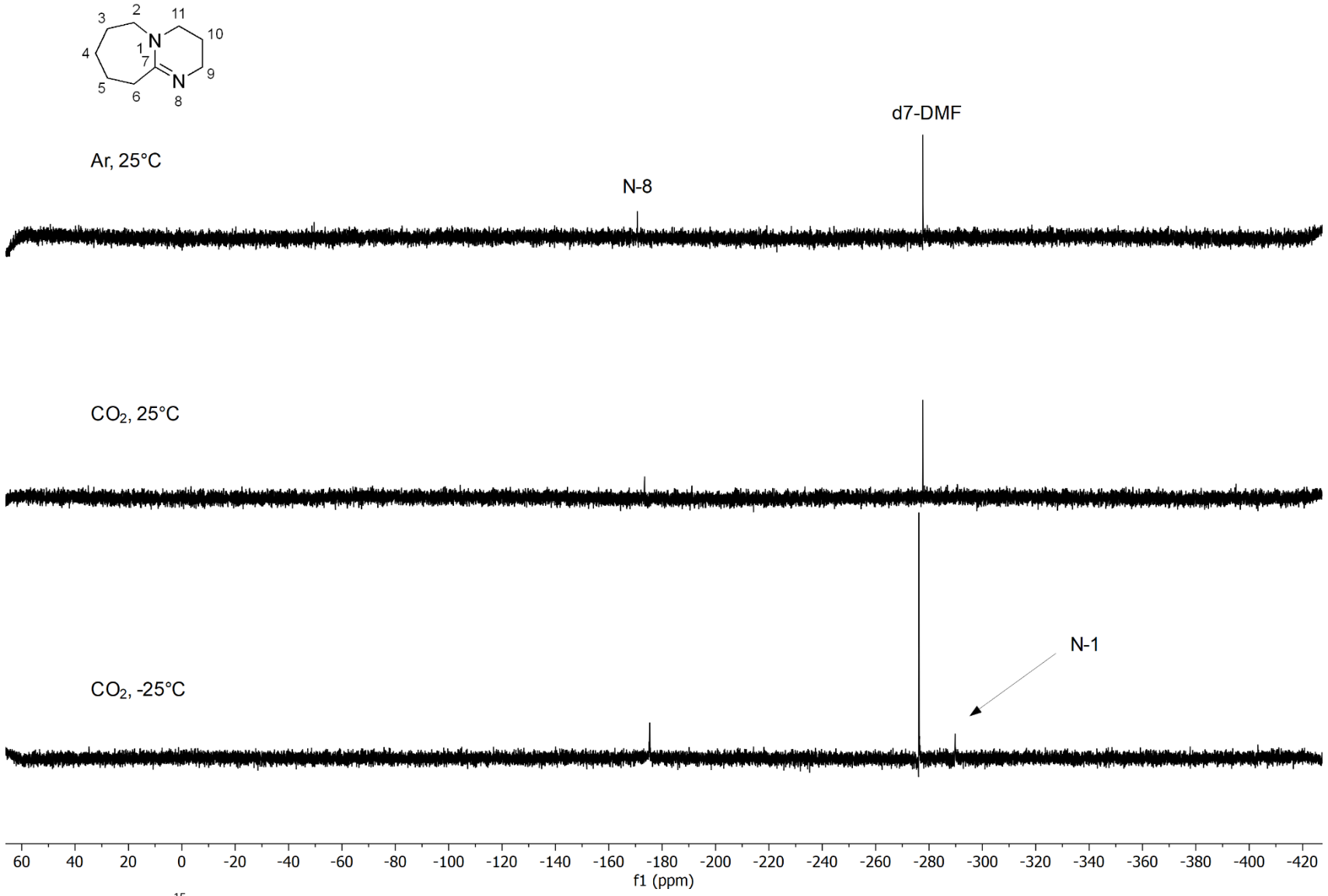

Figure S47. Stacked ^{15}N spectra (50.7 MHz) of DBU in d_7-DMF.

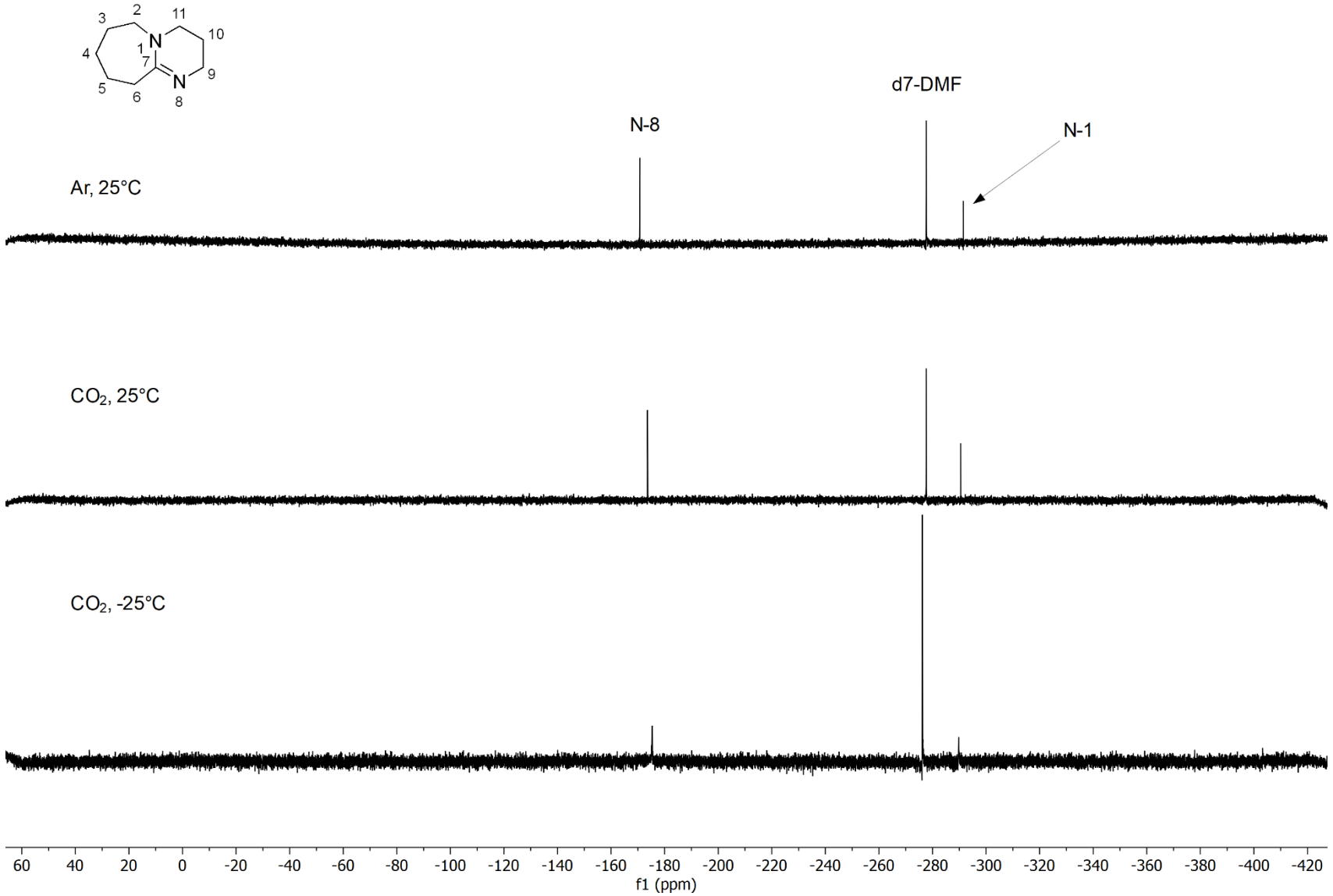

Figure S48. Stacked inverse gated ^{15}N spectra (50.7 MHz) of DBU in d_7-DMF. Experiment at -25°C is proton-coupled ^{15}N.

12. Thermogravimetric and Differential Thermal Analysis

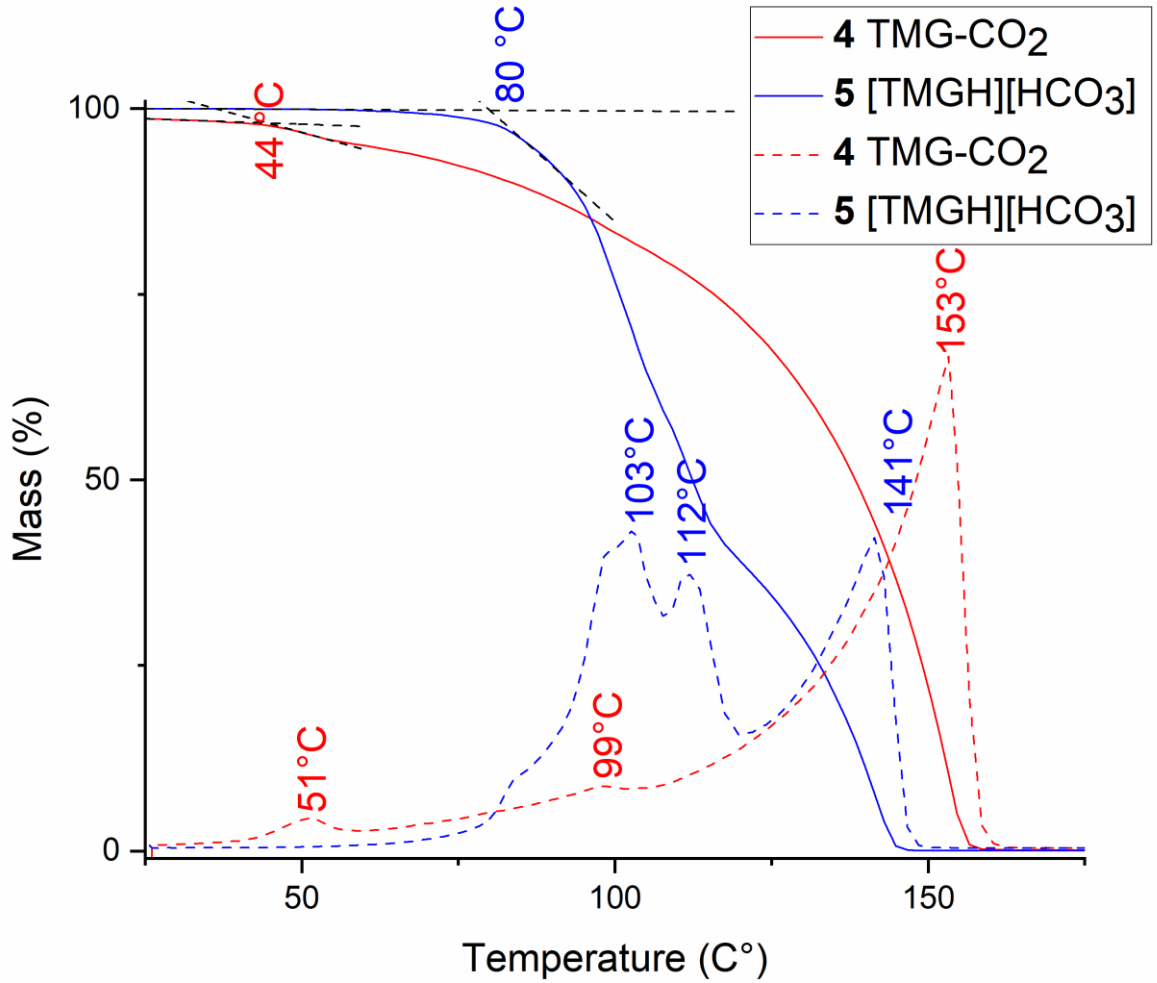

Figure S49. Thermogravimetric analysis (full line) and differential thermal analysis (dashed line) of zwitterion **4** and bicarbonate **5**. Intersection of black dashed lines indicate onset of thermal degradation. This image is a larger version of Figure 5 in the article.

13. Infrared Spectroscopy Data

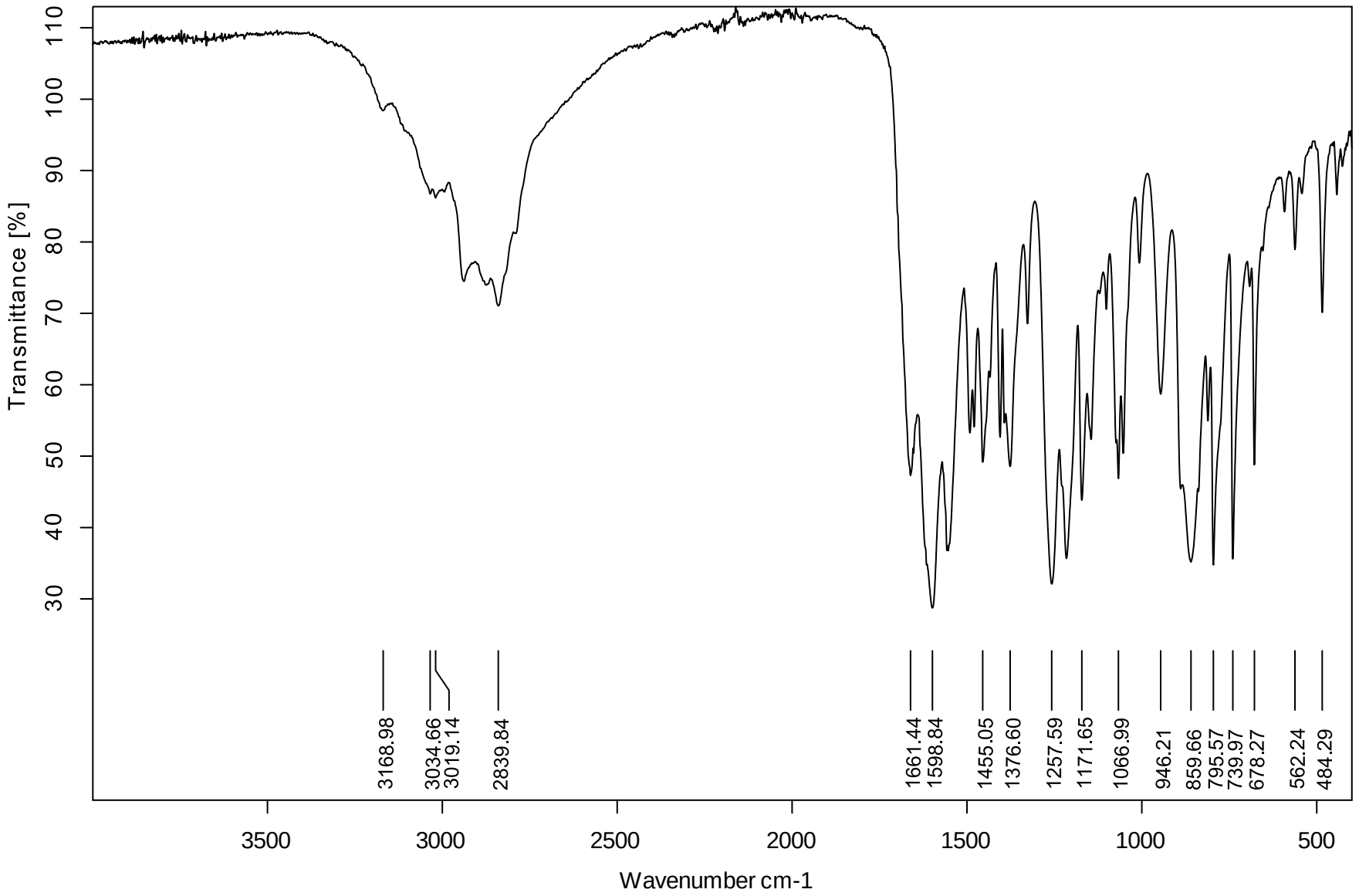

Figure S50. Infrared spectrum of zwitterion **4**, TMG−CO_2.

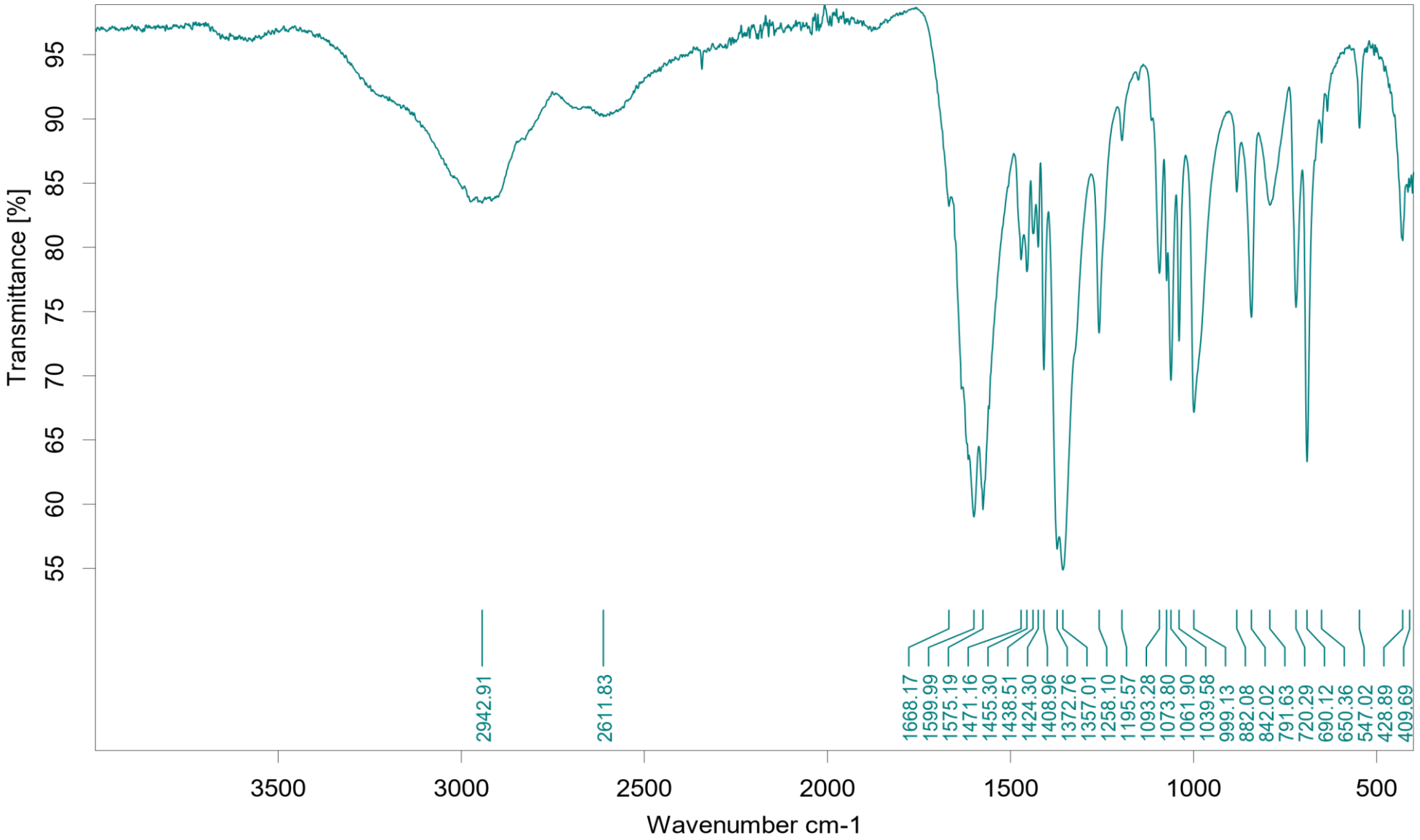

Figure S51. Infrared spectrum of bicarbonate **5**, $[TMGH^+][HCO_3^-]$.

14. Experimental Procedure for Stoichiometric Carboxylations in Glovebox

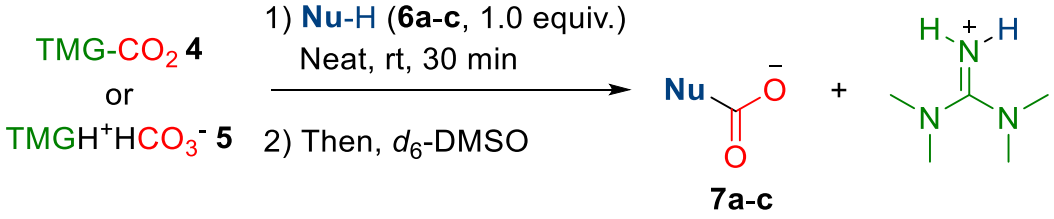

7a-c

Solid zwitterion **4** (TMG-CO_2, ca 1 g), stored in a 25 ml Schlenk tube under 1 atm of CO_2, was transported to an argon-filled glovebox. The zwitterion (0.5 mmol, 80 mg) was weighed into oven-dried 8 ml glass vials, and then an oven-dried stir bar was added to each vial. While stirring at room temperature, the corresponding protic nucleophile (0.5 mmol) was added by pipette in one portion to the open vial (not dropwise). This led to instant bubbling and formation of a gel, which slowly solidified (**Figure S52**). After 30 min, d_6-DMSO (0.7 ml) was added, and the suspension was stirred (ca 5 min), and finally mixed with a syringe until it became homogeneous. The solution was transferred to a J. Young NMR tube, which was sealed, and yields were determined by ^{1}H-NMR.

The procedure above was repeated using bicarbonate **5** (0.5 mmol, 88.6 mg). When the nucleophiles were added, no bubbles were observed, yet the mixtures became gels, which solidified within 30 min (except n-butanol).

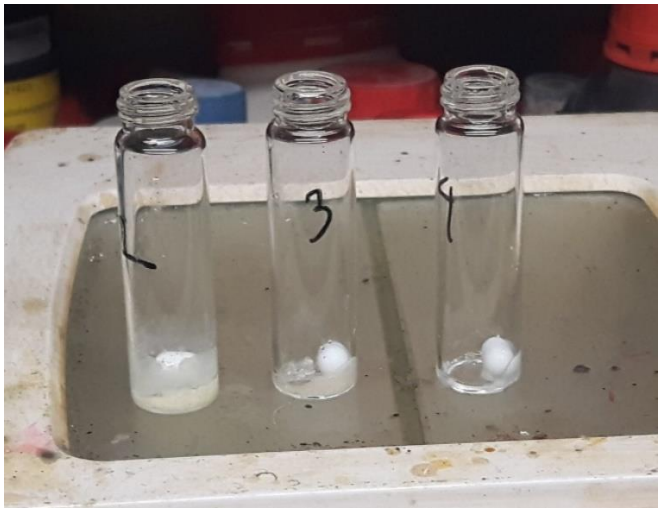

Figure S52. Zwitterion-mediated carboxylation without exogenous CO_2. The resulting solid/gel after 30 min of stirring. **Left** = 4-(Trifluoromethyl)aniline (solid), **Middle** = Pyrrole (wet solid), **Right** = 1-Butanol (gel).

4-(Trifluoromethyl)aniline

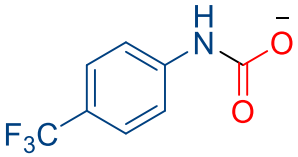

7a

For spectral characterization, please see the section **16** (in-situ formed mixed carbamates).

Experiments using bicarbonate **5**, resulting chemical shift of bicarbonate ion: **^{13}C{^{1}H} NMR** (125.8 MHz, d_6-DMSO, 25 °C): δ 159.0

Pyrrole

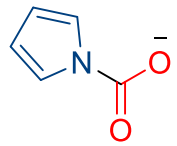

7b

Mixed carbamate:

^{1}H NMR (500 MHz, d_6-DMSO, 25 °C): δ 7.16 (overlap, 2H, br, =N**H**$_2$), 7.12 (overlap, 2H, t, *J* = 2.3 Hz, C**H**N), 5.90 (2H, t, *J* = 2.3 Hz, C**H**CHN), 2.74 (12H, s, NC**H**$_3$)

^{13}C{^{1}H} NMR (125.8 MHz, d_6-DMSO, 300 K): δ 162.3 (**C**=N), 150.5 (N**C**=OO), 119.3 (**C**HN), 107.2 (**C**HCHN), 39.3 (N**C**H$_3$)

Experiments using bicarbonate **5**, resulting chemical shift of bicarbonate ion: **^{13}C{^{1}H} NMR** (125.8 MHz, d_6-DMSO, 25 °C): δ 159.0

1-Butanol

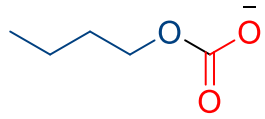

7c

Carbonate salt:

^{1}H NMR (500 MHz, d_6-DMSO, 25 °C): δ 5.90 (overlap, 2H, br, =N**H**$_2$), 3.60 (2H, t, *J* = 6.6 Hz, C**H**$_2$O), 2.68 (12H, s, NC**H**$_3$), 1.37 (overlap, 2H, m, C**H**$_2$), 1.28 (overlap, 2H, m, C**H**$_2$), 0.85 (overlap, 3H, t, *J* = 7.3 Hz, C**H**$_3$)

^{13}C{^{1}H} NMR (125.8 MHz, d_6-DMSO, 25 °C): δ 165.0 (**C**=N), 156.0 (O**C**=OO), 62.8 (**C**H$_2$O), 39.1 (N**C**H$_3$), 32.0 (**C**H$_2$), 19.0 (**C**H$_2$), 13.8 (**C**H$_3$)

Unreacted 1-butanol:

^{1}H NMR (500 MHz, d_6-DMSO, 25 °C): δ 3.38 (2H, t, *J* = 6.4 Hz, C**H**$_2$O), 1.37 (overlap, 2H, m, C**H**$_2$), 1.28 (overlap, 2H, m, C**H**$_2$), 0.86 (overlap, 3H, t, *J* = 7.3 Hz, C**H**$_3$)

^{13}C{^{1}H} NMR (125.8 MHz, d_6-DMSO, 25 °C): δ 60.3 (**C**H$_2$O), 33.7 (**C**H$_2$), 18.7 (**C**H$_2$), 13.8 (**C**H$_3$)

Experiments using bicarbonate **5**, resulting chemical shift of bicarbonate ion: **^{13}C{^{1}H} NMR** (125.8 MHz, d_6-DMSO, 25 °C): δ 158.8

15. Crystal Structure Determination of Bicarbonate 5, [TMGH$^+$][HCO$_3^-$]

Crystals suitable for X-ray diffraction study were grown by adding 0.1 ml of TMG to a 25 ml Schlenk tube with a stir bar in a glove box. The tube was taken out and connected to a Schlenk line under CO_2. Dry ACN (12 ml) and dry dioxane (3 ml) were added at room temperature under 1 atm CO_2 flow. The stopper was replaced with a rubber septum, which was pierced with a needle, and the solution was flushed with CO_2 for 20 min. The needle was removed, and the solution was transferred by through a syringe filter to a second oven-dried 25 ml Schlenk tube under CO_2 (1 atm). This removed small amounts of bicarbonate **5**, formed from residual water. The receiving tube had its septum replaced with a glass stopper, the Schlenk adapter was closed, and the tube was placed in a freezer for two weeks. A white precipitate formed (zwitterion **4**), but the crystals were of low quality, therefore the tube was left at room temperature for a week. During this time, the white precipitate dissolved and new long colorless needles formed, which were determined as bicarbonate **5**.

The single-crystal X-ray diffraction study of **5** was carried out on a Bruker D8 Venture diffractometer with PhotonII detector at 123(2) K using Cu-Kα radiation (λ = 1.54178 Å). Dual space methods (SHELXT for **5a**) [G. M. Sheldrick, *Acta Crystallogr.* 2015, **A71**, 3-8] were used for structure solution and refinement was carried out using SHELXL-2014 (full-matrix least-squares on F^2) [G. M. Sheldrick, *Acta Crystallogr.* 2015, **C71**, 3-8]. Hydrogen atoms were localized by difference electron density determination and refined using a riding model (H(N, O) free. A semi-empirical absorption correction was applied. Refinement with the listed atoms show residual electron density due to traces of solvent acetonitrile which could not be refined. In 2 voids are approx. 3 electron per void. Therefore the option "SQUEEZE" of the program package SQUEEZE [PLATON, A. L. Spek, *Acta Crystallogr.* 2009, **D65**, 148-155; A. L. Spek, *Acta Crystallogr.* 2015, **C71**, 9-18.] was used to create a hkl file taking into account the residual electron density in the void areas. The small fraction of the solvent acetonitrile was not included in the unit card (see cif.file for details).

5: colourless crystals, $C_5H_{14}N_3 \cdot CHO_3$, M_r = 177.21, crystal size 0.14 × 0.06 × 0.04 mm, monoclinic, space group $P2_1/n$ (No. 14), a = 7.4094(2) Å, b = 9.2008(2) Å, c = 14.0802(3) Å, β = 94.270(1)°, V = 957.22(4) Å^3, Z = 4, ρ = 1.230 Mg/m^{-3}, μ(Cu-K$_\alpha$) = 0.83 mm^{-1}, F(000) = 384, $2\theta_{max}$ = 144.2°, 9917 reflections, of which 1889 were independent (R_{int} = 0.027), 122 parameters, 3 restraints, R_1 = 0.031 (for 1746 I > 2σ(I)), wR_2 = 0.080 (all data), S = 1.04, largest diff. peak / hole = 0.19 / -0.17 e Å^{-3}.

CCDC 2044161 (**5**) contains the supplementary crystallographic data for this paper. These data can be obtained free of charge from The Cambridge Crystallographic Data Centre via www.ccdc.cam.ac.uk/data_request/cif. It is a redetermination of COWGON at 123 K using Cu-Kα radiation. COWGON: 1912766 V. Ramkumar, R.L. Gardas, *J. Chem. Eng. Data* **2019**, *64*, 4844-4855; DOI: 10.1021/acs.jced.9b00377.

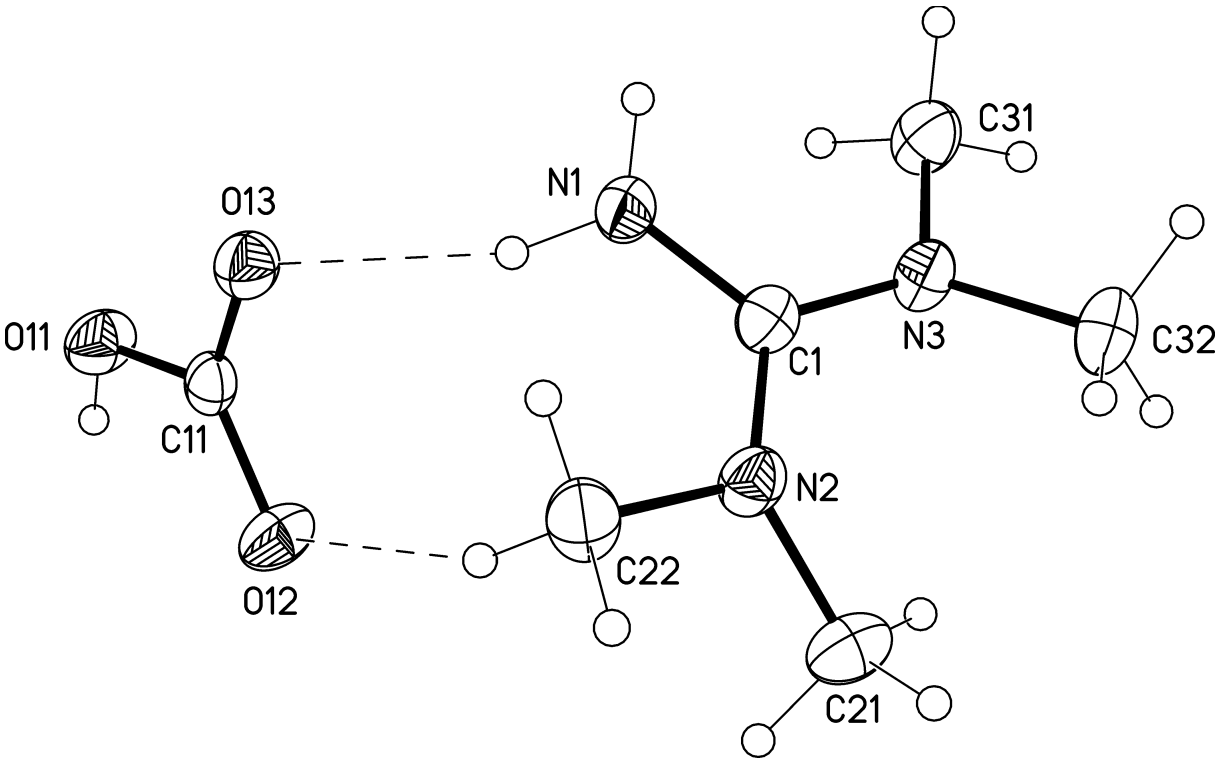

Figure S53. Molecular structure of **5** (displacement parameters are drawn at 50 % probability level).

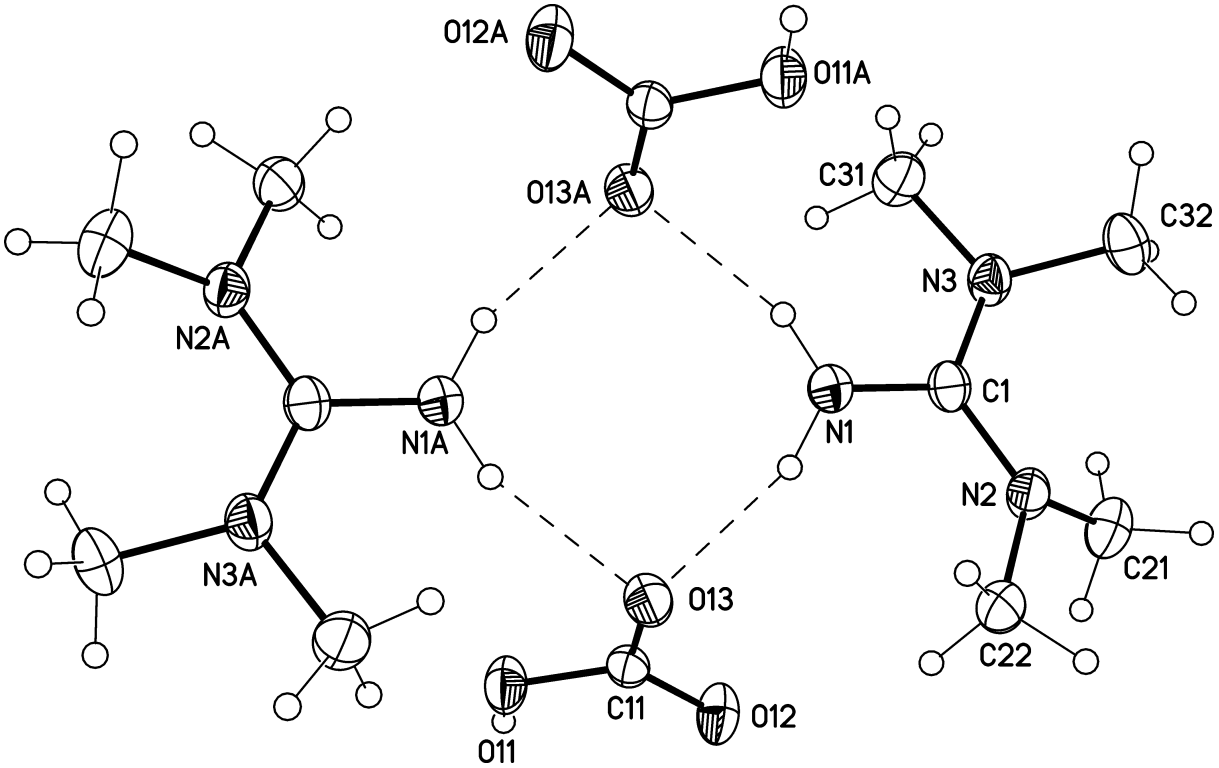

Figure S54. Structure of the dimer with C_i-symmetry of **5** (symmetry operator –x+1, -y+1, -z+1, displacement parameters are drawn at at 50% probability level).

16. Spectral Characterization of In-situ Formed Mixed Carbamates Using TMG

4-Methoxyaniline

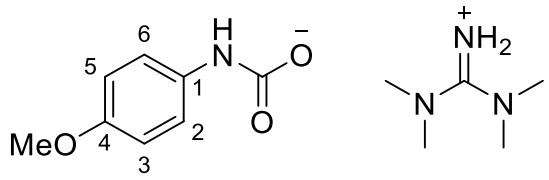

Mixed carbamate:

^{1}H NMR (500 MHz, d_6-DMSO, 25 °C): δ 9.37 (2H, br, =N**H$_2$**), 8.38 (1H, s, N**H**COO), 7.41 (2H, d, *J* = 8.7 Hz, 2-Ar**H** & 6-Ar**H**), 6.71 (2H, d, *J* = 9.0 Hz, 3-Ar**H** & 5-Ar**H**), 3.66 (3H, s, OC**H$_3$**), 2.84 (12H, s, NC**H$_3$**)

Quant ^{13}C{^{1}H} NMR (125.8 MHz, d_6-DMSO, 25 °C): δ 162.4 (**C**=N), 158.5 (N**C**=OO), 152.3 (4-Ar**C**OMe), 137.1 (1-Ar**C**N), 118.1 (2-Ar**C**H & 6-Ar**C**H), 113.4 (3-Ar**C**H & 5-Ar**C**H), 55.1 (O**C**H$_3$), 39.3 (N**C**H$_3$)

The formation of mixed carbamate is quantitative, because signals for unreacted 4-methoxyaniline are not observed.

4-Chloroaniline

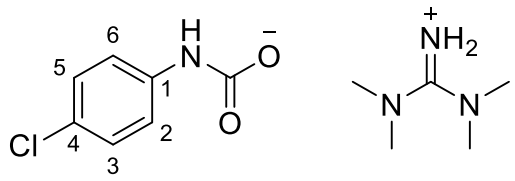

Mixed carbamate:

^{1}H NMR (500 MHz, d_6-DMSO, 25 °C): δ 8.96 (2H, br, =N**H$_2$**), 8.25 (1H, s, N**H**COO), 7.53 (2H, d, *J* = 8.7 Hz, 2-Ar**H** & 6-Ar**H**), 7.06 (2H, d, *J* = 8.9 Hz, 3-Ar**H** & 5-Ar**H**), 2.85 (12H, s, NC**H$_3$**)

Quant ^{13}C{^{1}H} NMR (125.8 MHz, d_6-DMSO, 25 °C): δ 162.0 (**C**=N), 158.0 (N**C**=OO), 143.4 (1-Ar**C**N), 127.6 (2-Ar**C**H & 6-Ar**C**H), 121.1 (4-Ar**C**Cl), 117.8 (3-Ar**C**H & 5-Ar**C**H), 39.3 (N**C**H$_3$)

Unreacted 4-chloroaniline:

^{1}H NMR (500 MHz, d_6-DMSO, 25 °C): δ 6.99 (2H, d, *J* = 8.5 Hz, 2-Ar**H** & 6-Ar**H**), 6.58 (2H, d, *J* = 8.1 Hz, 3-Ar**H** & 5-Ar**H**), 5.32 (2H, br, N**H$_2$**)

Quant ^{13}C{^{1}H} NMR (125.8 MHz, d_6-DMSO, 25 °C): Signal intensity is too low for accurate assignment (known compound).

4-(Trifluoromethoxy)aniline

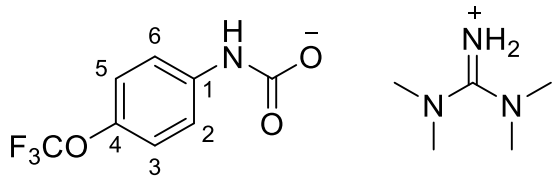

Mixed carbamate:

^{1}H NMR (500 MHz, d_6-DMSO, 25 °C): δ 8.94 (2H, br, =N**H$_2$**), 8.29 (1H, s, N**H**COO), 7.59 (2H, d, *J* = 9.0 Hz, 2-Ar**H** & 6-Ar**H**), 7.01 (2H, d, *J* = 8.5 Hz, 3-Ar**H** & 5-Ar**H**), 2.85 (12H, s, NC**H$_3$**)

Quant ^{13}C{^{1}H} NMR (125.8 MHz, d_6-DMSO, 25 °C): δ 162.0 (**C**=N), 157.9 (N**C**=OO), 143.8 (1-Ar**C**N), 139.9 (4-Ar**C**OCF$_3$), 120.8 (2-Ar**C**H & 6-Ar**C**H), 120.4 (q, *J* = 254.4Hz, O**C**F$_3$), 117.0 (3-Ar**C**H & 5-Ar**C**H), 39.3 (N**C**H$_3$)

Quant ^{19}F{^{1}H} NMR (470.4 MHz, d_6-DMSO, 25 °C): δ -57.37

Unreacted 4-(trifluoromethoxy)aniline:

^{1}H NMR (500 MHz, d_6-DMSO, 25 °C): δ 6.95 (2H, d, *J* = 8.3 Hz, 2-Ar**H** & 6-Ar**H**), 6.62 (2H, d, *J* = 7.3 Hz, 3-Ar**H** & 5-Ar**H**), 5.40 (2H, br, N**H$_2$**)

Quant ^{13}C{^{1}H} NMR (125.8 MHz, d_6-DMSO, 25 °C): Signal intensity is too low for accurate assignment (known compound).

Quant ^{19}F{^{1}H} NMR (470.4 MHz, d_6-DMSO, 25 °C): δ -57.58

4-(Trifluoromethyl)aniline

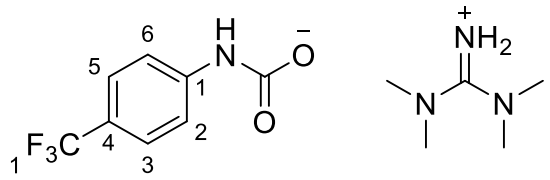

Mixed carbamate:

^{1}H NMR (500 MHz, d_6-DMSO, 25 °C): δ 8.63 (2H, br, =N**H$_2$**), 8.44 (1H, s, N**H**COO), 7.68 (2H, d, *J* = 8.5 Hz, 2-Ar**H** & 6-Ar**H**), 7.34 (2H, d, *J* = 8.8 Hz, 3-Ar**H** & 5-Ar**H**), 2.84 (12H, s, NC**H$_3$**)

Quant ^{13}C{^{1}H} NMR (125.8 MHz, d_6-DMSO, 25 °C): δ 162.2 (**C**=N), 157.5 (N**C**=OO), 148.3 (1-Ar**C**N), 125.3 (q, *J* = 270.4 Hz, 4-Ar**C**F$_3$), 125.1 (q, *J* = 3.8 Hz, 3-Ar**C**H & 5-Ar**C**H), 117.33 (q, *J* = 31.6 Hz, 4-Ar**C**CF$_3$), 115.7 (2-Ar**C**H & 6-Ar**C**H), 39.3 (N**C**H$_3$)

Quant ^{19}F{^{1}H} NMR (470.4 MHz, d_6-DMSO, 25 °C): δ -59.31

Unreacted 4-(trifluoromethoxy)aniline:

^{1}H NMR (500 MHz, d_6-DMSO, 25 °C): δ 7.28 (2H, d, *J* = 8.8 Hz, 2-Ar**H** & 6-Ar**H**), 6.69 (2H, d, *J* = 8.8 Hz, 3-Ar**H** & 5-Ar**H**), 5.96 (2H, br, N**H$_2$**)

Quant ^{13}C{^{1}H} NMR (125.8 MHz, d_6-DMSO, 25 °C): Signal intensity is too low for accurate assignment (known compound).

Quant ^{19}F{^{1}H} NMR (470.4 MHz, d_6-DMSO, 25 °C): δ -59.00

4-Cyanoaniline

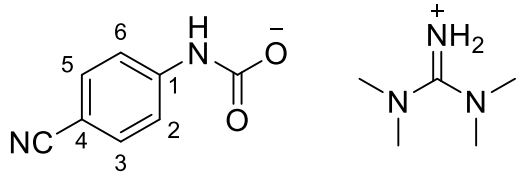

Mixed carbamate:

^{1}H NMR (500 MHz, d_6-DMSO, 25 °C): δ 8.61 (1H, s, N**H**COO), 8.49 (2H, br, =N**H$_2$**), 7.65 (2H, d, *J* = 8.6 Hz, 2-Ar**H** & 6-Ar**H**), 7.42 (2H, d, *J* = 9.0 Hz, 3-Ar**H** & 5-Ar**H**), 2.84 (12H, s, NC**H$_3$**)

Quant ^{13}C{^{1}H} NMR (125.8 MHz, d_6-DMSO, 25 °C): δ 162.0 (**C**=N), 157.0 (N**C**=OO), 149.2 (1-Ar**C**N), 132.4 (3-Ar**C**H & 5-Ar**C**H), 120.6 (4-Ar**C**N), 116.1 (2-Ar**C**H & 6-Ar**C**H), 98.0 (4-Ar**C**CN), 39.3 (N**C**H$_3$)

Unreacted 4-cyanoaniline:

^{1}H NMR (500 MHz, d_6-DMSO, 25 °C): δ 7.36 (2H, d, *J* = 8.9 Hz, 2-Ar**H** & 6-Ar**H**), 6.65 (2H, d, *J* = 9.2 Hz, 3-Ar**H** & 5-Ar**H**), 6.34 (2H, br, N**H$_2$**)

Quant ^{13}C{^{1}H} NMR (125.8 MHz, d_6-DMSO, 25 °C): 153.3 (1-Ar**C**N), 133.4 (3-Ar**C**H & 5-Ar**C**H), 120.8 (4-Ar**C**N), 113.5 (2-Ar**C**H & 6-Ar**C**H), 95.2 (4-Ar**C**CN)

4-Nitroaniline

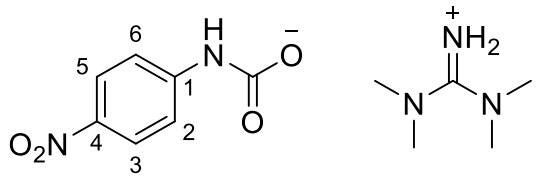

Mixed carbamate:

^{1}H NMR (500 MHz, d_6-DMSO, 25 °C): δ 9.05 (1H, s, N**H**COO), 8.25 (2H, br, =N**H$_2$**), 7.97 (2H, d, *J* = 9.6 Hz, 2-Ar**H** & 6-Ar**H**), 7.69 (2H, d, *J* = 9.2 Hz, 3-Ar**H** & 5-Ar**H**), 2.84 (12H, s, NC**H$_3$**)

Quant ^{13}C{^{1}H} NMR (125.8 MHz, d_6-DMSO, 25 °C): δ 162.2 (**C**=N), 156.3 (N**C**=OO), 151.8 (1-Ar**C**N), 137.3 (4-Ar**C**NO$_2$), 125.0 (3-Ar**C**H & 5-Ar**C**H), 115.1 (2-Ar**C**H & 6-Ar**C**H), 39.3 (N**C**H$_3$)

Unreacted 4-nitroaniline:

^{1}H NMR (500 MHz, d_6-DMSO, 25 °C): δ 7.92 (2H, d, *J* = 9.2 Hz, 2-Ar**H** & 6-Ar**H**), 7.02 (2H, br, N**H$_2$**), 6.66 (2H, d, *J* = 9.3 Hz, 3-Ar**H** & 5-Ar**H**)

Quant ^{13}C{^{1}H} NMR (125.8 MHz, d_6-DMSO, 25 °C): δ 156.1 (1-Ar**C**N), 135.4 (4-Ar**C**NO$_2$), 126.4 (3-Ar**C**H & 5-Ar**C**H), 112.4 (2-Ar**C**H & 6-Ar**C**H)

4-(Trifluoromethylsulfonyl)aniline

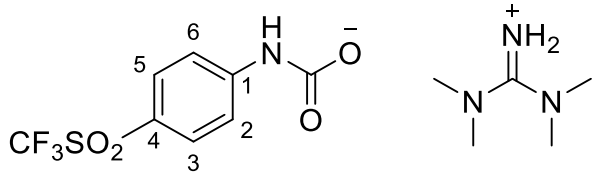

Mixed carbamate:

^{1}H NMR (500 MHz, d_6-DMSO, 25 °C): δ 9.17 (1H, s, N**H**COO), 8.12 (2H, br, =N**H$_2$**), 7.85 (2H, d, *J* = 8.3 Hz, 2-Ar**H** & 6-Ar**H**), 7.68 (2H, d, *J* = 8.8 Hz, 3-Ar**H** & 5-Ar**H**), 2.82 (12H, s, NC**H$_3$**)

Quant ^{13}C{^{1}H} NMR (125.8 MHz, d_6-DMSO, 25 °C): δ 162.5 (**C**=N), 156.0 (N**C**=OO), 153.3 (1-Ar**C**N), 131.8 (3-Ar**C**H & 5-Ar**C**H), 119.9 (q, *J* = 326.2 Hz, SO$_2$**C**F$_3$), 116.1 (2-Ar**C**H & 6-Ar**C**H), 113.7 (4-Ar**C**SO$_2$CF$_3$), 39.3 (N**C**H$_3$)

Quant ^{19}F{^{1}H} NMR (470.4 MHz, d_6-DMSO, 25 °C): δ -79.41

Unreacted 4-(trifluoromethylsulfonyl)aniline:

^{1}H NMR (500 MHz, d_6-DMSO, 25 °C): δ 7.59 (2H, d, *J* = 8.8 Hz, 2-Ar**H** & 6-Ar**H**), 7.22 (2H, br, N**H$_2$**), 6.83 (2H, d, *J* = 8.8 Hz, 3-Ar**H** & 5-Ar**H**)

Quant ^{13}C{^{1}H} NMR (125.8 MHz, d_6-DMSO, 25 °C): δ 157.4 (1-Ar**C**N), 132.8 (3-Ar**C**H & 5-Ar**C**H), 120.0 (q, *J* = 324.0 Hz, 4-ArSO$_2$**C**F$_3$), 113.6 (2-Ar**C**H & 6-Ar**C**H), 110.5 (4-Ar**C**SO$_2$CF$_3$)

Quant ^{19}F{^{1}H} NMR (470.4 MHz, d_6-DMSO, 25 °C): δ -79.55

4-Nitroaniline & Diisopropylamine (Instead of TMG)

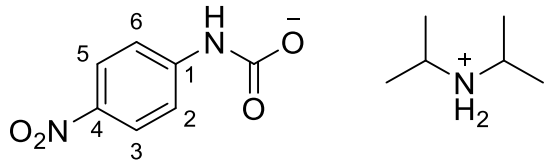

Mixed carbamate:

^{1}H NMR (500 MHz, d_6-DMSO, 25 °C): δ 8.73 (1H, s, N**H**COO), 7.99 (2H, d, *J* = 9.3 Hz, 2-Ar**H** & 6-Ar**H**), 7.69 (2H, d, *J* = 9.4 Hz, 3-Ar**H** & 5-Ar**H**), 3.90 (2H, br, N**H$_2$**$^+$, overlap), 3.81 (2H, m, C**H**(CH$_3$)$_2$, overlap), 1.13 (6H, C**H$_3$**), 1.11 (6H, C**H$_3$**)

^{13}C{^{1}H} NMR (125.8 MHz, d_6-DMSO, 25 °C): δ 156.7 (N**C**=OO), 151.2 (1-Ar**C**N), 137.9 (4-Ar**C**NO$_2$), 124.9 (3-Ar**C**H & 5-Ar**C**H), 124.2 (free CO$_2$), 115.4 (2-Ar**C**H & 6-Ar**C**H), 44.7 (**C**H(CH$_3$)$_2$, overlap), 20.9 (**C**H$_3$)

Unreacted 4-nitroaniline:

^{1}H NMR (500 MHz, d_6-DMSO, 25 °C): δ 7.94 (2H, d, *J* = 9.2 Hz, 2-Ar**H** & 6-Ar**H**), 6.72 (2H, br, N**H$_2$**), 6.61 (2H, d, *J* = 9.2 Hz, 3-Ar**H** & 5-Ar**H**)

^{13}C{^{1}H} NMR (125.8 MHz, d_6-DMSO, 25 °C): δ 155.7 (1-Ar**C**N), 135.7 (4-Ar**C**NO$_2$), 126.3 (3-Ar**C**H & 5-Ar**C**H), 112.4 (2-Ar**C**H & 6-Ar**C**H)

Unreacted DIPA:

^{1}H NMR (500 MHz, d_6-DMSO, 25 °C): δ 3.90 (1H, br, N**H**, overlap), 2.86 (2H, h, *J* = 6.2 Hz, C**H**(CH$_3$)$_2$), 0.97 (6H, s, C**H$_3$**), 0.96 (6H, s, C**H$_3$**)

^{13}C{^{1}H} NMR (125.8 MHz, d_6-DMSO, 25 °C): δ 44.7 (**C**H(CH$_3$)$_2$, overlap), 22.5 (**C**H$_3$)

4-Nitroaniline & Diisopropylethylamine (Instead of TMG)

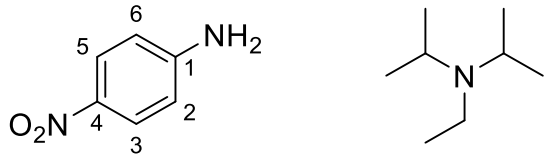

No carboxylation

Unreacted 4-nitroaniline:

^{1}H NMR (500 MHz, d_6-DMSO, 25 °C): δ 7.94 (2H, d, *J* = 9.2 Hz, 2-Ar**H** & 6-Ar**H**), 6.69 (2H, br, N**H$_2$**), 6.61 (2H, d, *J* = 9.2 Hz, 3-Ar**H** & 5-Ar**H**)

^{13}C{^{1}H} NMR (125.8 MHz, d_6-DMSO, 25 °C): δ 155.7 (1-Ar**C**N), 135.7 (4-Ar**C**NO$_2$), 126.3 (3-Ar**C**H & 5-Ar**C**H), 124.2 (free CO$_2$), 112.4 (2-Ar**C**H & 6-Ar**C**H)

Unreacted DIPEA:

^{1}H NMR (500 MHz, d_6-DMSO, 25 °C): δ 2.93 (2H, h, *J* = 6.6 Hz, C**H**(CH$_3$)$_2$), 2.39 (2H, q, *J* = 7.0 Hz, C**H$_2$**CH$_3$), 0.92 (6H, s, C**H$_3$**), 0.91 (2H, t, *J* = 7.1 Hz, CH$_2$C**H$_3$**), 0.91 (6H, s, C**H$_3$**)

^{13}C{^{1}H} NMR (125.8 MHz, d_6-DMSO, 25 °C): δ 47.7 (**C**H(CH$_3$)$_2$), 38.1 (**C**H$_2$CH$_3$), 20.6 (**C**H$_3$), 16.9 (CH$_2$**C**H$_3$)

17. Compound NMR Spectra

4-Methoxyaniline ^{1}H

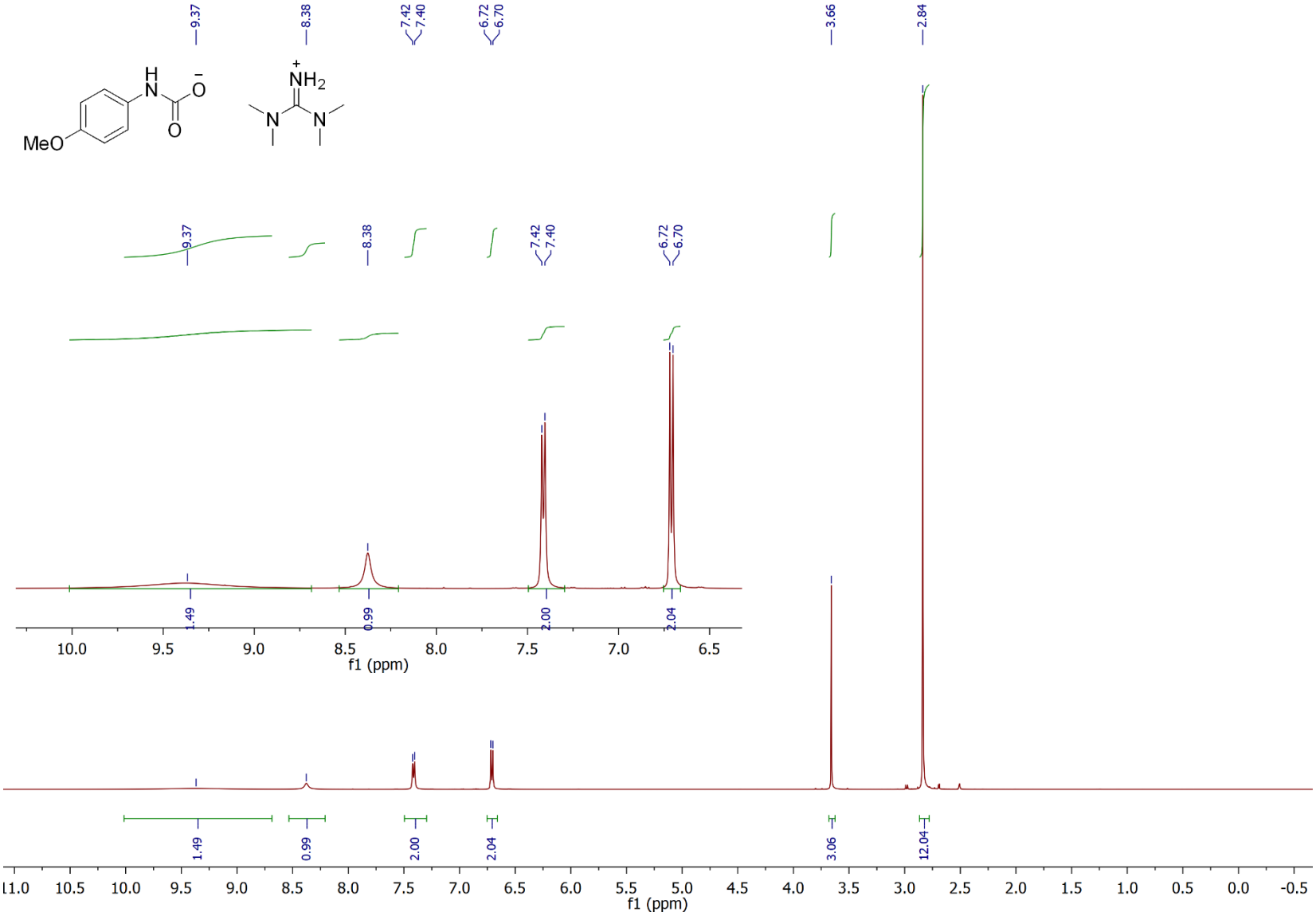

4-Methoxyaniline Quantitative $^{13}C\{^{1}H\}$

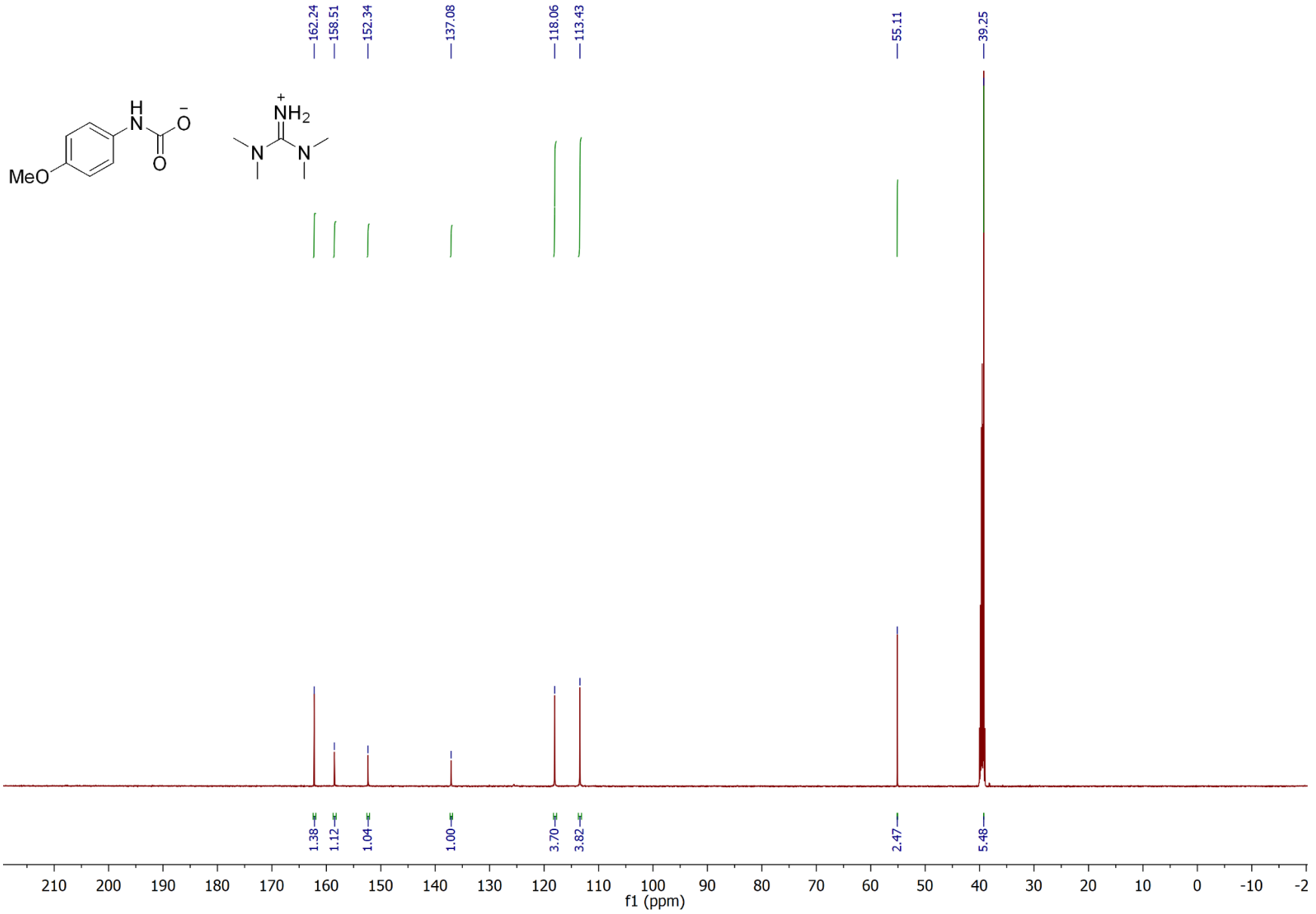

4-Methoxyaniline HMBC

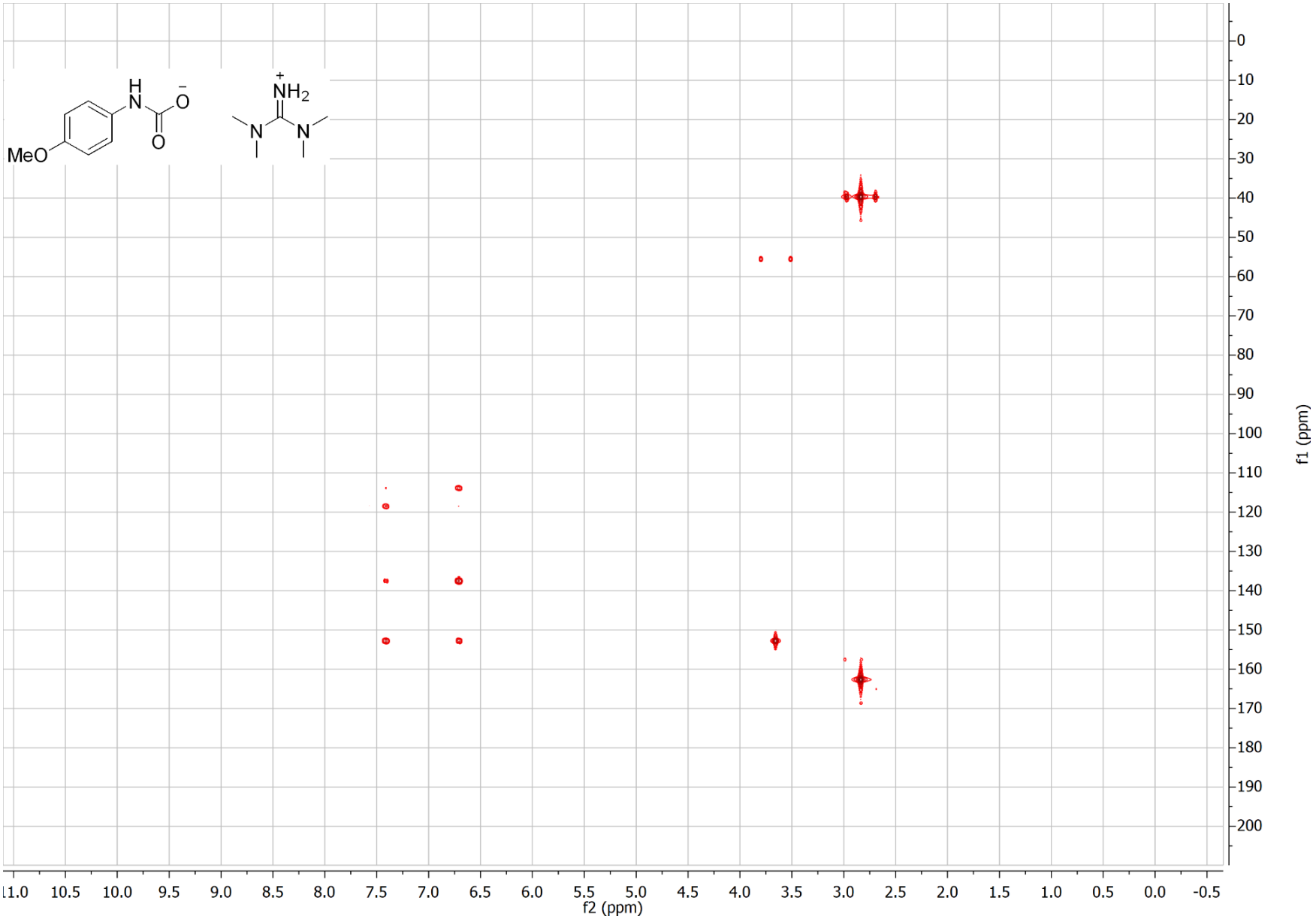

4-Chloroaniline ^{1}H

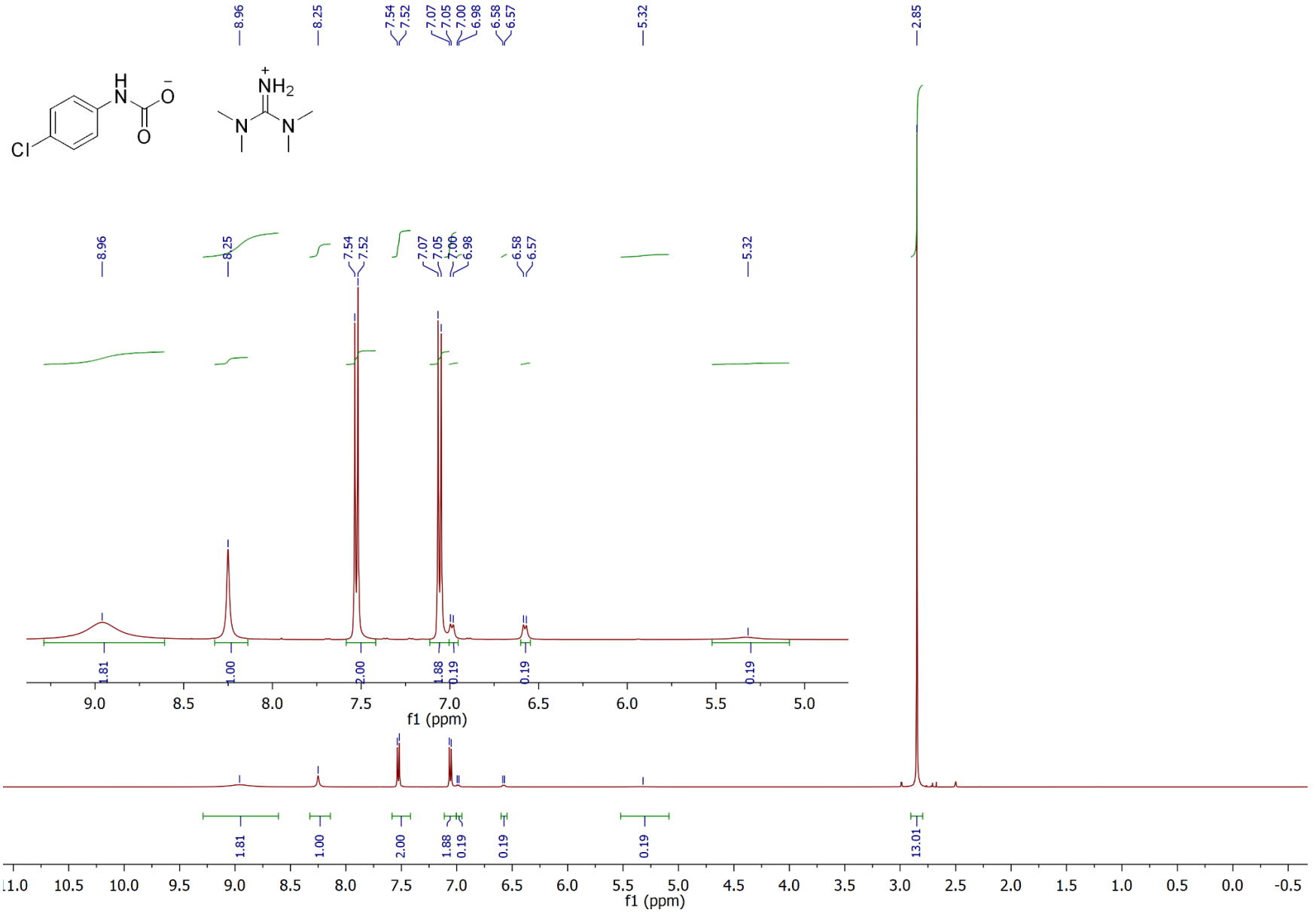

4-Chloroaniline ^{1}H (8 h later)

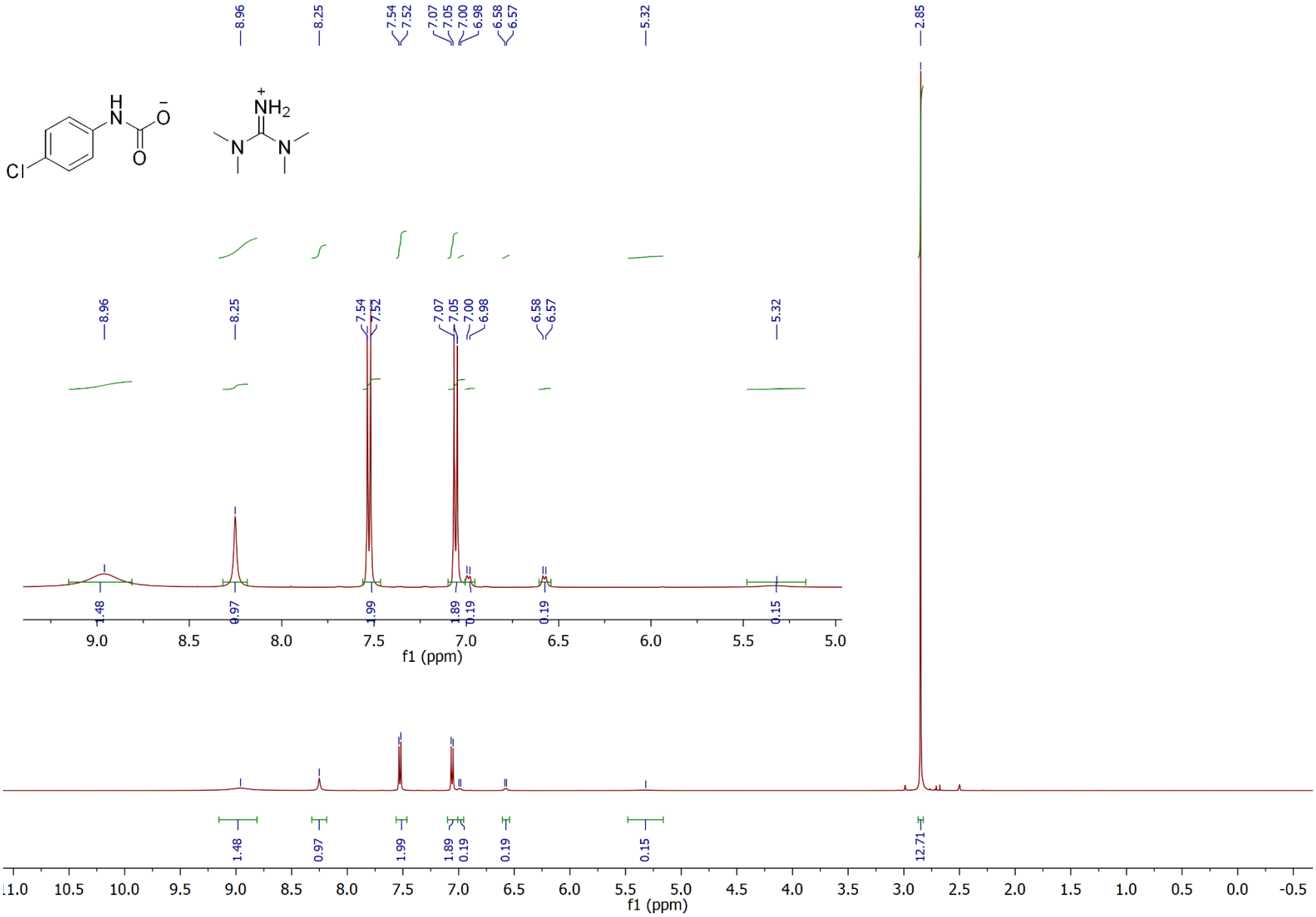

4-Chloroaniline Quantitative $^{13}C\{^{1}H\}$

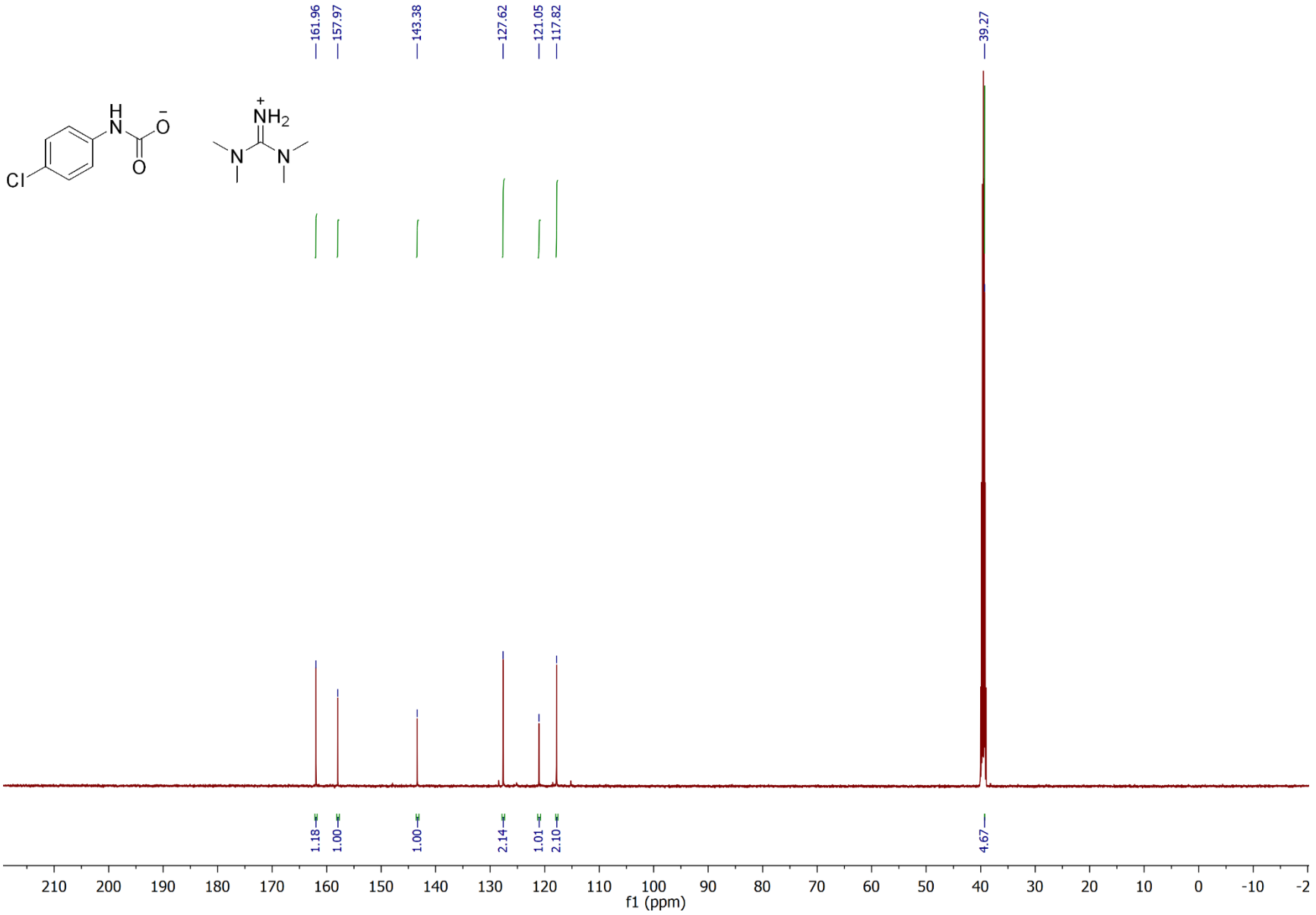

4-Chloroaniline HMBC

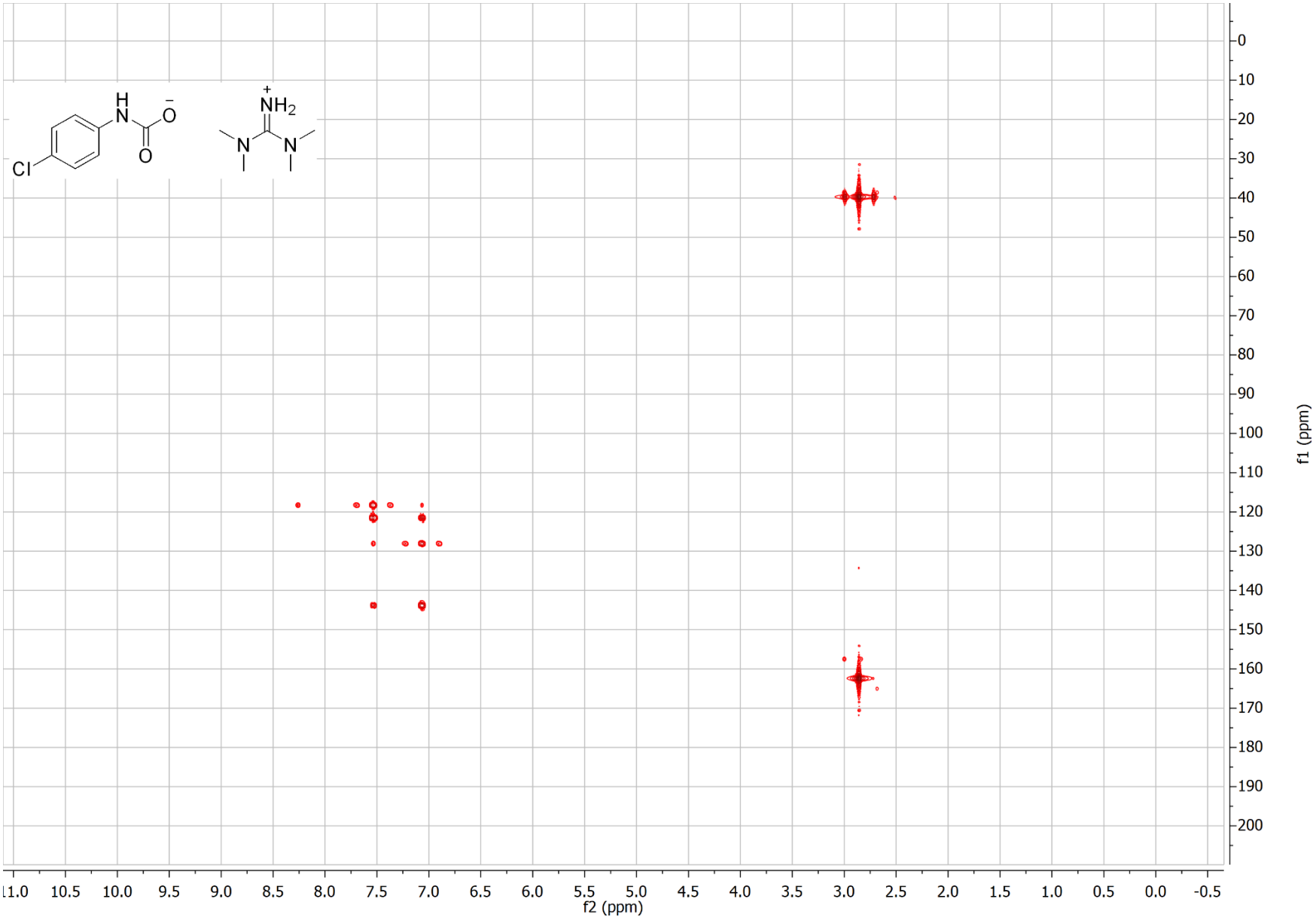

4-(Trifluoromethoxy)aniline ^{1}H

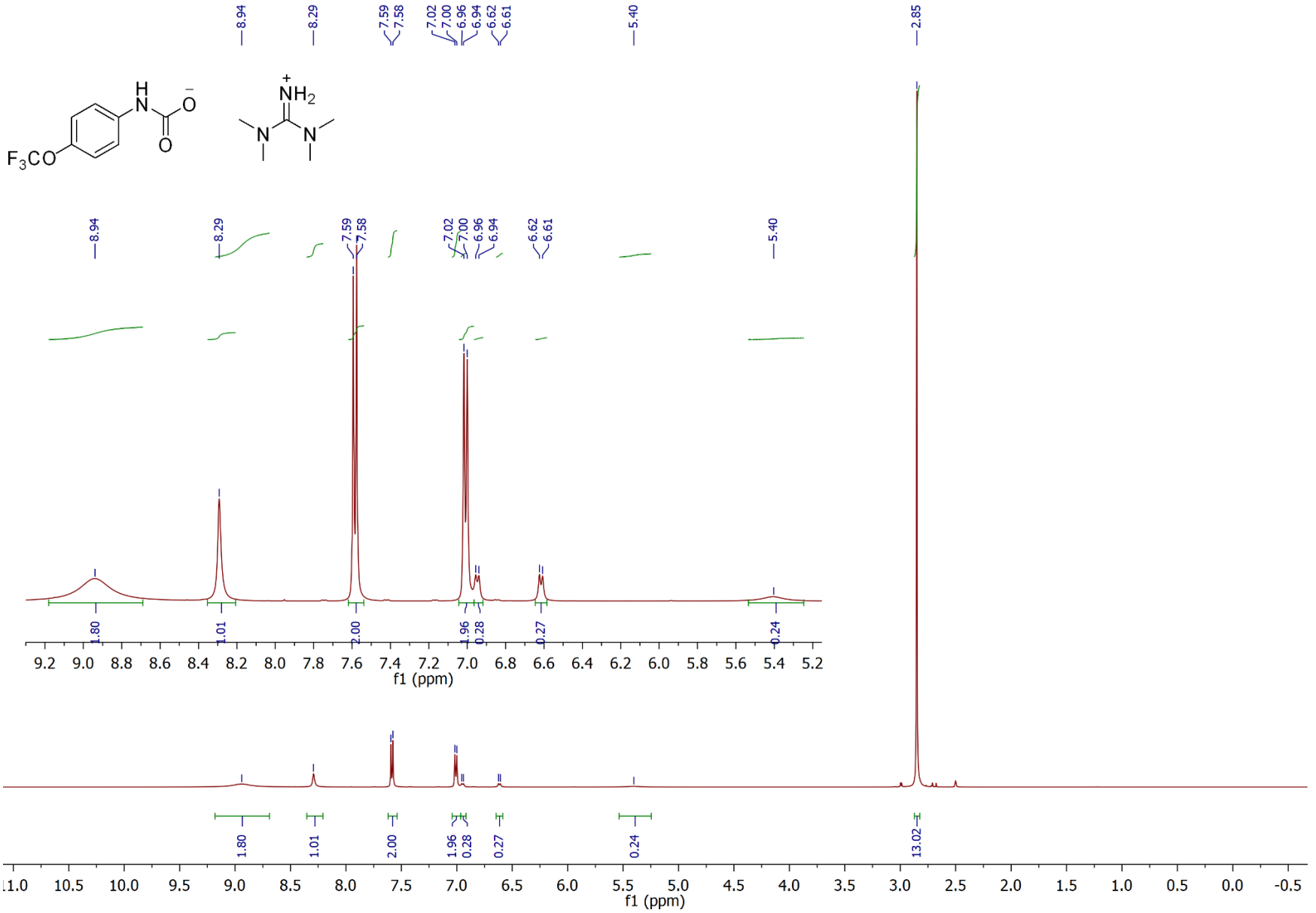

4-(Trifluoromethoxy)aniline Quantitative $^{13}C\{^{1}H\}$

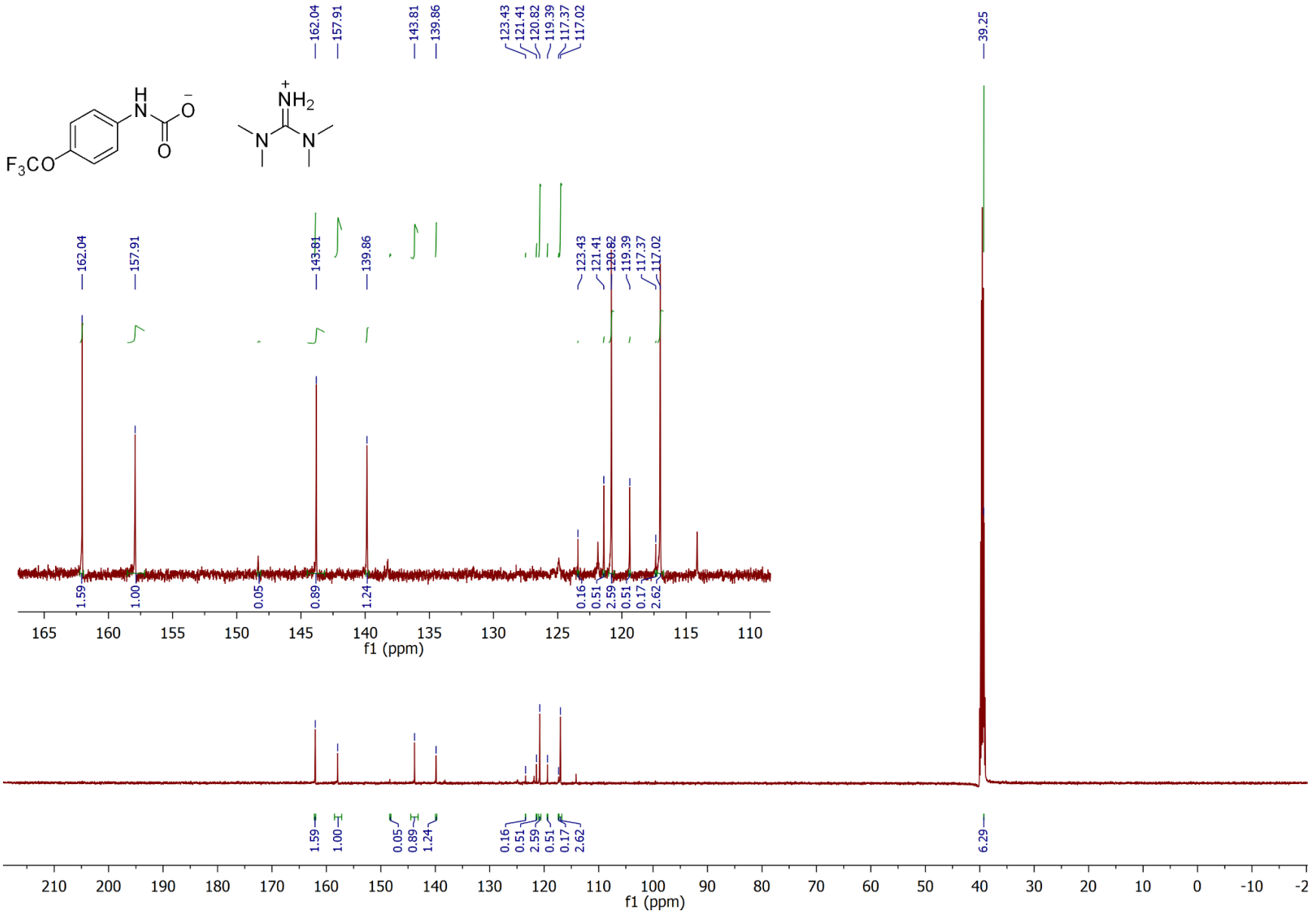

4-(Trifluoromethoxy)aniline Quantitative $^{19}F\{^{1}H\}$ (12 h later)

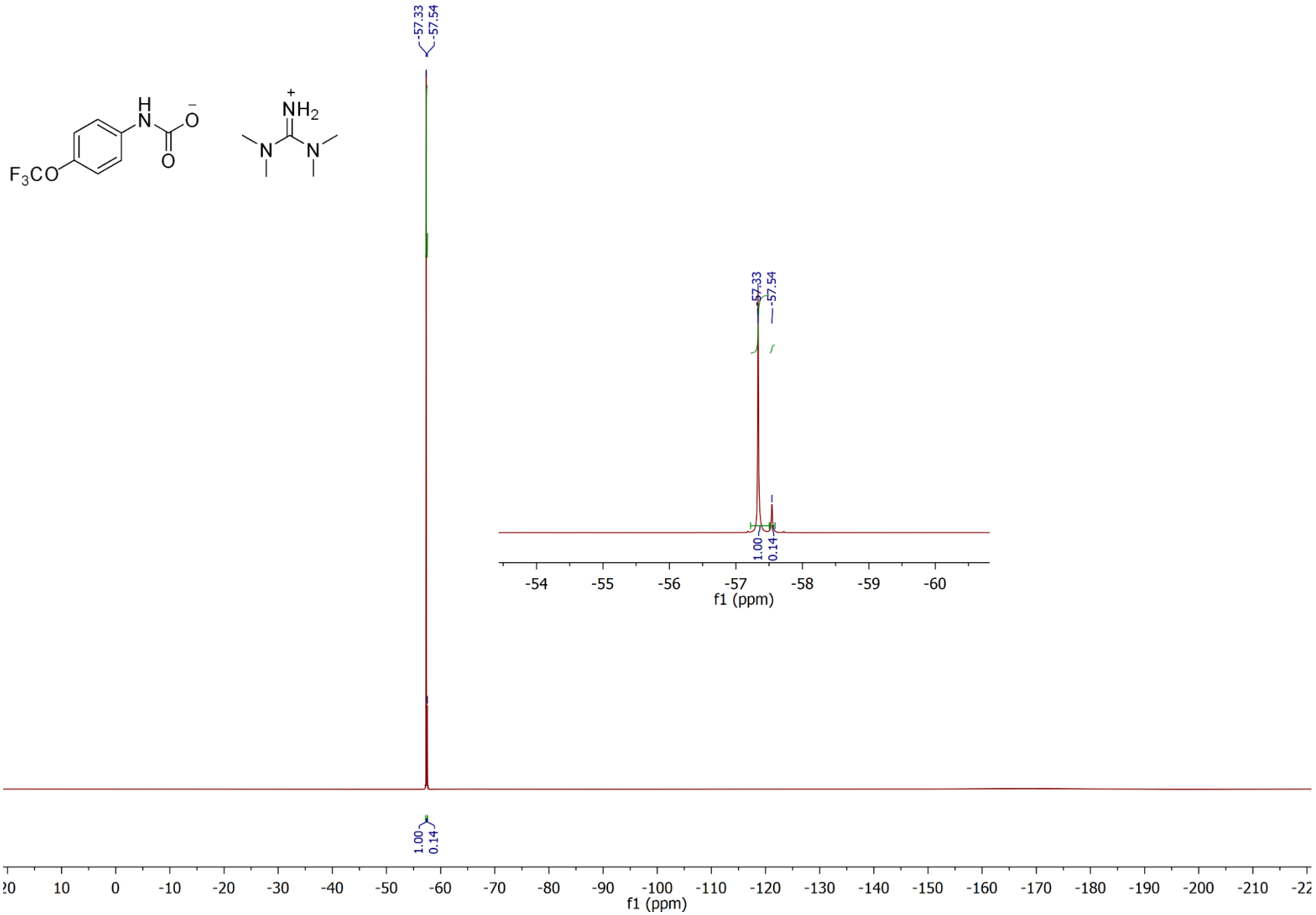

4-(Trifluoromethyl)aniline ^{1}H

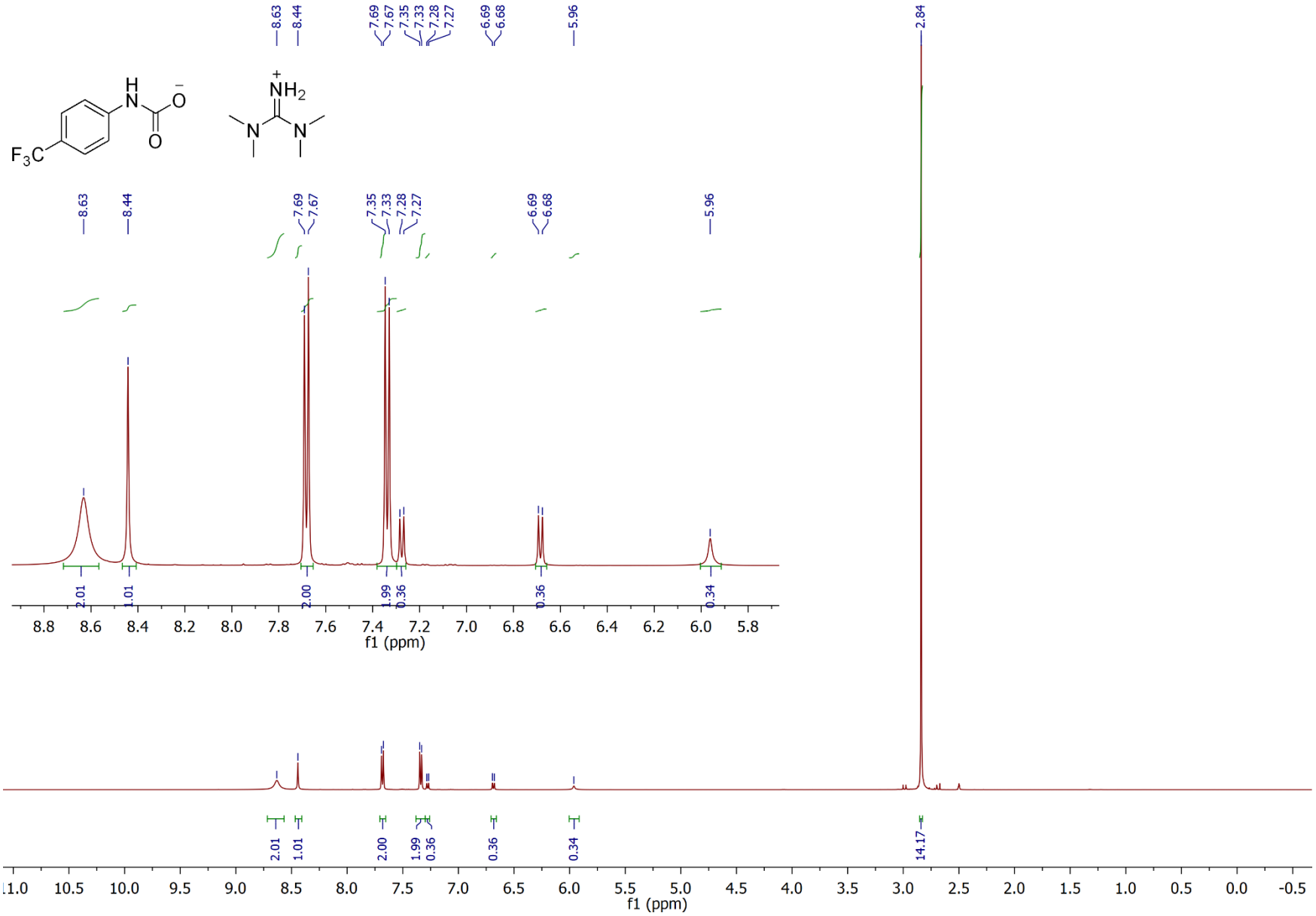

4-(Trifluoromethyl)aniline ^{1}H (12 h later)

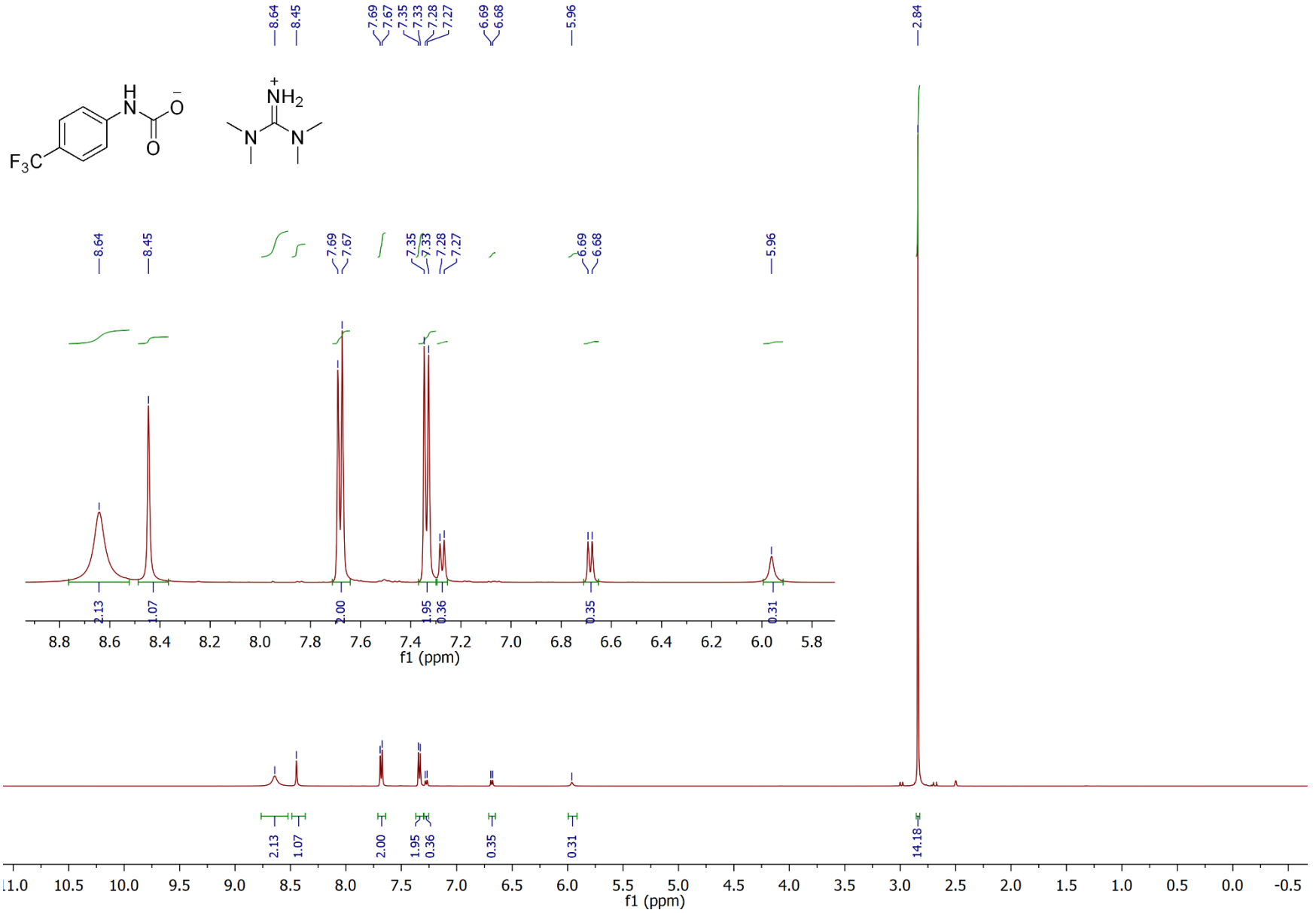

4-(Trifluoromethyl)aniline Quantitative $^{13}C\{^{1}H\}$

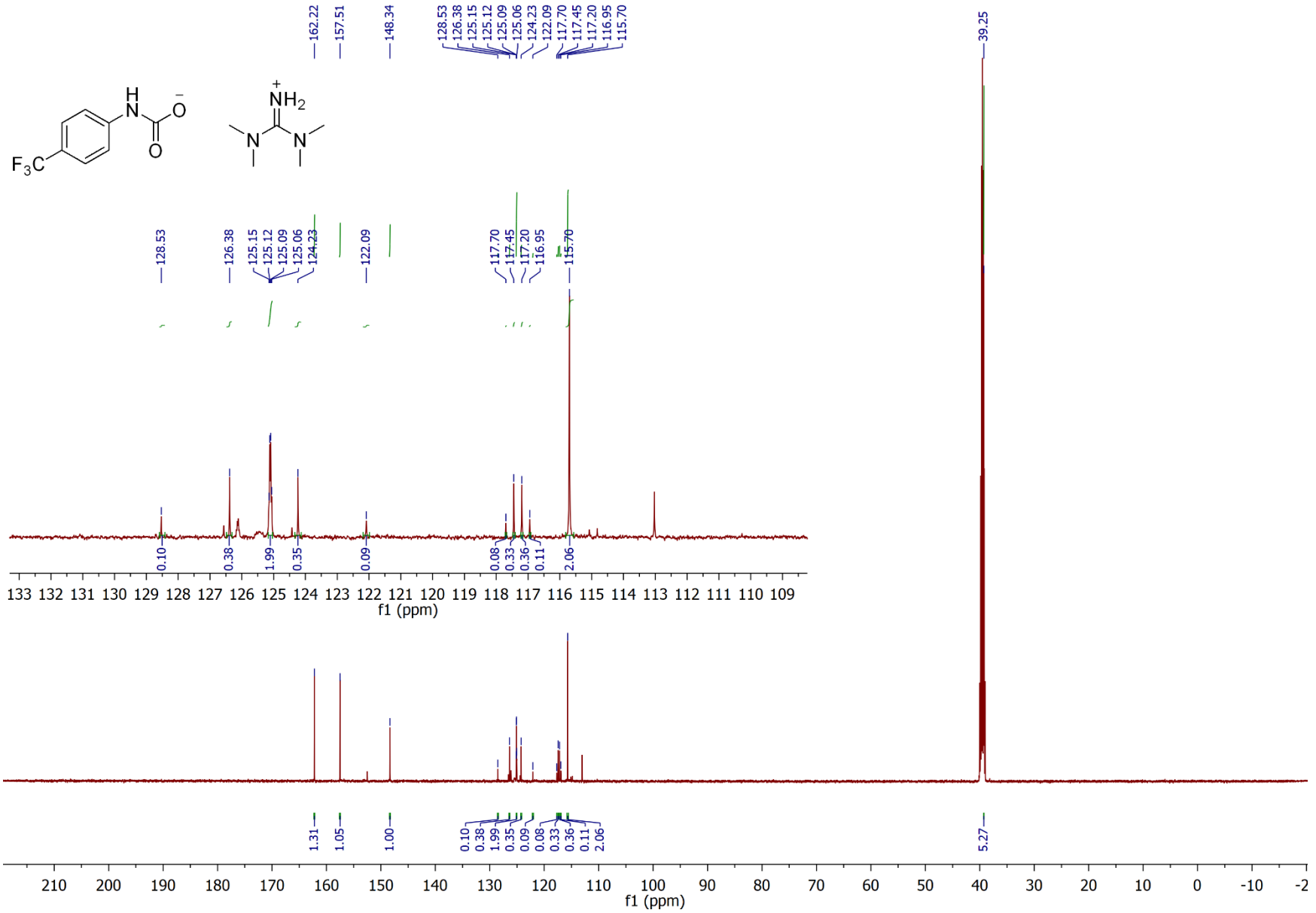

4-(Trifluoromethyl)aniline Quantitative $^{19}F\{^{1}H\}$

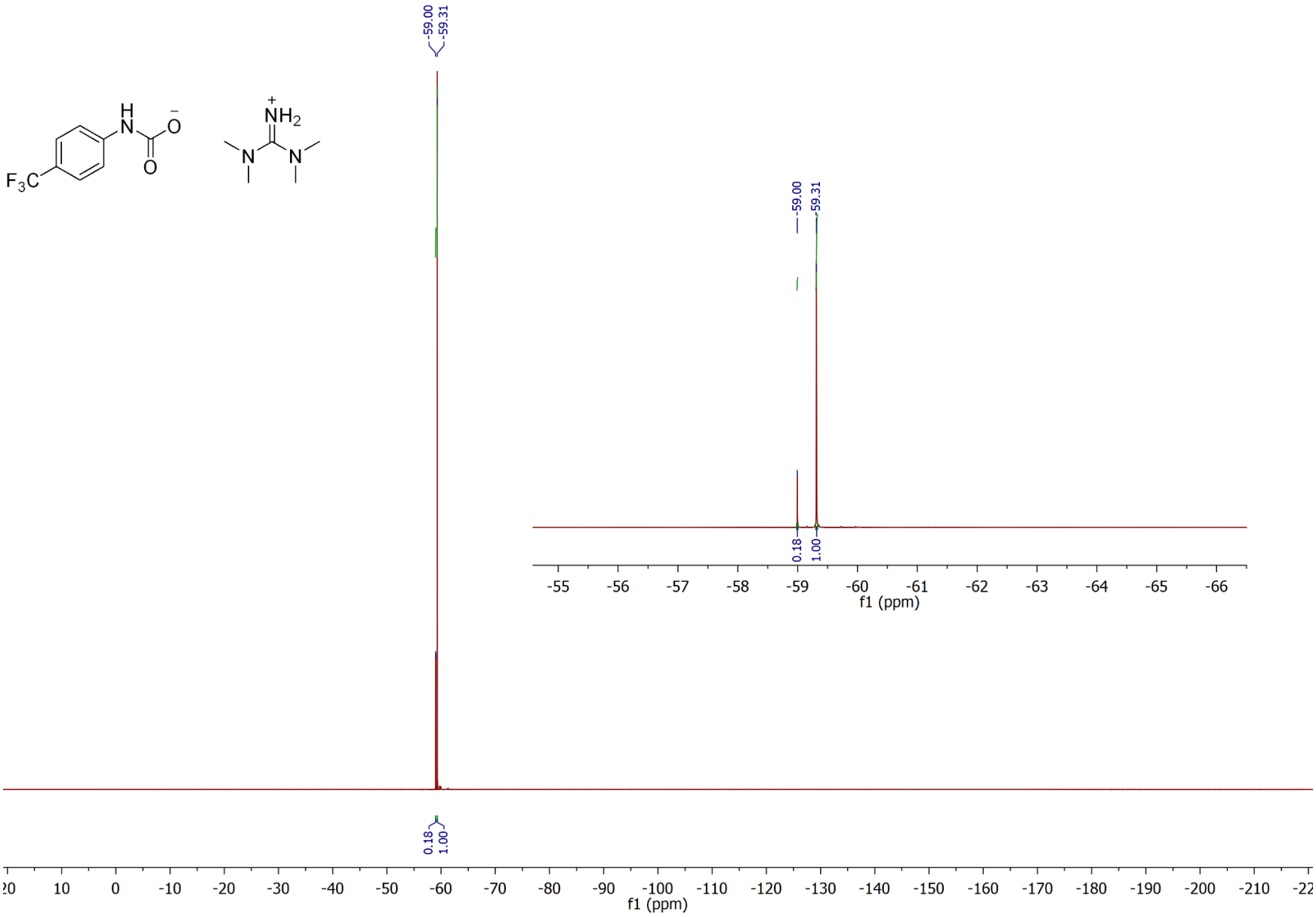

4-(Trifluoromethyl)aniline Quantitative $^{19}F\{^{1}H\}$ (12 later)

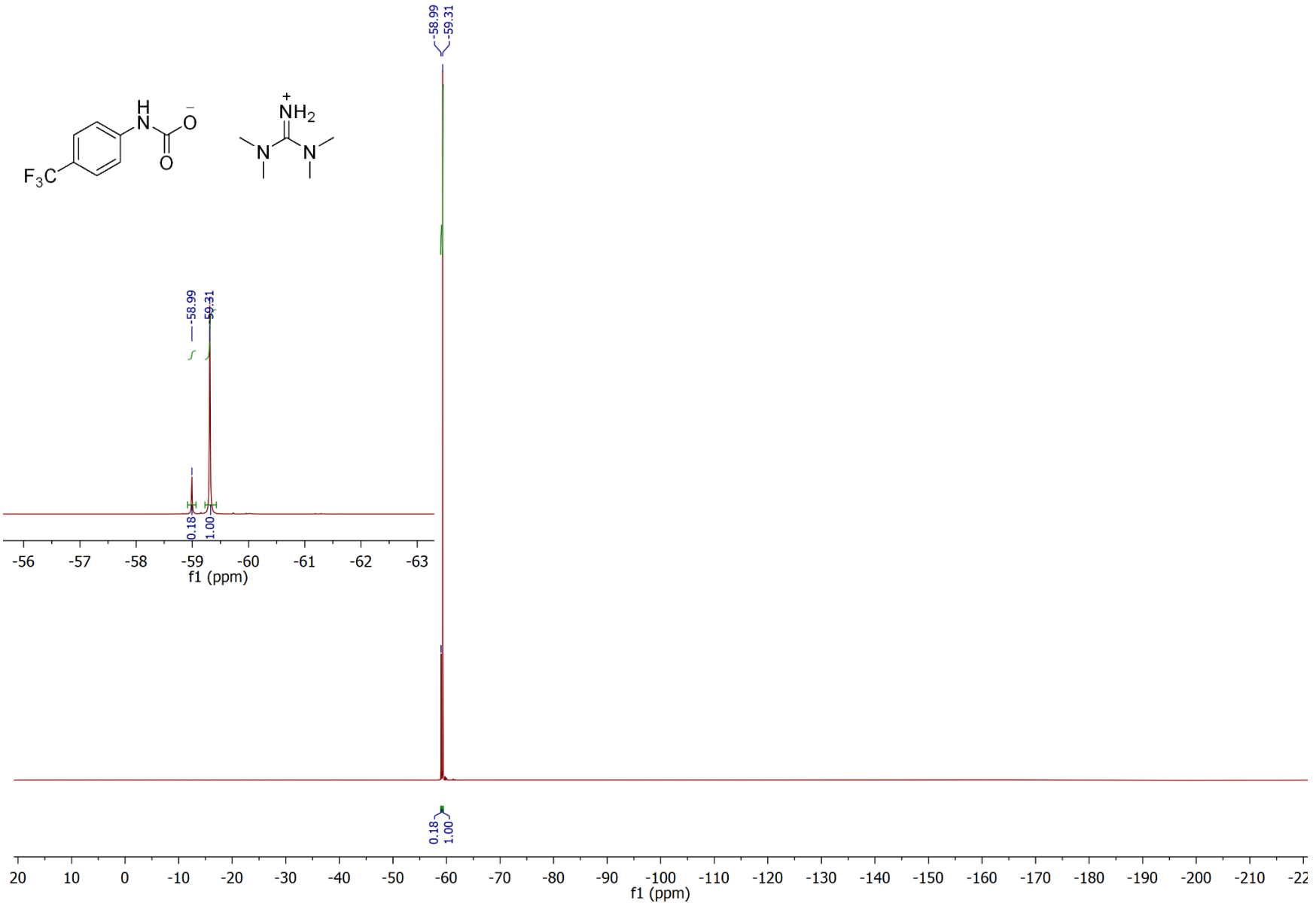

4-(Trifluoromethyl)aniline HMBC

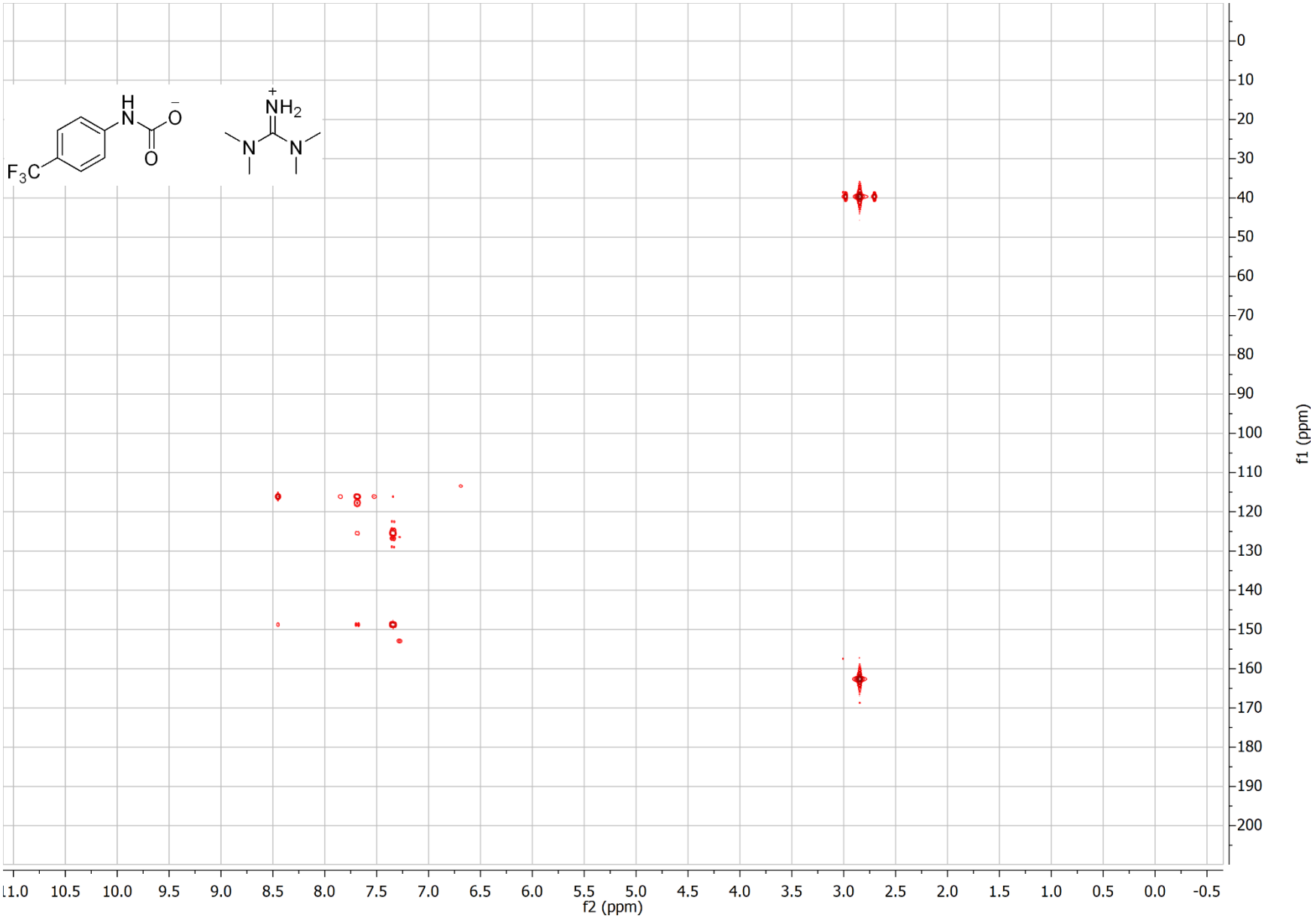

4-Cyanoaniline ^{1}H

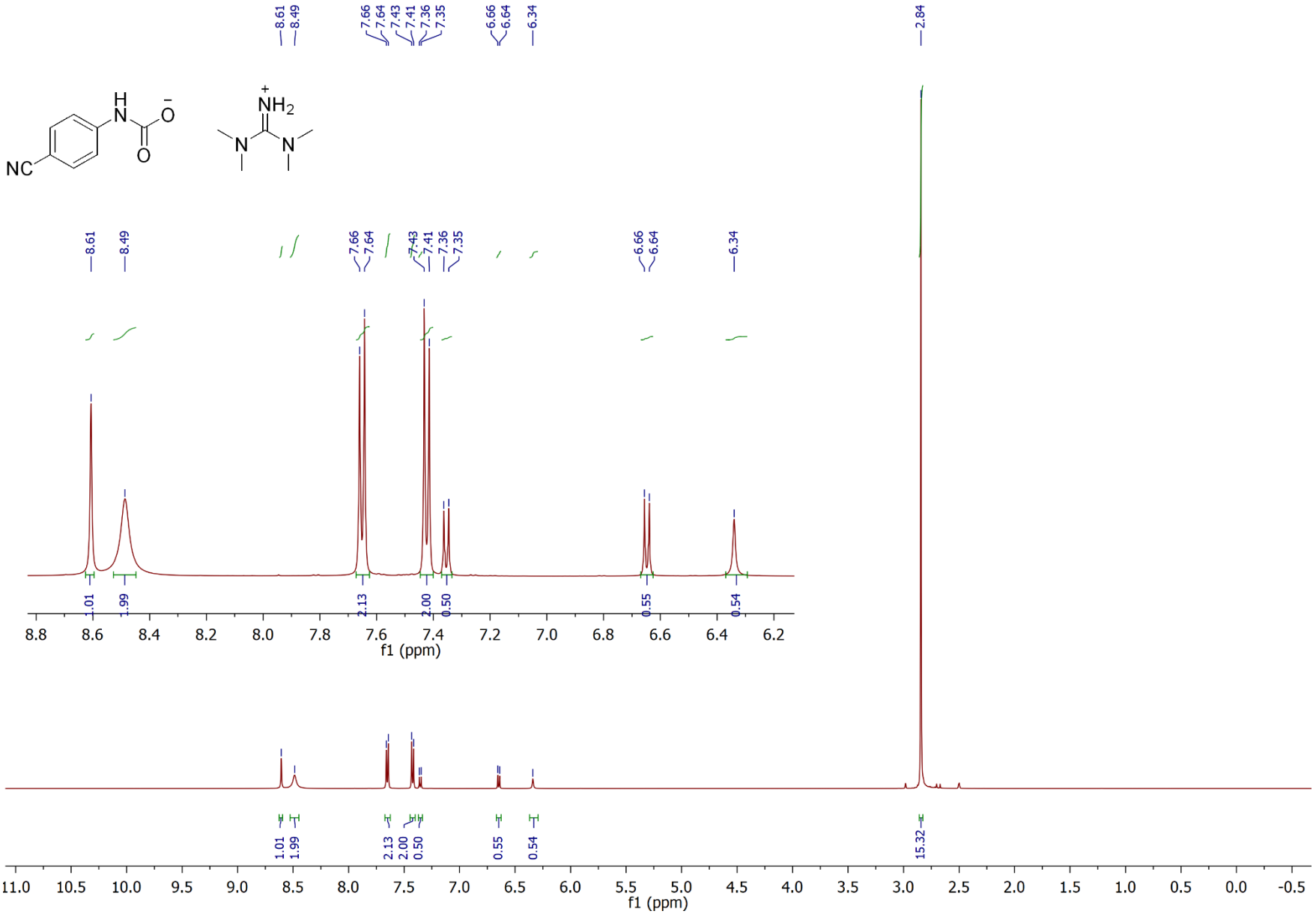

4-Cyanoaniline ^{1}H (8 h later)

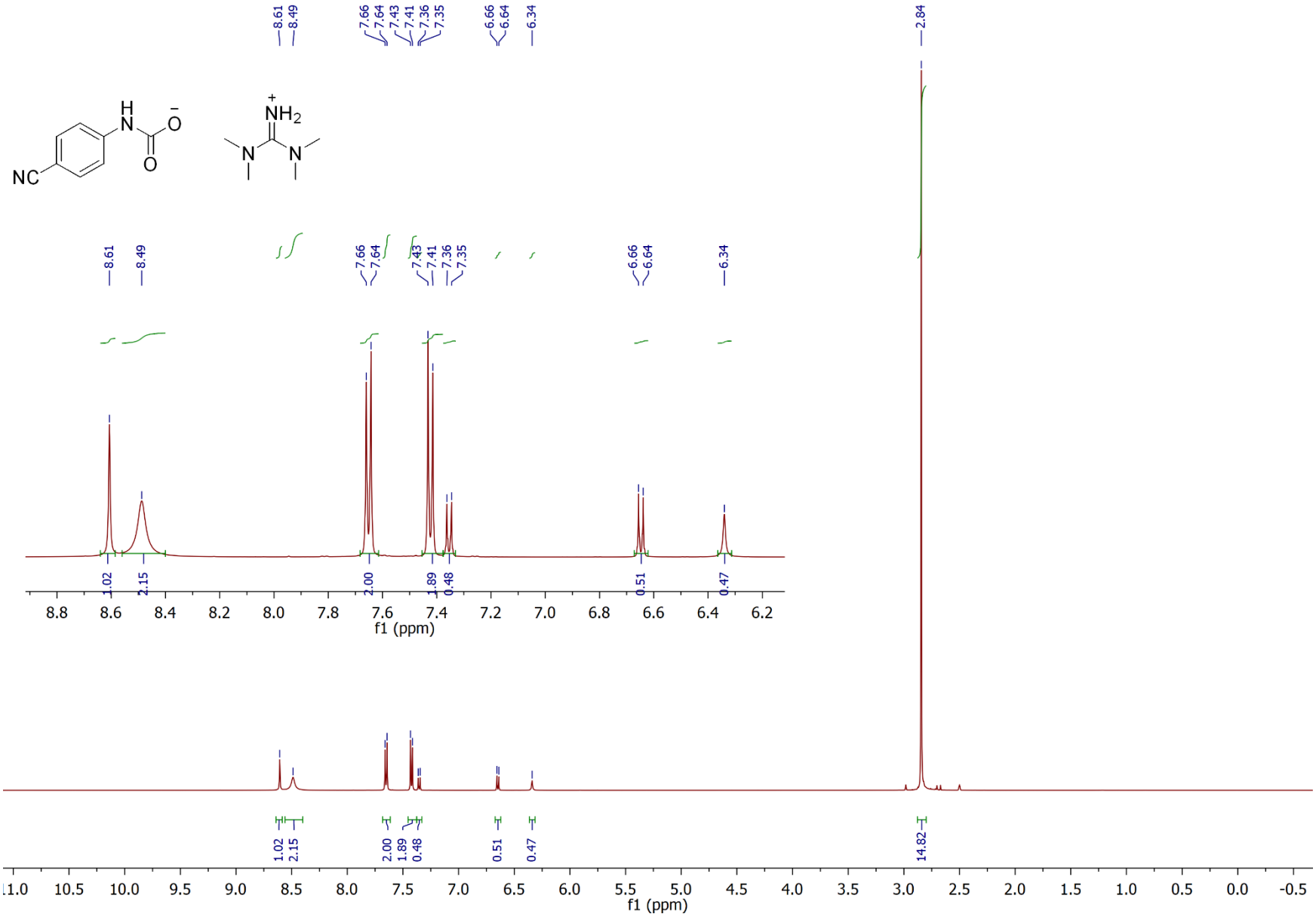

4-Cyanoaniline Quantitative $^{13}C\{^{1}H\}$

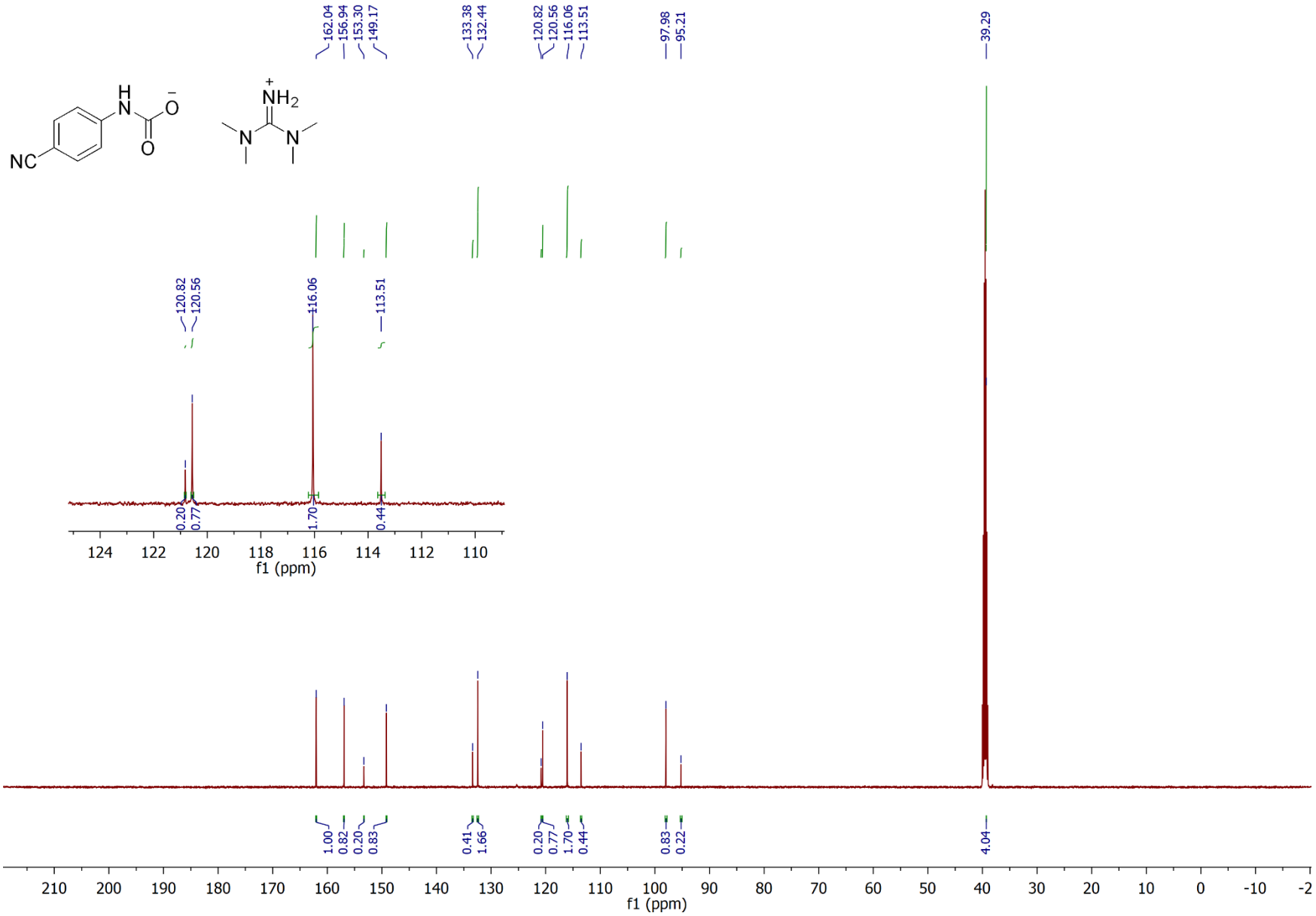

4-Cyanoaniline HMBC

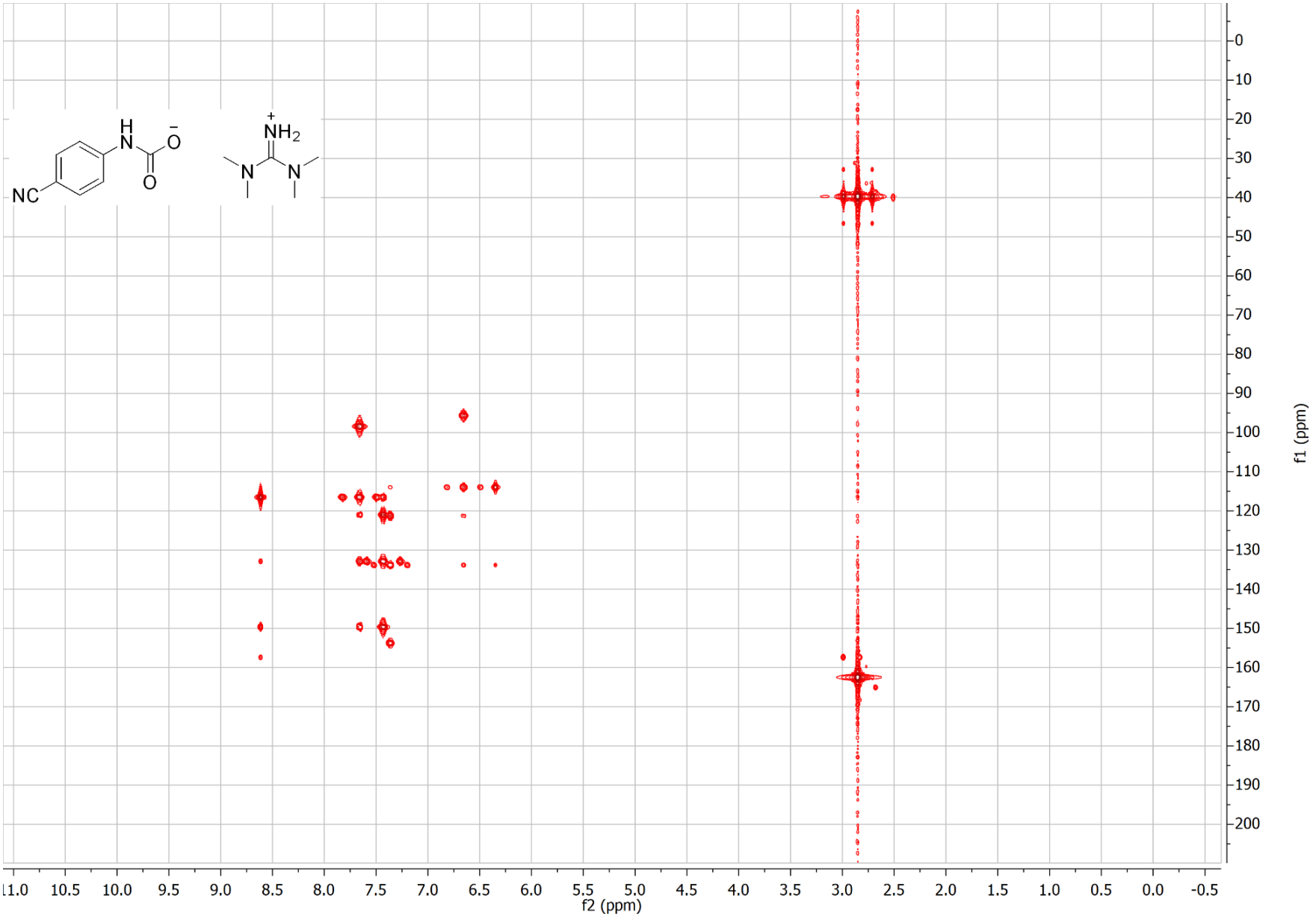

4-Nitroaniline ^{1}H

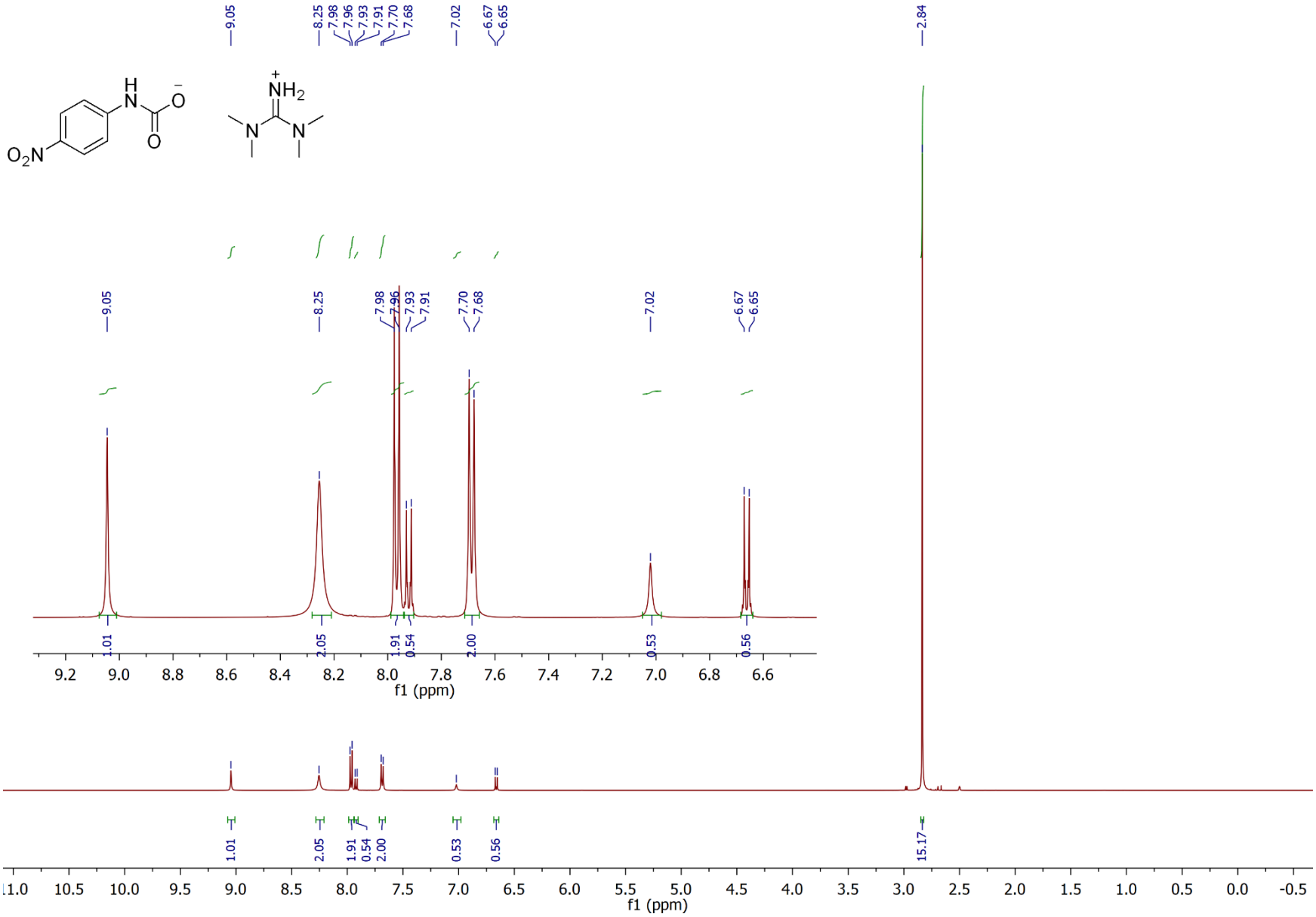

4-Nitroaniline ^{1}H (8 h later)

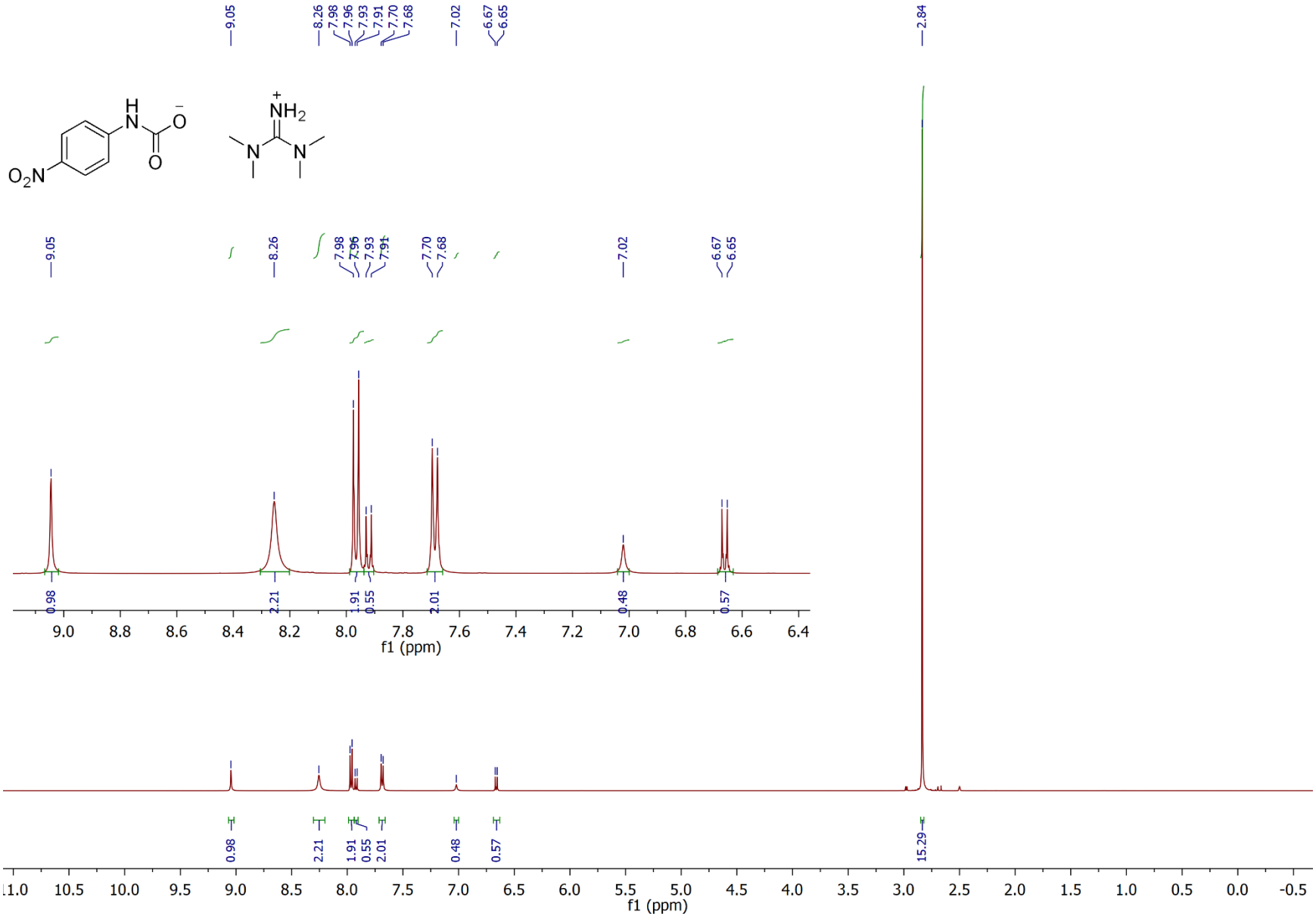

4-Nitroaniline Quantitative $^{13}C\{^{1}H\}$

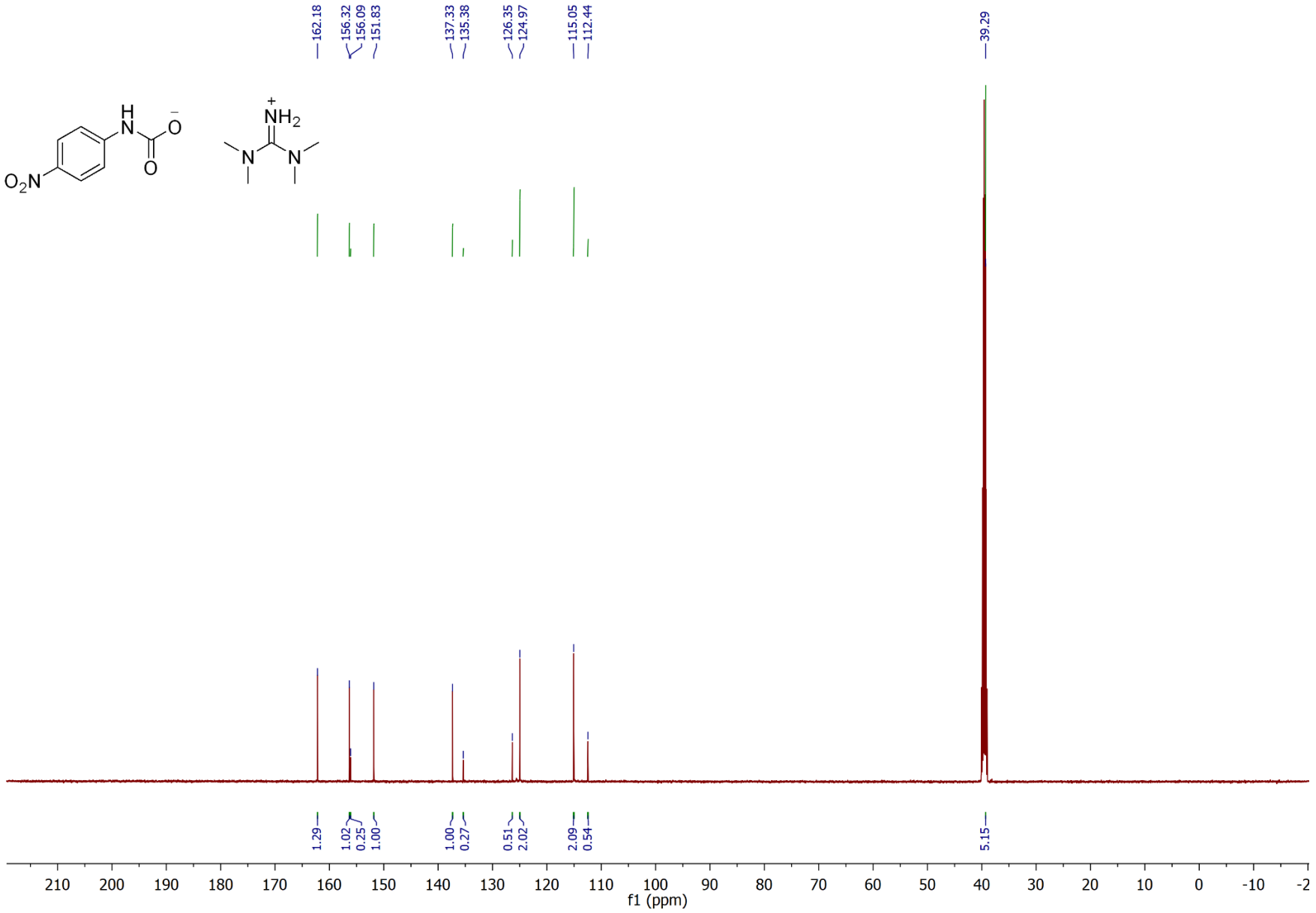

4-Nitroaniline HMBC

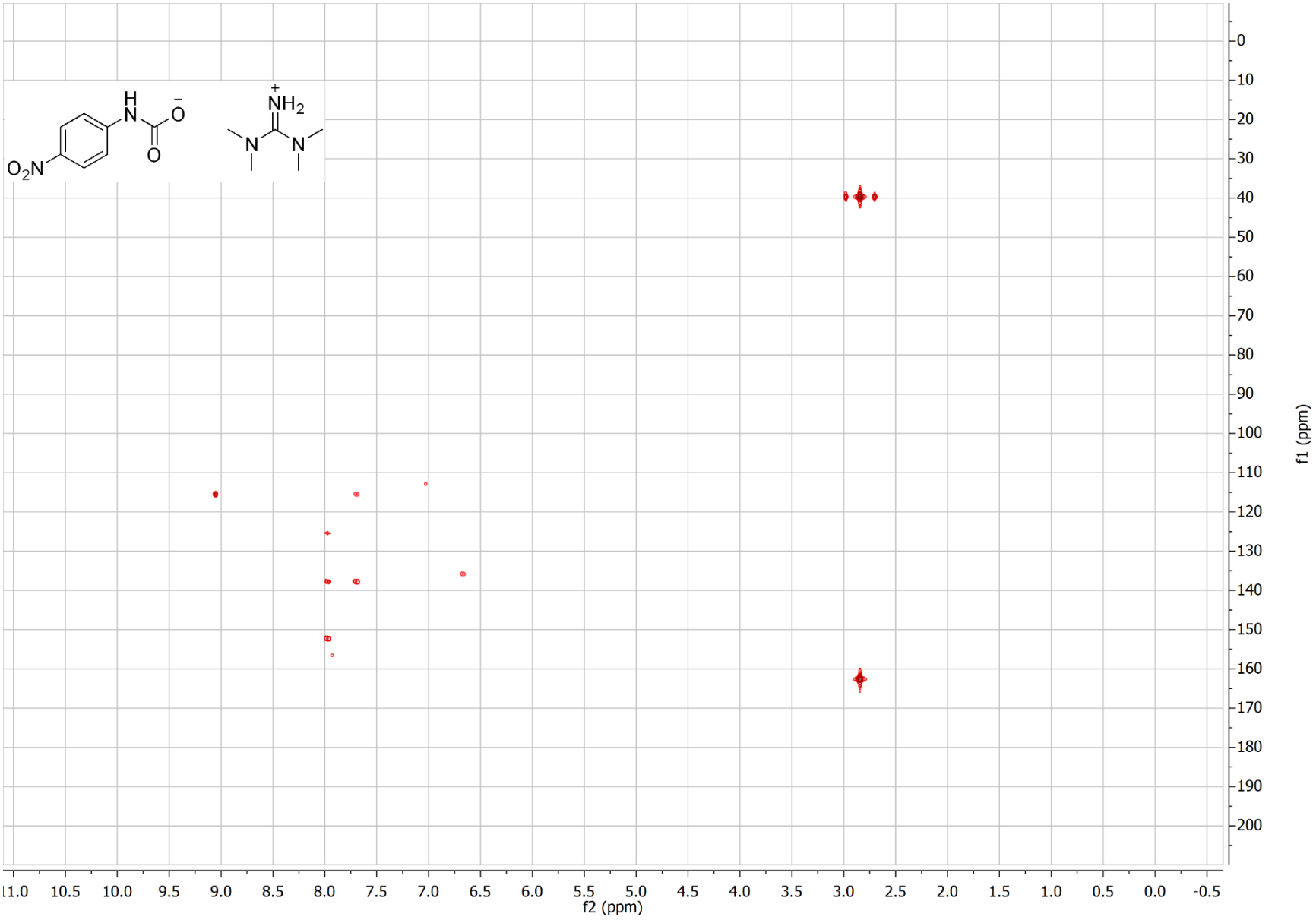

4-(Trifluoromethylsulfonyl)aniline ^{1}H

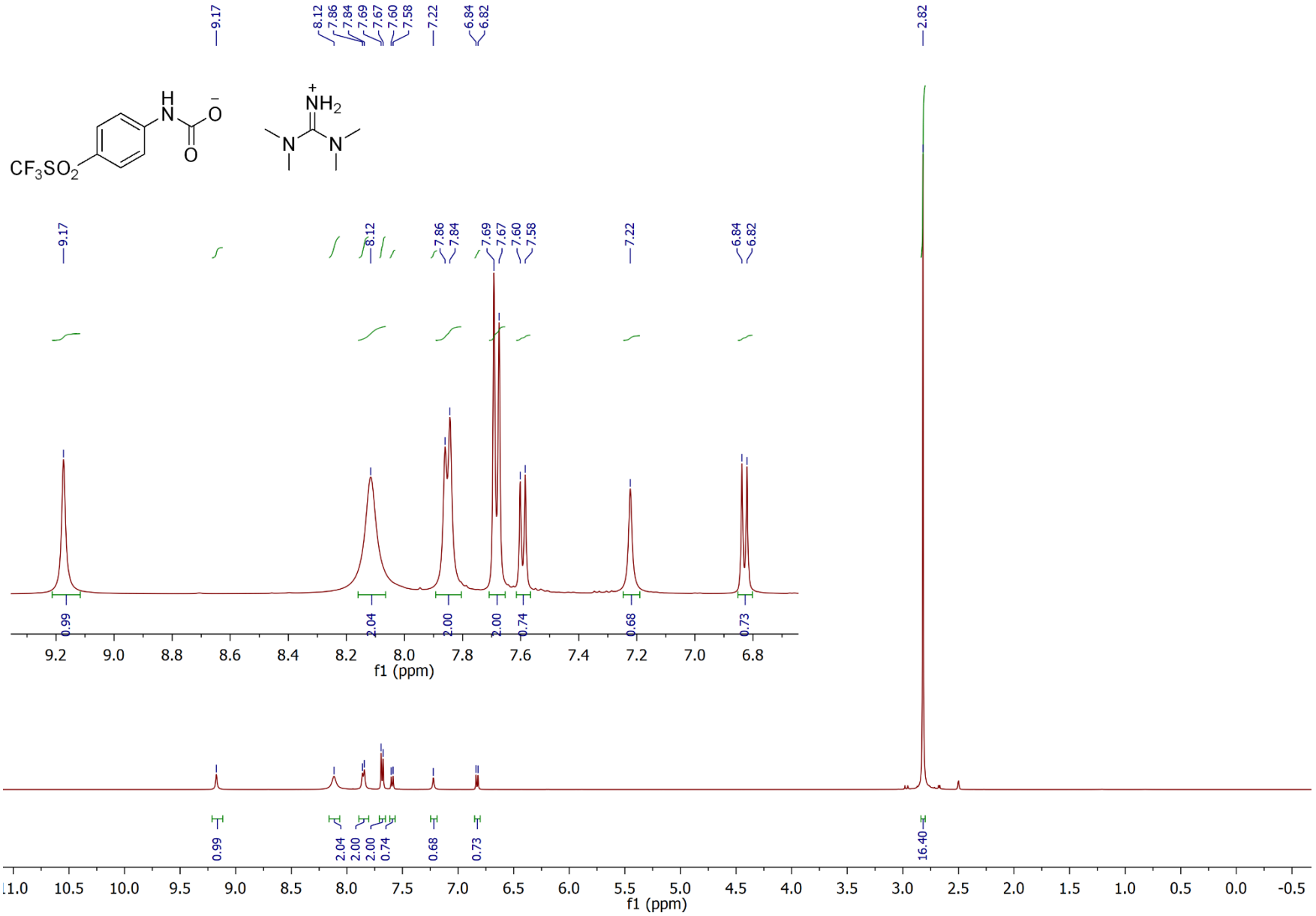

4-(Trifluoromethylsulfonyl)aniline Quantitative $^{13}C\{^{1}H\}$

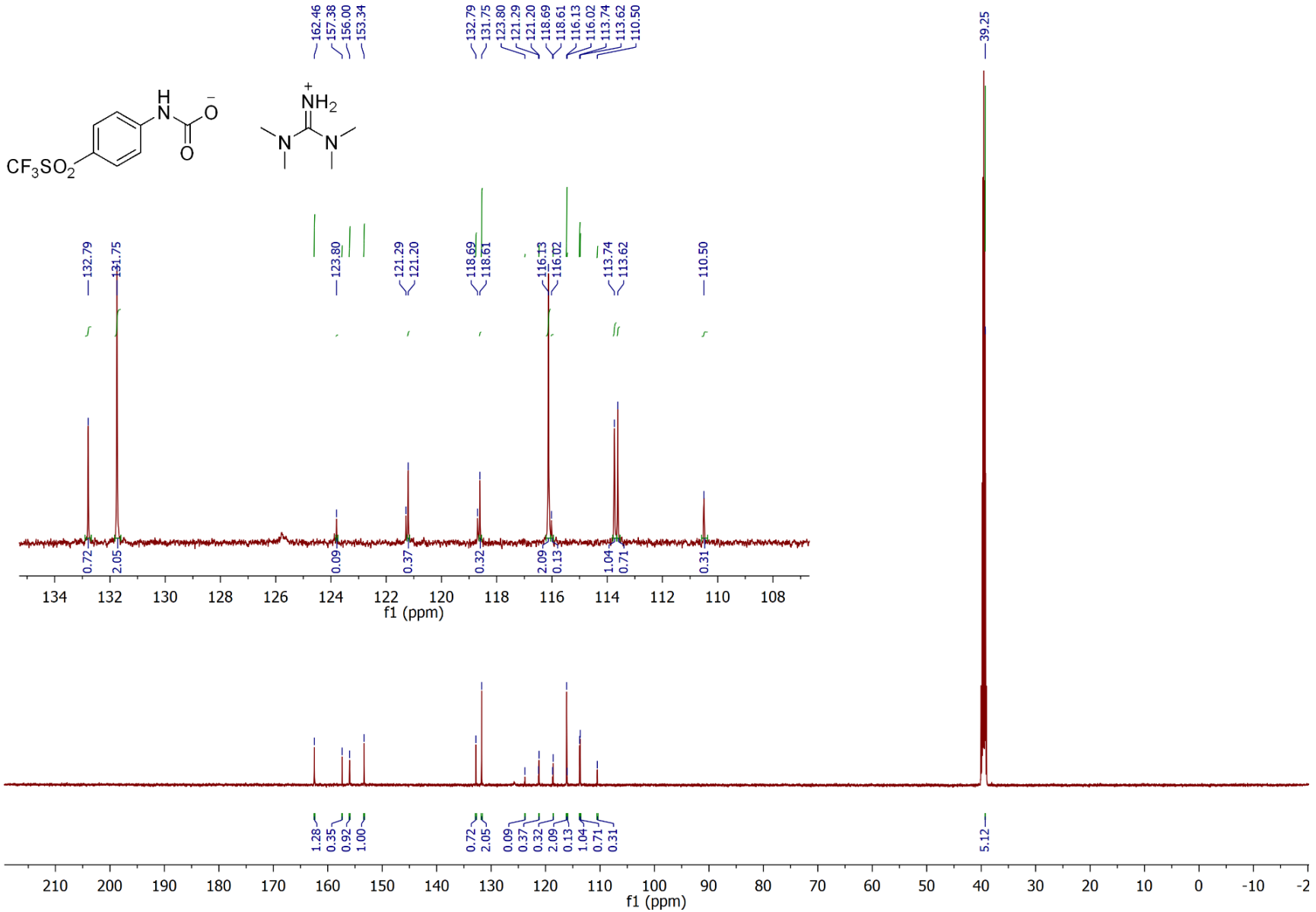

4-(Trifluoromethylsulfonyl)aniline HMBC

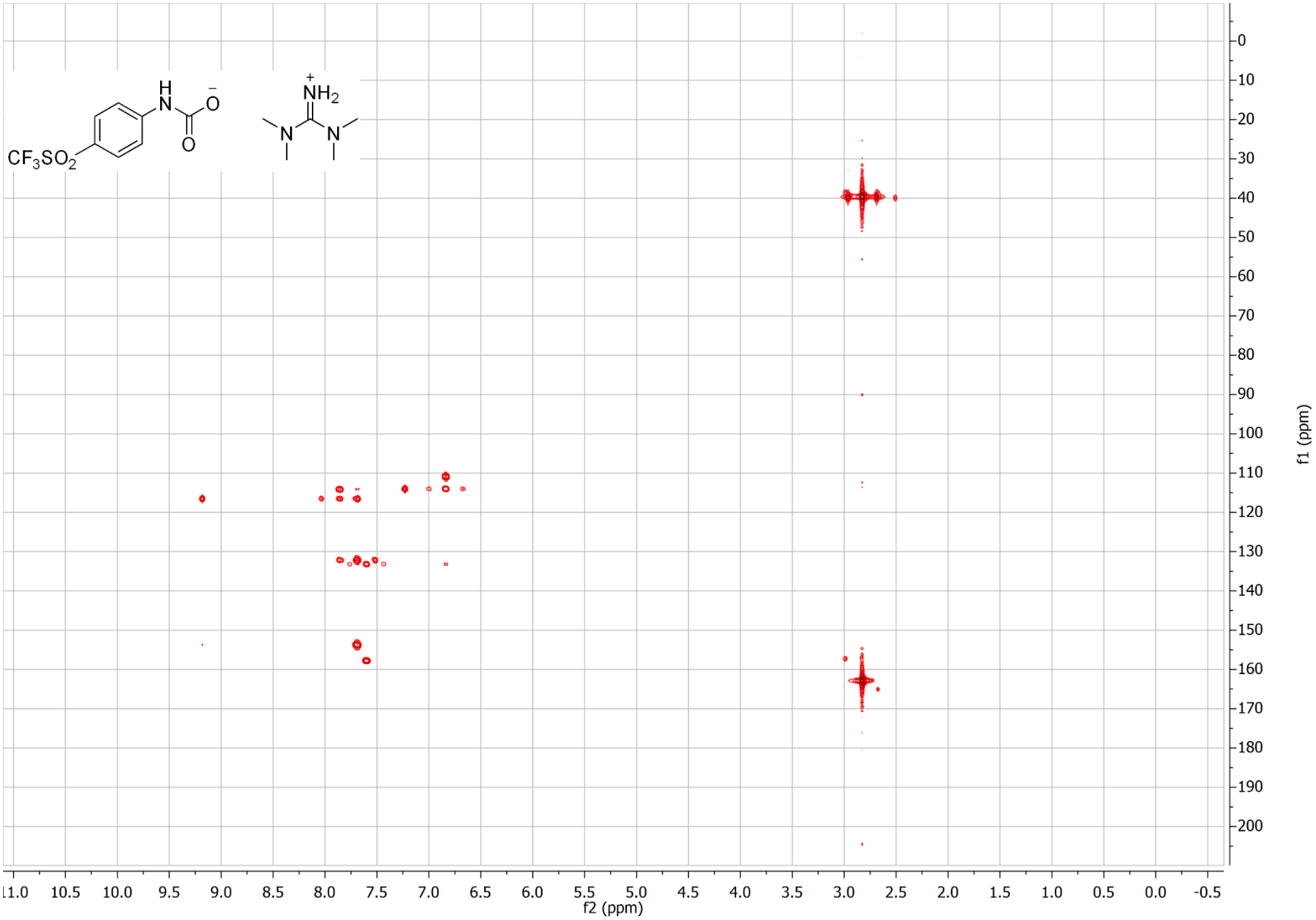

4-(Trifluoromethylsulfonyl)aniline Quantitative $^{19}F\{^{1}H\}$

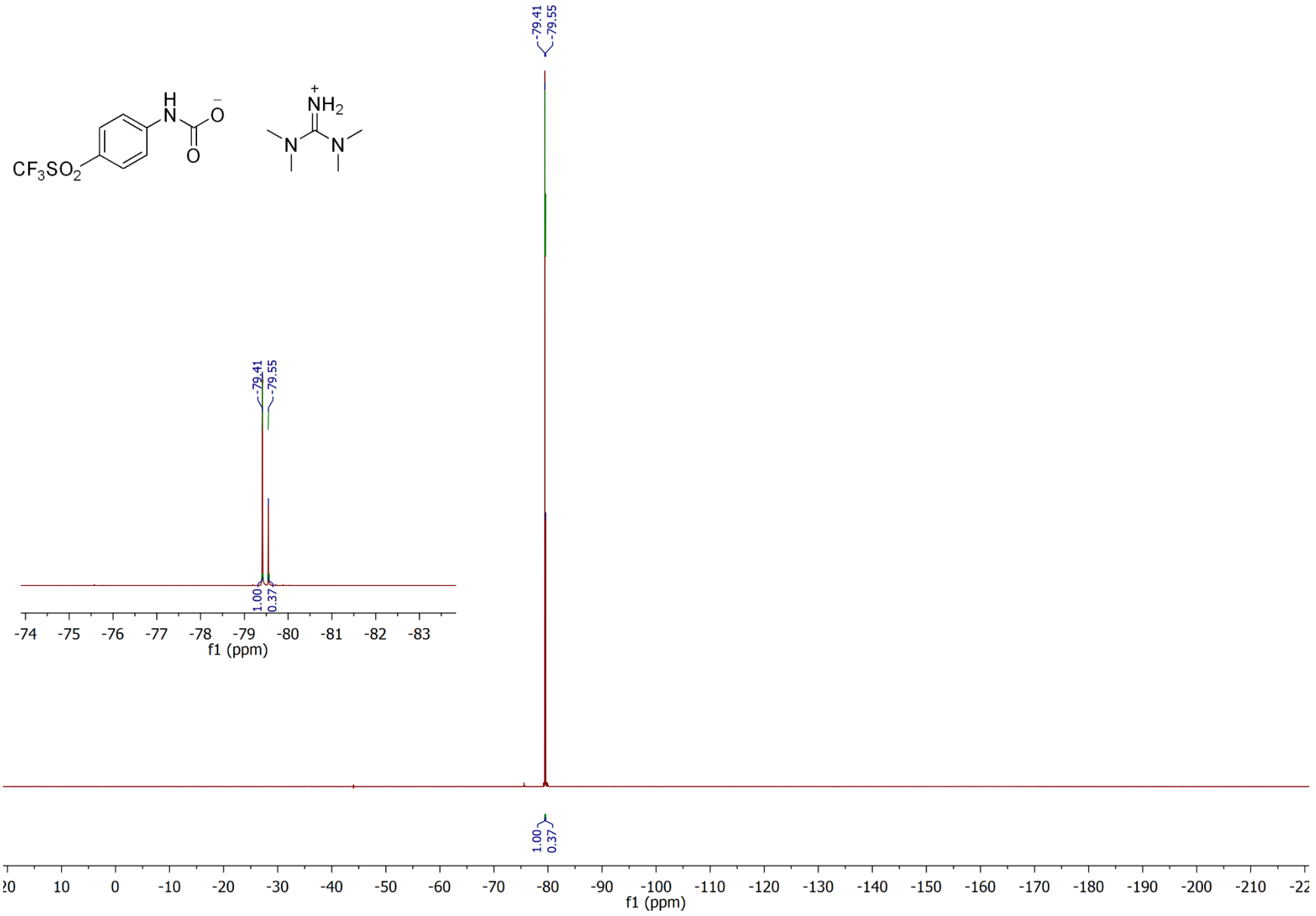

4-(Trifluoromethylsulfonyl)aniline Quantitative $^{19}F\{^{1}H\}$ (12 later)

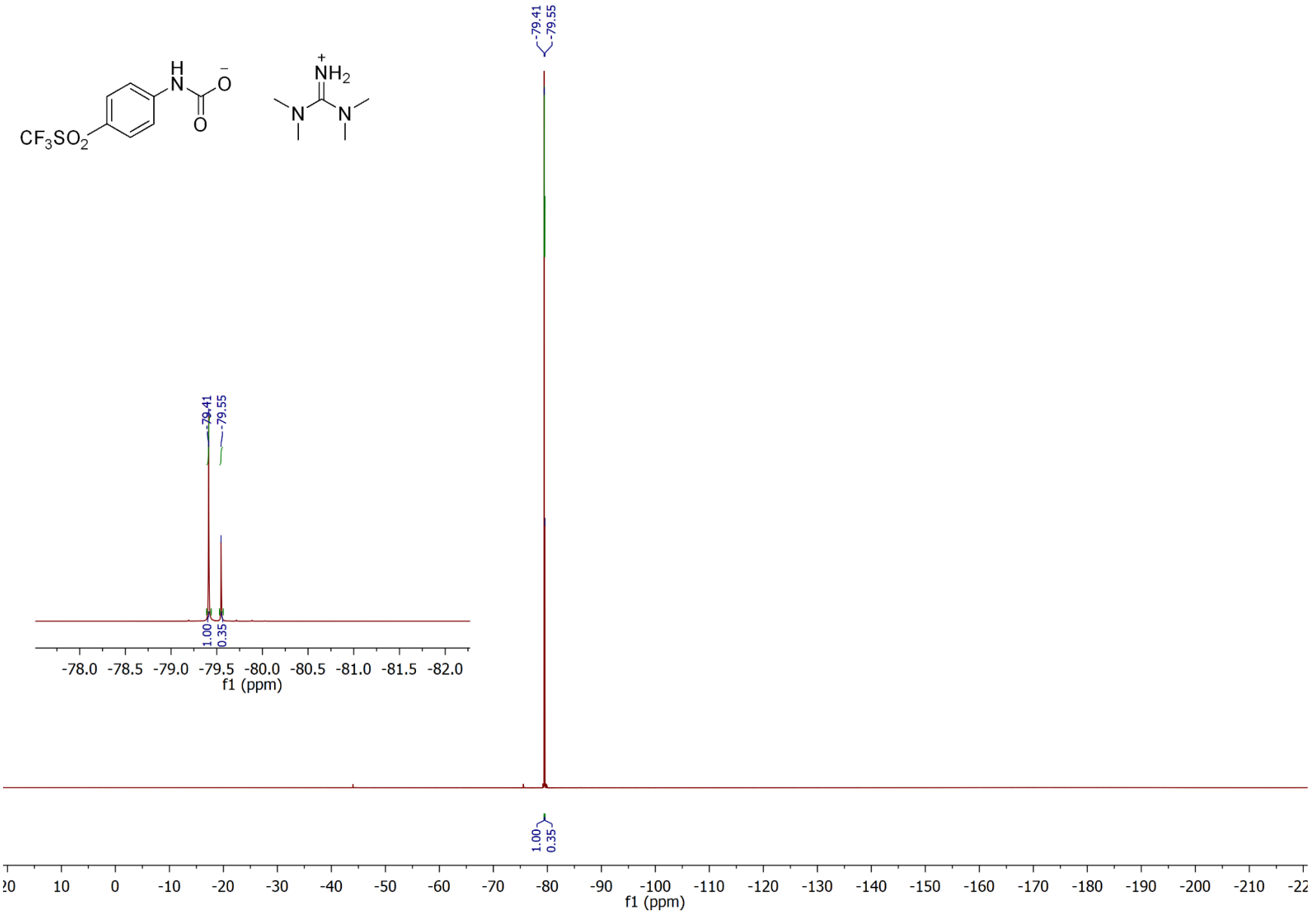

Effect of Base: 4-Nitroaniline (no added base, under Ar) ^{1}H

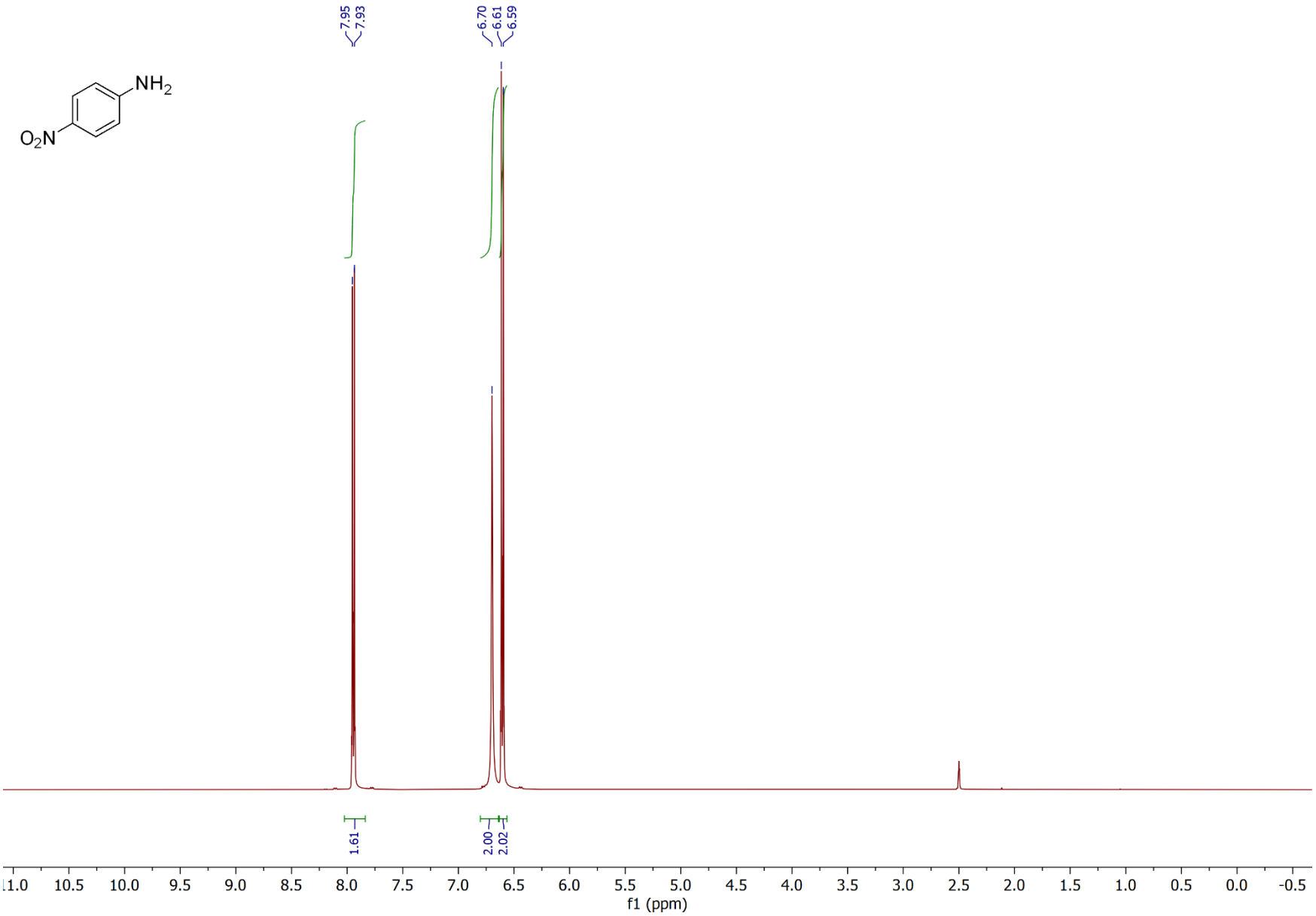

Effect of Base: 4-Nitroaniline (no added base, under Ar) $^{13}C\{^{1}H\}$

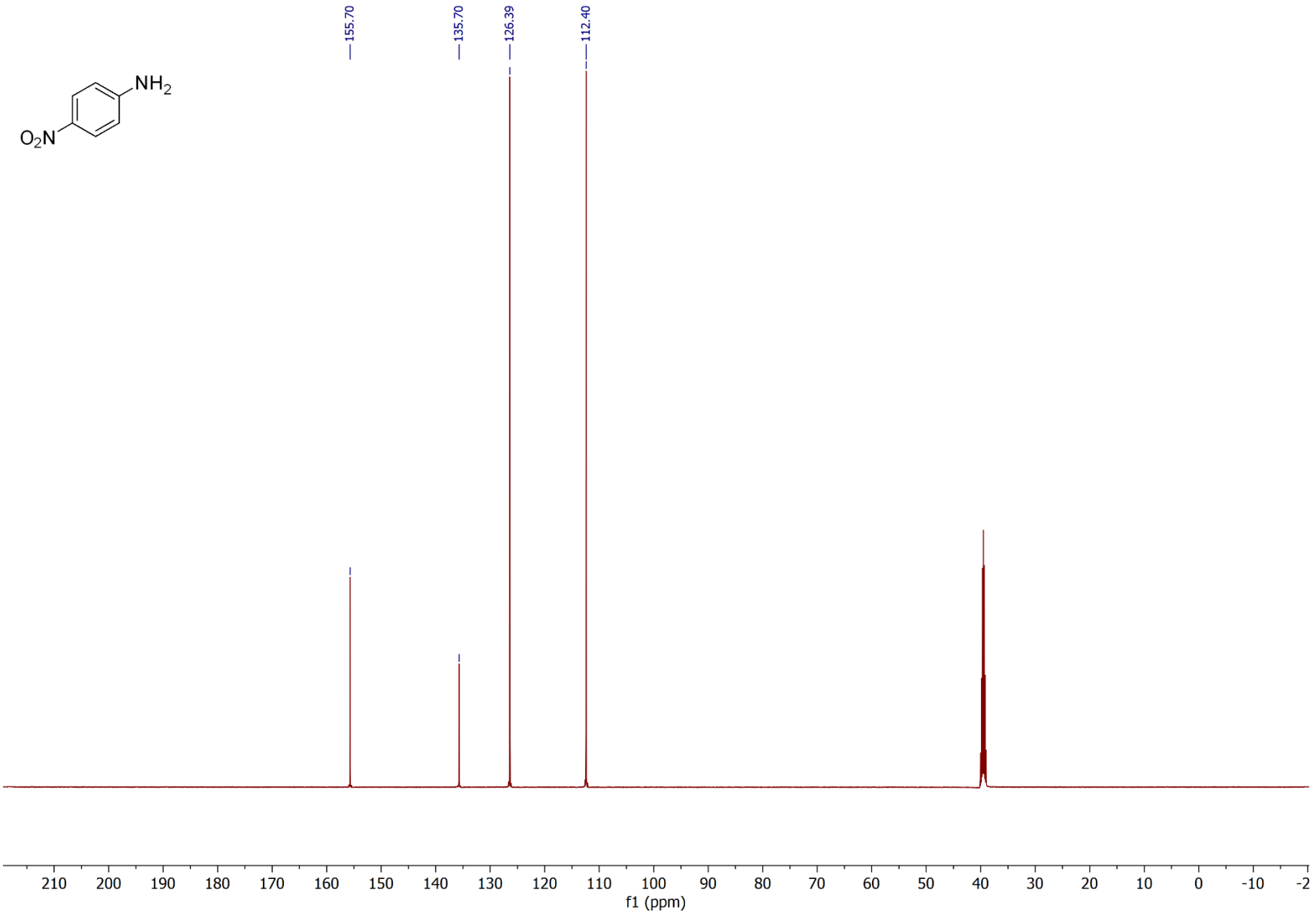

Effect of Base: 4-Nitroaniline (no added base, under CO_2) ^1H

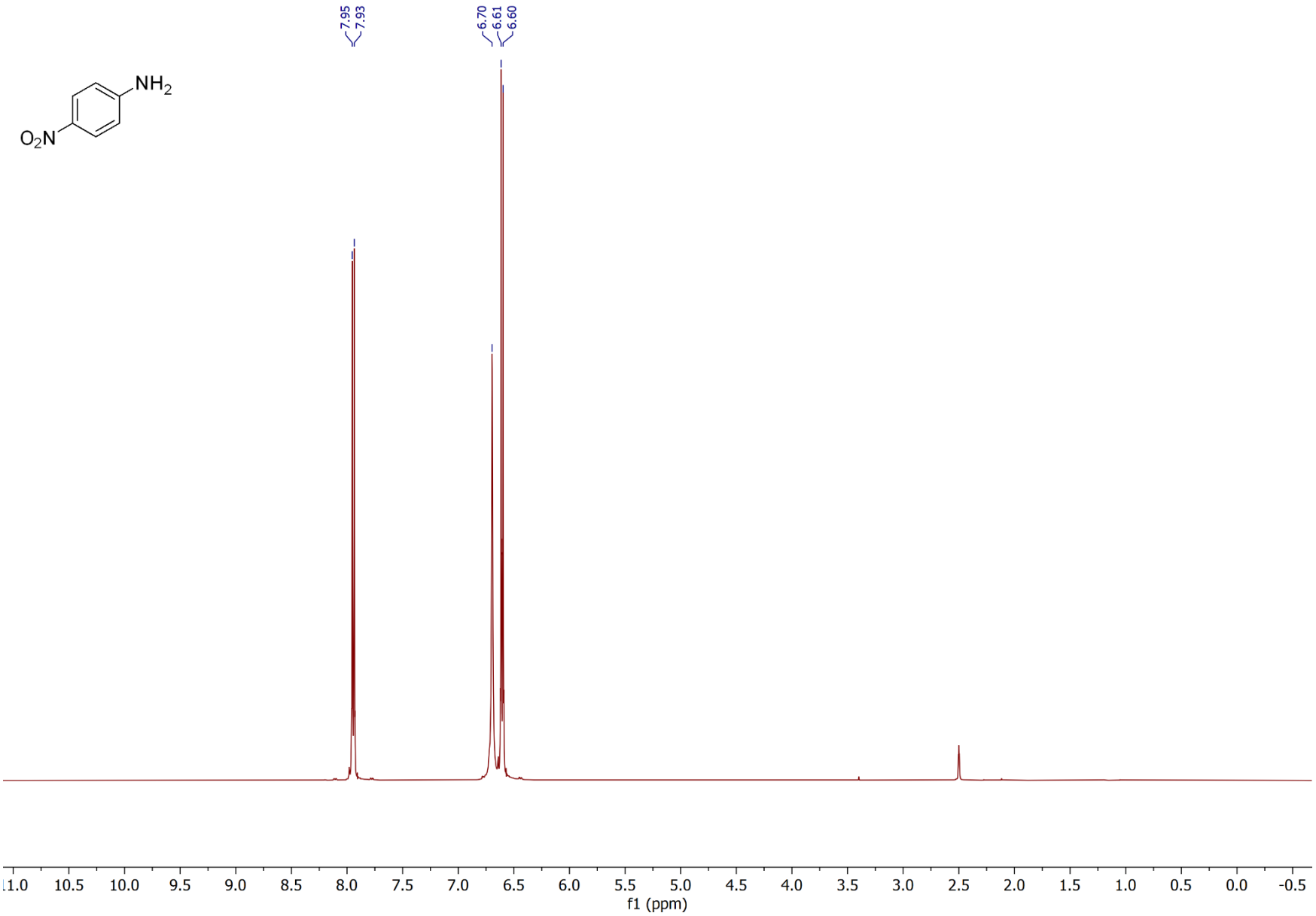

Effect of Base: 4-Nitroaniline (no added base, under CO_2) $^{13}C\{^1H\}$

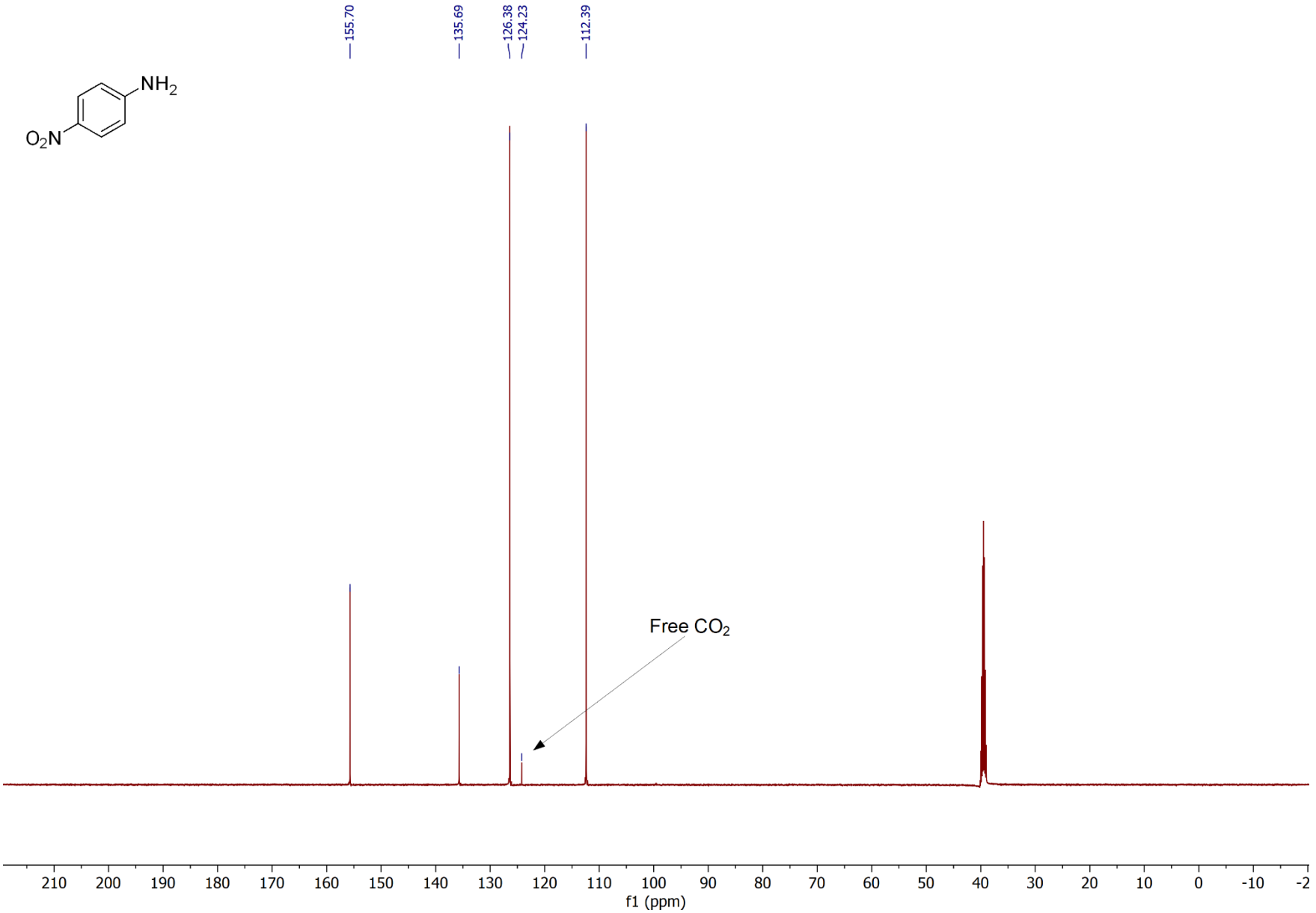

Effect of Base: 4-Nitroaniline & TMG (under Ar) ^{1}H

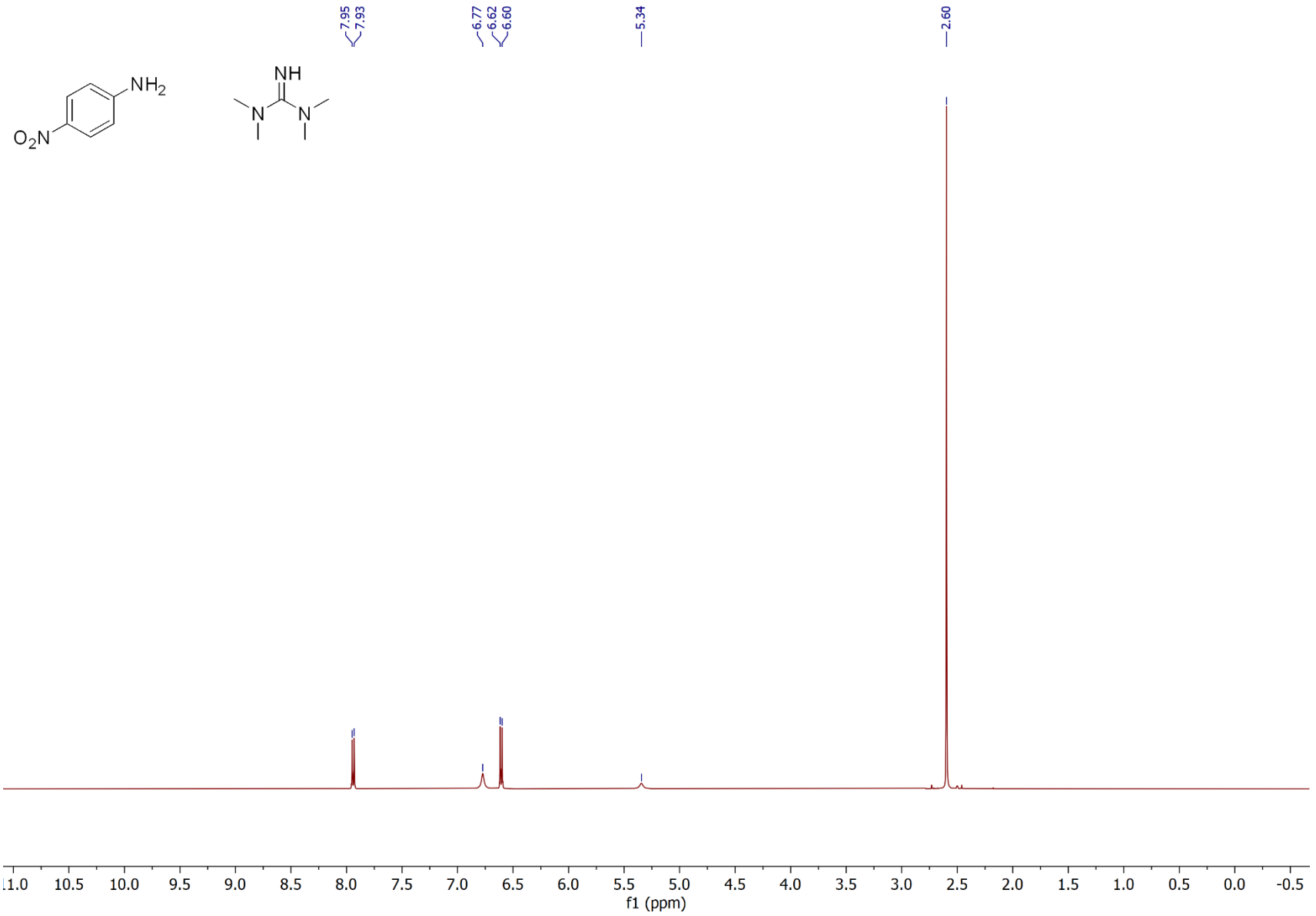

Effect of Base: 4-Nitroaniline & TMG (under Ar) $^{13}C\{^{1}H\}$

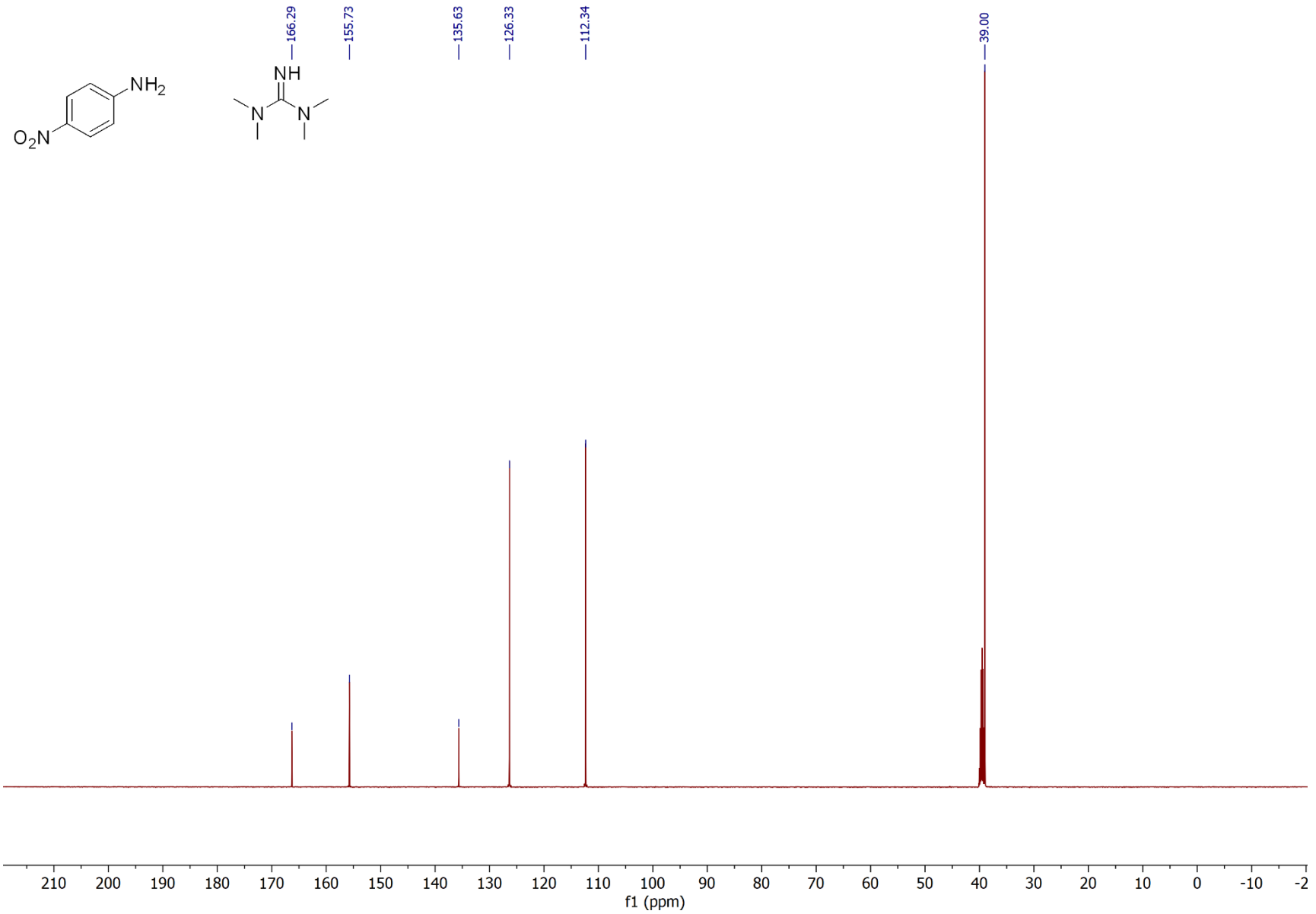

Effect of Base: 4-Nitroaniline & DIPA ^{1}H

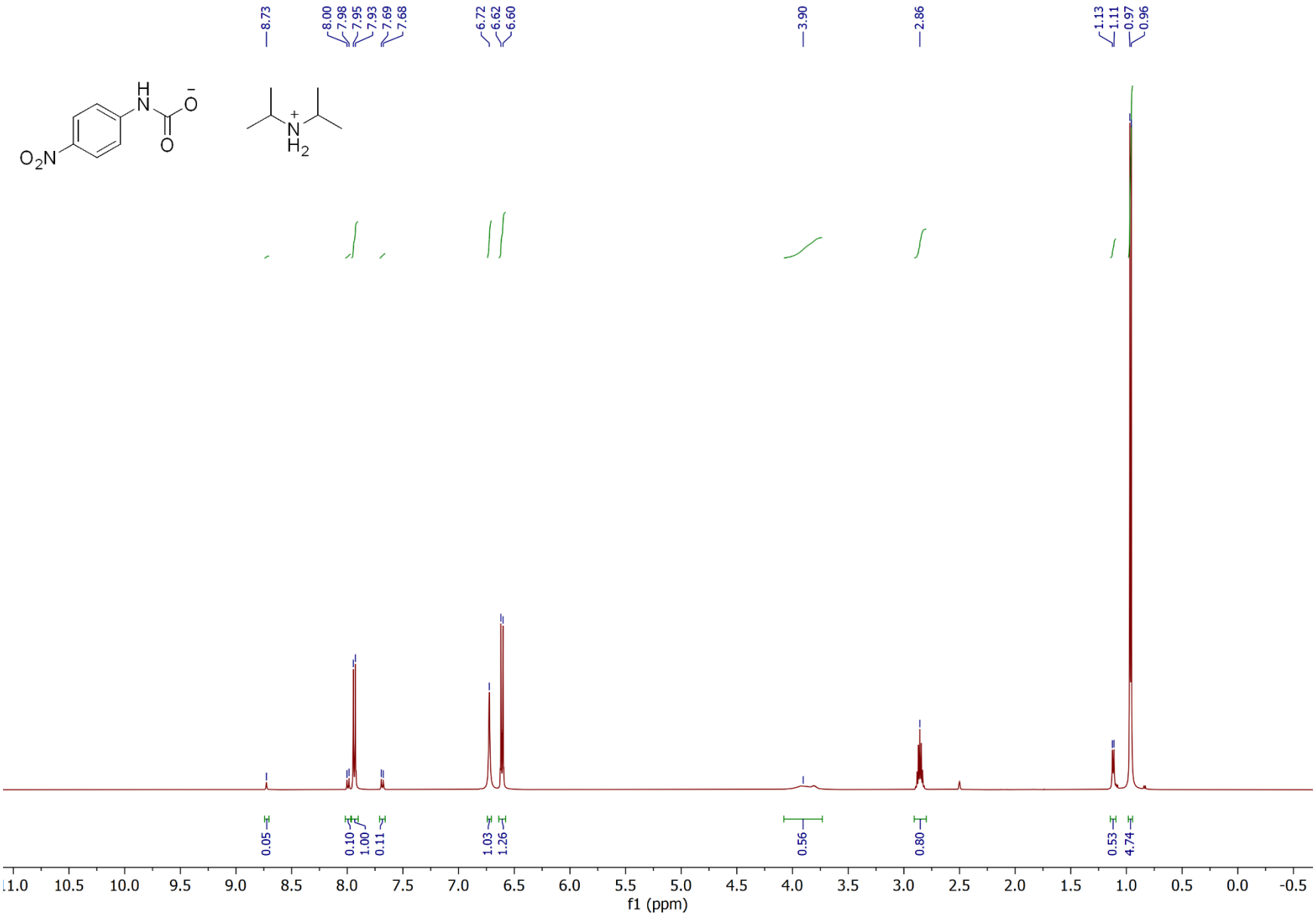

Effect of Base: 4-Nitroaniline & DIPA $^{13}C\{^{1}H\}$

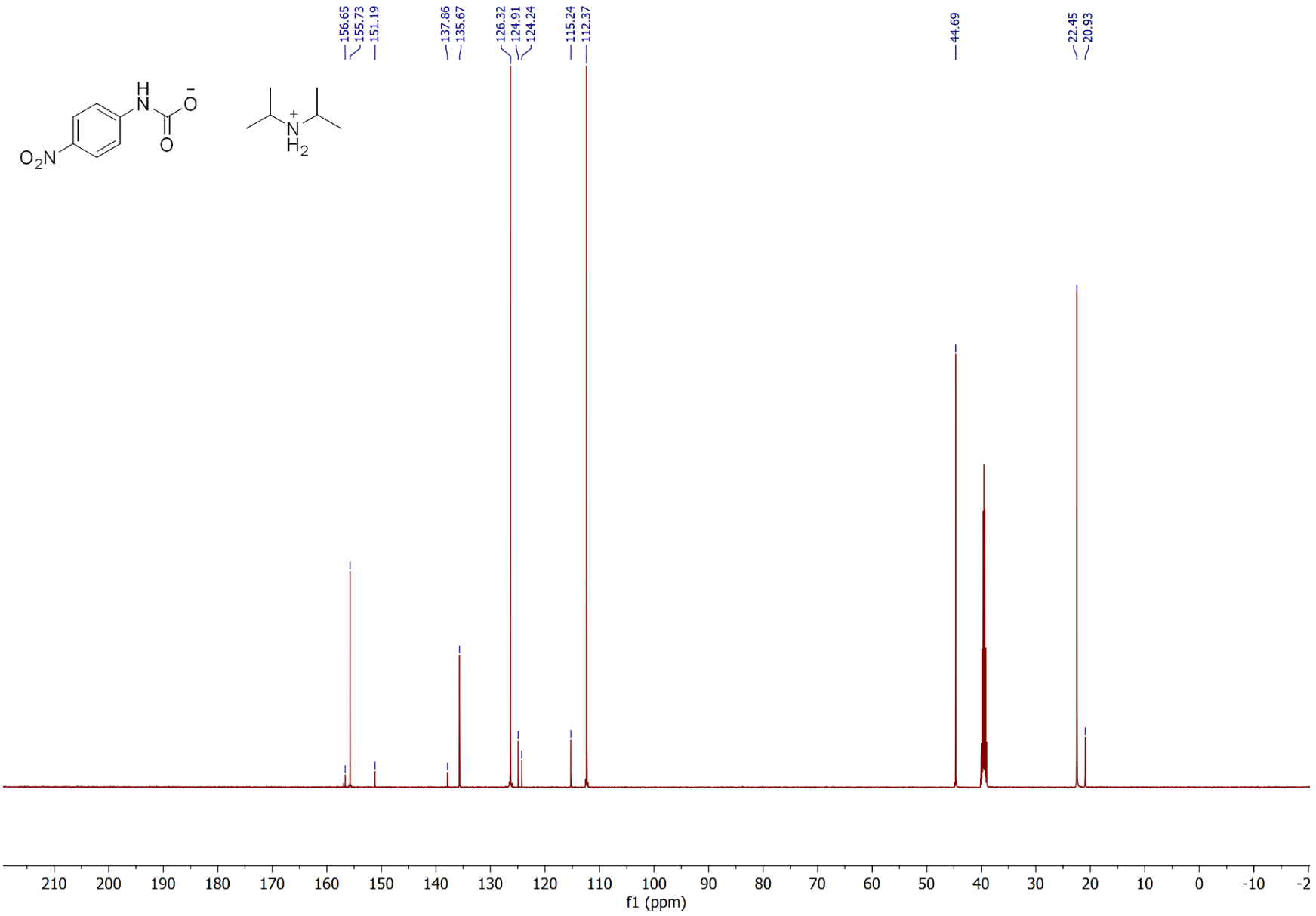

Effect of Base: 4-Nitroaniline & tBuTMG ^{1}H

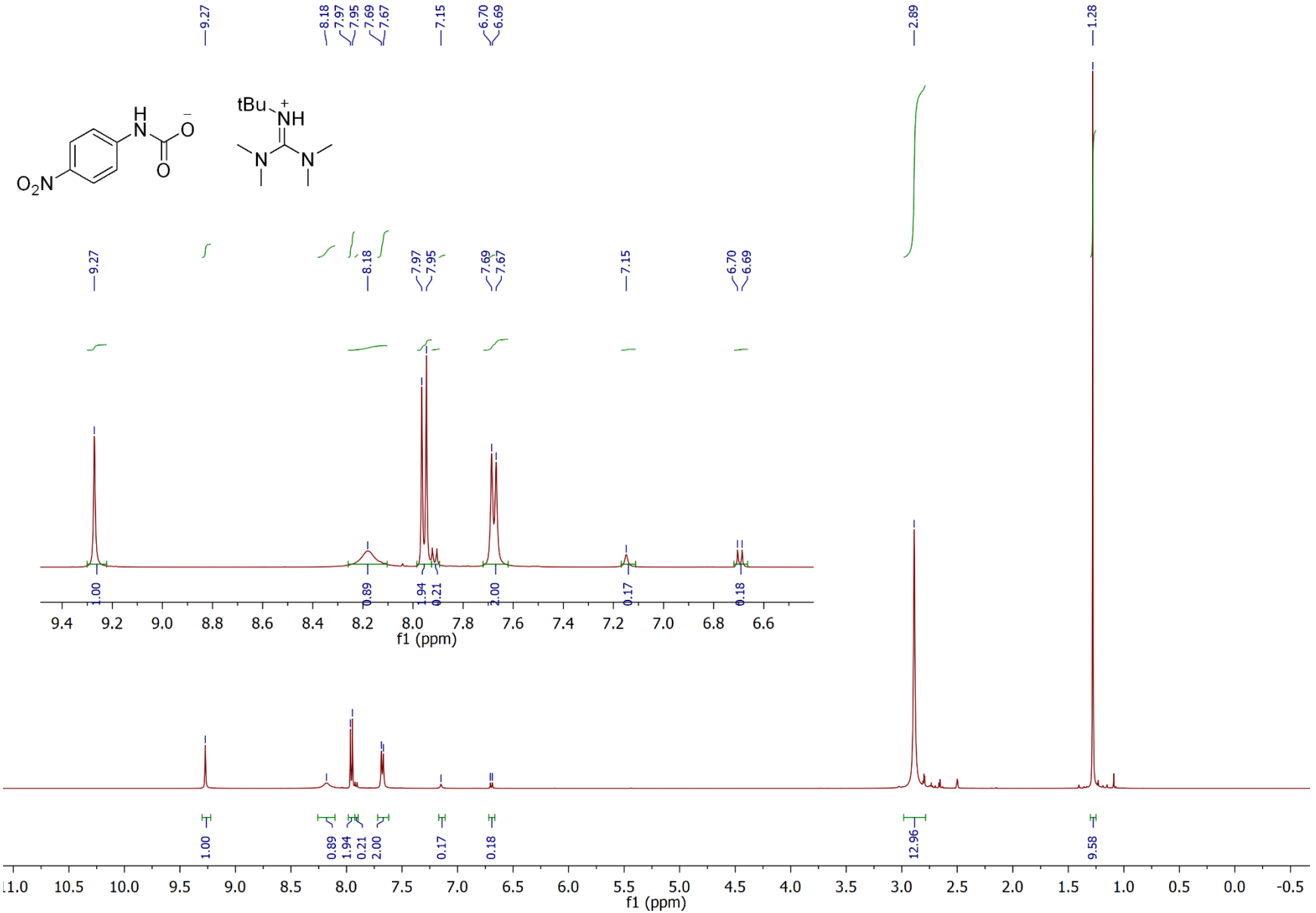

Effect of Base: 4-Nitroaniline & tBuTMG $^{13}C\{^{1}H\}$

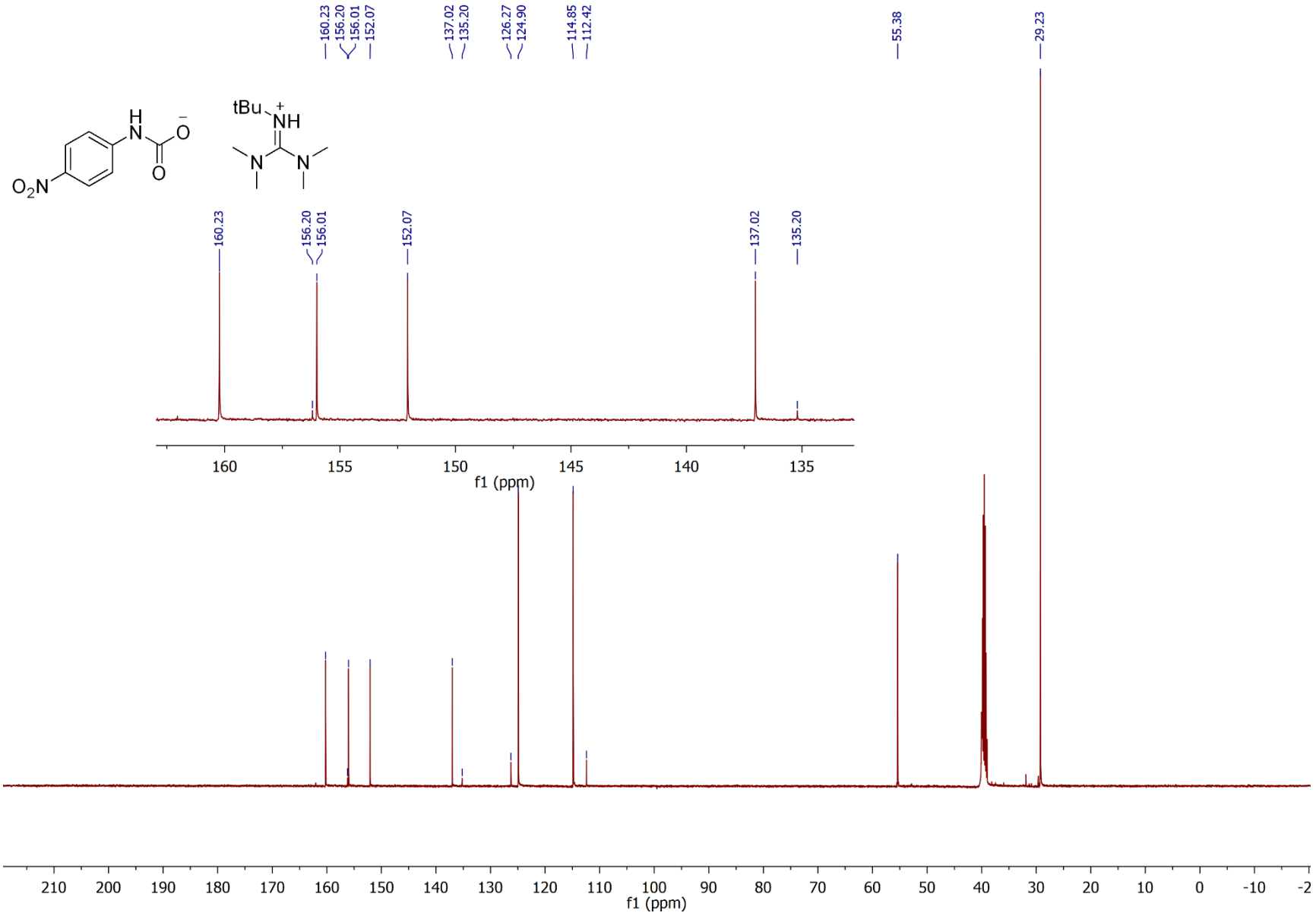

Effect of Base: 4-Nitroaniline & DBU ^{1}H

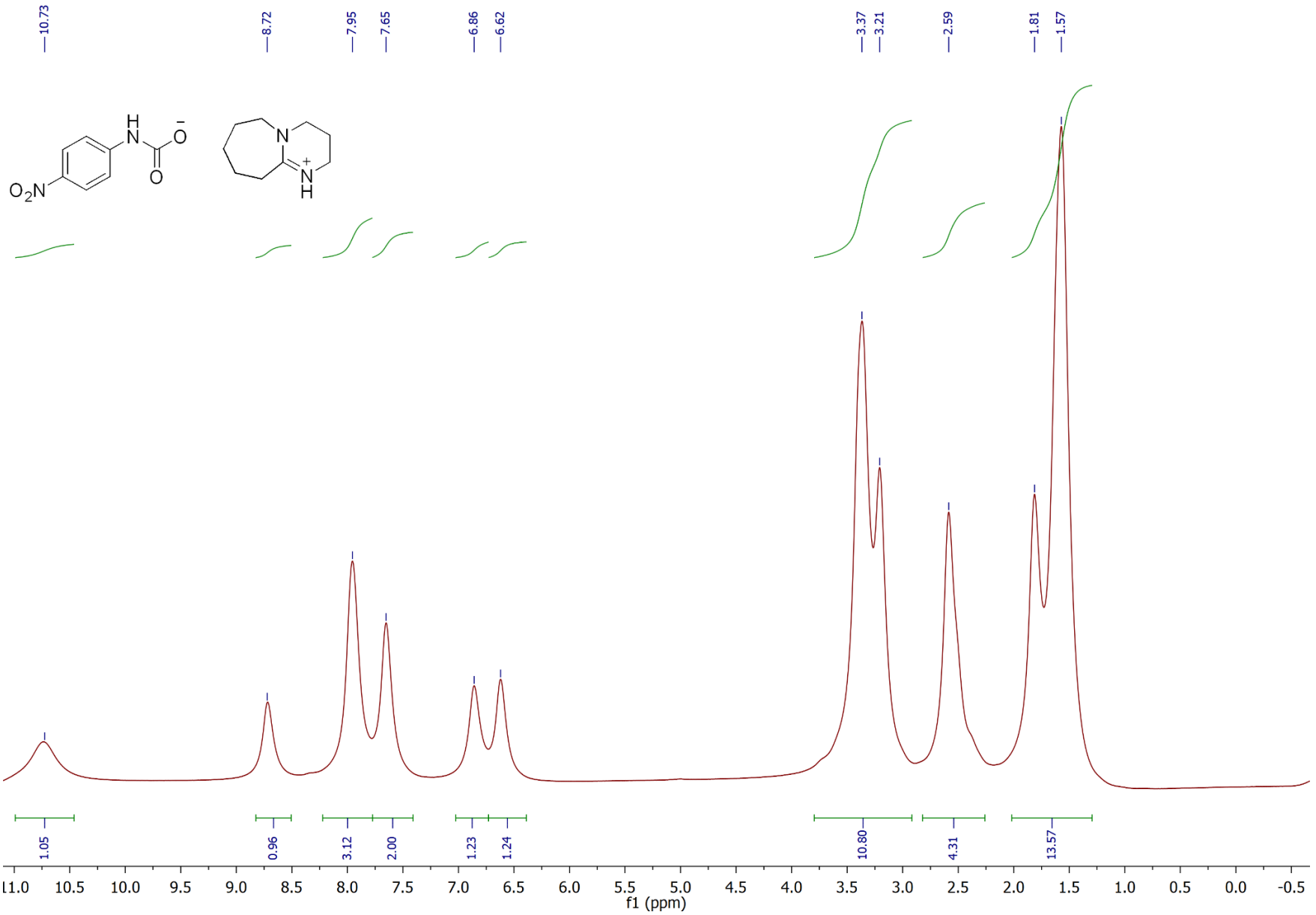

Effect of Base: 4-Nitroaniline & DBU $^{13}C\{^{1}H\}$

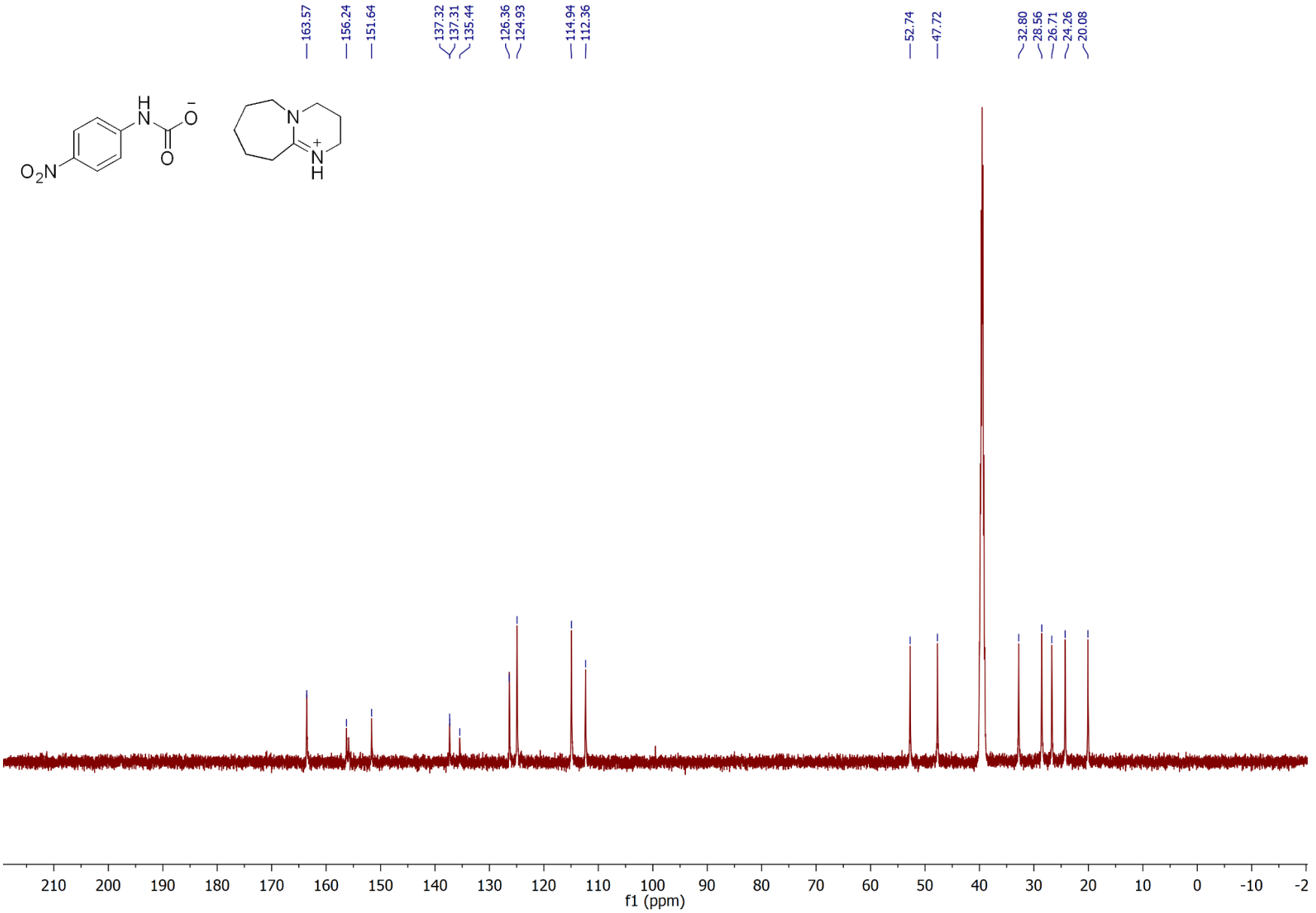

Effect of Base: 4-Nitroaniline, 1,3-Dimethoxybenzene & DBU (no CO_2) ^1H

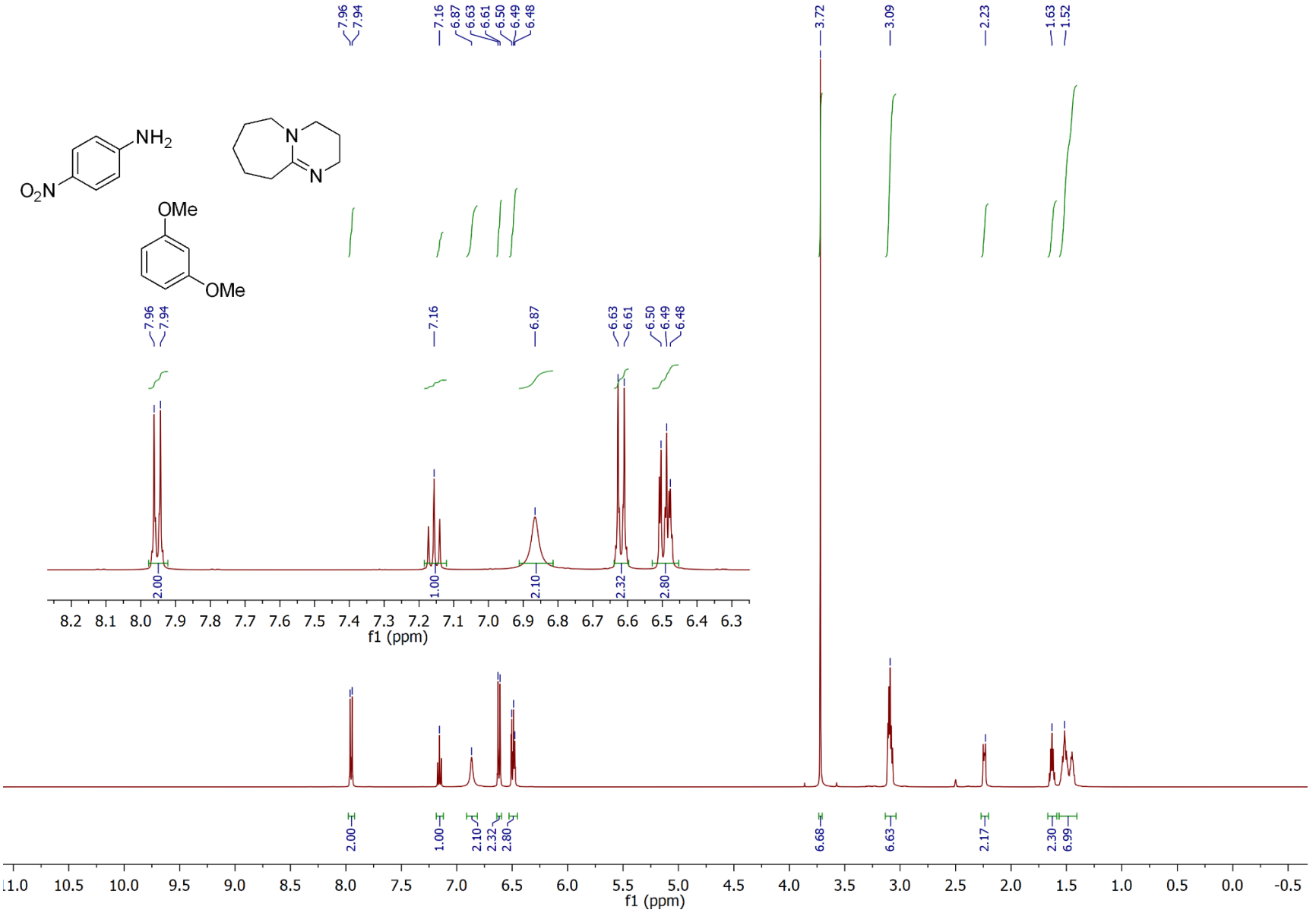

Effect of Base: 4-Nitroaniline, 1,3-Dimethoxybenzene & DBU (no CO_2) $^{13}C\{^1H\}$

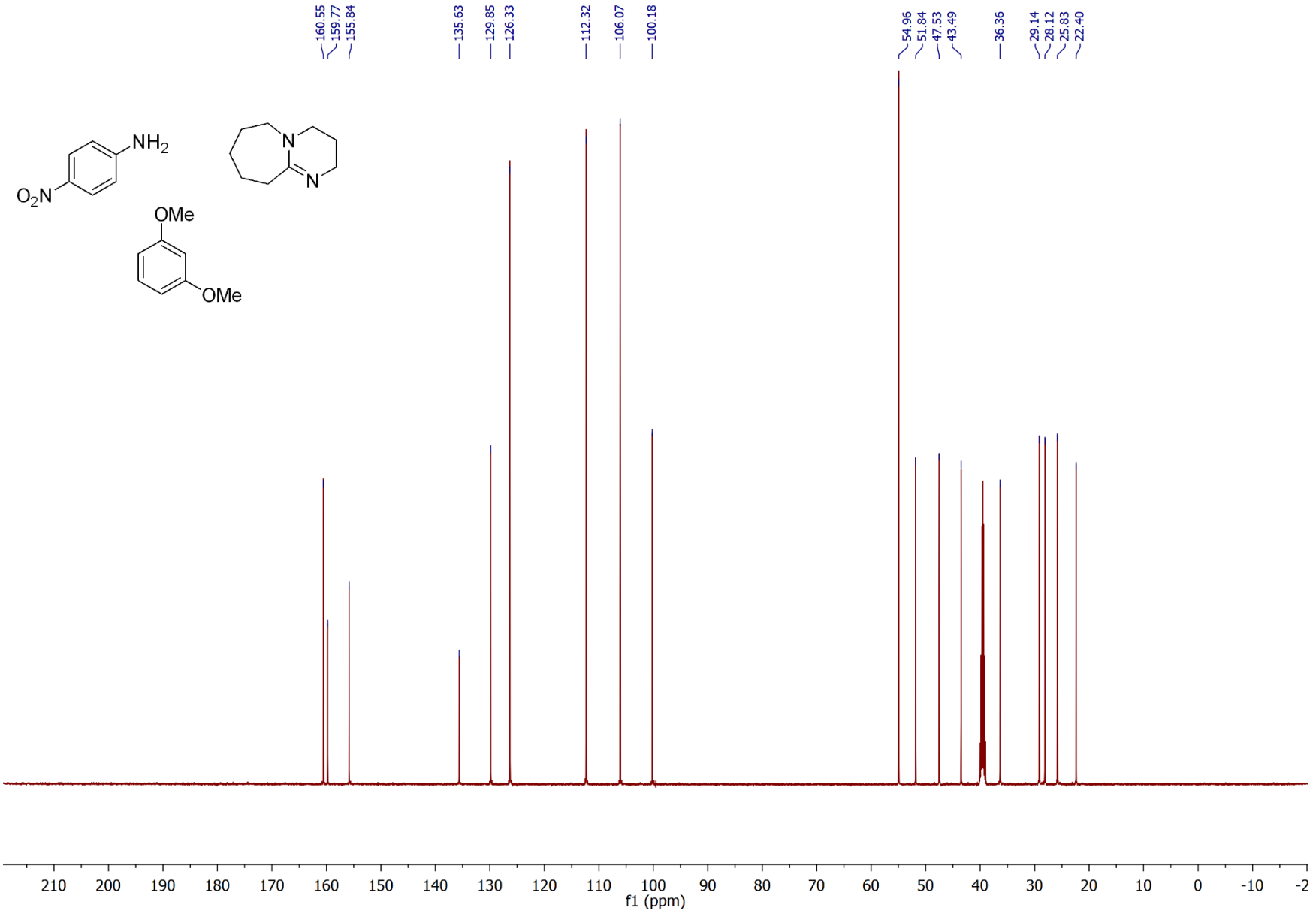

Effect of Base: 4-Nitroaniline, 1,3-Dimethoxybenzene & DBU (with CO_2) ^1H

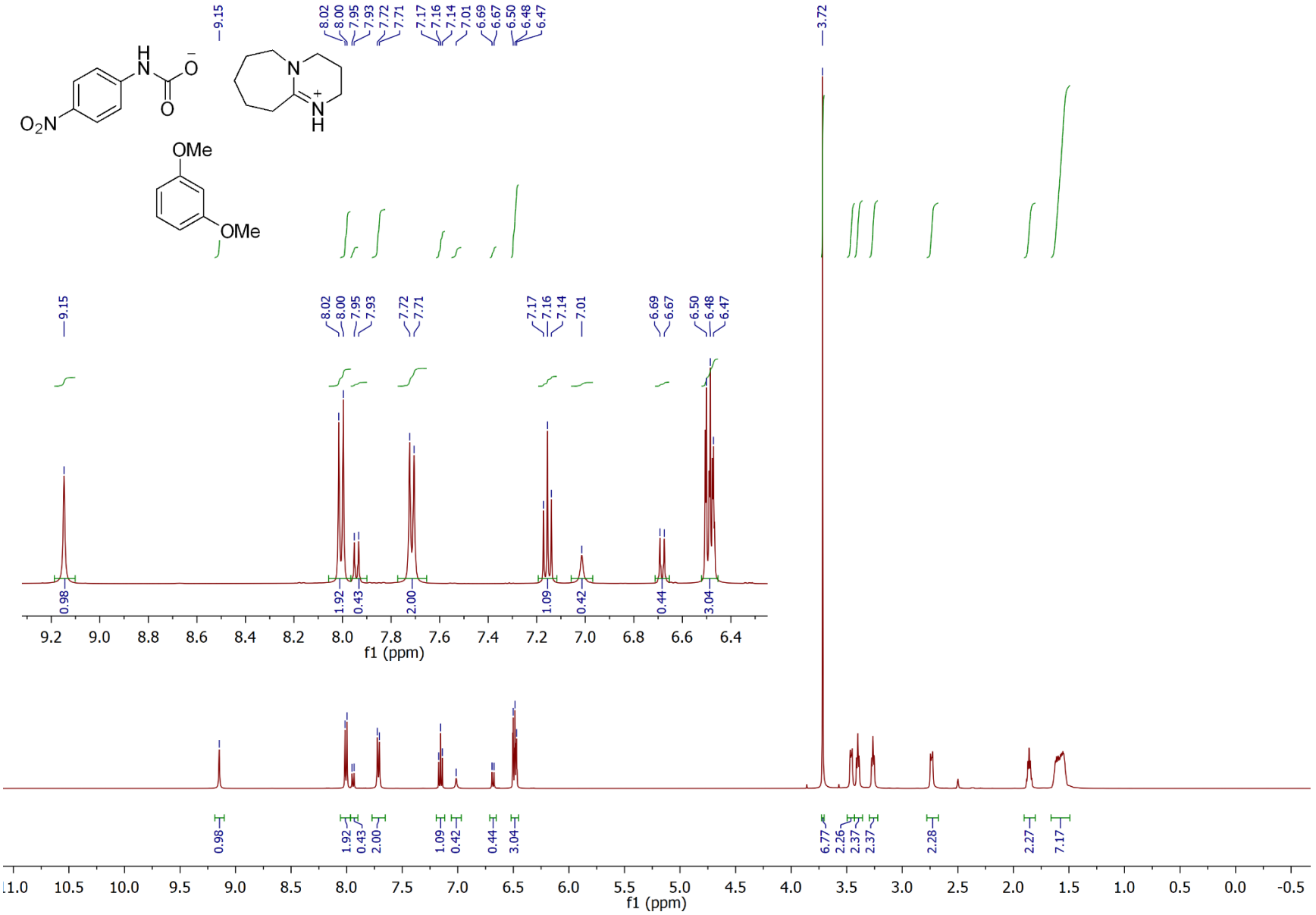

Effect of Base: 4-Nitroaniline, 1,3-Dimethoxybenzene & DBU (with CO_2) Quantitative $^{13}C\{^1H\}$

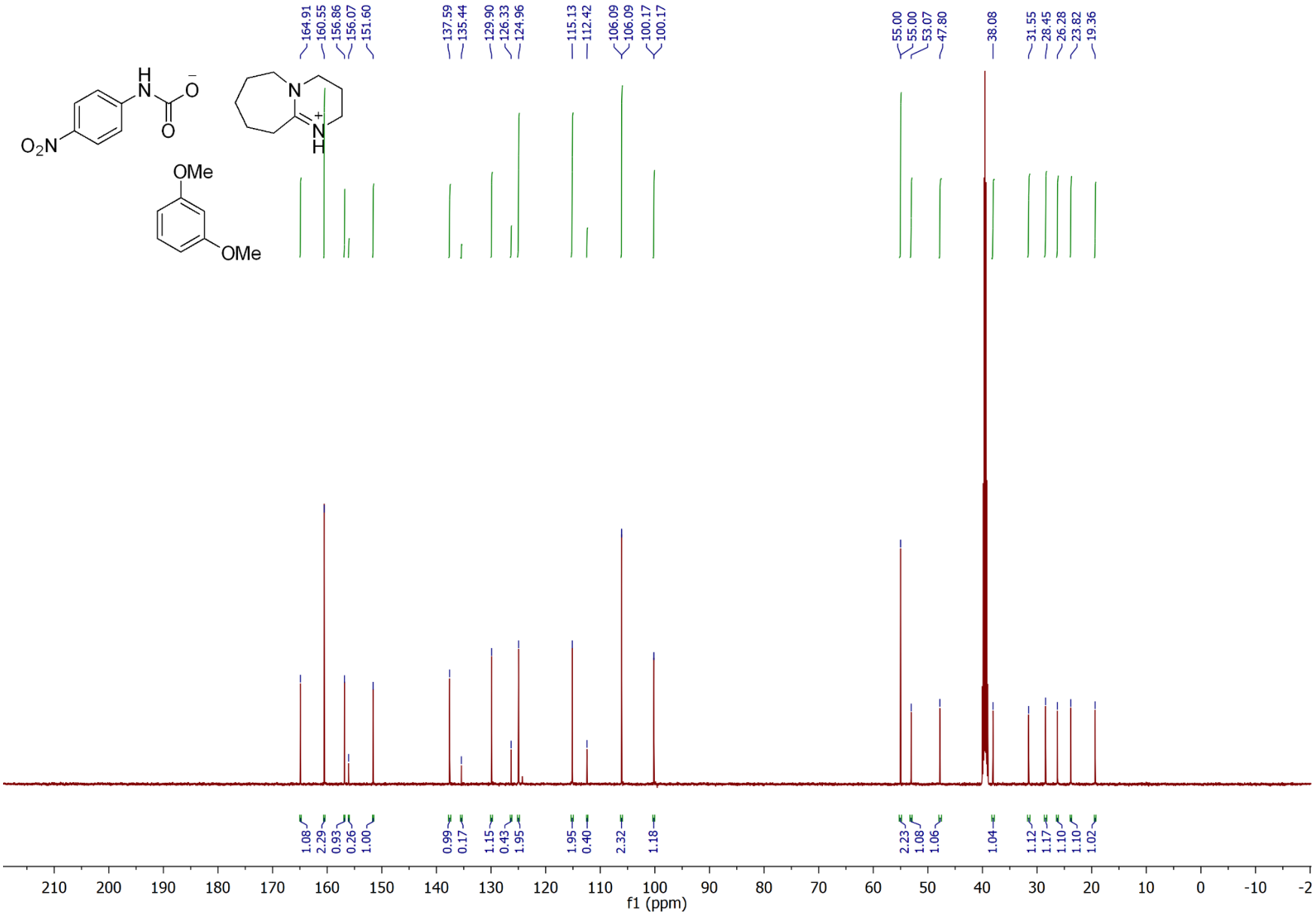

Effect of Base: 4-Nitroaniline, 1,3-Dimethoxybenzene & DBU (with CO_2) HMBC

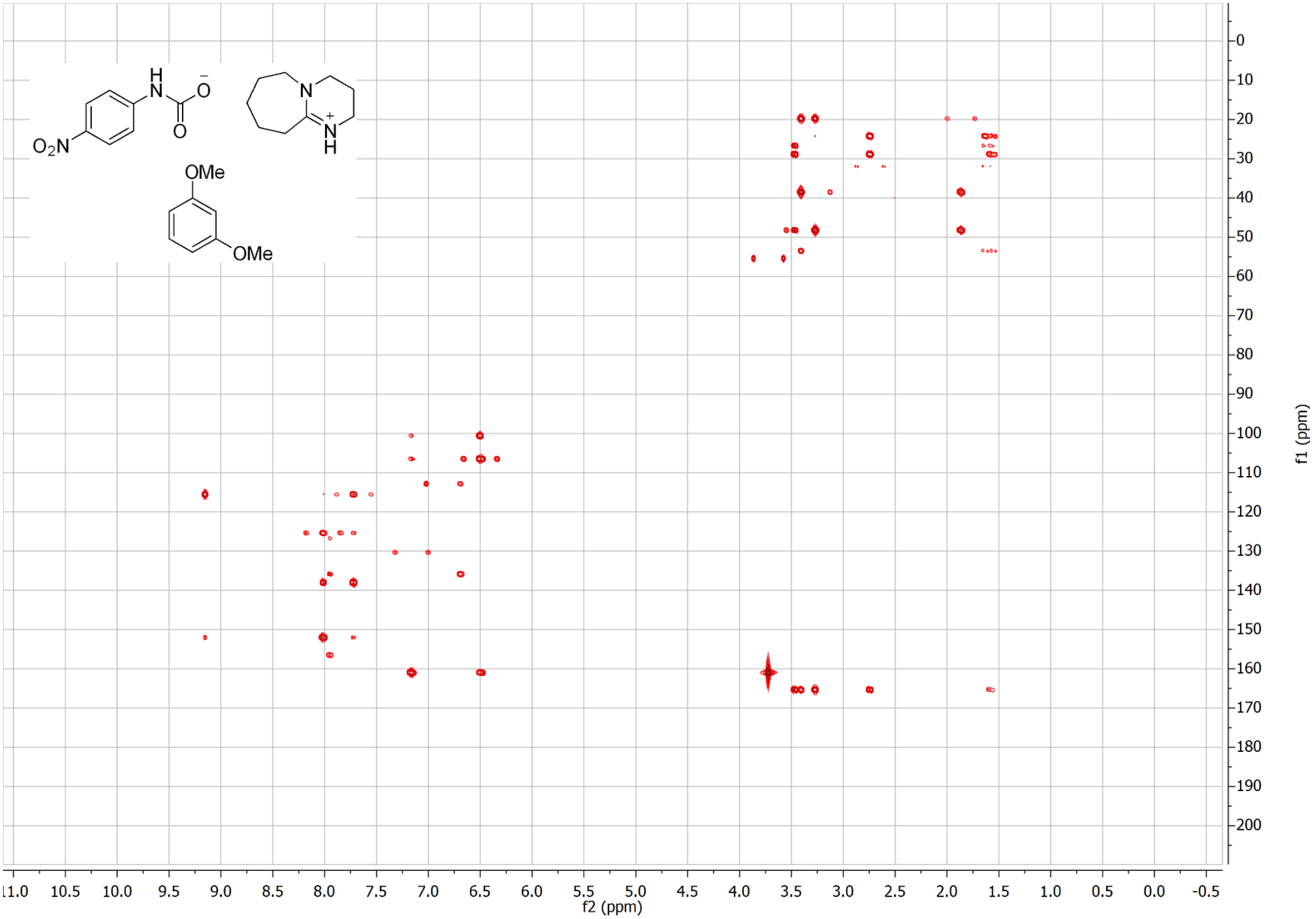

Effect of Base: 4-Nitroaniline, 1,3-Dimethoxybenzene & DBU (with CO_2) HSQC

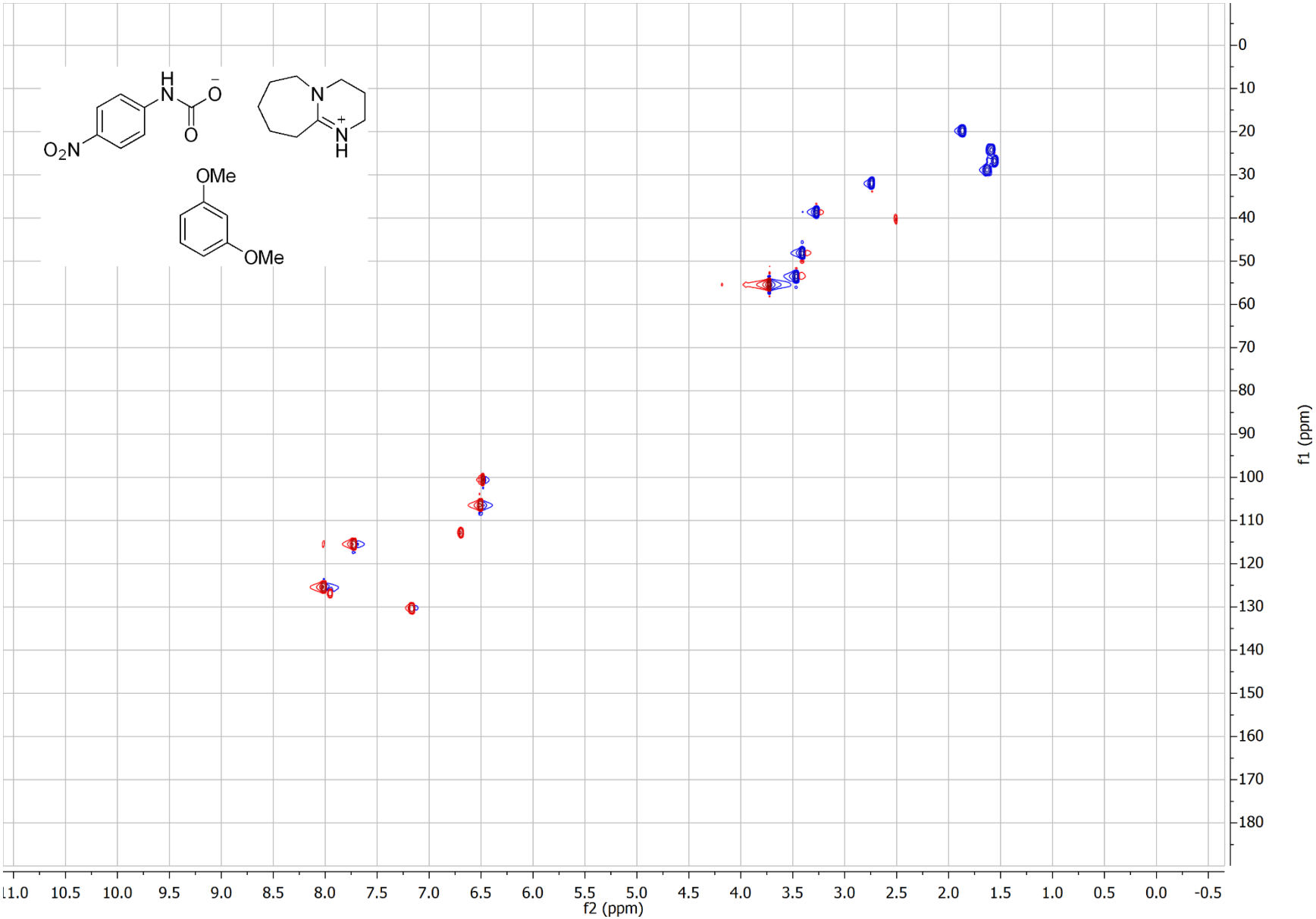

Effect of Base: 4-Nitroaniline & TBD ^{1}H

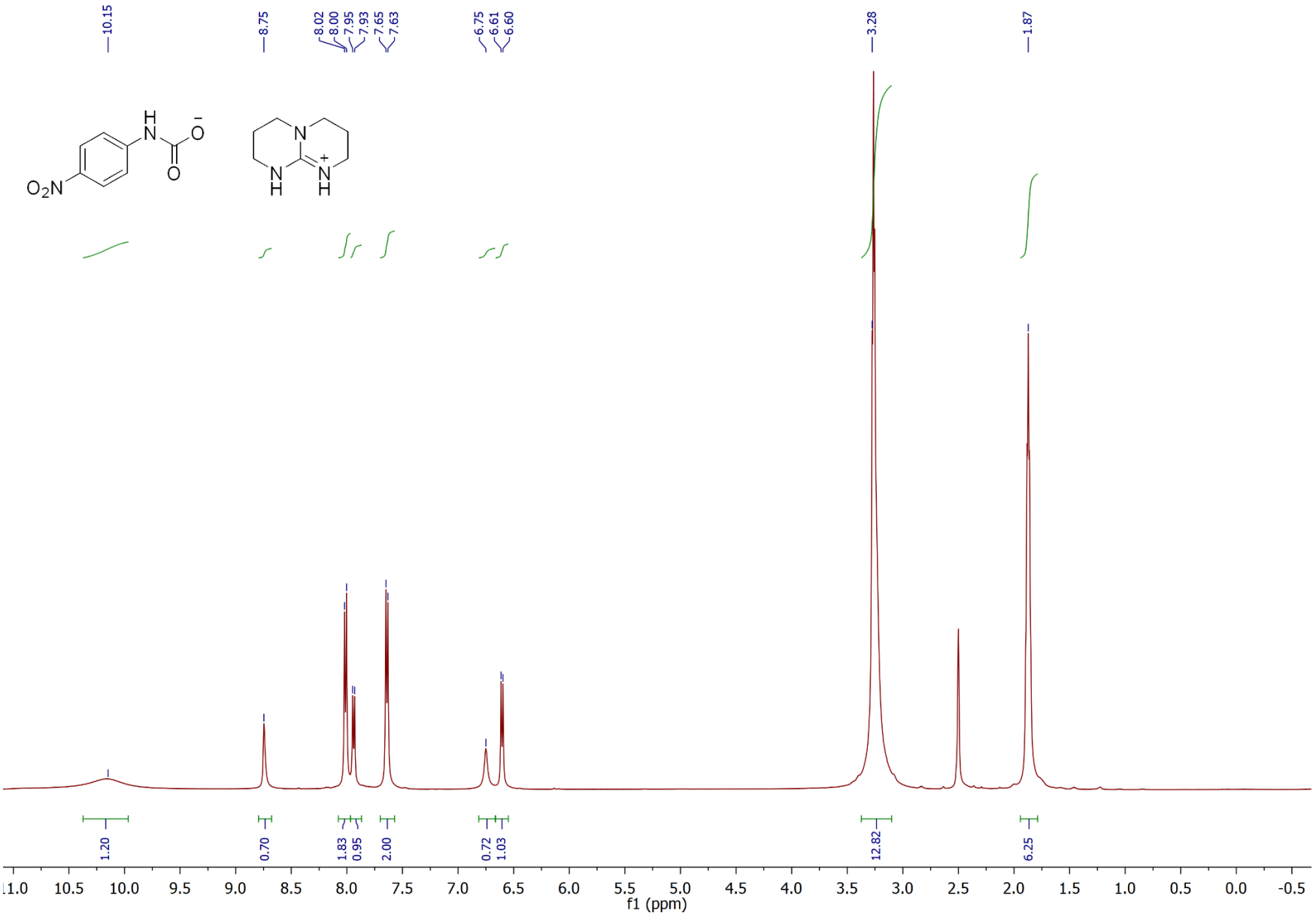

Effect of Base: 4-Nitroaniline & TBD $^{13}C\{^{1}H\}$

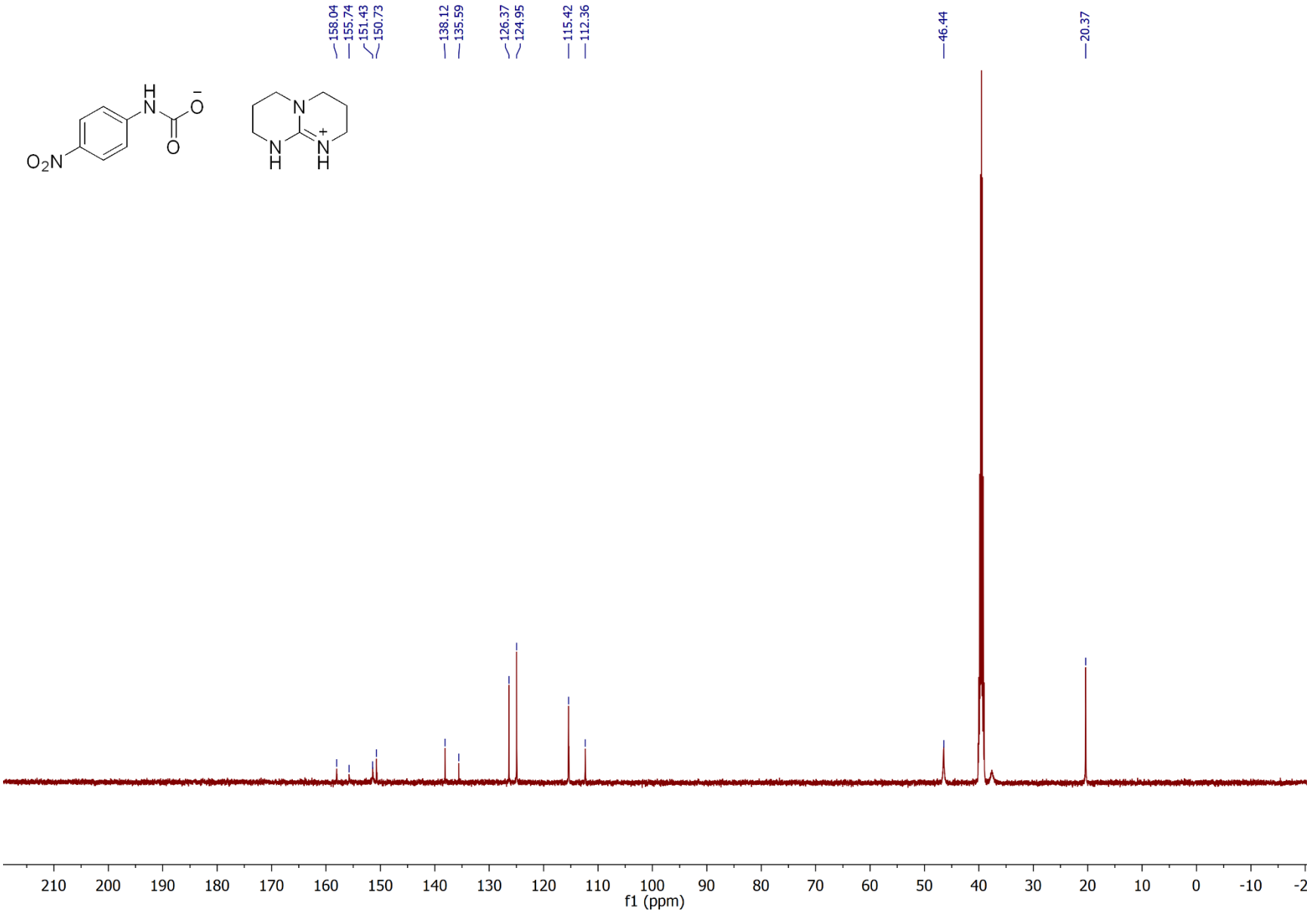

Effect of Base: 4-Nitroaniline & MTBD ^{1}H

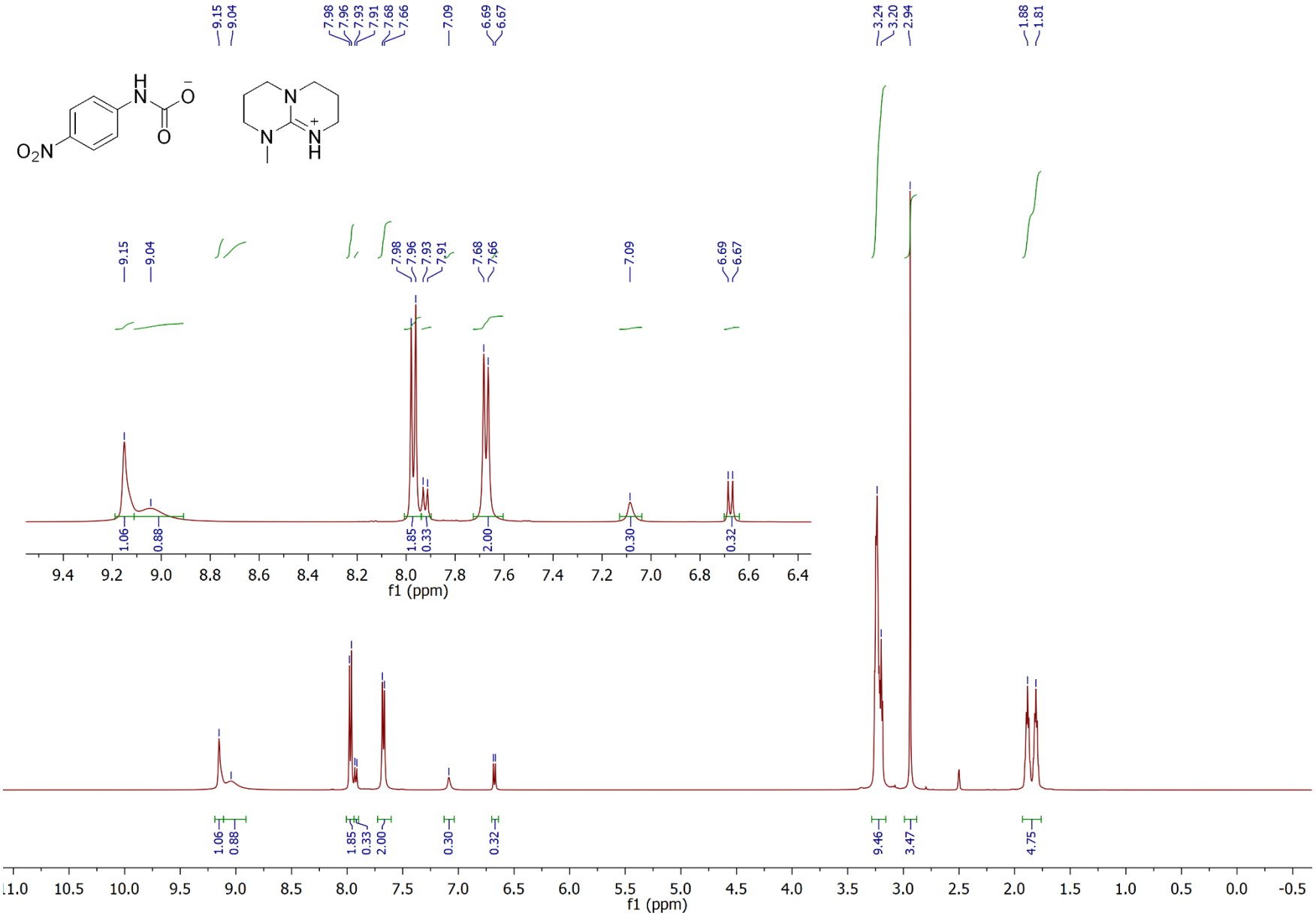

Effect of Base: 4-Nitroaniline & MTBD $^{13}C\{^{1}H\}$

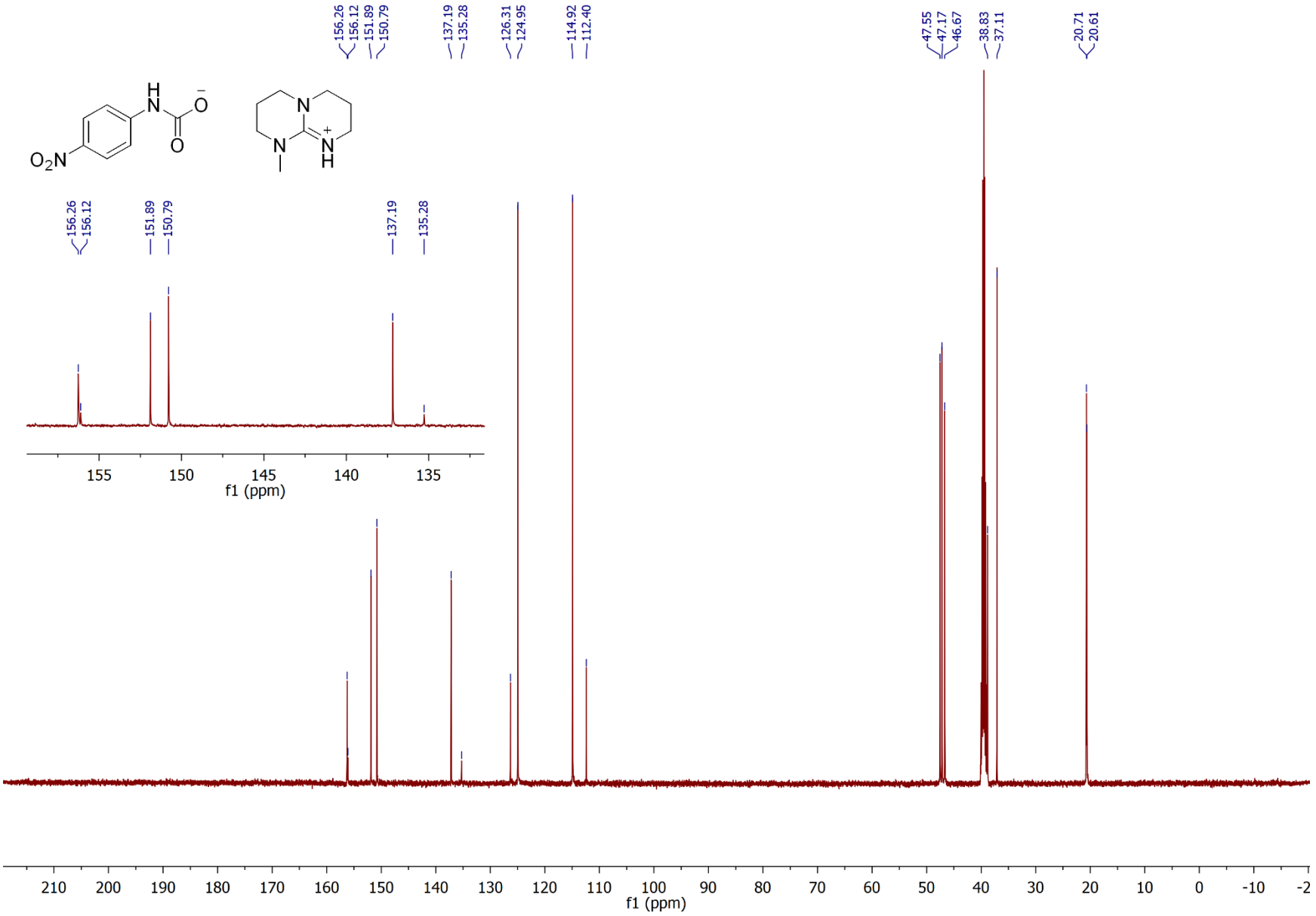

Effect of Base: 4-Nitroaniline & DIPA ^{1}H

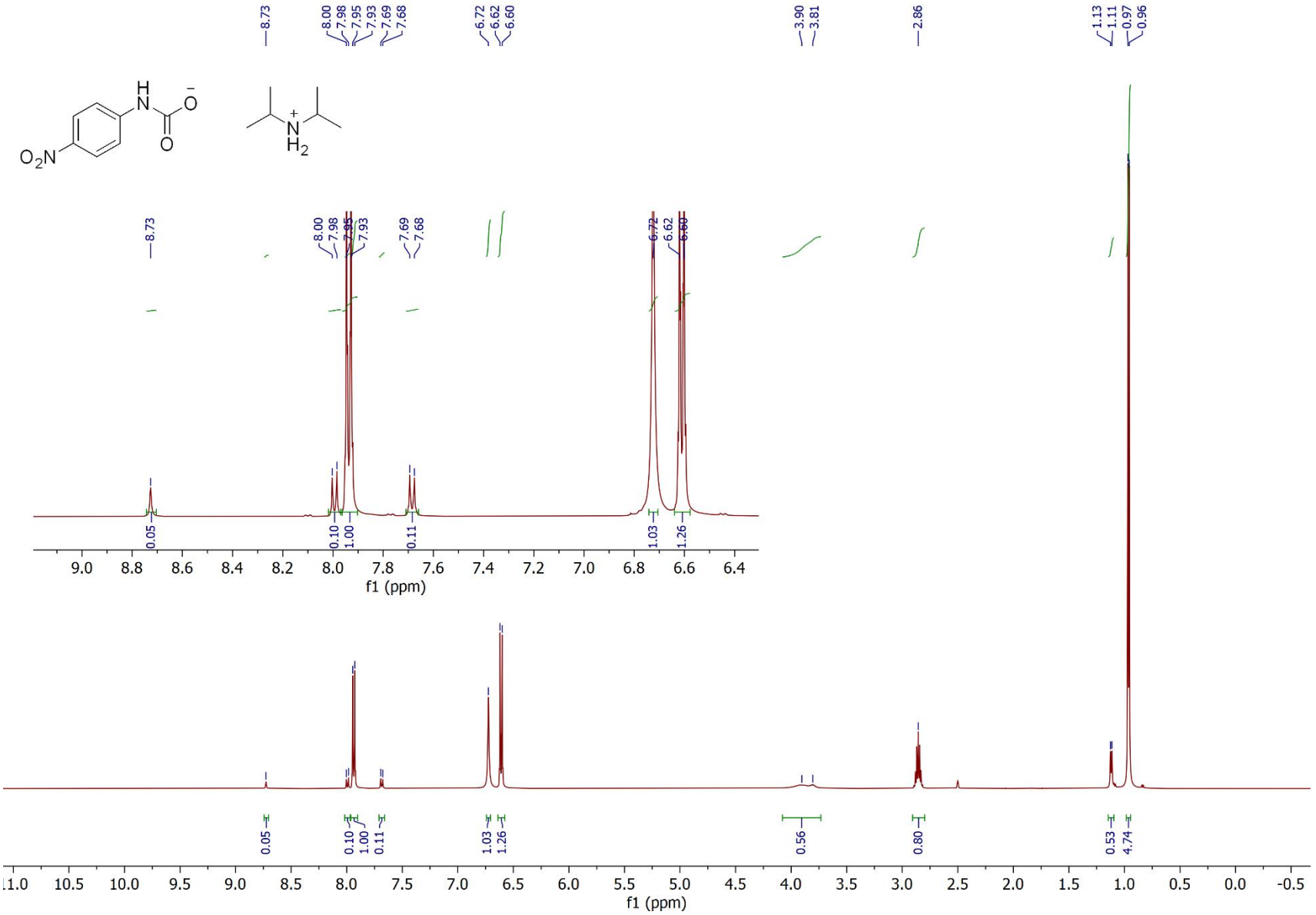

Effect of Base: 4-Nitroaniline & DIPA $^{13}C\{^{1}H\}$

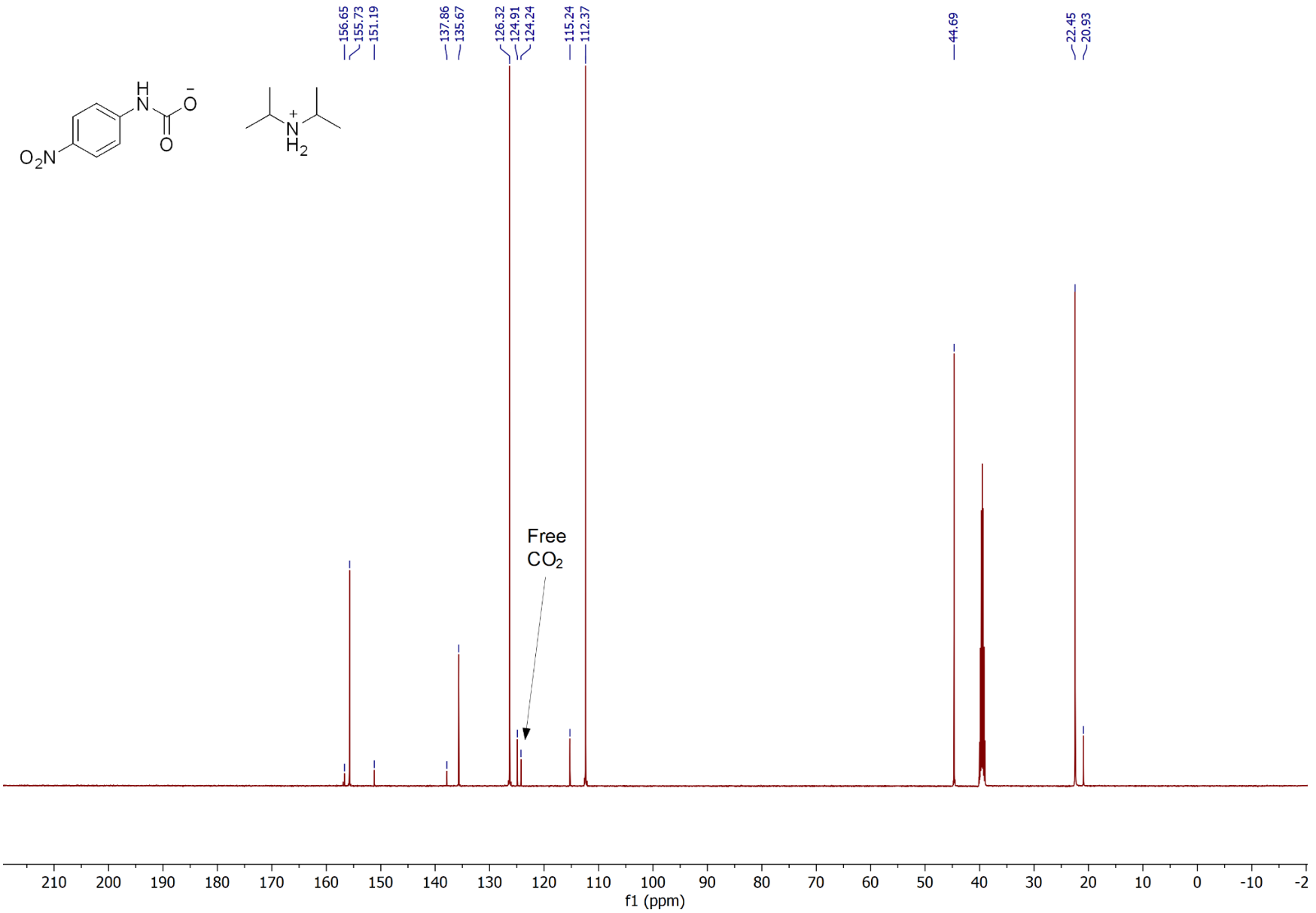

Effect of Base: 4-Nitroaniline & DIPEA ^{1}H

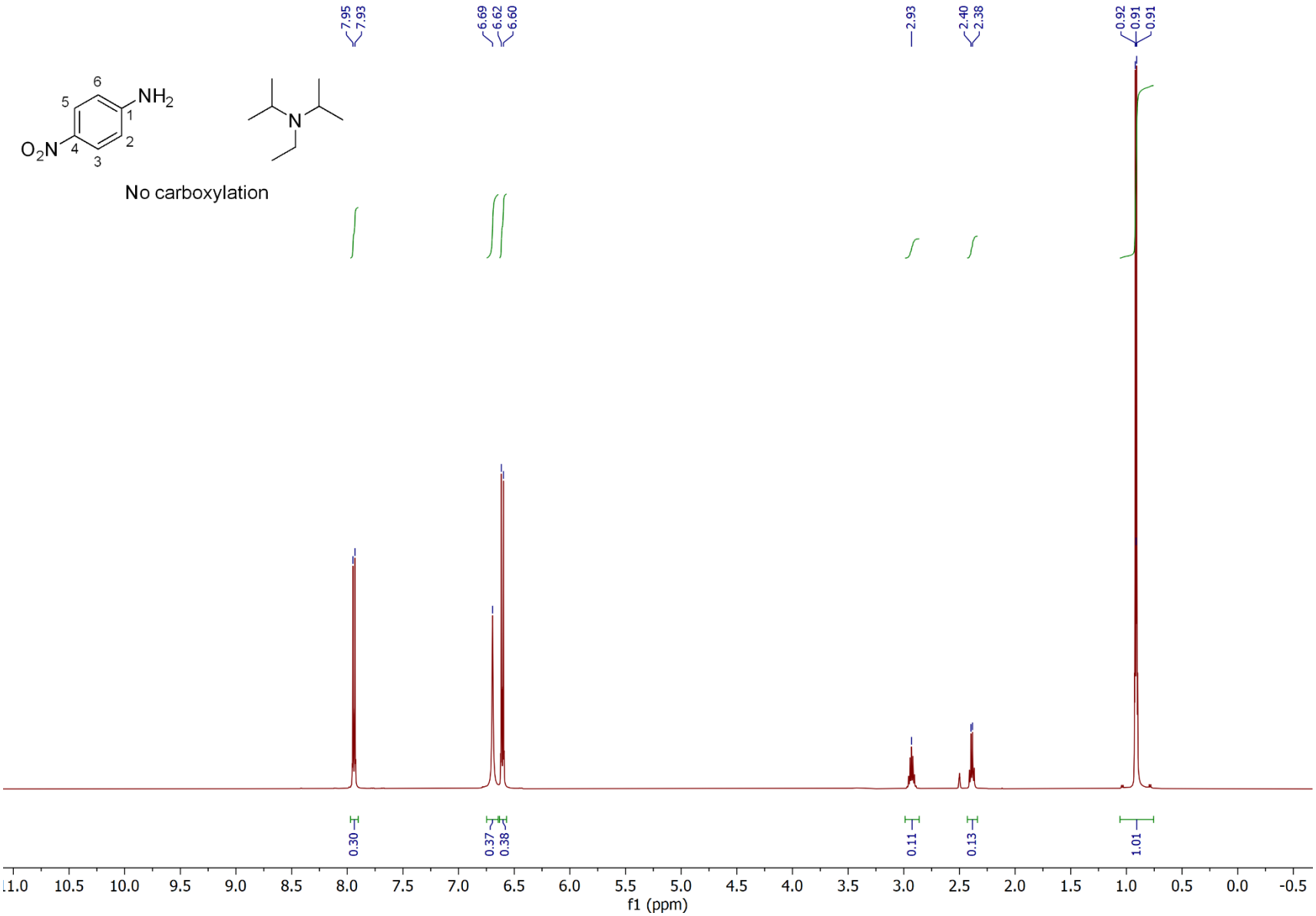

Effect of Base: 4-Nitroaniline & DIPA $^{13}C\{^{1}H\}$

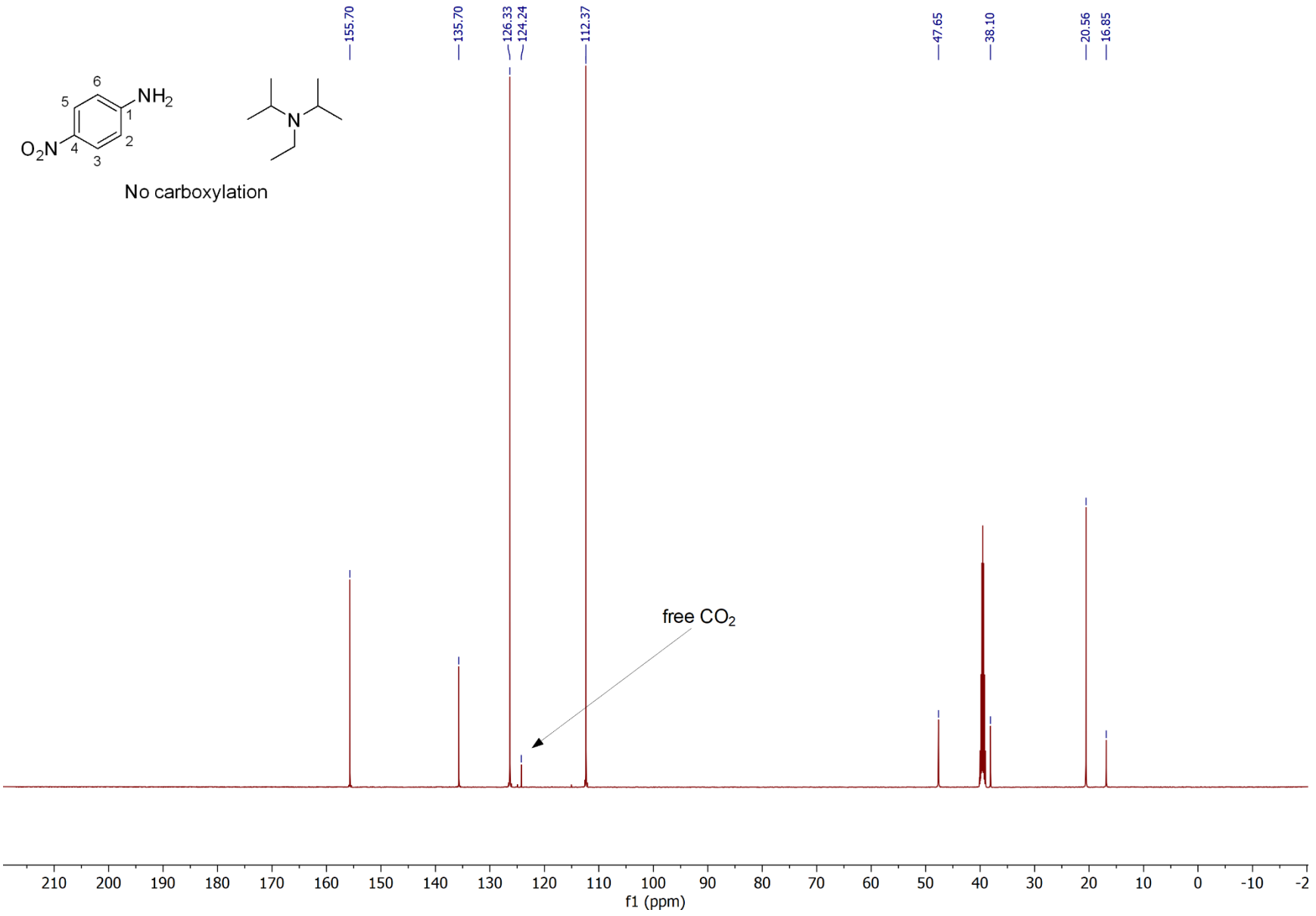

Carboxylation of 4-(Trifluoromethyl)aniline ^{1}H Using Zwitterion 4, TMG-CO_2

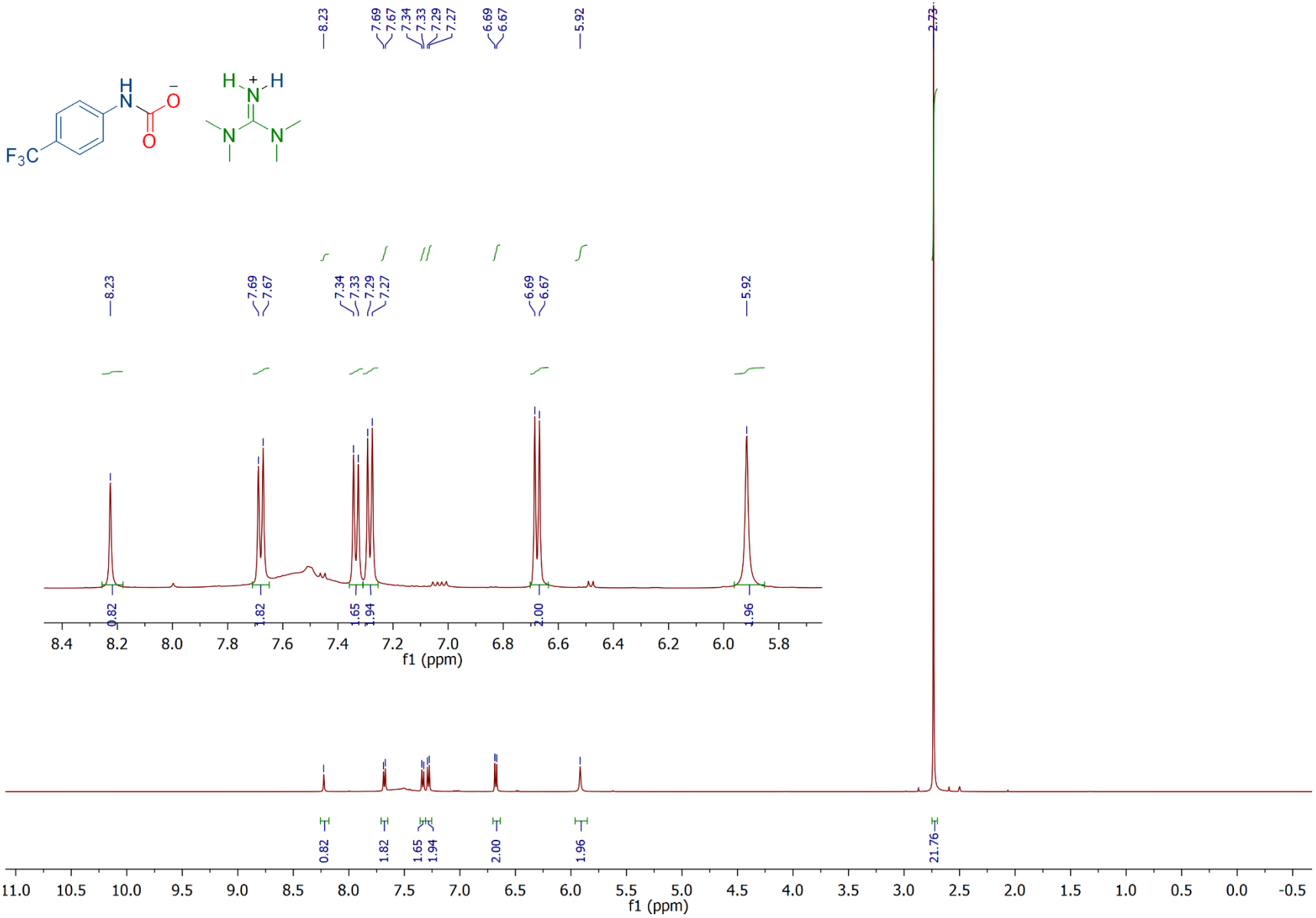

Carboxylation of 4-(Trifluoromethyl)aniline $^{13}C\{^{1}H\}$ Using Zwitterion 4, TMG-CO_2

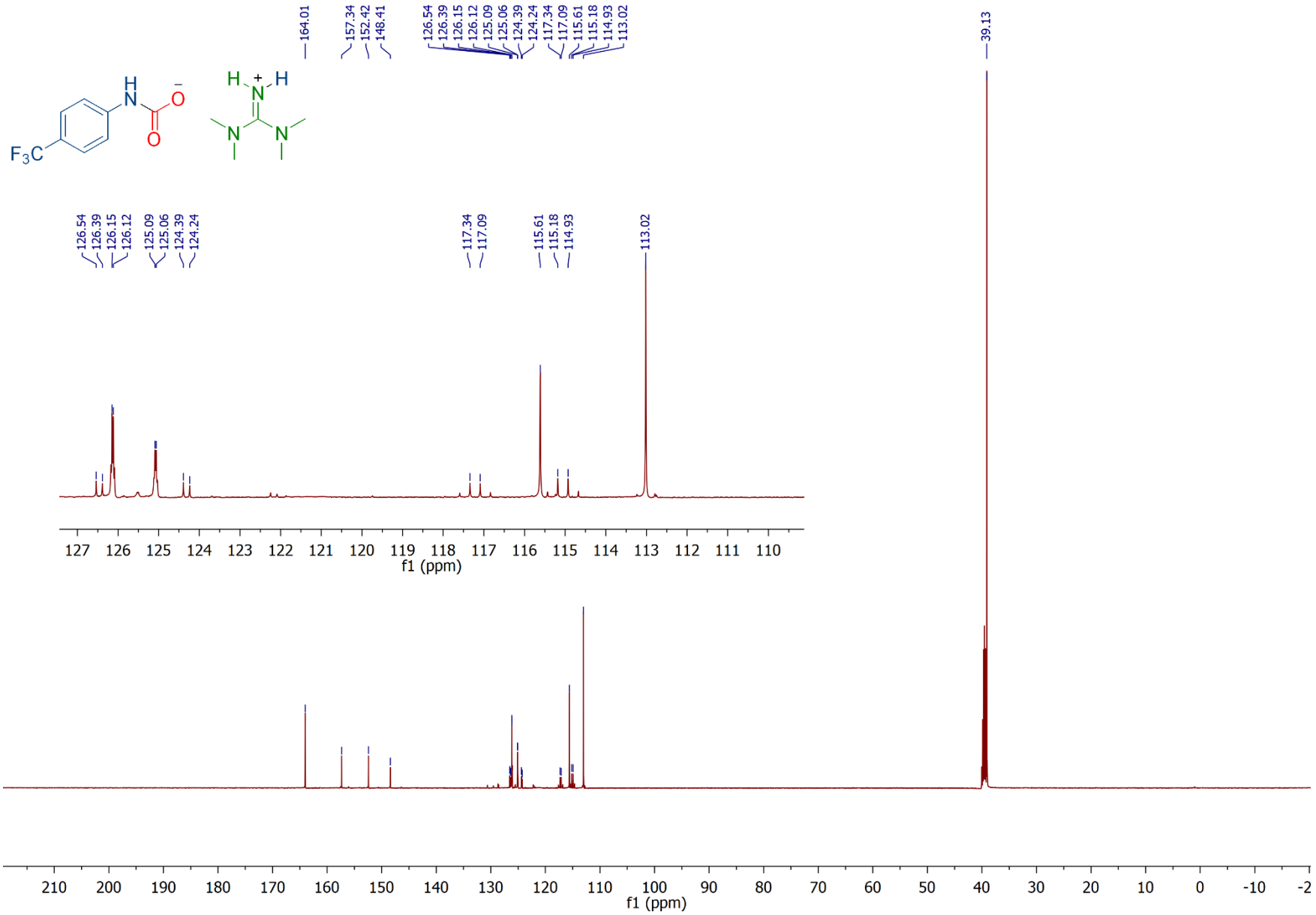

Carboxylation of 4-(Trifluoromethyl)aniline $^{19}F\{^{1}H\}$ Using Zwitterion 4, TMG-CO_2

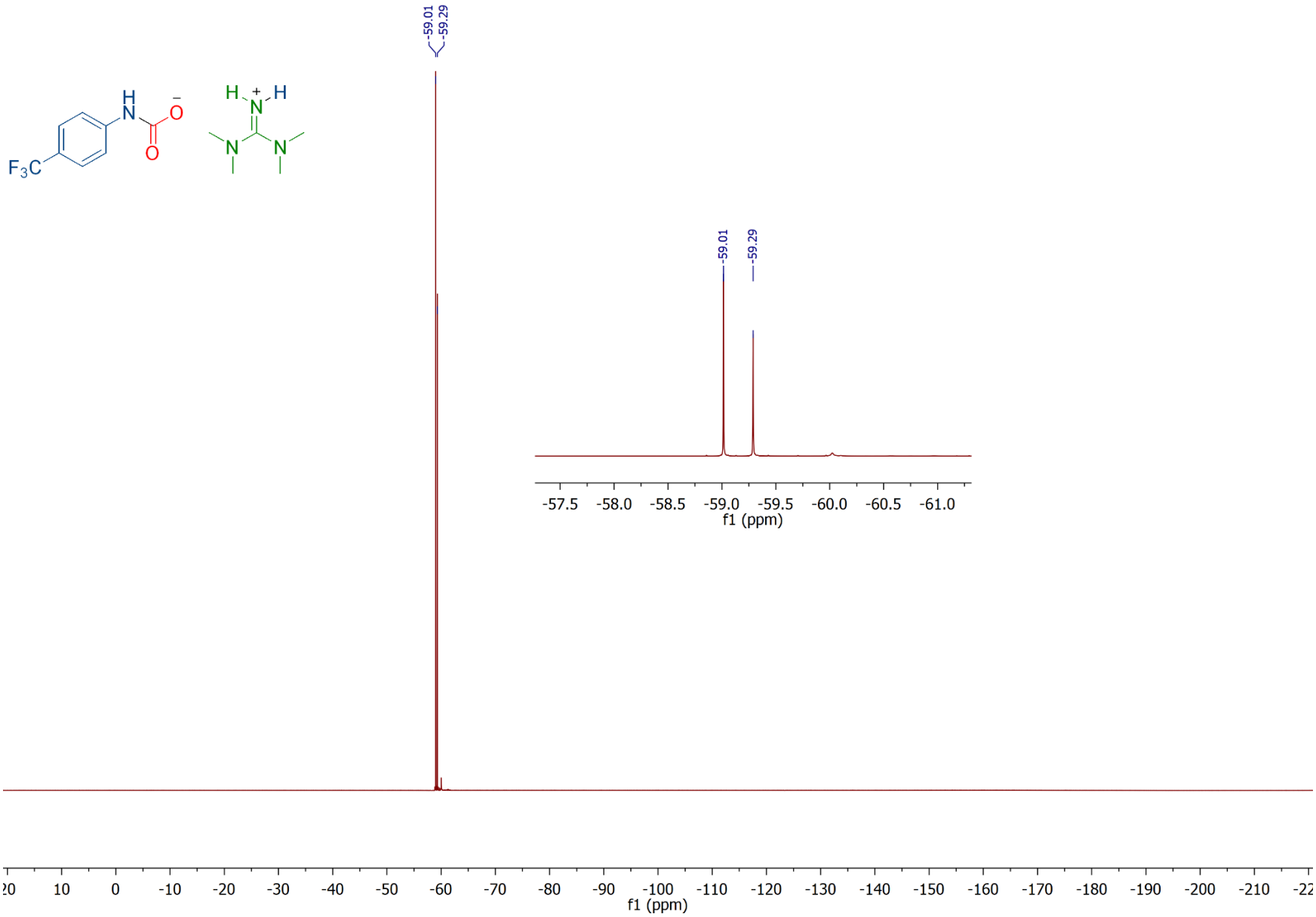

Carboxylation of Pyrrole ^{1}H Using Zwitterion 4, TMG-CO_2

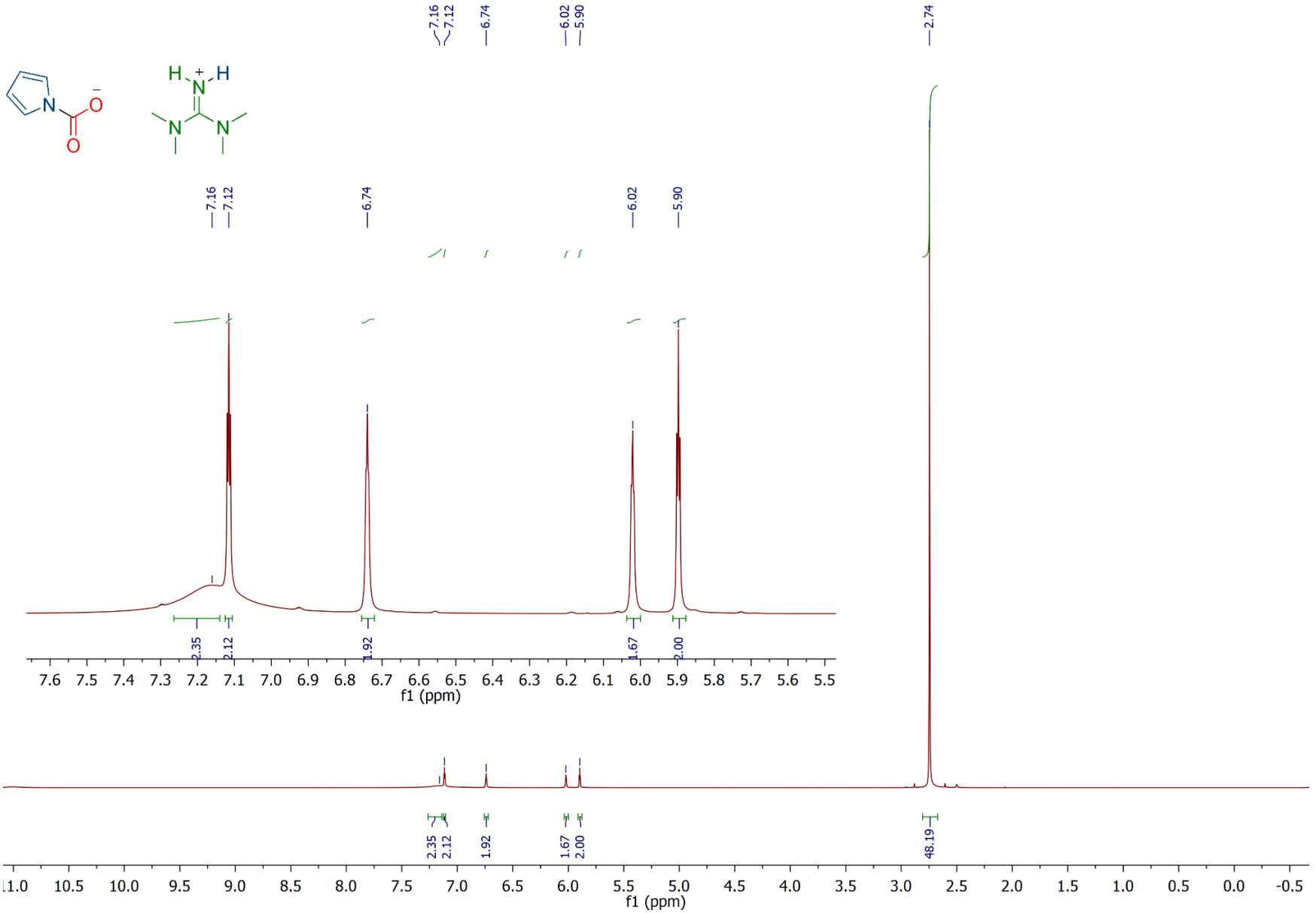

Carboxylation of Pyrrole $^{13}C\{^{1}H\}$ Using Zwitterion 4, TMG-CO_2

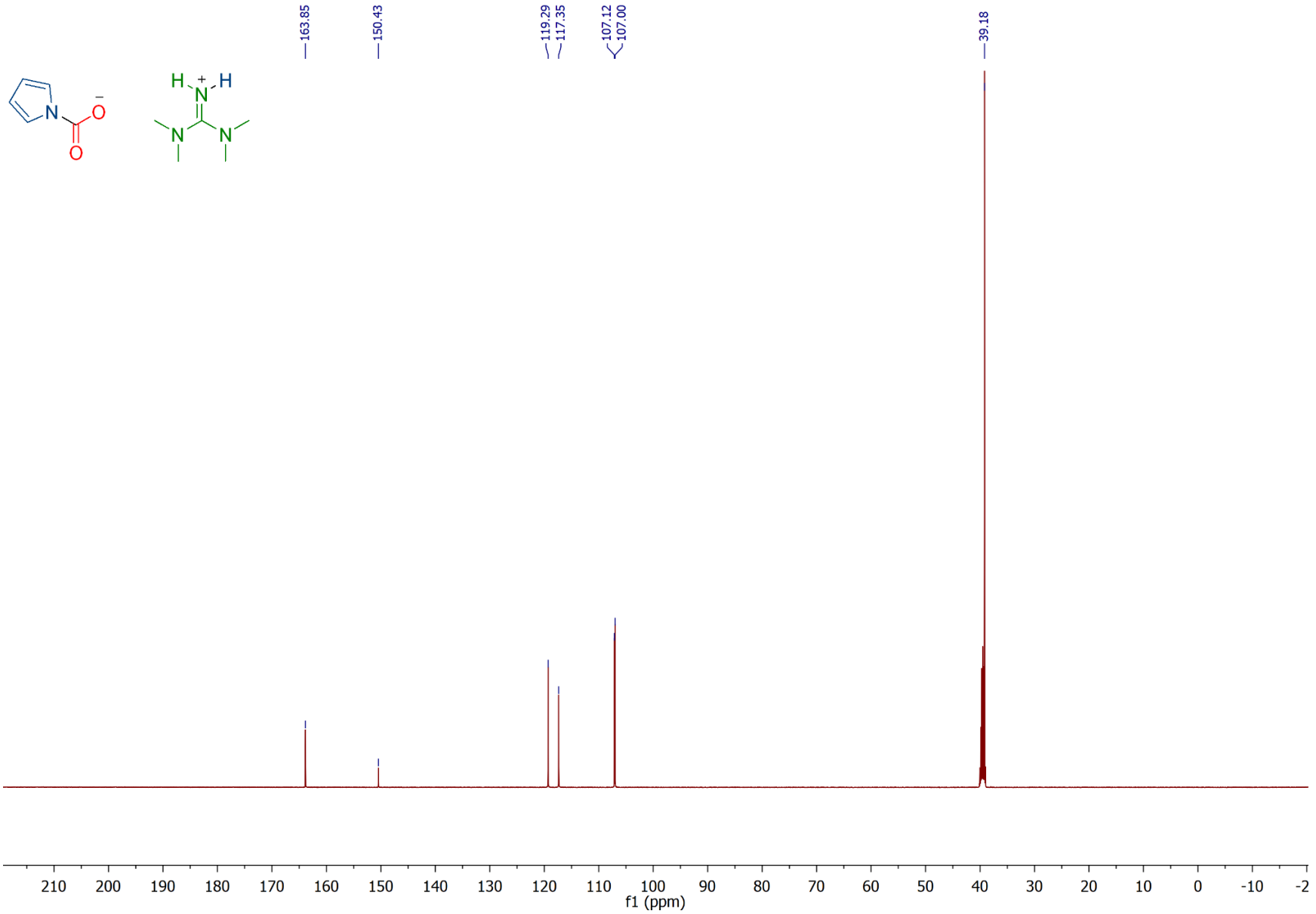

Carboxylation of 1-Butanol ^{1}H Using Zwitterion 4, TMG-CO_2

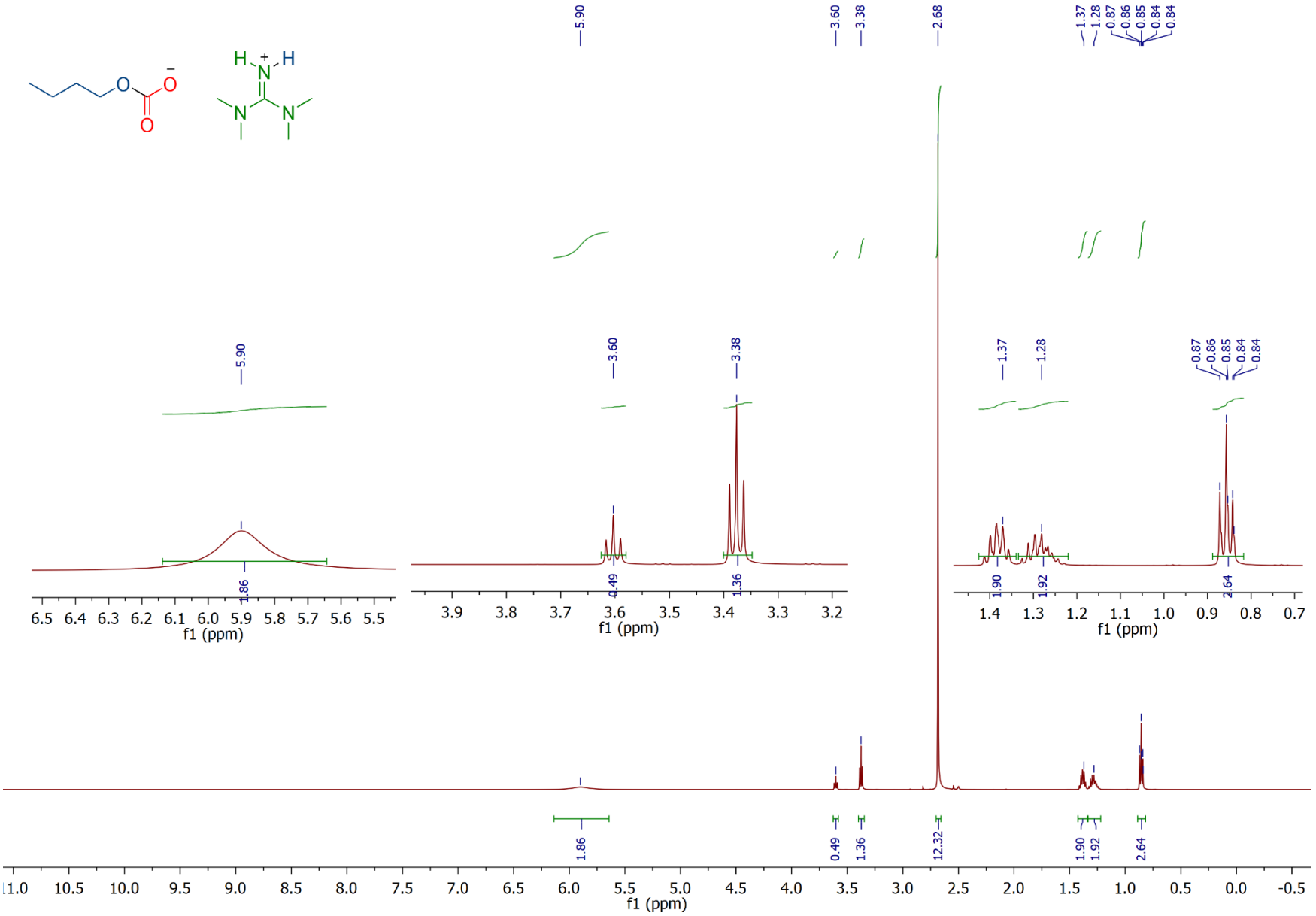

Carboxylation of 1-Butanol $^{13}C\{^{1}H\}$ Using Zwitterion 4, TMG-CO_2

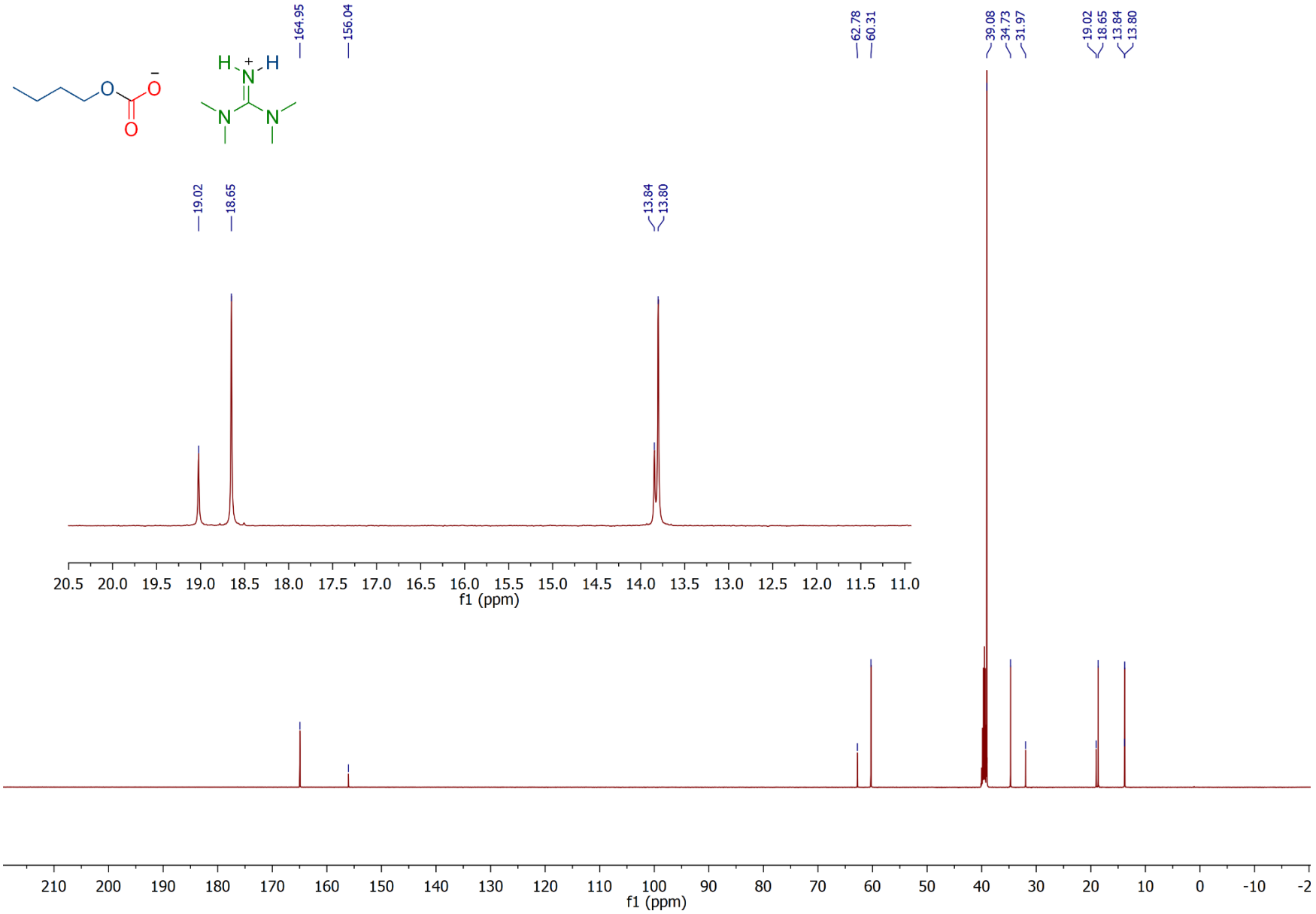

Carboxylation of 1-Butanol HSQC Using Zwitterion 4, TMG-CO_2

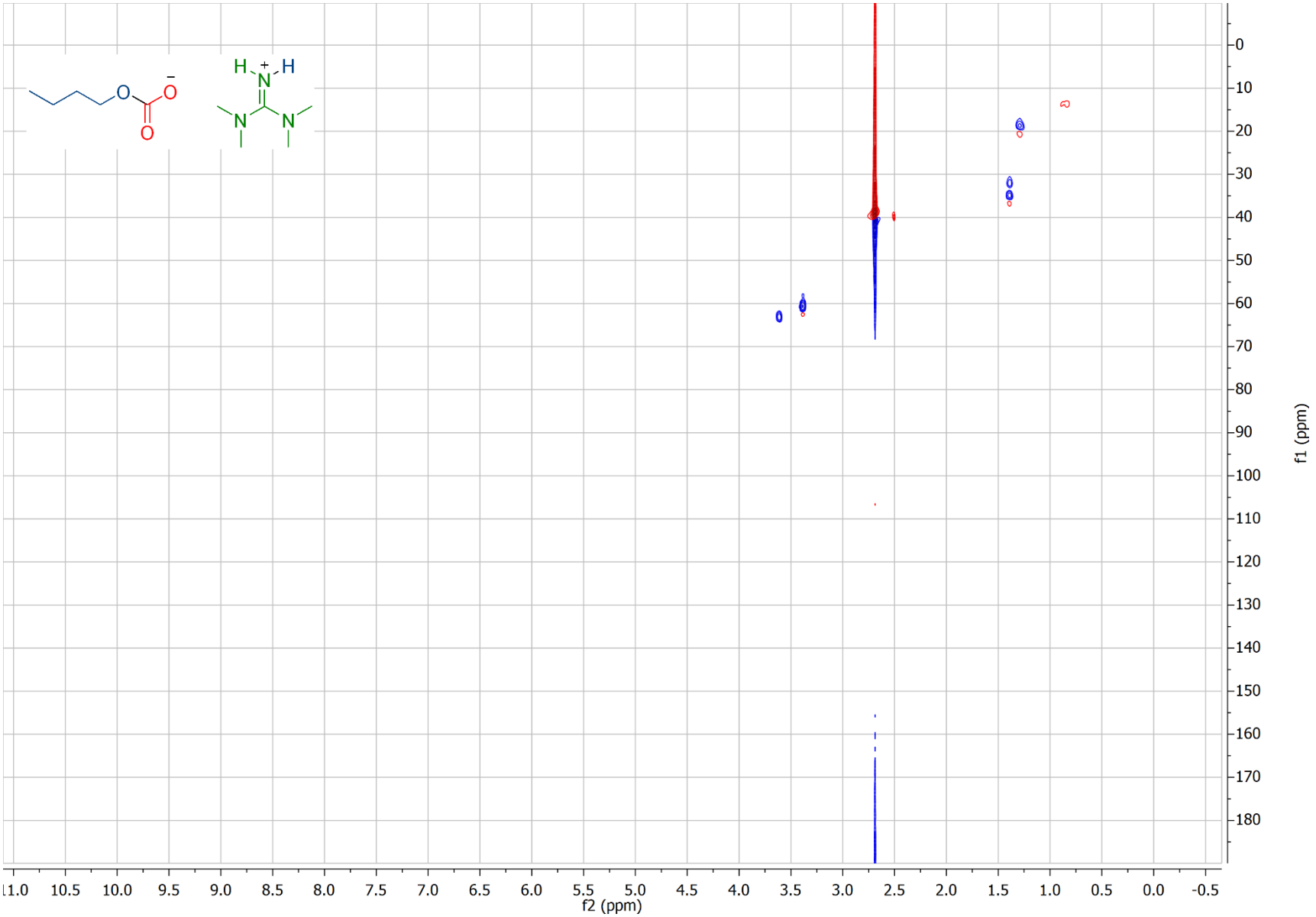

Carboxylation of 4-(Trifluoromethyl)aniline ^{1}H Using Bicarbonate 5, [TMGH^{+}][HCO$_3^{-}$]

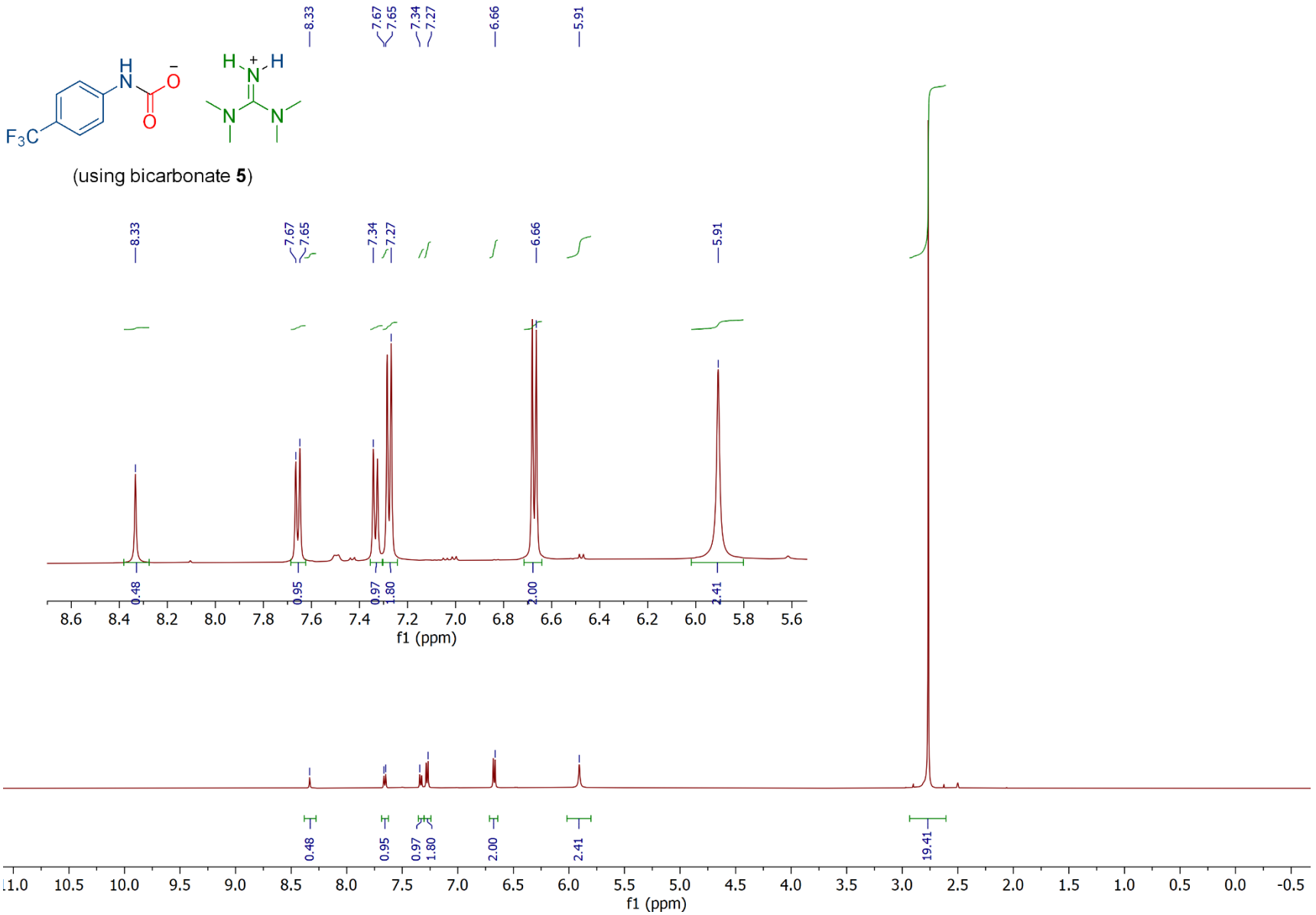

Carboxylation of 4-(Trifluoromethyl)aniline $^{13}C\{^{1}H\}$ Using Bicarbonate 5, [TMGH^{+}][HCO$_3^{-}$]

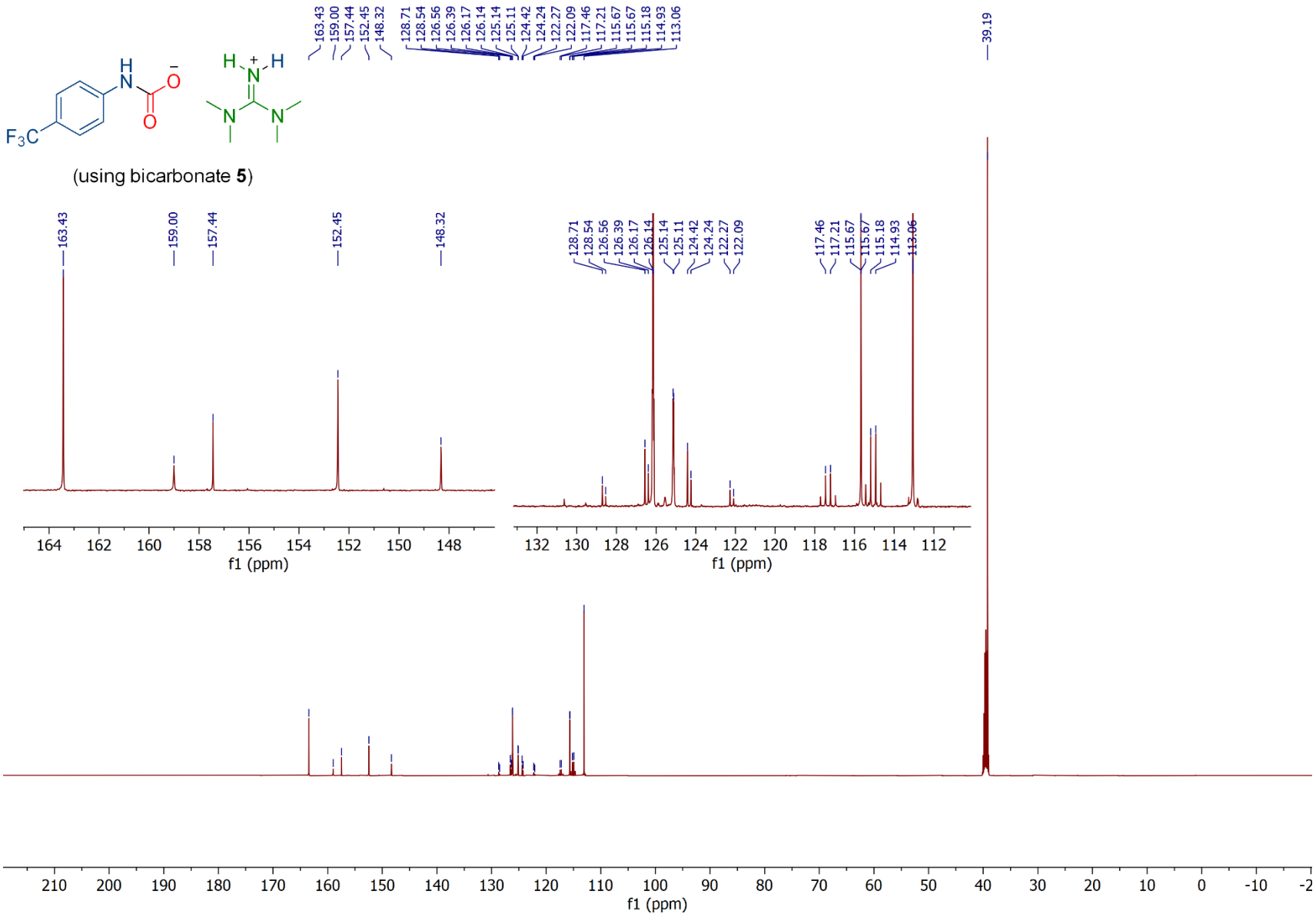

Carboxylation of 4-(Trifluoromethyl)aniline $^{19}F\{^{1}H\}$ Using Bicarbonate 5, $[TMGH^{+}][HCO_3^{-}]$

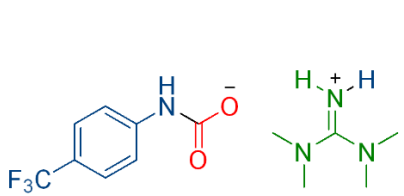

(using bicarbonate **5**)

Carboxylation of Pyrrole ^{1}H Using Bicarbonate 5, [TMGH^{+}][HCO$_3^{-}$]

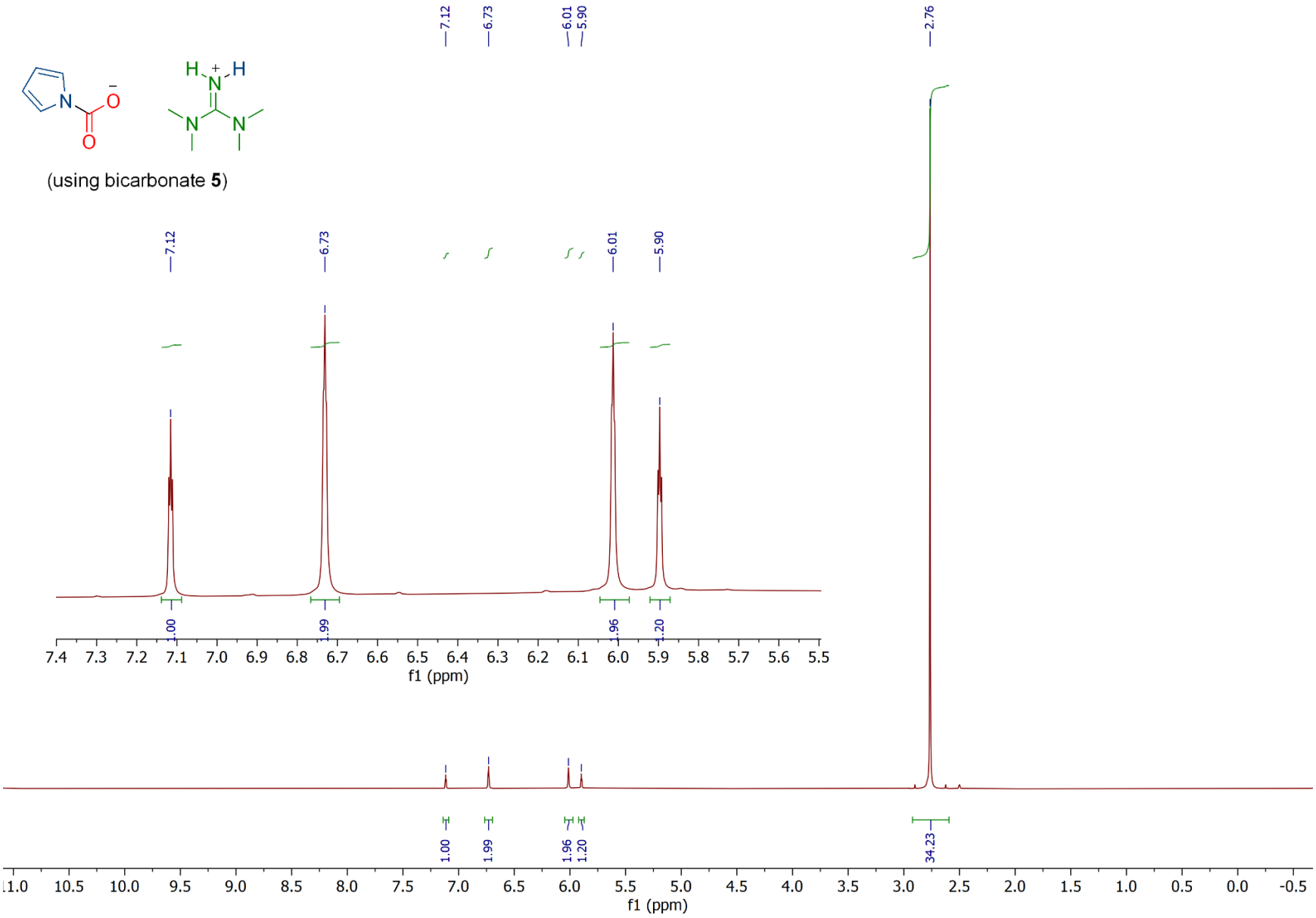

Carboxylation of Pyrrole $^{13}C\{^{1}H\}$ Using Bicarbonate 5, [TMGH^{+}][HCO$_3^{-}$]

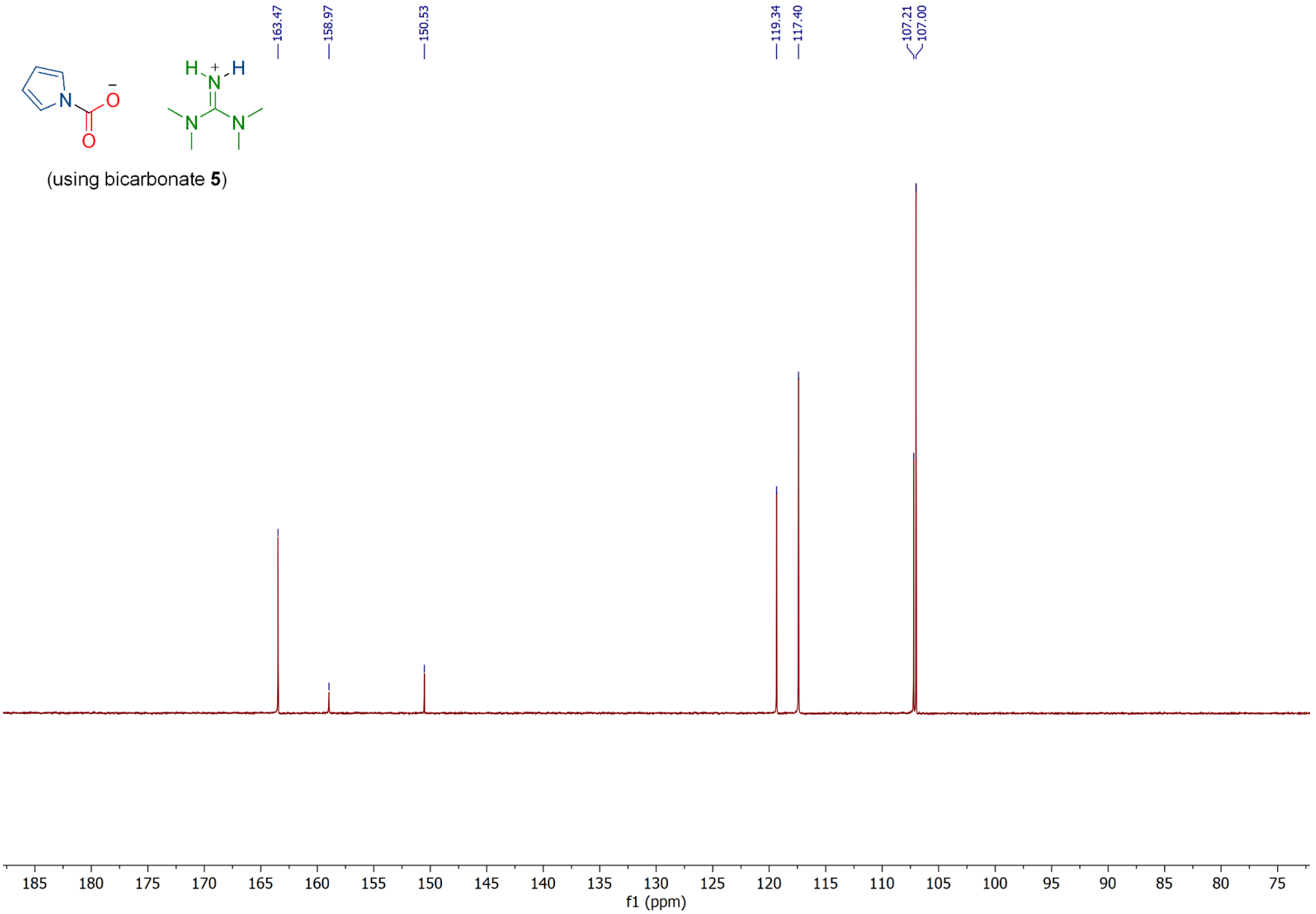

(using bicarbonate **5**)

Carboxylation of 1-Butanol ^{1}H Using Bicarbonate 5, [TMGH^{+}][HCO$_3^{-}$]

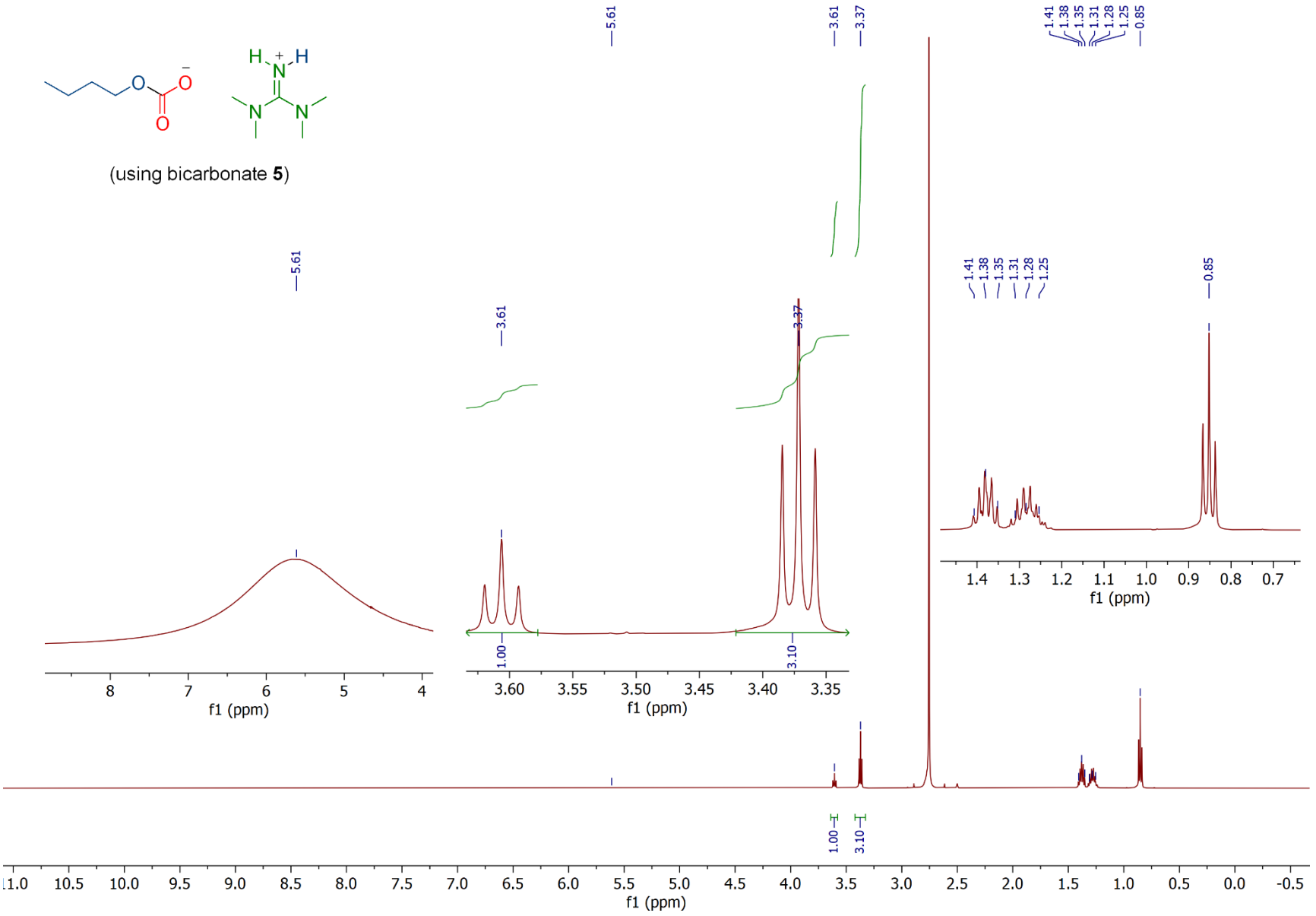

Carboxylation of 1-Butanol $^{13}C\{^{1}H\}$ Using Bicarbonate 5, [TMGH^{+}][HCO$_3^{-}$]

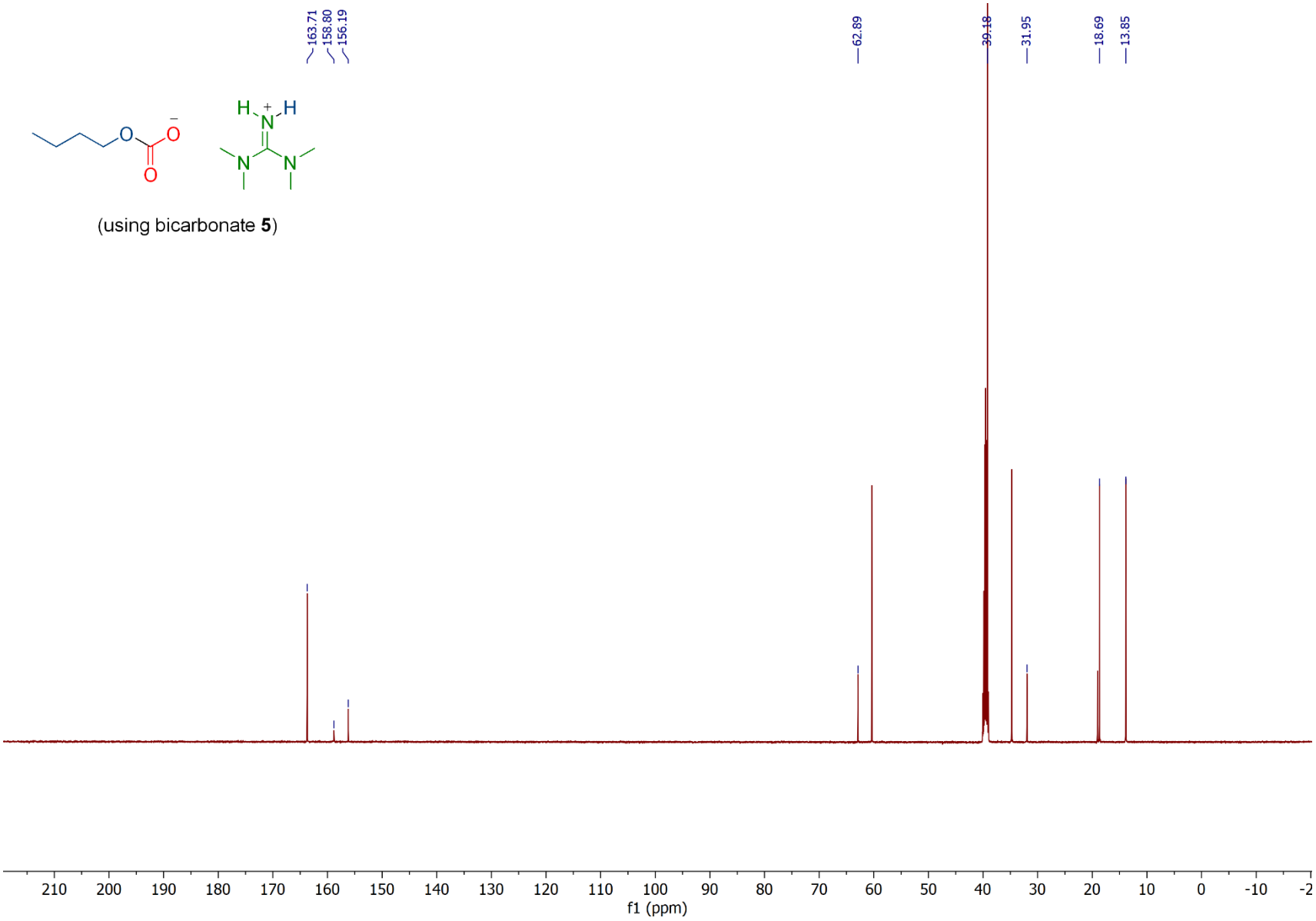

(using bicarbonate **5**)

Carboxylation of 1-Butanol HSQC Using Bicarbonate 5, [TMGH$^+$][HCO$_3^-$]

18. References

(1) Okaru, A. O.; Brunner, T. S.; Ackermann, S. M.; Kuballa, T.; Walch, S. G.; Kohl-Himmelseher, M.; Lachenmeier, D. W. Application of 19F NMR Spectroscopy for Content Determination of Fluorinated Pharmaceuticals. *J. Anal. Methods Chem.* **2017**, *2017*. https://doi.org/10.1155/2017/9206297.

(2) Srinivasan, P. R.; Lichter, R. L. Nitrogen-15 Nuclear Magnetic Resonance Spectroscopy. Evaluation of Chemical Shift References. *J. Magn. Reson.* **1977**, *28* (2), 227–234. https://doi.org/10.1016/0022-2364(77)90149-4.

(3) Fulmer, G. R.; Miller, A. J. M.; Sherden, N. H.; Gottlieb, H. E.; Nudelman, A.; Stoltz, B. M.; Bercaw, J. E.; Goldberg, K. I. NMR Chemical Shifts of Trace Impurities: Common Laboratory Solvents, Organics, and Gases in Deuterated Solvents Relevant to the Organometallic Chemist. *Organometallics* **2010**, *29* (9), 2176–2179. https://doi.org/10.1021/om100106e.

(4) Baidya, M.; Mayr, H. Nucleophilicities and Carbon Basicities of DBU and DBN. *Chem. Commun.* **2008**, No. 15, 1792–1794. https://doi.org/10.1039/b801811a.

(5) Gholamipour-Shirazi, A.; Rolando, C. Kinetics Screening of the N-Alkylation of Organic Superbases Using a Continuous Flow Microfluidic Device: Basicity versus Nucleophilicity. *Org. Biomol. Chem.* **2012**, *10* (40), 8059–8063. https://doi.org/10.1039/c2ob25215e.

(6) Frisch, M. J.; Trucks, G. W.; Schlegel, H. B.; Scuseria, G. E.; Robb, M. A.; Cheeseman, J. R.; Scalmani, G.; Barone, V.; Mennucci, B.; Petersson, G. A.; Nakatsuji, H.; Caricato, M.; Li, X.; Hratchian, H. P.; Izmaylov, A. F.; Bloino, J.; Zheng, G.; Sonnenberg, J. L.; Hada, M.; Ehara, M.; Toyota, K.; Fukuda, R.; Hasegawa, J.; Ishida, M.; Nakajima, T.; Honda, Y.; Kitao, O.; Nakai, H.; Vreven, T.; Montgomery, J. A., Jr.; Peralta, J. E.; Ogliaro, F.; Bearpark, M.; Heyd, J. J.; Brothers, E.; Kudin, K. N.; Staroverov, V. N.; Kobayashi, R.; Normand, J.; Raghavachari, K.; Rendell, A.; Burant, J. C.; Iyengar, S. S.; Tomasi, J.; Cossi, M.; Rega, N.; Millam, J. M.; Klene, M.; Knox, J. E.; Cross, J. B.; Bakken, V.; Adamo, C.; Jaramillo, J.; Gomperts, R.; Stratmann, R. E.; Yazyev, O.; Austin, A. J.; Cammi, R.; Pomelli, C.; Ochterski, J. W.; Martin, R. L.; Morokuma, K.; Zakrzewski, V. G.; Voth, G. A.; Salvador, P.; Dannenberg, J. J.; Dapprich, S.; Daniels, A. D.; Farkas, O.; Foresman, J. B.; Ortiz, J. V.; Cioslowski, J.; Fox, D. J. Gaussian 09, rev. D.01; Gaussian, Inc.: Wallingford, CT, **2013**.

(7) Perdew, J. P.; Burke, K.; Ernzerhof, M. Generalized Gradient Approximation Made Simple. *Phys. Rev. Lett.* **1996**, *77* (18), 3865–3868. https://doi.org/10.1103/PhysRevLett.77.3865.

(8) Adamo, C.; Barone, V. Toward Reliable Density Functional Methods without Adjustable Parameters: The PBE0 Model. *J. Chem. Phys.* **1999**, *110* (13), 6158–6170. https://doi.org/10.1063/1.478522.

(9) Grimme, S.; Ehrlich, S.; Goerigk, L. Effect of the Damping Function in Dispersion Corrected Density Functional Theory. *J. Comput. Chem.* **2011**, *32* (7), 1456–1465. https://doi.org/10.1002/jcc.21759.

(10) Cancès, E.; Mennucci, B.; Tomasi, J. A New Integral Equation Formalism for the Polarizable Continuum Model: Theoretical Background and Applications to Isotropic and Anisotropic Dielectrics. *J. Chem. Phys.* **1997**, *107* (8), 3032–3041. https://doi.org/10.1063/1.474659.

(11) Tomasi, J.; Mennucci, B.; Cance, E. The IEF Version of the PCM Solvation Method: An Overview of a New Method Addressed to Study Molecular Solutes at the QM Ab Initio Level - ScienceDirect. **2018**, *464*, 211–226.

(12) Tomasi, J.; Mennucci, B.; Cammi, R. Quantum Mechanical Continuum Solvation Models. *Chem. Rev.* **2005**, *105* (8), 2999–3094. https://doi.org/10.1021/cr9904009.

(13) Krishnan, R.; Binkley, J. S.; Seeger, R.; Pople, J. A. Self-Consistent Molecular Orbital Methods. XX. A Basis Set for Correlated Wave Functions. *J. Chem. Phys.* **1980**, *72* (1), 650–654. https://doi.org/10.1063/1.438955.

(14) Boys, S. F.; Bernardi, F. The Calculation of Small Molecular Interactions by the Differences of Separate Total Energies. Some Procedures with Reduced Errors. *Mol. Phys.* **1970**, *19* (4), 553–566. https://doi.org/10.1080/00268977000101561.

(15) Cramer, C. J. *Essentials of Computational Chemistry: Theories and Models.*; J. Wiley: West Sussex, England, 2002.

(16) Hopmann, K. H. How Accurate Is DFT for Iridium-Mediated Chemistry? *Organometallics* **2016**, *35* (22), 3795–3807. https://doi.org/10.1021/acs.organomet.6b00377.

(17) Hansch, C.; Leo, A.; Taft, R. W. A Survey of Hammett Substituent Constants and Resonance and Field Parameters. *Chem. Rev.* **1991**, *91* (2), 165–195. https://doi.org/10.1021/cr00002a004.

(18) Kanamori, K.; Roberts, J. D. A Nitrogen-15 NMR Study of the Barriers to Isomerization about Guanidinium and Guanidino Carbon-Nitrogen Bonds in L-Arginine. *J. Am. Chem. Soc.* **1983**, *105* (14), 4698–4701. https://doi.org/10.1021/ja00352a028.

(19) Wilm, L. F. B.; Eder, T.; Mück-Lichtenfeld, C.; Mehlmann, P.; Wünsche, M.; Buß, F.; Dielmann, F. Reversible CO 2 Fixation by N-Heterocyclic Imines Forming Water-Stable Zwitterionic Nitrogen-Base-CO 2 Adducts. *Green Chem.* **2019**, *21* (3), 640–648. https://doi.org/10.1039/c8gc02952k.

(20) Heldebrant, D. J.; Jessop, P. G.; Thomas, C. A.; Eckert, C. A.; Liotta, C. L. The Reaction of 1,8-Diazabicyclo[5.4.0]Undec-7-Ene (DBU) with Carbon Dioxide. *J. Org. Chem.* **2005**, *70* (13), 5335–5338. https://doi.org/10.1021/jo0503759.

(21) Wiench, J. W.; Stefaniak, L.; Grech, E.; Bednarek, E. Two Amidine Derivatives Studied by 1H, 13C, 14N, 15N NMR and GIAO-CHF Calculations. *J. Chem. Soc. Perkin Trans. 2* **1999**, No. 4, 885–889. https://doi.org/10.1039/a806259e.